UNIVERSIDAD DE ALCALÁ

ESCUELA POLITÉCNICA SUPERIOR

DEPARTAMENTO DE ELECTRÓNICA

"Optimization and Analysis of the Current Control Loop of VSCs Connected to Uncertain Grids through LCL Filters"

Ph.D. Thesis

Autor

Santiago Cóbreces Álvarez

Directores

Dr. D. Fco. Javier Rodríguez Sánchez
Dr. D. Emilio José Bueno Pena

2009

This thesis has been typeset using LaTeX and GNU Emacs.

Resumen

La presente tesis está centrada en el diseño y análisis del control de convertidores en fuente de tensión (VSC) conectados a la red mediante filtros LCL. Particularmente se centra en redes que presentan incertidumbre en sus parámetros dinámicos intrínsecos y en su influencia sobre el lazo de control de menor nivel del los convertidores: el control de corriente. Con este objetivo, la tesis aborda el estudio a tres niveles diferentes.

En primer lugar, la tesis estudia el modelo de red que en ella se considerará, sus parámetros inciertos y presenta una propuesta para estimarlos de manera recursiva. La estimación se basa en un proceso de optimización basado en mínimos cuadrados recursivos aplicados a las medidas obtenidas. El sistema de sincronización y la transformación a un sistema de referencia síncrono han sido específicamente diseñados para el sistema propuesto. El proceso de optimizatión se complementa con una función de evaluación de la estimación generada en tiempo real.

El estudio de la influencia de la incertidumbre en los parámetros de la red sobre la estabilidad del control de corriente de convertidores conectados a red constituye la segunda línea de trabajo de la presente tesis. En el caso de controladores lineales, se propone una análisis basado en la aplicación de la teoría del valor singular estructurado μ sobre un modelo de incertidumbre paramétrica que se describe en el presente documento. El método propuesto extrae un intervalo seguro de los parámetros de la red a partir de una planta y un controlador previamente definidos. Son objeto de especial atención los aspectos ligados a la implementación práctica como el tratamiento de incertidumbre real pura y el análisis de sistemas muestreados. Con el objetivo de probar las capacidades del método propuesto, la propuesta esta ilustrada mediante su aplicación a tres ejemplos prácticos: un controlador diseñado con un enfoque SISO, un servo-controlador MIMO y un diseño robusto basado en técnicas $\mathcal{H}_\infty$. Para el caso de controladores no lineales, la tesis presenta algunas conclusiones prácticas aplicables a controladores basados en comparadores con histéresis.

Tras este análisis, la tesis se centra en el problema complementario: el diseño de un controlador robusto para convertidores conectados a la red mediante un filtro LCL cuya estabilidad esté garantizada para un intervalo de parámetros de red previamente conocido. A modo de paso previo, la tesis presenta un servo-controlador óptimo LQ cuyo algoritmo puede ser complementado mediante el uso de observadores de estados. El control se afronta desde un marco de referencia síncrono y directamente controla las corrientes inyectadas en la red. Una vez que se ha establecido el entorno de trabajo, la tesis propone un diseño basado en conformado de lazo robusto $\mathcal{H}_\infty$ complementado con la herramienta de análisis ν-gap.

Palabras clave: Convertidor conectado a red, incertidumbre de red, identificación de la red, análisis robusto, control robusto, ν-gap, conformado de lazo, control $\mathcal{H}_\infty$.

Abstract

This thesis focuses on the design and analysis of the control of voltage source converters connected to the grid through LCL filters. Particularly it is centered on grids presenting uncertainty in their intrinsic dynamic parameters and their influence over the inner control loop of a grid converter: the current control. To that end, the thesis follows a three-fold discussion.

Firstly, the thesis studies the grid model, its uncertain parameters and presents a proposal to recursively estimate them. The estimation is based on a recursive least-squares optimization procedure applied to the current and voltage measurements, performed in the point of common coupling, expressed in a synchronous reference frame. The synchronization and the reference frame transformation process is specially designed for the proposed system. The optimization process is complemented with an estimation evaluation block that gives a real-time measure of the estimation quality.

The influence of those uncertain parameters over the stability of the current control loop of grid converters is the second topic of this thesis. For the case of linear controllers, the analysis is performed by applying the structured singular value μ theory to a parametric uncertainty model that is described in the document. The proposed method extracts safe grid parameters ranges from a previously defined controller and plant model. Special attention is payed to important practical considerations as pure real uncertainty and sampled-data systems analysis. To test the method performance and illustrate its behavior, this dissertation discusses the robustness of three particular examples: a SISO control approach, a MIMO servo-controller approach and a robust $\mathcal{H}_\infty$ design. For the case of nonlinear controllers, the thesis focuses on hysteresis controllers and presents some practical conclusions.

After that analysis, the thesis deals with the complementary problem: the design of a robust controller for grid converters connected through LCL filters to grids whose parameters range between known values. As a prior stage, the thesis presents an LQ servo-controller design procedure that may be complemented with the use of state estimators. The control is faced in a synchronous reference frame and directly controls the grid injected current. Once the framework is settled, the thesis proposes a design technique based on a robust Loop-shaping $\mathcal{H}_\infty$ design procedure complemented with the ν-gap analysis tool.

The final part of this dissertation describes the experimental set-up used for testing the presented proposals. After this, a summary of experimental results and waveforms is presented.

Index terms: Grid converter, grid uncertainty, grid identification, robust analysis, robust control, ν-gap, loop-shaping, $\mathcal{H}_\infty$ control.

Agradecimientos

La realización de la presente tesis ha involucrado muchas horas de trabajo, de discusión y dudas, de alegría y apatía y, en general, de convivencia con muchas personas que, con su esfuerzo, directa o indirectamente y en mayor o menor medida han dejado su huella en ella. Sirvan estas líneas para mostrarles mi profundo agradecimiento (espero no olvidarme de demasiados).

En primer lugar quisiera dar las gracias al Dr. Francisco Javier Rodríguez Sánchez. Su trabajo, experiencia, objetividad, rigor y conocimientos han resultado de gran valor durante todos estos años bajo su supervisión.

Me gustaría agradecer al Dr. Emilio José Bueno Peña su gran labor. Es la persona que me ha introducido en el mundo de la electrónica de potencia y esta tesis es, en gran parte, fruto de su duro trabajo en la dirección del grupo, del laboratorio y de mi investigación. Su actitud cercana, receptiva y positiva, su enorme conocimiento, su confianza y sus sabios consejos han sido ingredientes fundamentales para la culminación de este trabajo.

Quisiera dar muy especialmente las gracias a mi gran amigo Dr. Daniel Pizarro Pérez. Su apoyo tanto humano como técnico, su gran comprensión y su desinteresado compromiso han sido enormes. Si esta tesis pudiera tener varios autores, él estaría entre ellos, sin lugar a dudas.

Quisiera mostrar mi más sincero agradecimiento por sus desinteresada hospitalidad y ayuda a los grupos de investigación que me han acogido durante las diferentes fases de desarrollo del trabajo que aquí se presenta. Concretamente quisiera dar las gracias a todos los miembros del *Grup de recerca en electrònica de potència* (GREP) del Departament d'Enginyeria Electrònica de la Universitat Politècnica de Catalunya, y en especial al Dr. Josep Bordonau Farrerons. A los miembros del *Green Power Lab.* del Institute of Energy Technology de la Universidad de Aalborg, en Dinamarca, y en especial al Dr. Remus Teodorescu y al Dr. Frede Blaabjerg. A los miembros del grupo *Sistemes elèctrics d'energies renovables* (REES) del Departament d'Enginyeria Elèctrica de la Universitat Politècnica de Catalunya, y en especial al Dr. Pedro Rodríguez Cortés. Al Dr. Josep Mª Guerrero Zapata, del Departament d'Enginyeria Electrónica de la Universitat Politécnica de Catalunya.

Por otro lado quisiera agradecer a todos los miembros y colaboradores del grupo GEISER su implicación directa en la realización de la tesis. Gracias a ellos tenemos un laboratorio funcional y en el que se disfruta trabajando. Espero poder devolverles parte de la ayuda que me han prestado todos estos años.

Gracias también al resto de compañeros del Departamento de Electrónica por su completa disponibilidad y ayuda tanto a nivel personal como técnico. Quisiera agradecer especialmente al Dr. Ricardo García López y al Dr. Felipe Espinosa Zapata su ayuda con los temas más arduos de control y su valioso ofrecimiento para revisar partes del trabajo y

ofrecer su visión crítica.

No quisiera olvidarme de dos personas que han conseguido recordarme que hay mundo fuera de la universidad: Juan José Amor, siempre con sus grandes recomendaciones culturales y sus continuos ánimos y Miguel Casas Sánchez, compañero de cordada, aventura y gran corrector de inglés.

Dejo para el final a los más importantes.

Quisiera dar las gracias a mi padre, a mi hermana y al resto de mi familia por su paciencia, ayuda y constantes ánimos.

Y no podría acabar estos agradecimientos sin citar a mi novia, Mireia. Sin duda ha sido la persona que más ha sufrido mis ausencias y, sin embargo, siempre ha estado a mi lado para ayudarme en todo lo posible y para darme una palabra de aliento, confianza, alegría y cariño. A ella, un petó molt molt gran.

Alcalá de Henares, Nochevieja de 2008.

A mi madre

"And so you will sledge nearly alone,
but those with whom you sledge will not be shopkeepers: that is worth a good deal.
If you march your Winter Journeys you will have your reward,
so long as all you want is a penguin's egg."

Apsley Cherry-Garrard

Contents

Glossary

Symbols:

U_{DC}	DC-bus voltage
T_{SW}	PWM switching period
$\mathcal{P}$, Π	Uncertain set of plants
$\omega,\ \omega_0$	Grid fundamental frequency ($rad\ s^{-1}$)
$f,\ f_0$	Grid fundamental frequency (Hz)
u	Converter average output voltage
i	Current
u_c	Capacitor voltage in an LCL filter
e	Grid equivalent voltage source
$u_{PCC},\ v$	Voltage measured in the Point of Common Coupling
G_0, G	Nominal plant model
G_p	Perturbed plant model
x^*	Reference for variable x
$\hat{x}$	Estimate of variable x
$x^\star$	Complex conjugate of a complex variable x
x^T	Transpose of matrix x
x_g	Variable x of the grid model
$x_{a,b,c}$	Variable x of the phase a, b or c respectively
$x_{1,2}$	In the LCL model, variable x of the converter or grid-side branch resp.
$x_{d,q}$	d or q axis of variable x, respectively
$\langle x(t) \rangle_{T_{SW}}$	Average value of variable x during a switching period
$\boldsymbol{x}$	Complex variable x
$\mathbf{X}$	Complex matrix X
μ	Structured Singular Value
δ_ν	ν-gap
$\bar{\sigma}(X)$	Largest Singular Value of X
$\left[\begin{array}{c\|c} A & B \\ \hline C & D \end{array}\right]$	State space realization $C(zI-A)^{-1}B+D$ or $C(sI-A)^{-1}B+D$

Abbreviations:

AC	Alternating current
AWGN	Additive White Gaussian Noise
DC	Direct current
DPC	Direct Power Control
DPGS	Distributed Power Generation System

DSP	Digital Signal Processor
ECS	Electronic Control System
IMC	Internal Model Control
LFT	Linear Fractional Transformation
LQ	Linear Quadratic
LQG	Linear Quadratic Gaussian controller
LTI	Linear Time-Invariant
MIMO	Multiple-input Multiple-output
PCC	Point of Common Coupling
PES	Power Electronics System
PLL	Phase-Lock Loop
PV	Photovoltaic
PWM	Pulse-width modulation
SSV	Structured Singular Value
SISO	Single-input Single-output
RLS	Recursive Least-Squares
THD	Total Harmonic Distortion
VSC	Voltage Source Converter
ZOH	Zero Order Hold

Chapter 1

Introduction

1.1 Framework

The world economy is based on energy. The support of an economic progress for the each time bigger world population is accurately reflected on a maintained energy increase. The world energy consumption has almost doubled since 1970 and, despite the significant contributions and advances in energy processing and efficiency, the International Energy Agency predicts a more worrying evolution of the *Reference Scenario*[1] model in its annual publication World Energy Outlook[weo, 2006]: by 2015, the total global consumption is expected to increase by 33%, reaching by 2030 an increase of 52%. This increase is particularly stepped in populated currently developing economies such as China and India where energy efficiency and sustainability is better understood as a luxe more than a primary necessity.

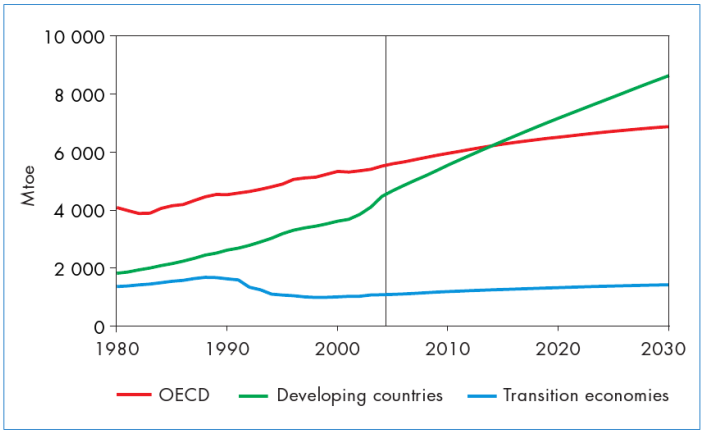

Figure 1.1: *World Primary Energy Demand by Region in IEA Reference Scenario. Extracted from* World Energy Outlook 2006 by International Energy Agency*[weo, 2006].*

[1]The term Reference Scenario is a mathematical model used in the annual publication World Energy Outlook of the International Energy Agency. It reflects the expectable situation considering the current legislative and productive situation.

Fossil fuels provide 80% of this energy. This fact is widely considered as a potential socio-economical instabilizing factor due to the marked oligopolistic nature of this market. Investment concerning oil and gas extraction and distribution is needed in order to provide the new developing areas with adequate infrastructures; unfortunately this is not expected.

In addition to these issues, global conscience about greenhouse effect is increasing. In 1998, several developed countries undersigned the Kyoto protocol [kyo, 1998]. This agreement settled a set of minimal objectives that supported a trial of keeping CO_2 at current or slightly lower levels. These objectives are revealing to be impossible to achieve in the current reference scenarios.

This increase in energy consumption is not only challenging because of generation issues but also in energy transportation, processing and use. The electric system is approaching its limit. Recent blackouts episodes [bla, 2005] are being related to power system design weaknesses, overuse and lack of redundancy. The repercussion of these power system faults is unlimited. Nowadays, the society and the economic system depend more than ever on a reliable, stable electric supply and the account of losses during a blackout is huge.

All these reasons are questioning the actual energy paradigm. There is a social, scientific and economical agreement in transforming this system in a multiple way: modifying the energy mix, trying to develop and improve alternative energy systems and trying to increase energy efficiency in socio-economical and technical terms.

E.U. position

The European Union is very concerned about these problems. In its green and white papers [gre, 2006] [whi, 1997] the European Commission made a strong criticism about its energetic situation. The facts: the energy balance indicates that half of the energetic demand is covered by energy that comes from outside its borders. This percentage is expected to increase to up to 66% before 2030. In the case of fossil fuel resources the situation is still more severe. Indigenous resources, such as the North Sea are in rapid decline and by 2030 84% of gas and 93% of oil will be imported. The origin of these materials is expected to be a very oligopolistic market. The diagnosis is clear: E.U. is in a clear vulnerable position.

In addition, in spite of the E.U. commitment to reduce greenhouse emissions, the evolution shows that far from reducing them, 5% increase is expected by 2030 [ene, 2007].

The strategy of the E.U. is remarkably ambitious. Far from limiting itself to study the possible solutions to try and repair these vulnerabilities, the European Commission is making strenuous efforts on turning this unfavorable situation into a great opportunity by creating an economic and industrial momentum that positions the E.U. as an energy sector global leader. More concretely:

- The EU has already undertaken to cut its own emissions by at least 20% and would increase this reduction under a satisfactory global agreement.
- It has also undertaken to improve the energy efficiency by 20% by 2020.
- And to raise the share of renewable energy to 20% by 2020.

Part of the way is covered: Europe is already world leader in renewable energy and has both a competitive and comparative advantage in the most promising and mature

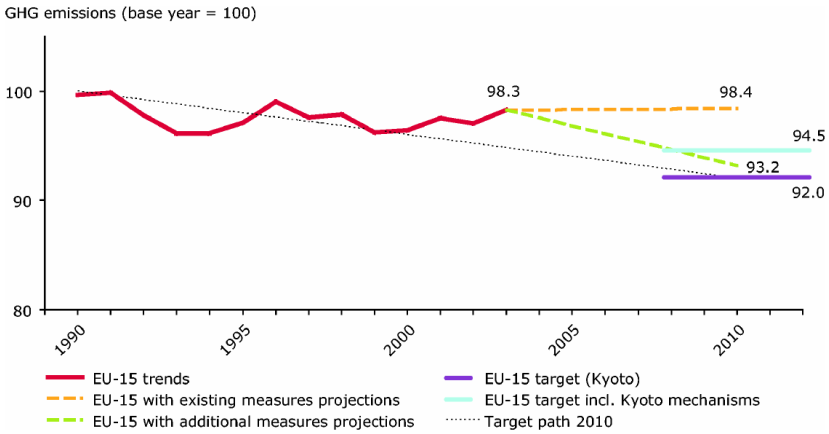

Figure 1.2: *Kyoto Protocol and possible evolutions. (Source: European Commission.)*

renewable technology, wind power. In 2004, European wind turbine manufacturers had a global market share of more than 60% [ene, 2007]. In the same direction, some of the countries belonging to the union are widely considered examples of grid integration of energy resources: Denmark, world leader in wind energy share, Germany, that after installing more than 1100 MW achieves an amount of PV facilities that represent 85.5% percentage of the total capacity installed in the European Union and Spain, approaching the 16.000 MW of wind generation capacity and holding ambitious plans of PV installation.

These three examples are locally approaching the considered maximum penetration safety margin. However, the transformation is not finished. When studied in the whole E.U. territory, the renewable resource share falls to only 3% of the European power needs[ewe, 2005]. This small percentage ensures a promising continuity in renewable energy technology investment in Europe that is likely to be extended to other world areas.

Spain position

Spain plays a distinguished role in the renewable energy sector. Several companies such as Gamesa, Acciona, Iberdrola and Isofoton operate abroad Spanish borders and are widely considered global market leaders in several fields.

Spain closely follows European guidelines. This way, its fundamental actions on this sector are specified by the *Plan de Energias Renovables 2005-2010* [per, 2005] and the *White book about electric generation regulatory framework*.

These plans specify a continued compromise to follow current policies in wind energy introduction until it achieves the maximum safety share: 30.3% in 2010 and a remarkably ambitious bet in the promotion of solar energy. More concretely, some specific purposes are stated in the following items and displayed in Fig. 1.3.

- 147% increase in wind energy production achieved by means of the installation of 12.000 MW. Total wind production will approximately reach 20.155 MW.

- 981% increase in photo-voltaic energy conversion system, achieved by means of the installation of 363 MW to get a production of approximately 400 MW.

- The installation of 500 MW of thermo-electric power producing plants. This kind of energy is practically not used currently in Spain.
- New PV energy installations together with new thermo-electrical generation plants will represent an increase in 2332% of the produced solar electric energy.

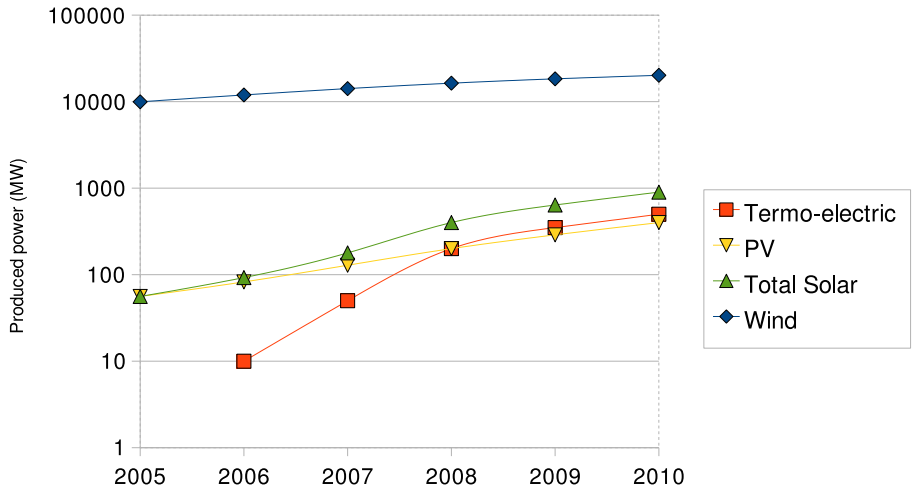

Figure 1.3: *Spanish renewable plan for the period 2005-2010. Source [per, 2005].*

The necessary increase in the power system efficiency and robustness, the introduction of new energy supplies into the grid and the need of a more flexible economic framework are causing a revolution in the way the power system is understood. One of the key points in this transformation is the decentralization in the power system operation. The distributed generation concept embodies this transformation.

The distributed generation paradigm

Most developed economies are arriving to the conclusion that one of the causes of last years electric problems is the obsolescence of a power system paradigm that uses one-century old technology and that is designed to resolve one-century old problems. This obsolescence is mainly detected in two directions: its structure and the power sources it contains.

The past and present electric paradigm is usually referred to as *Centralized or Traditional Generation paradigm*(see Fig. 1.4.a). Basically it is based on the existence of a (relatively) small number of big energy generation points. These generation points have traditionally been based on fossil fuel combustion (coal, oil and recently gas) or nuclear fission. The amount of energy injected into the power system is fully controlled by the power system operator relying on accurately consumption predictions and feedback.

This model presents some limitations. The centralized structure and the few generation points induce severe design vulnerabilities into the system. Few network points support a big generation responsibility and, in the case of a fault in some of the biggest generation nodes, the probability of a chained fault is higher than it should, even in the presence of back-up systems. A second limitation is its low efficiency regarding the distance from

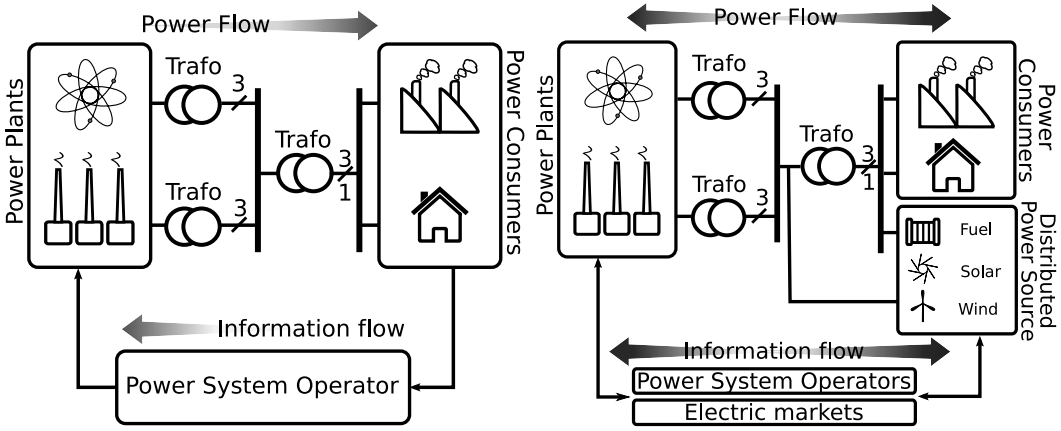

(a) Traditional generation. (b) Distributed generation.

Figure 1.4: *Power system paradigms.*

energy producers to energy consumers. Usually the placement of these big power plants is chosen to be far from populated places in order to minimize the adverse health effects over the consumers or simply near natural resources. Last but not least, these grids lack the desirable grade of cross-borders connection and management flexibility that could boost the economical possibilities of the electric market. Two main factors characterize this paradigm: its energy and information flow direction. As displayed in Fig.1.4.a, energy is always flowing from power plants through the transmission and distribution system to power consumers as domestic and industrial facilities. The information flows in the opposite direction: the system operator acquires the available consumption data, and sends commands to the generation points in order to balance the electric production.

Goverments and research institutions are increasingly focusing their attention on the improvement of the existing infrastructures and regulatory frameworks. Proof of it are the E.U. investments in these topics in the last Framework Programs and the documents [eus, 2006][sra, 2007]. The improvement of the power system following a *Distributed generation paradigm* (see Fig. 1.4.b) represents the common objective of the proposed transformations. This paradigm pays special attention to the bidirectional flow of power and information that would allow a more powerful control of the power system allowing the integration of extensive small distributed power sources, placed, or not, close to end users and its integration with large-scale central power generation, the participation of small producers in the electric market, the introduction of *quality of service* concepts in energy delivery, the ability to increase grid efficiency by equalizing power consumption along the day, etc.

Numerous transformations have to be performed to accomplish such objective. Many of them refer to economical and regulatory aspects but others are technical considerations related to the communication capabilities of distributed power sources and consumers and the reliability of the formers. A particular important role in this transformation is being played by the electronic interfaces used to connect the new distributed sources to the power system, that are being and (will be) the center of a huge research effort.

The Voltage Source Converter as electronic interface. Thesis work lines

The connection of distributed energy sources to the grid very often implies the use of power electronics interfaces. These interfaces increase the quality of the delivered energy and allow to control important conection parameters. One of the most popular topologies for this purpose is the *Voltage-Source converter*. This topology presents several important advantages:

- Bidirectional operation: The energy can flow from the DC-side to the AC-side or vice-versa. When associated in back-to-back configuration with another VSC, the resulting device behaves as a very versatile AC-AC converter.
- Control of active and reactive power consumed from or injected to the grid.
- Low ripple in the DC-side voltage and in the AC-side current, mostly if it is connected through an LCL filter.
- Configurable Power Factor displacement.

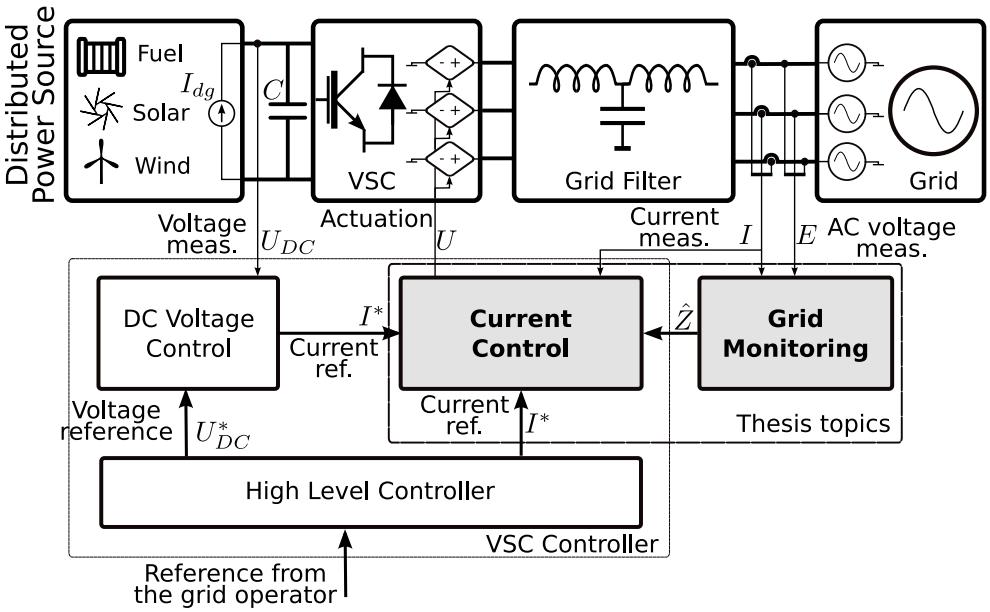

Figure 1.5: *VSC Cascaded control general block diagram.*

An important component of this kind of converters is the filter used in the grid connection (see Fig. 1.5). The selection of the line filter is important because it conditions the whole device dynamic behavior, its cost and the quality of delivered energy. This filter is aimed to achieve a certain attenuation at the switching frequency minimizing cost. Traditionally this filter was designed to be an inductor L in each phase, but achieving low THD current values implied bulky and expensive inductors. The employment of more complex structures such as LC or LCL filters opens the door of improving the current quality and decreasing costs. The design criteria for the filter components have been the topic of different documents and regulations from IEC, IEEE, etc.

The combination of an VSC and an LCL filter constitutes a powerful set for Distributed Generation Applications. It represents a flexible, efficient, high quality and low cost interface appropriate for most applications.

The connection of an energy source to the grid through this kind of interfaces is itself a dynamic system usually managed by means of automatic control strategies. The most widespread option is a control structure named *Cascaded VSC control*. This control strategy divides the control process in several control loops organized in hierarchical order (see Fig. 1.5). In general terms, these are the main three control layers:

- An outer application dependent control loop. This control loop may, for example, be the responsible, in the case of a wind-turbine connection, of the frequency-power or grid voltage regulation.
- An intermediate level control loop. This control loop keeps the DC-side voltage regulated at a desired value under different loading conditions. To achieve this, the outer control loop calculates the necessary output currents and assumes that they will be accurately delivered.
- An inner control loop stabilizes the actual VSC hardware. Its responsibility is to control the current in each of the phases of the AC-side at the reference value calculated by outer control loops. It is important to note that this control layer must provide a reliable base. Performance and robustness of outer control loops (and finally of the whole power converter) relies on this control loop operation.

This control scheme is known to present sensitivity to the characteristics of the PCC where it is connected. Unfortunately, the accurate modeling of the PCC performed when, for example, a new wind farm is installed is not scalable to other minor distributed resources as domestic solar panels or micro-turbines. This kind of energy sources, that play an important role in the *Distributed Generation paradigm*, are connected in very different situations, ranging from connections near to a transformer, in remote places connected through limited infrastructure or in local grids that may operate connected to or isolated from the mains.

The lack of a grid connection detailed study, the big amount of connection possibilities and its variation along time induce an uncertainty over the grid connection parameters that directly affects the control algorithm of the grid converter. A poor adaption of the VSC to a certain PCC may result in connection issues if the control algorithm of the power converter is not robust enough.

This thesis is focused on the analysis of the influence that an uncertain grid has over the inner current control layer of a grid converter. To this end, the thesis follows a three-fold strategy: the first work line of this dissertation is the design of a system able to estimate the fundamental parameters of the grid when viewed from the PCC. The resulting system should be recursive so that, in addition to its use for a measurement application or for controller design, it could serve as a base for an anti-islanding regulation compliant system. The analysis of the effect of the uncertainty in those grid parameters over the stability of traditional current controllers and the obtaining of safe grid limits for a given controller is the second topic of this dissertation. Once the effect is analyzed, the thesis will focus on the design of a grid converter current controller that is stable for a previously given set of possible grid parameters.

Fig. 1.5 shows a block diagram of the global control problem. The shaded blocks represent the main thesis topics.

1.2 Thesis development context

This thesis is developed inside the framework provided by the project CONDOR II, entitled *"Design and evaluation of protection and control solution for distributed generation systems in the presence of grid faults and disturbances"*. This project is funded by the Spanish Science and Technology Ministry (ENE2005-08721-C04-01). The project is developed by four research groups belonging to: Carlos III University, University of Valencia, Institute of Electric Technology of Valencia and University of Alcala. Its main objectives are:

- Design and development of control and protection systems for grid converters to fulfill current grid codes regulations.
- Design and development of a grid fault laboratory facility to test the proposed control techniques performance.
- Improvement and evaluation of magneto-resistive technology for the development of new low and medium voltage industrial measurement systems.
- The analysis and establishment of reference values to perform the measurements (and estimations) of electrical magnitudes for the control and protection of grid devices connected to power systems with high presence of distributed generation elements.

This thesis deals with the first project objective from a robust control design point of view. The approach is to try to find the relationship that exists in the trade decision between uncertainty in the connection model and the maximum achievable performance of the current controller. Robust control theory provides a valuable framework to deal with this kind of problems and is the chosen tool to resolve the problem.

Additionally, the thesis is also framed on the project funded by the University of Alcala ATICA, entitled *"Application of non-linear, adaptive and multi-variable control and identification techniques to improve the distributed generation grid connected converter behavior."*. The main objectives of this project are:

- The development of multi-variable control techniques to improve the current control design and performance of voltage source converters connected to the grid through high order filters.
- The development and testing of grid identification algorithms to estimate grid intrinsic parameters and provide power converters with grid support ancillary services.
- The development and testing of adaptive control schemes able to modify the grid converter control, optimizing its behavior according to the grid particular situation.
- The development of non-linear control techniques to improve the injected energy quality of voltage source converters connected to the grid through filters with low cost inductors operating in flux saturation zone.

This project scope is very close to this thesis objectives. First point of the project is to some extent common with CONDOR project and deals with control techniques that are proposed on this thesis. The second point of the project is related to the grid monitoring task considered in Fig. 1.5 also proposed in this document.

1.3 Document structure.

The present document is structured in seven chapters organized as follows:

- Chapter 2 is dedicated to a double objective. The first part is dedicated to make a review of the already published literature related with this thesis topics. The analysis covers three different sub-topics: the estimation of grid equivalent parameters, the study of the influence of uncertainty on those grid parameters over the current control loop of grid converters, and the current control of voltage source converters connected to the grid. Once the previous work has been analyzed, the second part of the chapter will describe the proposed objectives of the thesis.

- Chapter 3 proposes a grid impedance monitoring system for distributed power generation electronic interfaces. The chapter starts describing the assumed grid model that will be used for the estimation process. The described system estimates the previously described model from the voltage and current measurements performed in the point of common coupling. The estimation algorithm is based in a recursive least-squares algorithm implemented in the complex field. Simultaneously, the system evaluates the quality of the estimation, minimizing its influence over the grid and detecting islanding situations.

- Chapter 4 is dedicated to study the influence of uncertainty in the grid parameters over the current control of grid connected voltage source converters through LCL filters. To achieve this objective, the chapter starts making a detailed mathematical model of the converter grid connection in both the nominal and the uncertain case. Once the model is established, the chapter will analyze the influence of this uncertainty over converters controlled by means of linear and non-linear schemes.

- Chapter 5 is dedicated to propose a control design method that ensures stability of the current control loop of a voltage source converter connected to the grid through LCL filters given an initial uncertainty range.

- Chapter 6 also has a double objective. Its first part describes the experimental set-up that was used to verify the results proposed in this dissertation. The second part of the chapter presents a summary of the obtained experimental results and waveforms.

- Chapter 7 states the conclusions and contributions extracted from this thesis and elaborates a list of possible future lines of research and work.

Chapter 2

Knowledge review and thesis objectives

This chapter presents a review of the previous works related to this thesis topics and enumerates the thesis objectives.

2.1 Introduction

The work developed in this thesis is focused on the improvement of the behavior of grid-converters (VSC) connected to uncertain grids through LCL-structure filters.

This improvement is considered in three main directions:

1. Grid dynamics estimation.

2. Robustness analysis of current controllers when connected to grids with uncertain dynamics.

3. Robust current control design of a converter connected to uncertain grids.

The first part of this chapter presents a knowledge review of different previous approaches related to the main topics of this dissertation. The second part of the chapter is dedicated to extract a summary of the proposed objectives extracted from the study of the ideas and proposals outlined in the state of the art review part.

2.2 Knowledge review: Grid identification

The estimation of the dynamic parameters of a grid when seen from the PCC where a grid converter is connected has been an active research topic for years. Roughly speaking, the methods assume an initial model containing some unknown parameters and present different methods to estimate those parameters.

Proposed methods can be widely classified into two general groups according to the influence they have in the system under identification: *active* and *passive* methods.

2.2.1 Active grid identification

Active methods are intrusive. They require the systematic perturbation of the grid in order to extract the information needed to estimate the grid equivalent impedance.

Some remarkable strategies are the injection of single-tones of the frequency object of estimation [Asiminoaei et al., 2004] [Rhode et al., 1997]. The harmonic impedance can thus be estimated by performing a frequency analysis. The main handicap in this approach is the frequency masking produced by the grid fundamental frequency, which makes the estimation at exactly the fundamental frequency impossible. The adopted procedure usually interpolates this value by performing two simultaneous estimations in neighborhood's frequencies. Another known issue of these techniques is the possible interference between near converters that are executing similar methods without a previous frequency distribution.

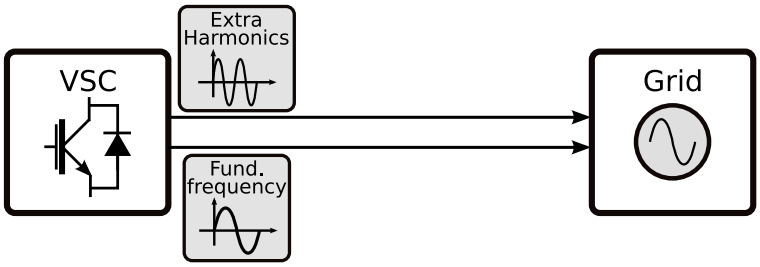

Figure 2.1: *Grid identification via tone injection.*

In order to gain information at more frequencies, some proposals extend the single-tone identification concept to the injection of a wide spectrum voltage or current disturbance into the grid [Sumner et al., 2004] [Sumner et al., 2002] [Staroszczyk, 2005]. By analyzing the relationship between the voltage and the current, the impedance spectrum can be estimated for several frequencies simultaneously. Again, fundamental frequency masking induces estimation problems and sharp notch filtering may be required.

A third set of methods bases the grid disturbance in the connection and disconnection of calibrated linear or non-linear loads from the PCC. A later analysis of the measured electric variables in the presence and absence of the extra load [de Oliveira et al., 1991] [Girgis and McManis, 1989] may give the searched information.

Finally, some recent references base their identification process in producing variations of the reactive and active power injected to the grid by a grid converter. Some remarkable works following this approach are [Ciobotaru et al., 2007] for single-phase cases and [Timbus et al., 2007] for three-phase cases. A similar approach from a different research group is [Tarkiainen et al., 2004]. These proposals are based in a periodic variation of the injected active and reactive power, usually following a square wave. The main limitation of these approaches are the difficulties in applying regression algorithms to the measurements that would improve the estimation results by reducing the negative effects of existing additive noise.

In [Fusco et al., 2000], the authors propose a least-squares based method that is able to estimate the grid intrinsic parameters from a quite general mathematical framework. Besides the systematic grid perturbation, the main drawback of this approach is the elevated computational load that produces the algorithm due to the constrained optimization algorithm and the use of Kalman filter for synchronization purposes.

2.2.2 Non-intrusive grid identification

Non-intrusive or passive methods present the characteristic of making an estimation without introducing disturbances into the grid. There are few publications proposing such methods. [Pedersen et al., 2003] proposed the use of the disturbances already inserted in the grid by existing converters in order to extract an estimate of the grid equivalent impedance. The proposed method showed important limitations in its application due to the lack of information on the measured signals and, in general terms, the performance has a strong dependency on the concrete application of the converter whose disturbances are being tracked. A similar approach is taken in [Girgis et al., 1993], where the existing current and voltage harmonics are processed with a regression model. In general terms, these methods offer bad results due to the complexity and variability of the grid: it is impossible to know if a certain harmonic is due to the converter connected to the grid or due to a close unknown device. Fundamental frequency masking is a major issue as well.

In [Liserre et al., 2005], an innovative approach based on the study of LCL resonances was presented. The proposal makes use of the fact that the transfer function of the LCL filter presents a medium frequency resonance. The position of this resonance is very dependent on the value of the grid equivalent impedance. If this resonance is excited in a controlled way, valuable information can be extracted from the produced oscillations. This method requires a very precise control: a mistake can take the converter to instability and it is also limited to its use with converters connected to the grid through LCL filters.

2.3 Knowledge review: Grid-converter current control

Current control plays an important role in the whole behavior of a grid-connected VSCs. It forms the basis of a great number of applications, such as FACTS, active filter, grid interface, etc. whose performance largely depends on the quality, accuracy and robustness of this control loop. Due to this importance, a great attention has been paid to this topic since it was introduced late in '70s [Plunkett, 1979] [Schauder and Caddy, 1982] [Brod and Novotny, 1985], giving as a result a great number of proposals published in the technical literature.

The heterogeneous nature of those proposals makes the task of classifying them by a single criterion become a hard objective. Below, several classification methods are exposed according to different criteria. These criteria tend to coincide with recurrent design decisions that often arise when facing a new application or design.

According to the control nature

Perhaps the most general classification of existing methods is the one made in [Kazmierkowski and Malesanti, 1998]. This article divides the proposed methods — up to the publication date — into two big groups: linear and non-linear controllers.

The concept of linear controllers stands for those schemes with a clear *Output-reference comparison, error compensation, voltage modulator* block structure (see Fig. 2.2), where the error compensation is carried out by a strictly linear time-invariant (LTI) transfer function.

The application of linear techniques could be questioned bearing in mind the intrinsic non-linear nature of a VSC converter. However, under certain circumstances, assuming

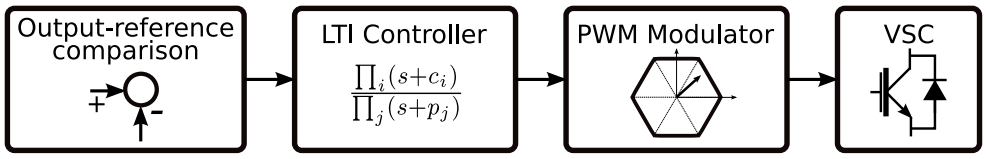

Figure 2.2: *Linear controller block diagram.*

the averaging hypothesis to be valid [Lindgren, 1998] [Svensson, 1997], the current control of grid converters can be considered a linear problem. This approximation brings the possibility of using well established linear techniques in the problem under study.

Due to its popularity, the family of PID controllers (usually implemented without the derivative part, i.e. PI) has received a great attention in this topic. In general terms, they provide a straightforward design process that results in high performance and easy to implement closed-loop systems. Some remarkable references are [Bueno et al., 2004] [Lindgren and Svensson, 1998] [Magueed and Svensson, 2005]. Their main drawbacks are their poor tracking performance when the problem is faced from a stationary reference frame, and, when the problem is translated into the *dq* rotating reference frame and the problem turns into a MIMO one, the design issues due to the the SISO design approach that is often taken.

The basic PI schema was later slightly modified to avoid the tracking issues when dealing with sinusoidal references. In [Yuan et al., 2002] [Liserre et al., 2006b] [Zmood and Holmes, 2003] [Blanco et al., 2005], the integral part of the controller was proposed to be modified by a generalized integrator. These generalized integrators provide infinite gains at an arbitrary frequency achieving perfect tracking performance. The concept has also been successfully extended to other harmonics control. Perhaps their main problems are: (i) the lack of a systematic design procedure, particularly when several similar controllers are associated, and (ii) the resonant poles displacement when the algorithm is programmed in a fixed-point digital signal processor (DSP).

Two popular approaches have to be remarked inside the scope of linear controllers: Dead-beat controllers and Internal Model Control. In fact, they represent a design criterion rather than a technique. Dead-beat controllers [Kuo and Golnaraghi, 2002] bring the possibility of reaching steady state in a small number of sampling periods (one, in the best case) provided the control effort is unlimited and the plant has no input delays and is perfectly known. In practice [Bueno et al., 2004] [Ottersten and Svensson, 2002] the zero-pole cancellations involved in the design are unefective under plant mismatch situations resulting in sensitive controllers. Actuators saturation and plant delays also reduce the expected performance. Anyway, in the strange case in which the plant is perfectly modelled, this technique yields superb performance. Internal Model Control (IMC), originally designed for chemical engineering processes [Morari and Zafiriou, 1989], gives a design procedure that offers a fair system robustness combined with an easy design process. It has been successfully used in VSC current control [Harnefors and Nee, 1998].

Predictive controllers have also been intensively explored for their appliance in the VSC current control [Rodriguez et al., 2007a] [Mattavelli et al., 2005] [Wipasuramonton et al., 2006] [Abu-Rub et al., 2004] [Bae and Ovaska, 2005] [Alepuz et al., 2008]. This family of controllers are remarkable because of the ease of design and concept, however, once again, they present performance issues when the plant is not correctly modelled.

Linear quadratic controllers have been slightly explored in the technical literature. [Pou, 2002] [Alepuz et al., 2005] [Alepuz et al., 2006] proposed Linear Quadratic Regulators to control the current generated by a VSC. These regulators can make use of sensors in order to measure all the state variables or be used together with an optimum estimator such as Kalman Filter [Kalman, 1960] getting a LQG controller [Brabandere, 2006]. In general terms, this family of controllers offers satisfactory results and allows a full MIMO design. However, two issues handicap their extensive use in VSC current control: their inappropriate design methodology based on energy optimization and stochastic properties of signals, and their inconvenient lack of robust behavior [Doyle, 1978].

In parallel, some authors have proposed non-linear controllers for the VSC control objective. These controllers break the controller-modulator structure depicted in Fig. 2.2, and most of them are based on relay feedback structures (see Fig. 2.3).

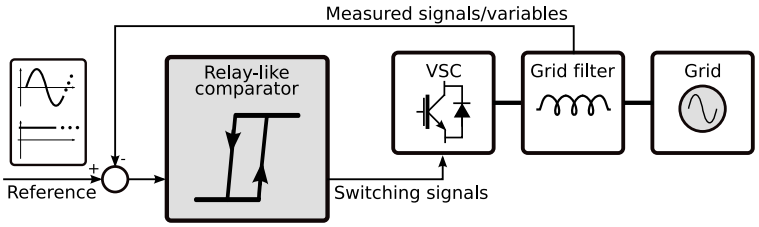

Figure 2.3: *Relay Feedback Structure based control.*

These structures base their operation in the establishment of an operation *band* around certain reference and switching continuous functions in the plant input depending on the operating point making the controlled signal stay inside the desired error band. These methods offer a superior reference tracking performance and a great ease in the design and implementation. Their main drawbacks are the natural variable switching frequency (if not corrected) that can rise to very high values when the grid equivalent impedance is low. This fact is quite usual in medium-high power applications. Other drawbacks for their application in industrial products are their partial incompatibility with digital control and the difficulty in extracting robustness conclusions. Most representative control schemes belonging to this relay feedback structure are hysteresis controllers [Bose, 1990] [Buso et al., 2000] [Bode and Holmes, 2001]. In a higher abstraction level, proposals such as Direct Power Control (DPC) [Malinowski et al., 2001] [Noguchi et al., 1998] join the inner current control loop and outer power control loop in a single stage. These proposals inherit the structure from Direct Torque Control from machine theory and apply it to the control of active and reactive power. Pros and cons are quite similar to the hysteresis case.

A second non-linear approach that plays a very important role is the sliding-based control. This kind of controllers give stability margins to plant parameters uncertainty, and, thus, are very interesting for their application in VSC control. Their application to LCL structures in their more general conception is still considered an open issue. Some remarkable references on this topic are [Jung and Tzou, 1996] [Utkin, 1993] [Miret et al., 2004].

According to the control reference frame and control structure

Naturally, most of the measurable and generated signals in three-phase grid converters are sinusoids whose amplitude and frequency tend to be constant in time. Historically, automatic control theory has specialized in dealing with constant signals, which eventually may have some step or ramp variation. This historical fact results in a great number of available control tools when the problem is expressed as a constant reference one. The Park transform [Krause et al., 1995] translates a three-phase sinusoidal problem into a two-phase constant-reference one when the reference frame is changed from a static one to a synchronous one.

As a result, three basic control approaches have been explored in the published literature:

- When the problem is faced from a three independent phases (i.e. in *abc* axes) point of view, without the appliance of the Park transform, the problem reduces to the control of several SISO independent linear plants with sinusoidal references and output signals. Some relevant related publications are: [Zmood et al., 2001] [Zmood and Holmes, 2003]. This approach is also suitable for single-phase grid converter [Teodorescu et al., 2004]. This approach is frequently used to reduce the Park transform computational charge or to avoid the computation of trigonometric functions and allows its use over different harmonics substantially increasing the current waveforms quality. From a structural point of view, the easiest approach — and also the most common — is the application of independent SISO controllers over each of the independent SISO systems.

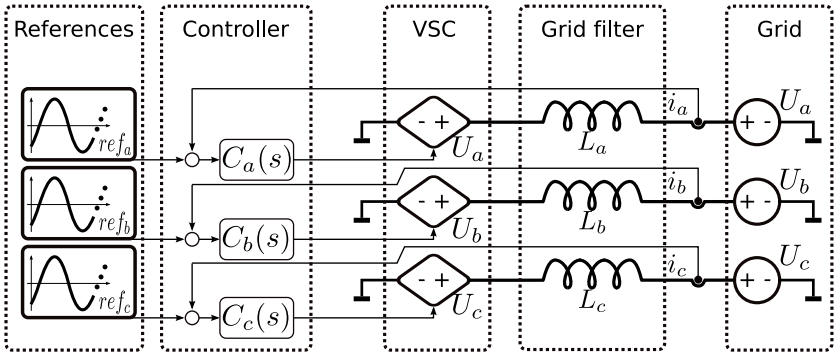

Figure 2.4: *Three-phase stationary reference frame control.*

- If the Clarke transform [Krause et al., 1995] is applied, *abc* axes can be converted to the sinusoidal $\alpha\beta$ axes. The obtained plant is an association of two independent SISO plants with sinusoidal references and signals but now, signals have an useful electric interpretation. This scheme increases the control design complexity but has demonstrated to be very useful when dealing with highly unbalanced situations. Again, this reference frame yields independent SISO channels that are easily faced with independent SISO controllers [Yuan et al., 2002]. The approach has also been successfully applied to the control of high order harmonics in active filters [Allmeling, 2004] producing computationally lighter controllers because of the removal of several Park transformations.

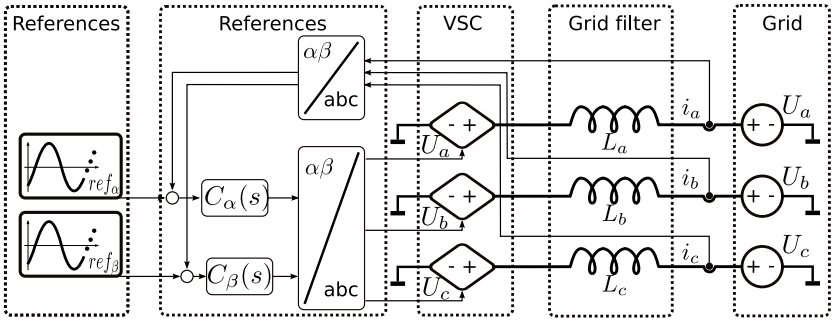

Figure 2.5: *$\alpha\beta$ synchronous reference frame control.*

- When the Park transformation is applied, the problem is approached from a synchronous reference frame (i.e. in *dq* axes). All fundamental frequency sinusoids are converted to constant magnitudes. This approach can be considered the most popular one as it gives a good reactive and active power interpretation and allows to apply classical control techniques to the problem. However, the resulting is a multi-input multi-output plant, which may need the use of modern MIMO techniques in order to analyze or control some of its variables. The number of technical proposals matching this group is huge, some interesting references could be [Bueno, 2005] [Kazmierkowsky et al., 2002].

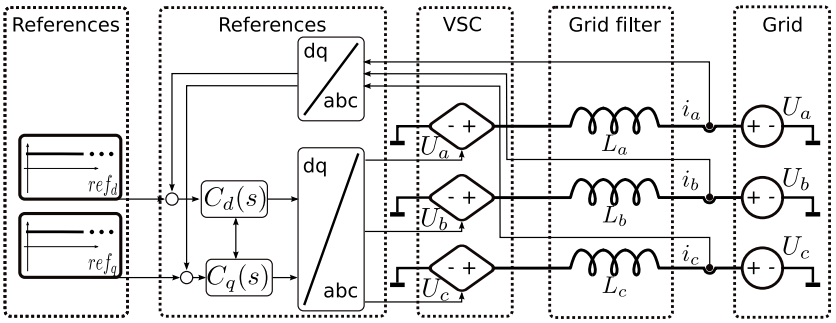

Figure 2.6: *dq synchronous reference frame control.*

From a structural point of view, this latter case is clearly a two inputs two outputs MIMO plant that, additionally, presents a high inter-channel coupling. Most of the published proposals have tried to face the problem considering independent (SISO) channels and trying to externally compensate the inter-channel coupling (see Fig. 2.6). Although this approach has yielded positive results and keeps the complexity in low bounds, it presents some lack of rigor due to the assumed approximations that make it difficult to design with some advanced criteria as robustness or perfect decoupling. Paradoxically, the use of MIMO techniques in the VSC current control problem is limited to some extent and there are not many previous works; some interesting references on this topic are [Botteron et al., 2003] [Alepuz et al., 2005] [Wu and Lehn, 2006].

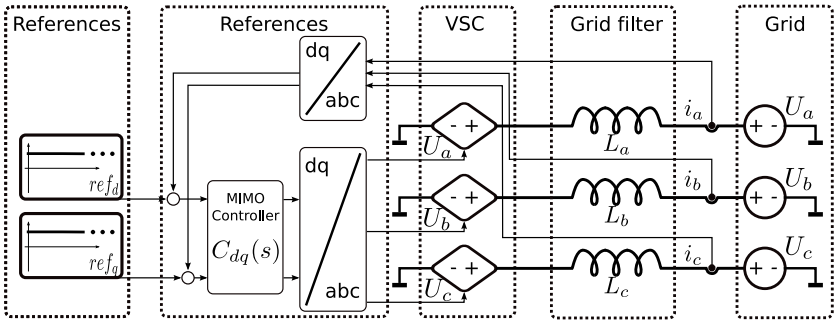

Figure 2.7: *dq synchronous reference frame multi-input multi-output control.*

Control structure is more complex when the interface filter is more complex than one inductor. In the case of using an LCL filter, a common approach for the control of the grid-side current is the sequential control of each of the state variables that are present in the filter transfer function. This process is depicted in Fig. 2.8. In this scheme, the reference is set over the grid-side current, then a simple controller for the grid-side current is applied assuming that the capacitor voltage is the actuation variable. This variable is not directly actuated as it depends on the converter-side current, a second simple control loop is settled where the actuation variable is assumed to be the converter-side current. Again, this variable depends on the converter output voltage, which is the actual actuation variable, and can be controlled by means of a third control-loop. This approach has been successfully applied and is reported in the related literature [Twining and Holmes, 2003][Bueno et al., 2004]. This design process is an extension of an L filter current control design. This fact has produced a good acceptance in the industry and research groups. However it presents several issues: channel coupling gets more intricate as it has to be compensated in three different stages. Furthermore, the design process is quite approximate and is difficult to settle robustness criteria.

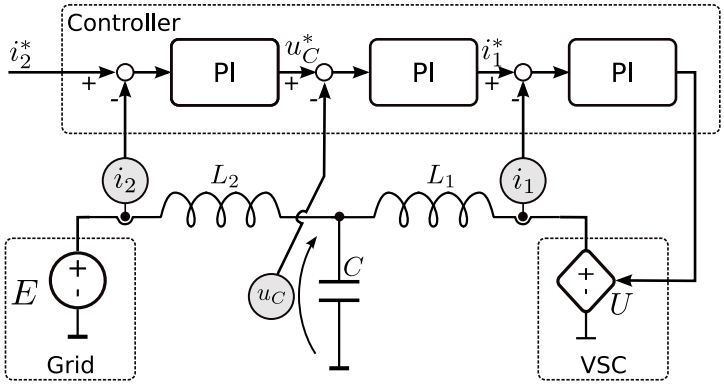

Figure 2.8: *LCL connected grid converter sequential current control structure.*

It is necessary to remark that all described approaches have been intensively used and investigated during past recent years by different research groups and companies. The result is that each method can be used together with known improvements in order to get some a-priori missing features or performance. Actually all approaches are being currently

used and the choice of one or another is more a matter of ease of design or personal preferences than an actual compromising decision.

According to the controlled variable

When the converter under control is connected to the grid through an LCL filter, another classification criterion can be settled regarding the variable under control. In fact, most control algorithms present, in one way or another, an internal state regulator that simultaneously keeps all the internal states in a controlled point. The term control variable is better understood as the desired variable to robustly follow an arbitrary external reference. Fig. 2.9 shows a simplified diagram of one phase, named j, of the LCL interface filter. Each phase has three main state variables: the converter-side current, named $i_{1j}(t)$, the capacitor voltages, $u_{Cj}(t)$, and the grid-side current, $i_{2j}(t)$:

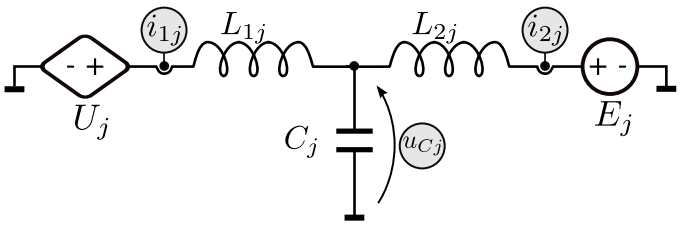

Figure 2.9: *Possible feedback variables in LCL current control.*

- The control of the converter-side current ($i_1(t)$) is probably the most common approach. Two main reasons justify this fact: quite often the converter and the grid filter (or at least the grid-side inductor) are not placed physically together. For this reason it is easier to place sensors for the converter-side currents, that also are VSC output currents. Additionally, the control of $i_1(t)$ can be considered to be easier because, under certain circumstances, the transfer function relating converter AC output voltage ($u_c(t)$) and $i_1(t)$ is quite similar to the transfer function in the L filter case. For this reason some popular current control techniques for the L filter case can be applied to this higher order filter. In the extreme case, some relay feedback based controllers as, for example, hysteresis or DPC, for the moment, can only be applied to the converter-side current. The philosophy here is to control the system described by the transfer function $\frac{I_1}{U_C}(s)$ and expect the grid-side current to be a filtered version of the converter-side one.

  This approach presents two limitations. First, the $\frac{I_2}{I_1}(s)$ transfer function presents a poorly undamped resonance that creates undesirable oscillations in the grid current. This problem is typically overcome by a family of algorithms named *Active damping*. The second limitation is the lack of actual closed-loop control of the grid current. This fact makes the system sensitive to grid impedance uncertainty and variation, making it necessary to add an extra control loop to correct the current reference phase, and consequently the active/reactive injected power balance.

- The direct control of the grid-side current has also been explored. It gives actual grid-current closed-loop control at the cost of an increase in the control complexity. Some remarkable references are [Bueno et al., 2004] [Magueed and Svensson, 2005].

- The control of the capacitor voltage can be usually found in micro-grids or Uninterrupted Power Supply (UPS) applications where a converter is responsible to keep the grid PCC voltage in a safe range. Usually this is accomplished by reducing the interface filter to a simpler LC structure (using the grid equivalent inductance as the grid-side inductance of the filter) and controlling the capacitor voltage [Loh and Holmes, 2005]. This kind of control structures are usually applied to droop distributed control.

According to the control objective

A possible last classification of grid converters current controllers can be made regarding the control objective. This stands for the main motivation of the design procedure. Among all the related published literature, four main motivations in the design process can be observed:

- *Design for closed-loop performance.* The objective of this design approach is to get a plant able to achieve a response to reference or disturbance events as fastest as possible. Perhaps the most representative strategy belonging to this tendency is the *dead-beat* controller [Ottersten and Svensson, 2002] [Bueno, 2005]: the objective is to gain the steady state in one sample period, if possible. Other remarkable techniques that offer outstanding performance are the family of so-called *resonant* controllers and the hysteresis controllers. Proof of their quick and accurate responses is their use in active filter applications.

- *Design for simplicity.* A recurrent motivation in the design of current controllers is the search for simplicity. This simplicity can be understood from a triple point of view: simplicity in the theoretical background of the algorithm, simplicity in the design process and simplicity in the execution. Simple algorithms are welcome in the industry because they are easy to understand and design and, in the case of simplicity in computation, they usually allow a reduction in the control platform costs. The main representatives of this philosophy are the feedback relay controllers in the different existing implementations (like current hysteresis [Bose, 1990] [Buso et al., 2000] [Bode and Holmes, 2001] or direct power control [Serpa et al., 2005] [Noguchi et al., 1998]) and the predictive controllers family [Rodriguez et al., 2007a] [Mattavelli et al., 2005] [Wipasuramonton et al., 2006] [Abu-Rub et al., 2004] [Bae and Ovaska, 2005].

- *Design for energy optimization.* The research for energy optimization in a feedback system is covered by the optimal LQ theory. These techniques, originally designed for aerospace applications have also been applied to the problem of controlling the output current of a VSC [Alepuz et al., 2006] [Pou, 2002] [Brabandere, 2006]. They represent design processes with good success guarantees, flexible and suitable for complex LCL structures. In general terms, they offer an adequate compromise between robustness, performance, computational payload and design complexity, although the energy optimization is not very adequate for the VSC current control problem.

- *Design for robustness.* The objective of this design approach is the design of a controller that, while maintaining a certain minimum performance regarding the con-

verter reference tracking and disturbance rejection, is able to overcome an arbitrary amount of uncertainty in model parameters.

Uncertainty is always present in power applications. Particularly in the case of the grid converter current control, plant model quality is degraded by filter components tolerance and drift, grid uncertainty, unmodelled fast dynamics in switching devices, etc. This uncertainty, if not considered, has a direct influence on reliability.

Unfortunately, very few proposals have approached such a design principle in VSC current control. The sliding-mode controllers family [Dias et al., 2008] [Jung and Tzou, 1996] [Miret et al., 2004], some $\mathcal{H}_\infty$ proposals [Rahim and Kandlawala, 2004] have been published, most of them dedicated to L-filter structures and others based on other interesting tools as, for example, Linear Matrix Inequalities (LMI) [Gabe et al., 2007].

2.4 Knowledge review: Grid influence analysis

Very few studies have dealt with the dynamic effect of a non-ideal grid over the performance or stability of the internal current control loop of grid converters. Perhaps, the most remarkable work in this topic is [Liserre et al., 2006c]. This work presented a study of the poles and zeros displacement when modifying the grid equivalent resistance and inductance. The proposal introduces very interesting issues by comparing the grid dynamic characteristics in *weak* and *strong* or *stiff* grid scenarios.

The article presented good conclusions that may result useful for converter design. However, this article scope is limited to the effect of the grid over converters controlled with a proportional+resonant scheme and does not generalize to extract conclusions for other structures.

Another remarkable paper from the same group makes an indirect analysis of the grid influence over VSC controllers in a work dedicated to propose an islanding detection algorithm [Liserre et al., 2006a], which analyzes the effect of the uncertainty in grid impedance over the estimation of grid voltage disturbance.

2.5 Statement

As a statement, it could be said that the measurement of the parameters of the grid, the analysis of the influence of an uncertain grid over the current control loop of a grid converter or the design considering this uncertainty, remain open topics.

A more detailed knowledge of the grid connection, its uncertainty effect over current controllers and the design constraints that arise when it is not perfectly known may improve grid-converters reliability, decrease their costs, improve their behavior and, more important, contribute to increase the power system stability.

The study of the interaction between grid dynamics and grid converter current control is the main motivation of this thesis, whose objectives are described below.

2.6 Thesis objectives

This thesis studies the connection of grid converters to uncertain grids. The following objectives are proposed and detailed in following subsections:

- Propose a method to implement an on-line grid dynamic parameters estimation procedure.
- Study the influence of those grid dynamic parameters over the behavior of the converter current loop.
- In the case that some influence is found, study the design of a control algorithm that minimizes the sensitivity to grid parameters uncertainty.

2.6.1 Grid equivalent impedance identification

Past experiences in grid impedance identification have made clear that it is extremely complicated to achieve good accuracy and precision with purely passive identification methods. Several facts back up this statement:

- Grid connected applications are supplying or consuming power at the fundamental grid frequency the major part of the time. The optimization process according to the information obtained in only one frequency is clearly undetermined.
- The grid is a dynamical structure and it is difficult to segment behaviors caused by grid dynamic parameters or by exogenous perturbations introduced by other grid converters or loads.

On the other hand, active methods get better results but, usually, at the cost of deteriorating the quality of the injected energy and, even more important, creating potential interference when several devices connected at close locations apply the same algorithm.

This thesis aims to propose a method that combines positive features of both trends: to minimize the influence over the grid nearly as much as passive methods and to achieve a precision and accuracy comparable to those obtained with active ones.

To this end, this thesis proposes to support the identification method on a monitoring task able to detect how good the estimation is: if the estimation quality is acceptable, the converter continues operating regularly without introducing disturbances in the grid. This is the default mode. Whenever the estimation quality falls beyond some arbitrary threshold, the converter would introduce singular disturbances until quality returns inside the threshold.

The method should be able to have a very good behavior in the presence of additive and switching noise by applying regressive methods that cancel sample noise by using history records.

2.6.2 Grid converter current control stability analysis

The second objective of this thesis is the analysis of the effect of a non-ideal or uncertain grid over the performance and stability of the inner current control loop of grid converters.

This objective implies very different approaches depending on the nature of the control scheme under study. While powerful tools are available to study it when linear controllers are being applied, complete tools are rarely accessible when dealing with non-linear schemes. This reason forces to apply different analysis for each case.

For the linear case, the objective is to face the problem following a formal procedure. First step of the analysis will cover the influence of the assumed grid model over the model perceived from the current control level of a grid converter connected through an LCL filter, making use of the uncertainty concept.

A key step in the fulfillment of this objective is the development of a *structured parametric uncertainty* model of the perturbation induced by grid parameters. This model, that is explained in chapter 4, extracts the uncertainty from the plant model, splitting a set of possible plants into a norm-bounded perturbation block and an LTI system. A scheme of such a process is depicted on Fig. 2.10, that displays the process of extracting internal uncertainty into an independent transfer function block. This process will play an important role during the chapter 4 development.

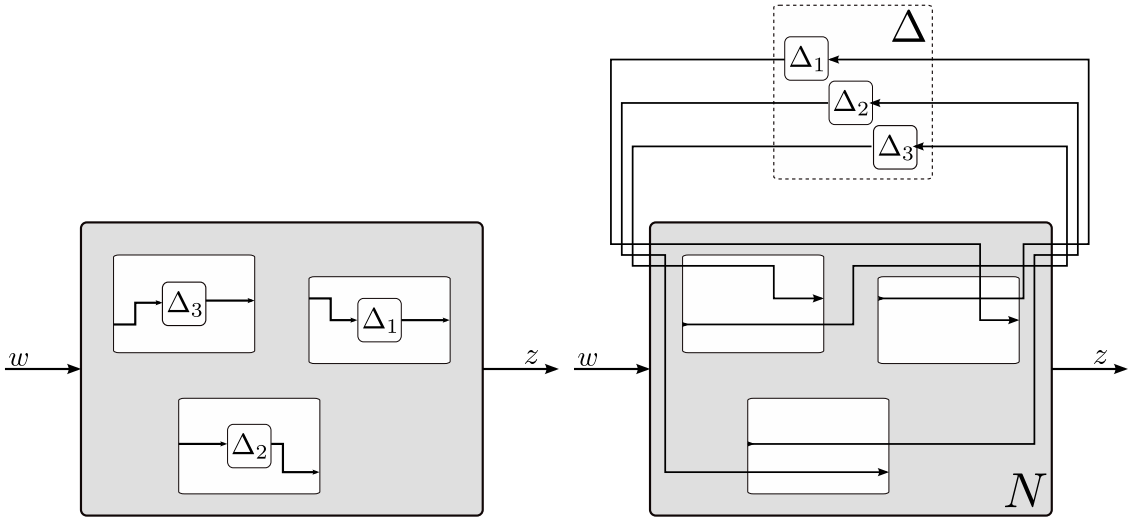

(a) Regular model with internal uncertainty. (b) Structured parametric uncertainty model.

Figure 2.10: *Rearrangement of an uncertain model to build the Structured parametric uncertain model (N Δ - structure).[Skogestad and Postlethwaite, 2005].*

The extraction of all the uncertainties out of the plant model allows the application of advanced systematic analysis tools to assess the maximum allowable model perturbation that keeps the system stable. In other words, the maximum allowable variation in the grid dynamics for a certain controller. Concretely, this analysis will be carried out using the *structured singular value* μ, that will be introduced later in this dissertation.

The study will be applied to some already presented techniques, which will increase the clarity of the discussion.

The non-linear case lacks a systematic analysis tool and stability conclusions are much harder to get. The objective here is to present a study of grid effects over, perhaps, the most used non-linear scheme: the hysteresis regulator.

2.6.3 LCL grid current control

Assuming a negative impact of grid parameters uncertainty over the current control loop of grid converters, the next natural objective is to research for a controller design process able to deal with this kind of problems. This core problem forms the basis of the last and main objective of this thesis.

More concretely, the objective is to propose a control design method that, given an initial expected grid equivalent parameters variation range, gives a controller that ensures stability for all possible conditions. It is clearly a robustness driven design method: robustness of the closed loop is the primary objective. Obviously, simplicity and performance are optimized as much as possible but these goals remain secondary.

Besides the main objective, the following constraints are also imposed:

- The proposed technique will assume the averaging hypothesis to be valid. This is to assume that PWM harmonics are placed well above the process dynamics, and, thus, the plant can be assumed to be fully linear. This assumption opens the door to the application of firmly established linear robust control techniques.
- The proposed technique will face the problem from the *dq* synchronous reference frame. This approach facilitates the design process to some extent by dealing with constant reference signals. In the same direction, the control problem will be assumed to be MIMO. This way SISO approximations that could produce invalid robustness conclusions are avoided.
- The proposed technique must be suitable for DSP programming. This constraint implies the following two:
  - Be applicable for discrete-time systems.
  - Be able to cope with input computational delays.
- The proposed technique must be compatible with the application of an anti-windup technique to properly deal with actuators saturations.

2.7 Conclusions

As a conclusion, the primary objective of this thesis is the improvement of the behavior of VSC connected to uncertain grids through LCL filter following three main directions: identification of uncertain grid parameters, analysis of the robustness of already proposed controllers when connected to uncertain grids and proposal of a more direct method to control such devices.

Chapter 3

Grid impedance monitoring

This chapter proposes a grid impedance monitoring system for distributed power generation electronic interfaces. The described system estimates the grid equivalent impedance and voltage source from the voltage measurements performed in the point of common coupling. The estimation algorithm is based on a recursive least-squares algorithm implemented in the complex field. Simultaneously, the system evaluates the quality of the estimation, minimizing its influence over the grid and detecting islanding situations. The proposed system performance has been evaluated under simulation and experimental testing.

3.1 Introduction

The range of the grid connection electric parameters that may face up a DPGS grid converter is wide and uncertain. For example, a grid converter operating in a *micro-* or *nano*-grid should be able to operate connected to the mains, or supplying several local loads in island mode, perhaps in co-operation with other DPGS sources. The grid model that perceives a grid converter in the former situation substantially differs from the one it would perceive in the latter. A critical grid parameter in these cases is the grid equivalent impedance that a grid converter sees from the point of connection, usually named Point of Common Coupling (PCC). Experience demonstrates that it often results difficult to have an accurate a-priori knowledge of its value. These difficulties are more severe in DPGS environments where additionally this value can get high impedance values as well as important variations along time.

The grid equivalent impedance has a demonstrated influence over the behavior of converters connected to the grid. As concluded in [Liserre et al., 2004b][Liserre et al., 2006c] and chapter 4 of this thesis, it influences the inner current control loop of grid converters in both the linear and non-linear case. It also influences the behavior of voltage control loops in both active power conditioners and grid converters [Tarkiainen et al., 2004]. In both cases an incorrect pre-estimation of the grid equivalent impedance (particularly in the inductive part of this impedance) would degrade the converter performance or even make it unstable under certain circumstances. A grid monitoring system, able to accurately estimate this model parameters, as the one in Fig. 3.1, would give a valuable information for adaptive control schemes.

In addition to this influence, grid impedance value could give an useful information in order to comply with the each time more stringent standard requirements regarding DPGS

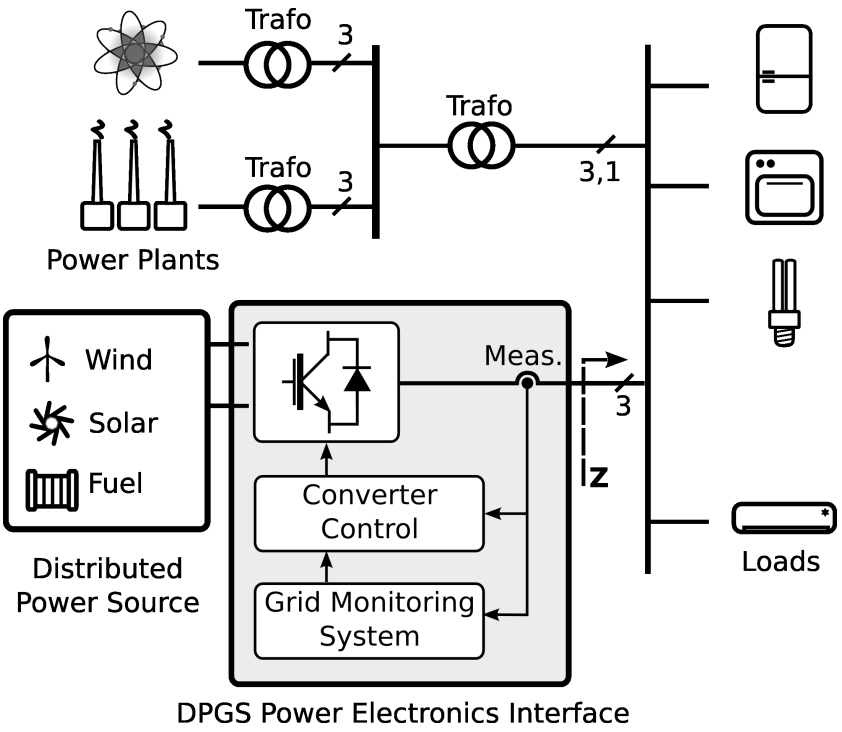

Figure 3.1: *Grid monitoring system situation diagram.*

connection to the grid. Particularly important are the anti-islanding regulations as, for example, the German standard VDE0126 for grid connected photo-voltaic (PV) systems. The standard requirement is to isolate the supply within 5s after an impedance change of 1 ohm. A possible way to comply with this standards is to add an equivalent impedance measuring function or *ancillary service* to grid converters that would indicate whether the converter should remain connected to the mains or not [Ciobotaru et al., 2007] [Timbus et al., 2004] [Timbus et al., 2007]. This situation is shown in Fig. 3.1.

As described in chapter 2, proposed methods can be widely classified into two general groups attending to the influence they have in the system under identification: *active* and *passive* methods.

Passive methods present the characteristic of making an estimation without introducing disturbances (non-intrusive). They are based on the study of the relationship between the voltage and the current measured in the PCC. These magnitudes contain dynamic information induced by non-linearities and harmonic information of devices that are connected to the grid during the estimation process. Some remarkable non-intrusive methods are [Girgis et al., 1993] or [Pedersen et al., 2003]. Although these methods are the most convenient due to their null influence over the quality of the delivered energy, some of them present drawbacks in their empirical application due to the lack of information in the grid converters used for certain applications. For the case of power converter connected to the grid through LCL filters, a remarkable method was presented in [Liserre et al., 2005]. This method is based on the use of the oscillation created by a resonance that exists in the transfer function of the LCL filter. This resonance position is very dependent of the grid equivalent inductance and, thus, its study can give valuable information for grid estimation

purposes.

Active methods are intrusive. They require the systematic perturbation of the grid in order to extract the information needed to estimate the grid equivalent impedance. Some remarkable strategies are the injection of single-tones of the frequency object of the estimation [Asiminoaei et al., 2004] [Rhode et al., 1997], the study of the relationship between the voltage and current in the point of common coupling (PCC) during the injection of wide spectrum voltage or current disturbances [Sumner et al., 2002] [Sumner et al., 2004] [Staroszczyk, 2005], the switching of certain known linear or non-linear loads from the PCC [de Oliveira et al., 1991] [Girgis and McManis, 1989], or the variation in the active or reactive power injected to the grid [Ciobotaru et al., 2007] [Timbus et al., 2007] [Fusco et al., 2000] [Tarkiainen et al., 2004].

This chapter presents a new estimation algorithm that makes use of regular converter operation information to estimate the grid equivalent impedance and, when the estimation quality falls beyond some quality threshold, the algorithm is able to improve it introducing eventual disturbances. This way, the algorithm achieves a precision comparable to the active methods, minimizing its influence over the grid nearly as much as the passive methods. The algorithm is decomposed into two fundamental tasks. The first task function is to obtain an estimate of the grid equivalent impedance. This impedance is estimated by means of a Recursive Least Squares algorithm (RLS in the following) applied to the PCC measured currents and voltages expressed in a *dq* synchronous reference frame. This way, the algorithm maintains the recursive nature of the proposal in [Fusco et al., 2000] decreasing the mathematical complexity by translating the problem into a complex one by means of expressing it in a synchronous reference frame. Special attention is dedicated to the description of the synchronization and prefiltering stage because its behavior is critical in the algorithm performance. The second function is to give a measurement of the quality of the estimation process. This second function would make the algorithm suitable for anti-islanding detection and is, in fact, a core part of the estimation algorithm as it decides whether is necessary to perturb the grid or not, giving to the system its actual *quasi-passive* nature.

Next section of this chapter will describe the assumed grid model. Section 3.3 will describe the proposed method from its theoretical base to its recursive final implementation describing important system blocks as grid synchronization and measurement of the quality of the estimation. Finally, Section 3.4 presents some simulation and experiments which verify the theoretical development and the validity of the system. The last section of the chapter is dedicated to make a statement of the extracted conclusions and contributions.

3.2 Grid modeling

The grid model dictates the relationship between the current and voltage measured in the PCC.

Simplest control approaches applied to power electronics systems consider the grid as a perfect sinusoidal voltage source. Qualitatively, this assumption implies an independence between the current that the power converter is delivering — consuming — from the grid and the voltage that could be measured at this point. This model is usally called in the related literature *stiff grid*. In the opposite pole, a grid may be considered *weak* when the influence of the PCC current over its voltage is not neglectable anymore.

In fact, the *weakness* of a grid is relative to the size (in power) of a certain converter respect to the grid where it is connected to. In practical applications, influence of the current over the voltage in the PCC ranges from being neglectable (*stiff* case) to the extreme case of affecting the power system frequency and voltage stability as is the case when considering one generator of the small grid of an aircraft or all the installed wind power in a country grid.

This thesis focuses on an intermediate level where the PCC voltage is assumed to present an affine behavior (linear + a voltage source) with regard to the injected current, assuming the grid frequency to be an independent variable.

Different models have been used under the same assumptions in the technical literature as [Girgis and McManis, 1989] [Enslin and Heskes, 2004].

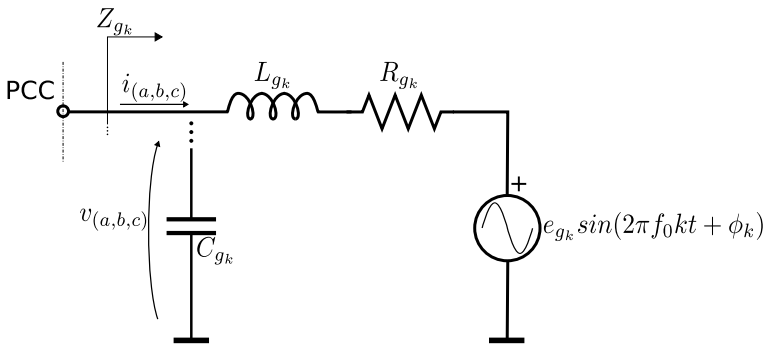

Figure 3.2: *Phase grid model.*

In general terms, three main effects are present in the grid dynamic behavior as shown on Fig. 3.2[1]. Inductive and resistive effect are the most important [Enslin and Heskes, 2004], and are mainly created by electric lines intrinsic parameters, and transformer and generator output impedances. This way, long lines situated in rural areas are associated with a high inductive and resistive behavior. Paralelly, some authors include, as well, a shunt capacitance. This capacitance gains importance in residential environments [Enslin and Heskes, 2004]. This model is represented in Fig. 3.2.

From a practical point of view, this capacitor creates a resonance that is usually placed above the firsts kHz in the bode plot and, thus, does not have such a big influence on control loop stability as it usually falls outside the converter close-loop bandwidth. Actually, stability is mainly compromised by an underestimation in the inductive behavior of the grid as shown in [Liserre et al., 2006c][Cobreces et al., 2007] and chapter 4 of this dissertation. On the other hand, the resonance also affects in a limited way the harmonic impedance in typical power conditioning applications whose scope, usually, is the control of the converter in harmonics below 1 kHz.

For this reason, several studies, including this dissertation, prefer to neglect the effect of higher frequencies capacitors reducing the effect to a resistive-inductive one.

[1]For simplicity reasons, the standard notation for the PCC measured voltage, u_{PCC}, that appears in the Glossary, is substituted by v in this chapter

3.3 System Description

3.3.1 System overview

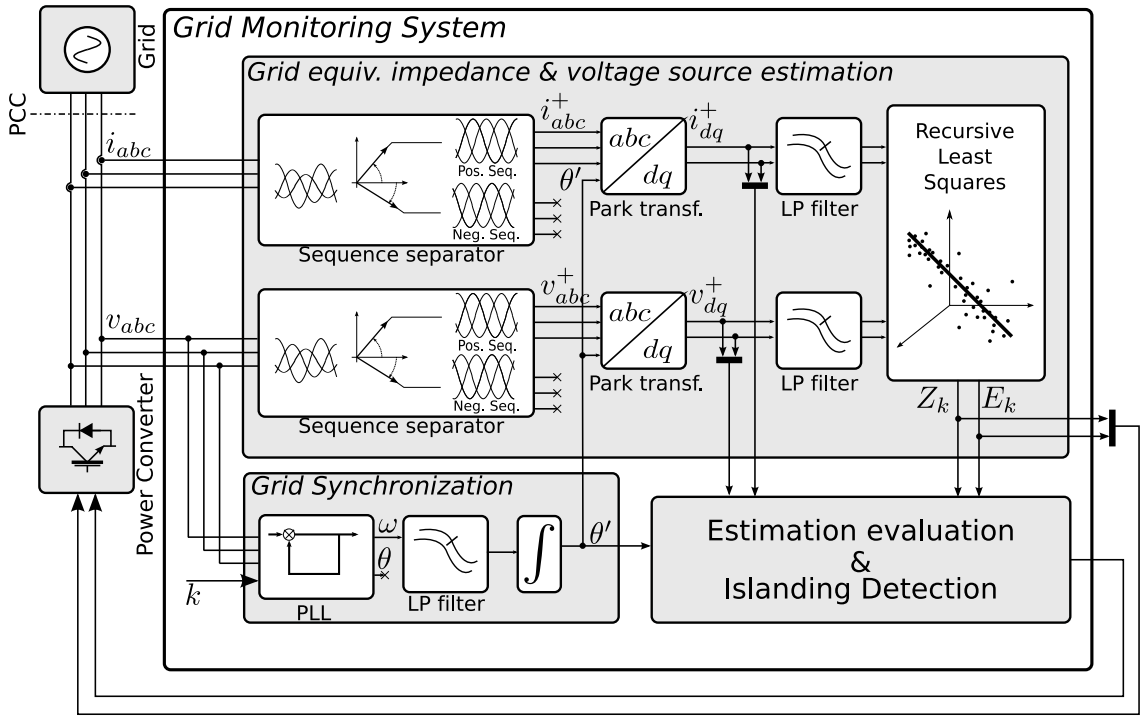

Figure 3.3: *Block diagram of the presented grid monitoring system.*

The grid monitoring system is decomposed in three main functions, as displayed in the block diagram of Fig. 3.3. The core function, named *Grid equivalent impedance and voltage source estimation* takes as inputs the voltage and current measurements performed in the PCC and a synchronization angle coming from the *Grid synchronization* block. Its operation begins with a preprocessing stage which firstly eliminates the negative sequence from the three-phase measurements [Fortescue, 1918]. So, if the original grid was unbalanced, the resulting three-phase equivalent system will be balanced and will comply with the grid model described in Fig. 3.2. The resulting three-phase signals are, then, transformed into a *dq* rotating synchronous reference frame synchronized with the frequency of the grid. This frequency is estimated by the *Grid synchronization* block. Voltage and current measurements in this transformed reference frame are the inputs of the actual estimation process, whose outputs are the estimated impedance and voltage source.

Simultaneously, the block named *Estimation evaluation and Islanding Detection* evaluates the estimates. The estimation is evaluated by means of an integrated windowed re-projection error. As it will be shown later, this integrated error gives a value of the quality of the estimation. This value is compared with a chosen threshold that represents the minimum allowable precision. In the case this error is too high, meaning that probably the estimation is not good, this block would send a signal to the converter global control to indicate the necessity of introducing some extra disturbances in the grid to improve the estimation. One of the possible reasons of an increase in the estimation error is an islanding

situation. This block is described in detail in subsection 3.3.4.

3.3.2 Estimation algorithm

Let us consider a three-phase grid converter connected to a resistive-inductive grid as the one described in section 3.2. The converter is assumed to be delivering — consuming — P and Q active and reactive power to — from — the grid. In this situation, let us assume known the three instantaneous phase voltages (v_a, v_b and v_c). And the three instantaneous phase currents (i_a, i_b, i_c).

When the converter is working in permanent regimen, the following expression verifies:

$$\boldsymbol{v} = \boldsymbol{i} \cdot \boldsymbol{Z} + \boldsymbol{e}, \tag{3.1}$$

where $\boldsymbol{v}, \boldsymbol{i}, \boldsymbol{e} \in \mathbb{C}$ represents the expression in the dq rotating reference frame of the vectors (v_a, v_b, v_c) (voltages measured in the PCC), (i_a, i_b, i_c) (currents measured in the PCC) and (e_a, e_b, e_c) (equivalent voltage source value) respectively. $\boldsymbol{Z} \in \mathbb{C}$ represents the complex expression of the line impedance:

$$\boldsymbol{Z} = R_g + j\omega L_g = R_g + jX_g. \tag{3.2}$$

By taking n different *measurement points* (i.e. algorithm inputs) in m different *operation points* (i.e. combinations of active, P, and reactive, Q, power) the following set of linear n equations can be built:

$$\begin{cases} \boldsymbol{v}_0 = \boldsymbol{i}_0 \cdot \boldsymbol{Z} + \boldsymbol{e}_0 \\ \boldsymbol{v}_1 = \boldsymbol{i}_1 \cdot \boldsymbol{Z} + \boldsymbol{e}_1 \\ \vdots \\ \boldsymbol{v}_{n-1} = \boldsymbol{i}_{n-1} \cdot \boldsymbol{Z} + \boldsymbol{e}_{n-1} \end{cases} \tag{3.3}$$

Assuming a stationary grid during the measurement process, it can be said that $\boldsymbol{Z}_0 = \boldsymbol{Z}_1 = \cdots = \boldsymbol{Z}_{n-1} = \boldsymbol{Z}$ and $\boldsymbol{e}_0 = \boldsymbol{e}_1 = \cdots = \boldsymbol{e}_{n-1} = \boldsymbol{e}$. This assumption is quite accurate as changes in the grid parameters are usually sparse steps changes. Eq. (3.3) can be easily re-written in matricial form,

$$\mathbf{Y} = \mathbf{A} \cdot \mathbf{X}, \tag{3.4}$$

where $\mathbf{Y} \in \mathbb{C}^{Nx1}$, $\mathbf{A} \in \mathbb{C}^{Nx2}$, $\mathbf{X} \in \mathbb{C}^{2x1}$. $\mathbf{X}$ is named parameters vector. They have the following structure:

$$\mathbf{Y} = \begin{pmatrix} \boldsymbol{v}_0 \\ \boldsymbol{v}_1 \\ \vdots \\ \boldsymbol{v}_{n-1} \end{pmatrix}, \ \mathbf{A} = \begin{pmatrix} \boldsymbol{i}_0 & 1 \\ \boldsymbol{i}_1 & 1 \\ \vdots & \vdots \\ \boldsymbol{i}_{n-1} & 1 \end{pmatrix}, \ \mathbf{X} = \begin{pmatrix} \boldsymbol{Z} \\ \boldsymbol{e}_0 \end{pmatrix}$$

At this point, the problem is reduced to a linear regression problem expressed in the complex field. This situation is depicted in a simplified way in Fig. 3.4. As shown, the algorithm keeps sampling measurement points around an *operation point*. The points are grouped in a cloud because of the deviation due to additive noise or due to small variation in the P and Q combination. In the moment the converter moves to a different *operation*

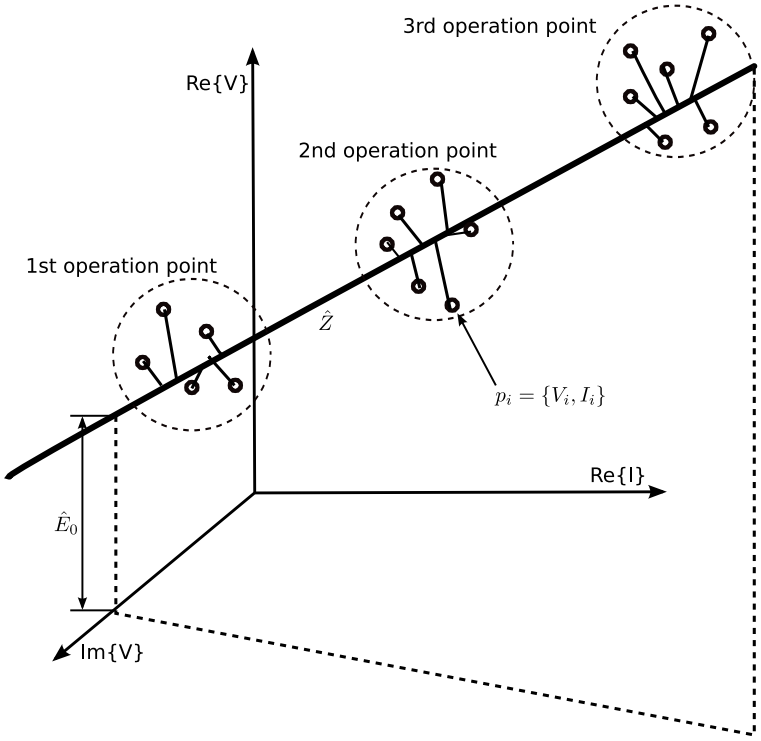

Figure 3.4: *Example of regression algorithm.*

point and starts sampling *measurement points*, there is enough data to estimate a line, and consequently the grid equivalent impedance and voltage source.

Let us assume an estimated parameters vector $\hat{\mathbf{X}} = (\hat{\boldsymbol{Z}} \quad \hat{\boldsymbol{e}_0})^T \in \mathbb{C}^{2x1}$. The following matricial expression can be written:

$$\mathbf{Y} = \mathbf{A} \cdot \hat{\mathbf{X}} - \mathbf{Q}, \tag{3.5}$$

where $\mathbf{Q} \in \mathbb{C}^{Nx1}$ is the error vector representing the error between the estimated voltage value calculated by the product between $\mathbf{A}$ and $\hat{\mathbf{X}}$ an the actual measured output $\boldsymbol{v}_i$.

The problem of finding a best-fit for the estimated parameters vector $\hat{\mathbf{X}}$ can be solved by minimizing the error — cost — function $J \in \mathbb{R}$.

$$J = |\mathbf{Q}|^2 = \mathbf{Q}^{T\star} = (\mathbf{A}\hat{\mathbf{X}} - \mathbf{Y})^{T\star}(\mathbf{A}\hat{\mathbf{X}} - \mathbf{Y}). \tag{3.6}$$

$$\frac{\partial J}{\partial \hat{\mathbf{X}}} = 0 \tag{3.7}$$

should give a vector $\hat{\mathbf{X}} \in \mathbb{C}^{2x1}$ that minimizes the quadratic error function J. Developing the expression:

$$\begin{gathered} \frac{\partial J}{\partial \hat{\mathbf{X}}} = \frac{\partial (\mathbf{A}\hat{\mathbf{X}} - \mathbf{Y})^{T\star}(\mathbf{A}\hat{\mathbf{X}} - \mathbf{Y})}{\partial \hat{\mathbf{X}}} = \\ \frac{\hat{\mathbf{X}}^{T\star}\mathbf{A}^{T\star}\mathbf{A}\hat{\mathbf{X}} - \hat{\mathbf{X}}^{T\star}\mathbf{A}^{T\star}\mathbf{Y} - \mathbf{Y}^{T\star}\mathbf{A}\hat{\mathbf{X}} + \mathbf{Y}^{T\star}\mathbf{Y}}{\partial \hat{\mathbf{X}}} = 0. \end{gathered} \tag{3.8}$$

Applying the properties of complex Jacobian, it produces the following equation:

$$\mathbf{A}^T\mathbf{A}^\star\hat{\mathbf{X}}^\star - \mathbf{A}^T\mathbf{Y}^\star = 0, \tag{3.9}$$

that verifies for the following optimal parameters vector:

$$\hat{\mathbf{X}} = (\mathbf{A}^{T\star}\mathbf{A})^{-1}(\mathbf{A}^{T\star}\mathbf{Y}). \tag{3.10}$$

Eq. (3.10) gives an optimal estimation once all the measurements are available. It is an *off-line* procedure and is not valid for the purposes of the proposed system. However, it is easy to transform it into a recursive algorithm. That is, to express the estimated parameters vector in the instant k, $\hat{\mathbf{X}}_k$ as a function of the previous estimation $\hat{\mathbf{X}}_{k-1}$ and of the last input measurement $\boldsymbol{p}_k = (\boldsymbol{v}_k, \boldsymbol{i}_k)$.

Rewriting (3.5):

$$\begin{pmatrix} \boldsymbol{y}_0 \\ \boldsymbol{y}_1 \\ \vdots \\ \boldsymbol{y}_k \\ \boldsymbol{y}_{k+1} \end{pmatrix} = \begin{pmatrix} \boldsymbol{i}_0 & 1 \\ \boldsymbol{i}_1 & 1 \\ \vdots & \vdots \\ \boldsymbol{i}_k & 1 \\ \boldsymbol{i}_{k+1} & 1 \end{pmatrix} \cdot \begin{pmatrix} \hat{\boldsymbol{Z}} \\ \hat{\boldsymbol{e_0}} \end{pmatrix} - \begin{pmatrix} \Delta\boldsymbol{e}_0 \\ \Delta\boldsymbol{e}_1 \\ \vdots \\ \Delta\boldsymbol{e}_k \\ \Delta\boldsymbol{e}_{k+1} \end{pmatrix} \tag{3.11}$$

Applying now, eq. (3.10). The optimum parameters vector $\hat{\mathbf{X}}_{k+1}$ gets the value:

$$\hat{\mathbf{X}}_{k+1} = (\mathbf{A}_{k+1}^{T\star}\mathbf{A}_{k+1})^{-1}(\mathbf{A}_{k+1}^{T\star}\mathbf{Y}_{k+1}) \tag{3.12}$$

that, when expanded, results in:

$$\begin{pmatrix} \hat{\boldsymbol{Z}} \\ \hat{\boldsymbol{e_0}} \end{pmatrix}_{k+1} = \left\{ \begin{pmatrix} \boldsymbol{i}_0^\star & \dots & \boldsymbol{i}_k^\star & \boldsymbol{i}_{k+1}^\star \\ 1 & \dots & 1 & 1 \end{pmatrix} \begin{pmatrix} \boldsymbol{i}_0 & 1 \\ \vdots & \vdots \\ \boldsymbol{i}_k & 1 \\ \boldsymbol{i}_{k+1} & 1 \end{pmatrix} \right\}^{-1} \left\{ \begin{pmatrix} \boldsymbol{i}_0^\star & \dots & \boldsymbol{i}_k^\star & \boldsymbol{i}_{k+1}^\star \\ 1 & \dots & 1 & 1 \end{pmatrix} \begin{pmatrix} \boldsymbol{v}_0 \\ \vdots \\ \boldsymbol{v}_k \\ \boldsymbol{v}_{k+1} \end{pmatrix} \right\} \tag{3.13}$$

which identifying the matrices $[\mathbf{A}]$ and $[\mathbf{Y}]$ in instant k, can be re-written as:

$$\begin{pmatrix} \hat{\boldsymbol{Z}} \\ \hat{\boldsymbol{e_0}} \end{pmatrix}_{k+1} = \left\{ \left([\mathbf{A}^{T\star}]_k \quad | \quad \begin{matrix} \boldsymbol{i}_{k+1}^\star \\ 1 \end{matrix} \right) \left(\begin{array}{c|c} [\mathbf{A}]_k & \\ \hline \boldsymbol{i}_{k+1} & 1 \end{array} \right) \right\}^{-1} \left\{ \left([\mathbf{A}^{T\star}]_k \quad | \quad \begin{matrix} \boldsymbol{i}_{k+1}^\star \\ 1 \end{matrix} \right) \left(\begin{array}{c} [\mathbf{Y}]_k \\ \hline \boldsymbol{v}_{k+1} \end{array} \right) \right\} \tag{3.14}$$

Let us consider the following matrices:

$$\mathbf{P}_k = ([\mathbf{A}^{T\star}]_k[\mathbf{A}]_k)^{-1}, B = \begin{pmatrix} \boldsymbol{i}_{k+1}^\star \\ 1 \end{pmatrix} \tag{3.15}$$

$$\mathbf{W}_{k+1} = \mathbf{P}_k\mathbf{B}(\mathbf{I} + \mathbf{B}^{T\star}\mathbf{P}_k\mathbf{B})^{-1} = \mathbf{P}_{k+1}\mathbf{B} \tag{3.16}$$

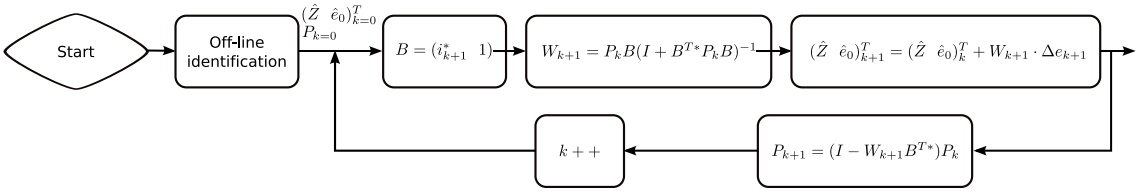

Figure 3.5: *Final recursive impedance estimation algorithm.*

it can be demonstrated [Ljung, 1986] that

$$\begin{pmatrix} \hat{\boldsymbol{Z}} \\ \hat{\boldsymbol{e}_0} \end{pmatrix}_{k+1} = \begin{pmatrix} \hat{\boldsymbol{Z}} \\ \hat{\boldsymbol{e}_0} \end{pmatrix}_{k} + \mathbf{W}_{k+1} \cdot \Delta \boldsymbol{e}_{k+1}. \tag{3.17}$$

Eq. (3.17) gives a straightforward method to recursively estimate the grid equivalent impedance at its equivalent generator. Fig. 3.5 shows a flux diagram of the proposed algorithm. The algorithm presents the following features.

- The algorithm simultaneously estimates the grid equivalent generator and equivalent voltage source.
- The algorithm presents a light computational charge. Due to the small dimensions of the regression problem, the key step — the matrix inversion in the computation of $\mathbf{W}_{k+1}$ (Eq.(3.15)) — reduces to a complex number inversion that is very fast to calculate.
- The algorithm inherits the optimal behavior of RLS under white Gaussian noise in the measurements.

As a consequence of its intrinsic recursive nature, the method requires an original matrix $\mathbf{P}_0$ and an original estimation for the grid impedance $(\hat{\boldsymbol{Z}}\ \ \hat{\boldsymbol{e}_0})^T_0$. Although algorithm convergence is mathematically ensured if $\mathbf{P}_0$ matrix is semi-definite positive, inaccurate values will make the algorithm initial convergence longer, as it must compensate the initial error. An approach that has proven to be useful in practice is to extract these matrices from an initial off-line estimation procedure. The first measurement *operation point* may, for example, be the voltage measurement in open circuit situation, that is, when $\boldsymbol{i} = 0$. It is important to remark that the matrix $\mathbf{P}_k$ controls the convergence speed of the estimation algorithm. The RLS algorithm naturally makes this matrix evolve so that the resulting convergence speed is optimal for the actual noise in the measurements. Under certain events, such as an impedance change detection, accuracy is not so important, but it is desirable to get faster responses. This issue is solved in the estimation evaluation subsystem by configuring $\mathbf{P}_k$ to quickly track the new changes and then let it evolve to increase the accuracy.

3.3.3 Grid synchronization

The influence of the grid synchronization over the performance of the monitoring system is critical: if grid phase — or frequency — is not correctly estimated, the *dq* reference frame

transformation will be erroneous, producing data that would not verify the assumed model. This would translate into an incorrect estimation.

Phase Locked Loop algorithms offer an easy way to extract the phase information of a periodic signal and there are several reported solutions for its application in three-phase systems [Bueno et al., 2005][Rodriguez et al., 2007b]. Usually, these systems use the PCC voltage measurements in order to extract their phase and synchronize the whole system with them forcing either the d or q coordinate of the transformed voltage to be null.

This approach, however, is not valid in this situation because voltage (and particularly its phase information) in the PCC is influenced by the injected current: when the converter moves to a different *operation point* by changing its injecting current, the PCC voltage is also changed and consequently the phase information provided by a PLL will be affected. This change in the phase moves the whole identification problem to a different reference frame, introducing errors.

To avoid this problem, the proposed system extracts the phase by integrating a grid frequency estimation:

$$\theta'(t) = \int_0^t \hat{\omega}(\tau) d\tau \tag{3.18}$$

Most PLL systems present a frequency intermediate signal, that is integrated in order to obtain the phase of the reference signal. When applied to a power system, this frequency signal is usually a constant (50-60 Hz) signal with small variations due to the power system situation. When the current injected by the power converter into the grid presents amplitude or phase jump, for instance during an *operation point* change, the grid voltage measured in the PCC is affected, as well. This quick change in the voltage signals may be reflected on a phase jump estimated by the PLL. In the PLL frequency signal, this translates into a — theoretically infinite — impulse. When integrated again, this impulse induces errors in the synchronous reference frame and in the estimation process.

To eliminate this transitory effects, two simultaneous strategies are applied. First, as shown on Fig. 3.3, the frequency signal is sharply low-pass filtered. This way, the high frequency components of the estimated frequency signal are reduced, giving a more stable synchronous reference frame. The cut-off frequency can be arbitrary low. This may generate low transients in the initial convergence of the synchronization subsystems that do not influence the system operation.

However, phase change impulses cannot be completely removed with this technique. With a linear filtering, peak value of the impulses is reduced, but they are also spread along time. The presented subsystem applies a transient removal procedure to solve this issue.

In general terms, transient removal procedures are difficult and unstable techniques because the unpredictable nature of transitories and their difficult detection. In the case under study, however, transients are fully predictable as they are generated by the grid converter itself.

Thus, when a transient is generated, the control system sends a signal to the monitoring system. The latter substitutes the frequency estimation by a moving average of the last detected frequencies during half a fundamental frequency cycle. Although this frequency is again an estimation, this can be considered to be valid because of the slow dynamics of power system frequency. This procedure is described in Fig. 3.6.

This system presents the advantage of making use of a regular PLL, which is usually already present in all converter control schemes. However, the monitoring system could be implemented with other reported frequency estimation algorithms [Mojiri et al., 2007].

3.3.4 Estimation evaluation algorithm, system behavior and anti-islanding capabilities

The ability of the system to make an on-line evaluation of the estimation characterizes it as a quasi-passive one and, in fact, dictates the whole system behavior.

From the description of the estimation algorithm it is easy to extract the clear relationship that exists between the chosen *operation points* and the quality of the estimation. Intuitively, *operation points* separated by a small *distance*, when contaminated by the measurement noise, will yield worse estimations that *operation points* situated in the different limits of the converter operation range. This creates a trade between the influence of the monitoring system over the grid and the obtained precision. Or in other words, a trade between the number and importance of the grid disturbances and the amount of information extracted from it.

In order to avoid a systematic perturbance of the grid, the proposed system incorporates an evaluation subsystem. The evaluation is based on the computation of a windowed error variable, named Γ and its comparison with a threshold named $\Gamma\gamma$. The variable Γ in time k takes the value:

$$\Gamma_k = \frac{1}{2k} \sum_{i=k-n}^{k+n} \frac{\left\| \boldsymbol{v}_i - \boldsymbol{i}_i \hat{\boldsymbol{Z}}_i + \hat{\boldsymbol{e}}_i \right\|^2}{|\boldsymbol{i}_i|} \tag{3.19}$$

This *error measurement* is the basis of the system behavior, described in state flow diagram of Fig. 3.7.

The monitoring system operation begins in the *Idle* state. During this state, the system samples points that belong to the no-current *operation point*. This *operation point* gives rich information about the grid equivalent voltage source but it is not enough to get a valid estimation of grid parameters. Eventually, the grid converter will start delivering or consuming power, and the grid monitoring system will then have the minimum two *operation points* to start the estimation process. The monitoring system enters, then, into a *regular operation* state, where the converter keeps working in the same *operation point*. Although the *measurement points* sampled during this stage belong to a single *operation point*, its introduction into the estimation algorithm improve the estimation quality as it contributes to compensate the additive noise always present in the measurements. It will remain in this state as long as the Γ measure keeps below the chosen threshold. When this condition fails, the monitoring system assumes that the estimates are not valid anymore (probably because of a potential change in the grid equivalent parameters) and moves to the *History clear* state. During this state, the $\mathbf{P}_k$ is reset to its initial value. This reset is performed to speed up the estimation algorithm dynamics and allow it to quickly converge to the new grid equivalent parameters.

Once this operation is fulfilled, the system needs two new *operation point*s to get a new valid estimation. The first *measurement points* can perfectly be sampled in the current one. After that, the system creates a disturbance in the grid — changing the *operation point* — to try and get a new valid estimation. The grid monitoring system will stay in

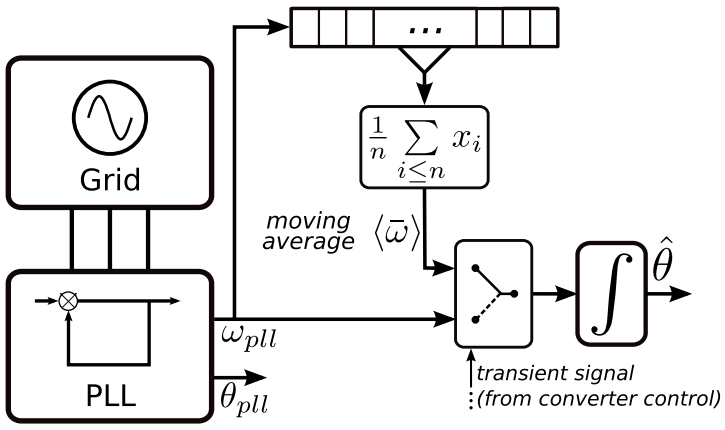

Figure 3.6: *Transient removal procedure.*

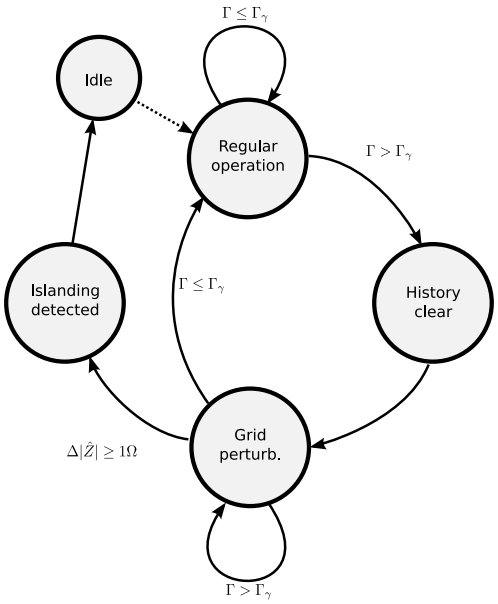

Figure 3.7: *Global system behavior (ENS detection) state flow.*

this *Grid perturbation* state until $\Gamma \leq \Gamma_\gamma$. When this condition is verified, the estimated grid equivalent impedance and voltage source is assumed to be valid. If the equivalent impedance value differs from the previous one in more than the allowed amount given by the power system operator (e.g. 1 Ω) the monitoring system assumes that the converter is working in an island and would move it to the initial *Idle* situation. Otherwise, the system returns to the *Regular operation* state.

3.4 Results

The different components of the grid impedance monitoring system exposed in this chapter have been verified under simulation environment and evaluated under experimental testing.

3.4.1 Grid equivalent impedance and voltage source estimation subsystem

Given the varying nature of the problem, it results difficult, in many cases, to have an a-priori knowledge of the grid fundamental parameters (i.e. equivalent impedance and generator). This fact makes difficult to directly validate the proposed algorithm. For this reason, the algorithm validation has been divided in three phases:

- Complete simulation evaluation.
- Application of the algorithm to a pure passive load without grid generator.
- Application of the algorithm to an unknown grid.

This way, the algorithm will be, first, theoretically evaluated and, once its theoretical performance is demonstrated, it will be applied to growing complexity experimental situations.

Application of the algorithm to a simulation set-up

Its important to remark the importance of a correct and realistic simulation of this algorithm. It is only under simulations when the estimation of the grid impedance and equivalent voltage generator can be truly evaluated as its actual value is exactly known.

The simulation environment consists in a MATLAB environment connected to PSIM simulator. The simulation setup consists in a three-phase converter connected to a fictitious grid composed of an ideal sinusoidal voltage generator connected in series with a resistance and an inductance, as displayed in Fig. 3.2. The simulated grid has an actual resistance value of 1 Ω, a reactance value of 0.6 Ω and a peak grid equivalent generator value of $220 * \sqrt{(2)}$ V.

Fig. 3.8 shows the evolution of the grid impedance estimation. In $t = 0.4\ s$ the algorithm is connected. The evolution is a typical exponential function and presents a great accuracy. A little bias appears in the estimates. This bias is due to the fact that noise over input signals (currents and voltages) is not so white but a bit colored. The existence of this error can be mathematically demonstrated and compensated. However, for most purposes, this error is acceptable and there would be no need of applying the more complex Extended Least Squares algorithm [Ljung, 1986].

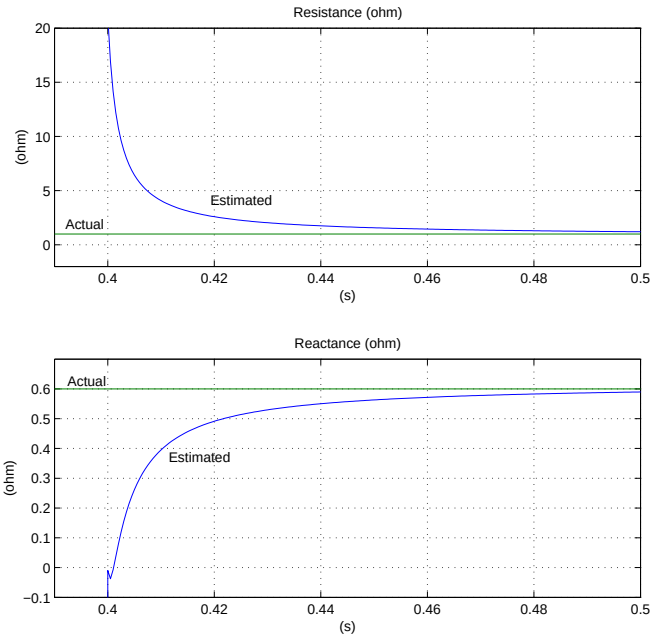

Figure 3.8: *Simulated time evolution of the grid impedance estimation.*

Fig. 3.9 shows the time evolution of the grid equivalent generator estimation. As it is shown in the figure, the algorithm convergence is fast and accurate.

Experimental passive load identification

The performance of the algorithm can be exactly evaluated if it is applied to a calibrated inductive-resistive load. Under this situation, the algorithm should return a null estimation of the grid generator and a correct estimation of the calibrated load. The great advantage of this test is the possibility to calibrate the passive load with a measurement equipment and use its actual value to compare it with the estimated one.

Fig. 3.10 shows the evolution of the estimated resistance and inductance when applying the algorithm to a balanced load of 1.5 Ω and 3.67 mH. The algorithm results very robust and accurate. In all tests, the estimated equivalent grid generator values were negligible.

Experimental grid identification

Finally, the identification algorithm has been tested on a real situation. The grid converter is connected to a 50 Hz grid through a pattern series R-L filter as shown in Fig. 3.11.

Two executions of the algorithm have been launched simultaneously, the first one, applied over the actual PCC (point 1 in Fig. 3.11), and another one applied over the new fictitious PCC (point 2 in Fig. 3.11). Assuming an invariant grid during the experiment execution, the algorithm can be assumed to work properly if the estimated impedance on both points differs exactly in the amount added by the pattern R-L serial network, and the estimated grid equivalent generator is the same in both cases.

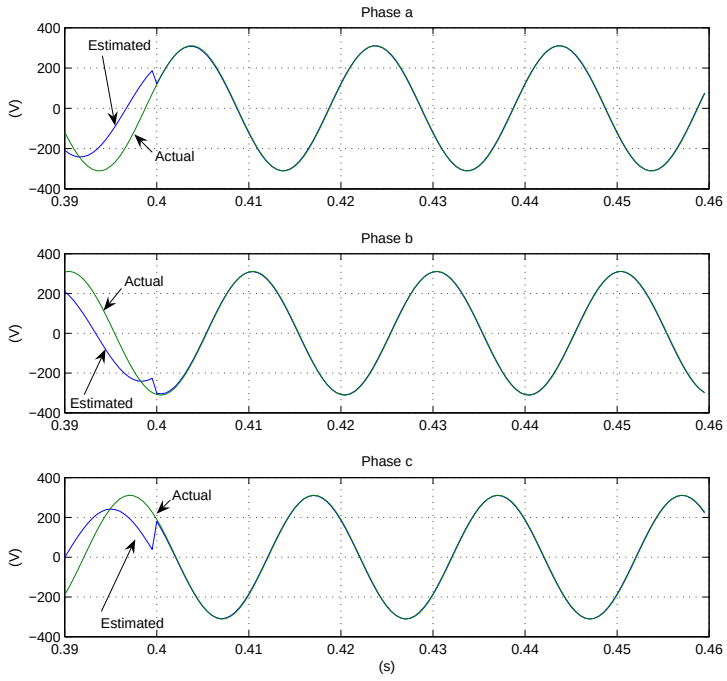

Figure 3.9: *Simulated time evolution of the grid equivalent generator estimation.*

Fig. 3.12 shows the currents applied to the grid, with the typical changes in *operation point*, and the sensed PCC voltages. It's important to remark the perceptible variations of the PCC voltage. The bigger the change in the *operation point* is, the bigger distance from the new group of clustered points to the previous ones will be and, consequently, the better the precision obtained will be. Fig. 3.13 shows those measurement transformed into the rotating *dq* reference frame. These are the data that are actually entering the estimation algorithm.

Fig. 3.14 shows the experimental impedance estimated values that offers the algorithm when the pattern R-L serial network presents a resistance of 1 Ω and an inductance of 0.5 mH. The upper part of Fig. 3.14 shows the evolution of the resistance estimation for the algorithms launched at points 1 and 2 of Fig. 3.11. Both algorithm executions are launched in different time instants to ensure that the data used by the algorithms is different. In both cases, the estimated values get some mistaken values until the second *operation point* arrives; once it arrives, the convergence to the final value is fast and accurate. The estimated value difference between points 1 and 2 closely approximates the resistance of the pattern R-L network (1 Ω). The lower part of the plot displays the inductance estimation. Conclusions about this estimation are similar to those obtained in the resistance case.

Fig. 3.15 shows the experimental grid equivalent generator estimated values that offers the algorithm in the same experiment. Both estimations reach very close values, validating the proposed algorithm.

Fig. 3.16 compares the behavior of the algorithm when the system is operating under a big amount of low order harmonics and white Gaussian additive noise. Fig. 3.16.a and b,

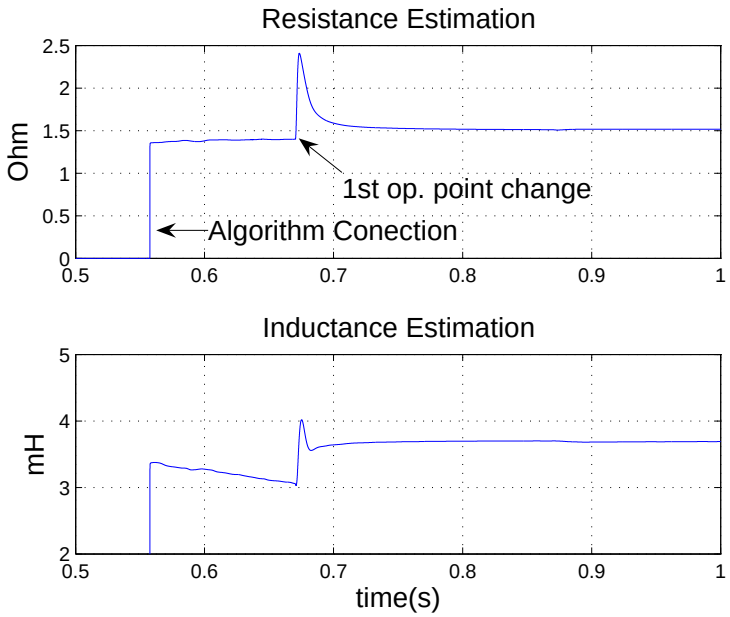

Figure 3.10: *Experimental identification of a passive load.*

evaluates system behavior when the voltage signal from the grid is contaminated with 0%, 25%, 50% and 100% of fifth harmonic. The system presents a very robust behavior as a consequence of its preprocessing and synchronization stage. Fig. 3.16 evaluates the system behavior when the current measurements are contaminated with additive white Gaussian noise of variance 0%, 25%, 50% and 100% (note that this variance values are referenced, also, to the peak value of the current fundamental harmonic. i.e. if the current peak value is 1 A, a noise with 100% variance is a noise whose variance equals 1 A). Plots show some influence over the estimates due to the magnitude of the noise, and also due to the fact that the noise is not totally white. Even under these conditions, the convergence is fast and accurate.

Fig. 3.17 shows simultaneously the sensed PCC voltage grid and the same reconstructed voltage by means of the estimated grid impedance and generator and the sensed PCC

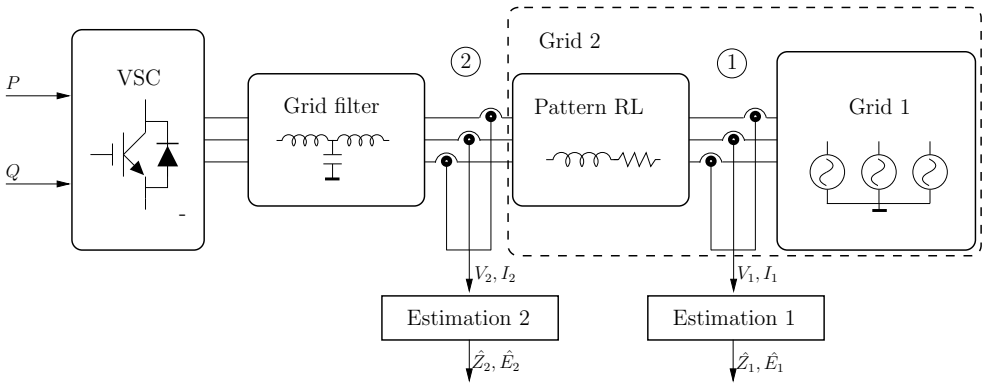

Figure 3.11: *Set-up for complete experimental grid identification.*

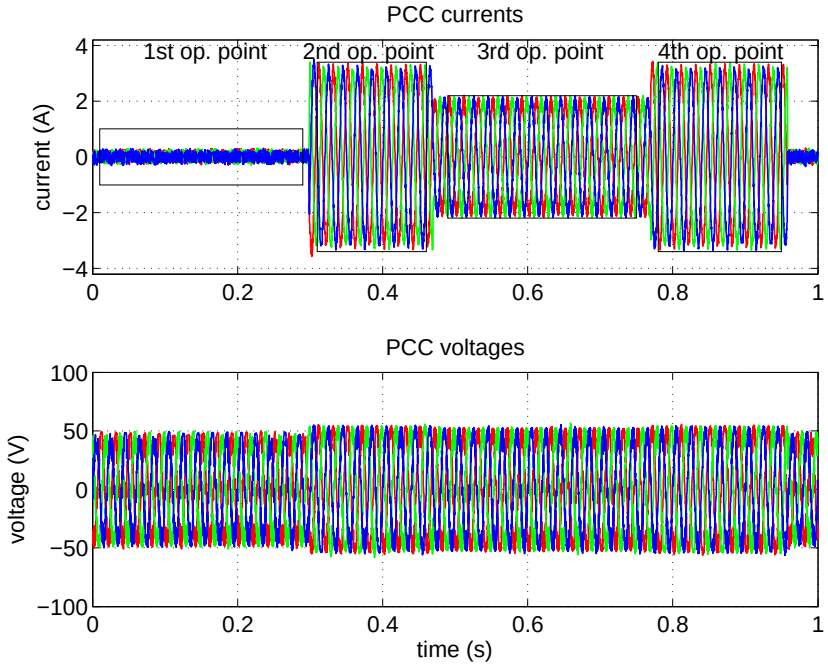

Figure 3.12: *Experimental identification sequence.*

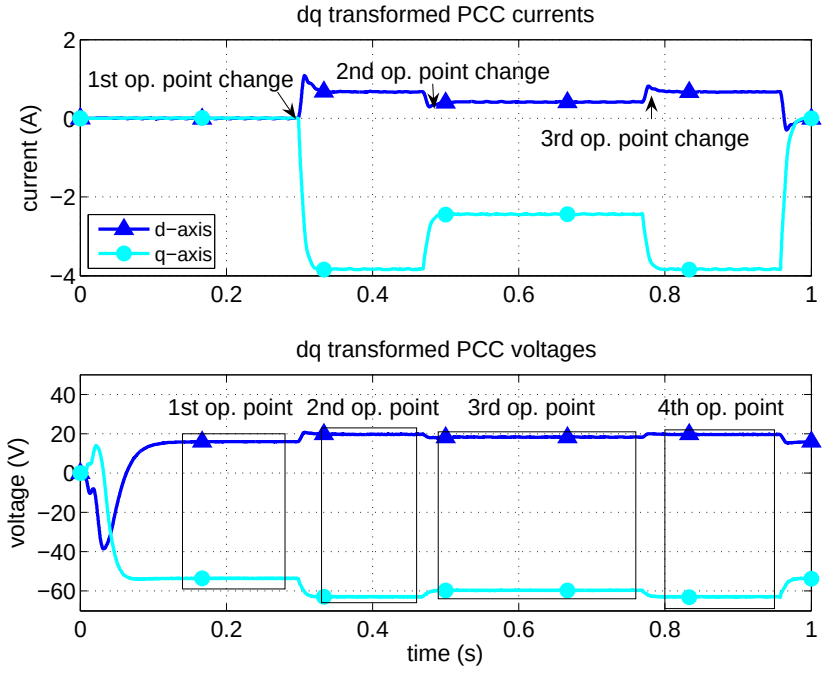

Figure 3.13: *Values of the measured currents and voltages in PCC transformed into dq reference frame.*

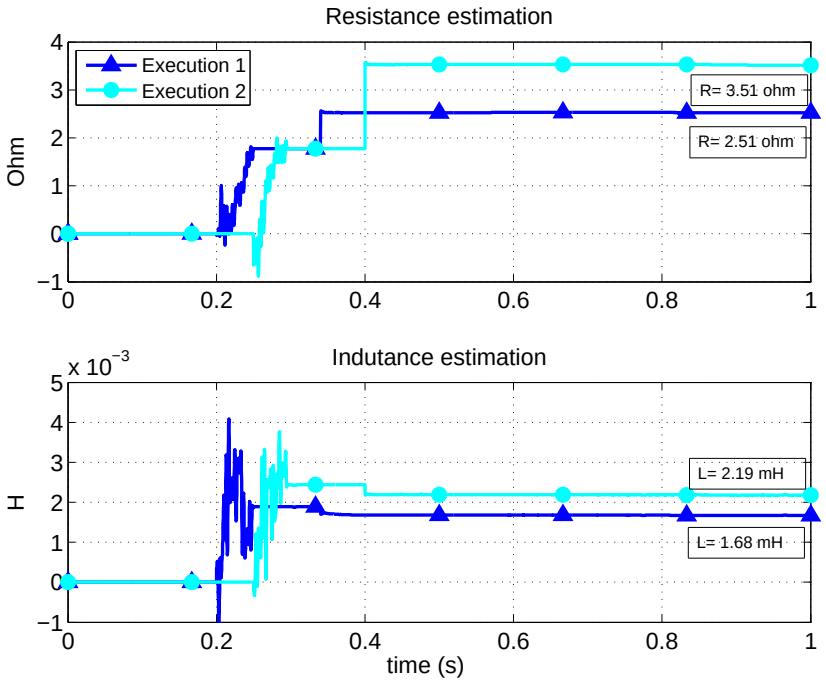

Figure 3.14: *Experimental impedance estimation.*

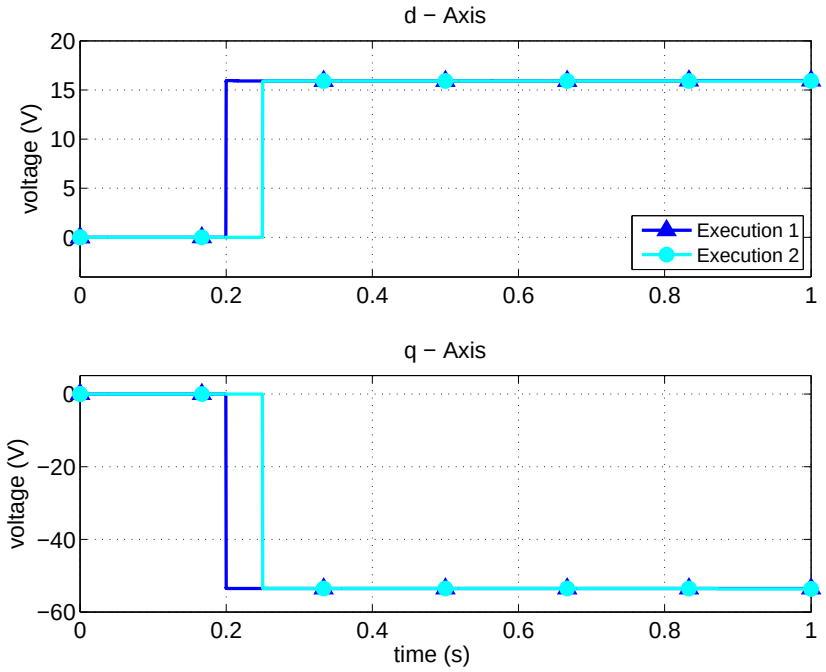

Figure 3.15: *Experimental grid equivalent voltage source estimation.*

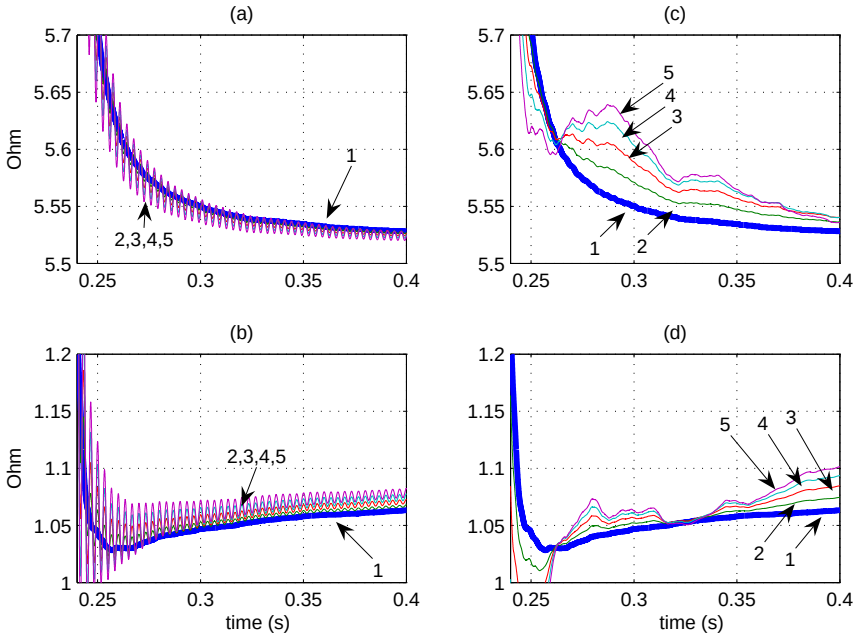

Figure 3.16: *Estimation algorithm under disturbances. (a)(b) Resistance and inductance estimation with fifth harmonic (Amplitude: 1:0%, 2:25%, 3:50%, 4:75%, 5:100%). (c)(d) Resistance and inductance estimation with aditive white gaussian noise in the current meas. (Variance: 1:0%, 2:25%, 3:50%, 4:75%, 5:100%)*

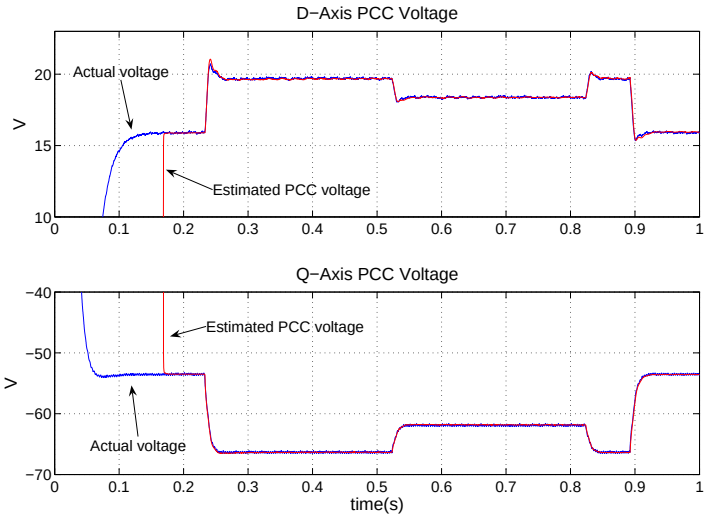

Figure 3.17: *Estimation error.*

currents. Consequently, it represents the error of the estimation algorithm prior to *Gamma* computation. This measure gives an idea of the accuracy obtained by the algorithm, and indirectly assesses the assumed grid model.

3.4.2 Grid synchronization and pre-processing stage

As comented in previous sections, the most sensitive steps in the operation of the presented impedance monitoring system are the grid synchronization unit and the estimation pre-processing stage.

The grid synchronization subsystem primary function is to extract an estimation of the frequency of the grid harmonic under consideration; usually the grid fundamental frequency. Fig. 3.18 shows the temporal evolution of the synchronization system. The upper part of the figure shows the raw PCC voltage measurements during an small change in the *operation point* (in t=0.52 s). The middle part of the plot shows the frequency estimation. It can be seen that the grid syncrhonization subsystem is working properly as the *operation point* change does not reflect on this estimated magnitude. The lower part of the plot shows the phase information that is used to represent the problem in a synchronous reference frame. Also in this case, the *operation point* step change does not have a perceptible influence over the phase estimation.

The pre-processing stage, located in the *Grid equivalent impedance & voltage source estimation* block (see Fig. 3.3) is the responsible of presenting a filtered and balanced *dq* input signals to the RLS estimator. Fig. 3.19. shows the evolution of the this stage when the input voltage signals are unbalanced and polluted with switching ripple. As displayed in the lower part of the figure, the system behaves in a satisfactory way.

3.4.3 Estimation evaluation algorithm and anti-islanding capabilities

Fig. 3.20 shows the evolution of the system when the grid equivalent impedance is suddenly increased in 1.8 Ω. The upper part of the figure shows the evolution of the estimated

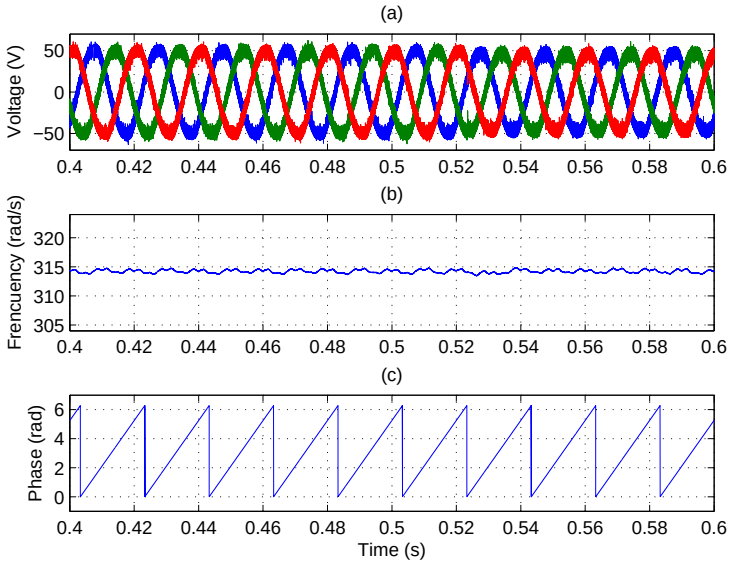

Figure 3.18: *Time evolution of the Grid synchronization subsystem. (a) Three-phase PCC voltage measurement. (b) Frequency estimation. (c) Phase estimation.*

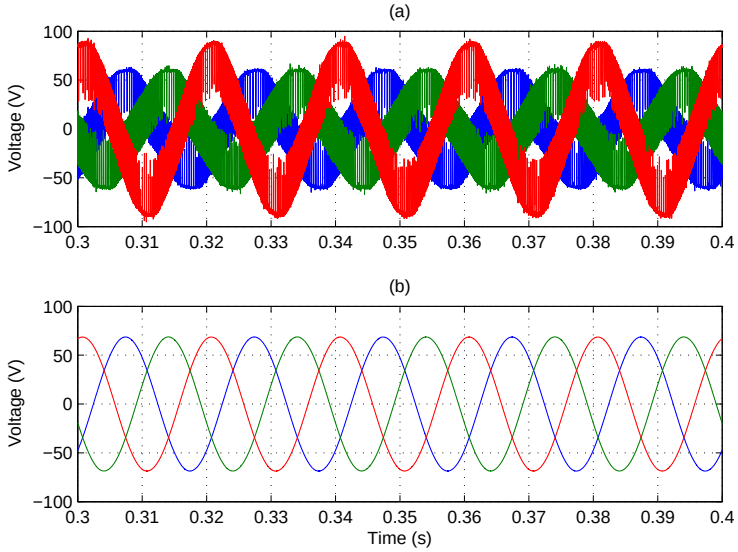

Figure 3.19: *Pre-processing stage experimental results. (a) Unbalanced three-phase PCC voltage measurement. (b) Output of the pre-processing stage.*

equivalent resistance. The middle row, shows the evolution of the error variable Γ and the associated threshold Γ_γ. Finally, the lower part shows the corresponding grid injected current. The step in the impedance value is created in $t = 0.05\ s$. As expected, the variable Γ quickly increases its value crossing the threshold Γ_γ. From this moment, the monitoring system exits the *Regular operation* state and enters the *History Clear* state. The matrix $\mathbf{P}_k$ is reset approximately in $t = 0.1\ s$ (see Fig. 3.20). After that, some *measurement points* are sampled in order to settle a first *operation point*. In $t = 0.13\ s$, the monitoring system sends the signal to the converter control to change the *operation point*. In a short period the Γ variable falls beyond the threshold Γ_γ. As the equivalent impedance has suffered a big increase, the monitoring system disconnects the converter from the grid, as corresponds in an islanding situation.

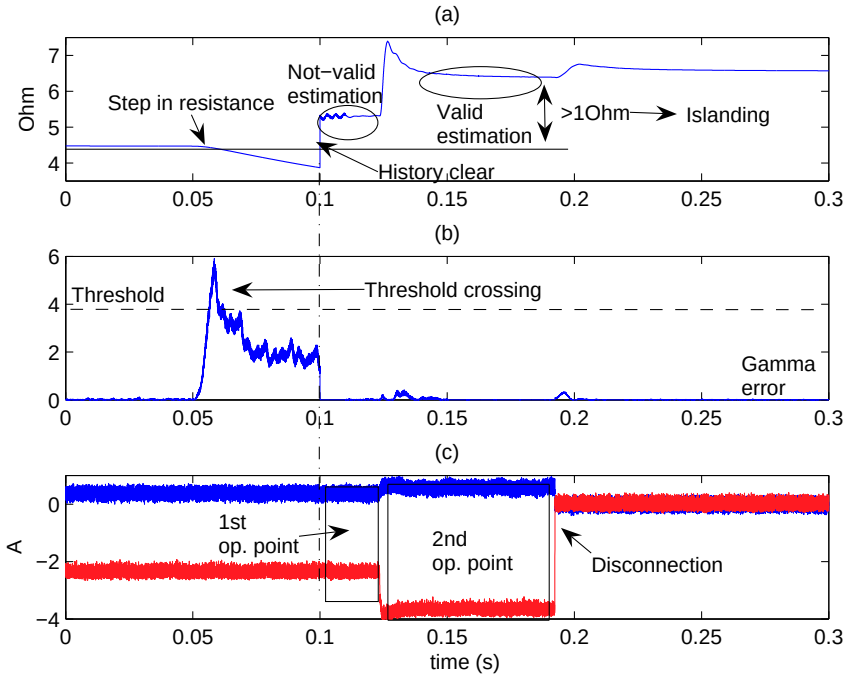

Figure 3.20: *Evolution of the estimation evaluation algorithm under a islanding situation. (a) Resistance estimation. (b) Γ evolution. (c) Injected currents expressed in dq axis.*

3.5 Conclusions and main contributions

This chapter has presented a system for the monitoring of grid equivalent impedance. Following lines state the main extracted conclusions and contributions.

The presented system is sustained on an optimization process based on the use of a linear regression algorithm, operating in a synchronous reference frame (dq axes). The use of a least-squares based algorithm ensures a good behavior in the presence of additive noise, harmonics and switching ripple. The translation of the problem into a synchronous reference frame allows to substantially decrease the computational load with respect to

previous published proposals.

To complement its operation, the chapter has proposed a novel estimation quality method that calculates a quality index related to the estimation validity in real time. This method allows to implement a quasi-passive identification process that avoids the classical systematic grid perturbation that is present in active proposals, minimizing its influence. The method also enables to quickly track big impedance change and, thus, could serve as a basis for islanding detection.

The chapter proposes a synchronization method that can be utilized to generate a synchronous reference frame that spins at the grid frequency but removes line voltage phase dependency.

The last part of the chapter benchmarks the system performance applying different tests. In all tests, the system demonstrated a good behavior. This good behavior is mainly due to the quasi-optimal behavior of the system under additive white Gaussian noise that inherits from RLS algorithm and the strong pre-filtering and synchronization stage.

The system design forces the converter current controller to be fully stable in order to get valid estimates. This fact limits the application of the algorithm in adaptive control schemes.

Chapter 4

Analysis of the influence of grid dynamics over stability of current controllers

Previous chapter of this dissertation has presented a method to recursively estimate the grid dynamic parameters when viewed from the point of connection of a power converter. Experimental tests have shown that this parameters are difficult to predict and are time variant. The objective of this chapter is to analyze the influence of those grid uncertain parameters over the stability of current controllers used for the connection of grid converters. The analysis covers general linear controllers and hysteresis controllers.

4.1 Introduction

One of the main concerns of this thesis is about reliability. The current power market paradigm forces grid connected converters to operate 24×7. For example, renewable energy contracts are increasingly introducing clauses guaranteeing a minimum uptime of the system and specifying the expenses of an eventual service interruption. In this thesis, reliability is understood at the current control level and particularly at its global stability. As described in the introductory chapter, this inner control loop is itself a core component of the global converter control structure so, the stability of outer controllers, and finally of the whole grid interface, depends on it.

The process that has to face up this control loop is hardly non-linear. Power devices, such as IGBT, MOSFET, etc., are used as switches, making the plant transfer function discontinuous. This chapter will deal with these non-linearities and the way to approximate the non-linear model and obtain a linear model.

Besides this non-linear nature, the involved models present several uncertainty sources. The less critic of them are due to grid filter components tolerance. At the cost of an expenses increase, this values could be calibrated during the manufacturing process, achieving accurate models. However, there are still other internal non-correctable uncertainty sources as temporal drifts, coil flux saturation or lack of detail in the assumed physical model.

A major uncertainty source is the grid. As explained in previous chapter, the grid is a complex dynamic system whose conditions vary along time. Moreover, even under the assumption of an invariant grid, electrical analysis of the Point of Common Coupling of

power converters is expensive, rarely presents the required precision and, in low power applications, it is often missing. This lack of knowledge translates, also, into grid model uncertainty. The grid is an external system, but, except in few connection topologies (L filter connection, to some extent, for example), its mathematical model is integrated inside the model of the process to stabilize by the current controller, that will inherit the uncertainty.

The problem of analyzing the stability of this current control loop is different depending on the control approach used. In general terms, SISO controllers applied to SISO systems as, for example, resonant controllers applied to independent or $\alpha\beta$ phases, can be formally analyzed by means of classical analysis tools. Gain and phase margins, together with Nyquist and/or Nichols plots, form a toolbox suitable for stability analysis purposes.

When the control is faced from a, more common, synchronous reference frame, (dq axes), the plant turns into a MIMO system. It does not matter which procedure was used to design the controller: popular methods use approximations to face the problem from a SISO point of view. But the problem is MIMO anyway. Gain and phase margins, even when studied for each of the channels, are incorrect indicators and cannot ensure robust stability. Simulations offer good information about the system, but it is difficult to extract conclusions under the presence of multiple uncertainty sources and, occasionally, some very slow unstable modes can remain hidden and generate problems after several hours of operation.

Very few studies have been published regarding this topic. One of the most important is [Liserre et al., 2006c]. This work presented a study of the poles and zeros displacement when modifying the grid equivalent resistance and inductance. However, this article scope is limited to the effect of the grid over converters controlled with a proportional+resonant scheme and does not generalize to extract conclusions for other SISO or MIMO structures. Another remarkable paper from the same group makes an indirect analysis of the grid influence over VSC controllers in a paper dedicated to propose an islanding detection algorithm [Liserre et al., 2006a], which analyzes the effect of the uncertainty in grid impedance over the estimation of grid voltage disturbance.

This chapter proposes an analysis method suitable for the study of the influence of grid dynamics uncertainty over stability of the inner current control loop of grid connected power converters valid for the more general MIMO problem.

First part of the chapter focuses on how this grid uncertainty is reflected in the model of a converter connected to an uncertain grid. The effect is two-fold: over model parameters, and as an external disturbance added to the plant output.

Once the problem is correctly modelled, the chapter proposes an stability analysis method for linear current controllers. The analysis is performed by using the μ structured singular value. The topic is dealt from a rather practical point of view, focusing on practical and implementation issues. Three illustrative practical cases serve as demonstration of this tool capabilities.

For the non-linear controller case, the analysis complexity is drastically increased. For this reason, the analysis is centered over a particular controller, a hysteresis controller. Stability bounds are extracted for the L-connection case, and some conclusions are given for the LCL-case.

4.2 Grid converter modelling

In general terms, an AC converter connected to the grid is composed of the blocks displayed in Fig. 4.1. The process of modelling a PWM converter consists in extracting mathematical expresions that describe the behavior of each of the blocks in Fig. 4.1, except the controller.

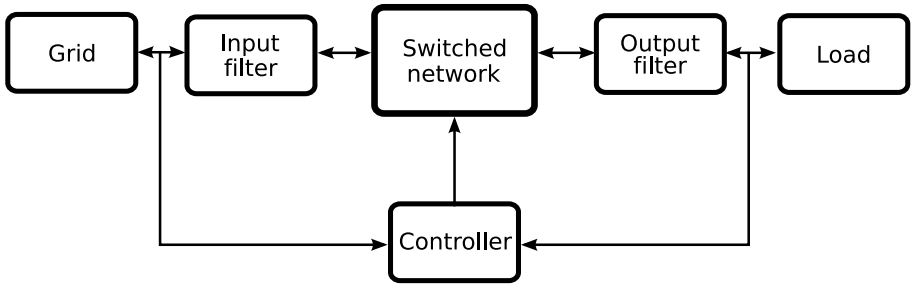

Figure 4.1: *General structure of a power converter.*

Several methods to model a PWM converter have been reported in the related technical literature. Fig. 4.2 [Boroyevich, 2000] is a statement of the fundamentals:

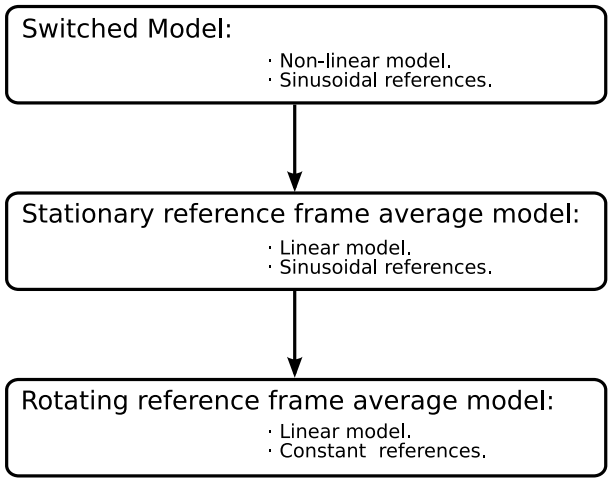

Figure 4.2: *Steps in PWM power converters modelling.*

- **Switched model:** The inputs to the converter are directly the switching devices (IGBT, MOSFET, etc.) control signals. The result is a non-linear model. Additionally, the reference signals (e.g. reference currents in each of the phases) are (usually) sinusoidal.

- **Stationary reference frame average model:** The switching functions produced by the system inputs are averaged during a PWM period T_{SW} by means of the average operator:

$$\langle x(t) \rangle_{T_{SW}} = \frac{1}{T_{SW}} \int_{t-T}^{T} x(\tau) d\tau \tag{4.1}$$

This averaging process allows to work with the average voltage value of the switching signals in each of the phases instead of the PWM generator and the switched network, i.e. $u_a(t)$, $u_b(t)$, $u_c(t)$. This model still presents the problem of having sinusoidal reference signals as it is still represented in a stationary reference frame. However some control proposals [Yuan et al., 2002] [Zmood and Holmes, 2003] [Liserre et al., 2006b] have successfully faced the problem from this point of view.

- **Rotating reference frame average model:** If additionally to the averaging process the reference frame is rotated at an angular speed equal to the grid one (e.g. $2\pi 50\ rad/s$), the sinusoidal signals of the fundamental frequency turn into constant ones. A known approach for this operation is the application of the Park transform [Krause et al., 1995].

The latter two models are almost equivalent for stability analysis purposes. In fact, the procedure that is proposed in this chapter could be equally applied in both cases. However, this last averaging approach [Lindgren, 1998] [Svensson, 1997] is very used in converter control design, and is the starting point of the two models that will be extracted in this section:

- A linear nominal model that assumes that the parameters of the actual plant match with the ones in the plant model. Thus, no uncertainty is present in model parameters.

- An uncertain model that assumes that for some of the plant parameters, only a range of possible values is known. In fact, an uncertain model is a set of possible models generated by the possible combinations in the uncertain parameters. Usually, an uncertain model is also referred to as uncertain set and is represented by $\mathcal{P}$ or Π. A particular plant inside this set is the nominal plant, usually denoted by $G_0(s) \in \mathcal{P}$ or simply $G(s) \in \mathcal{P}$. The rest of the particular perturbed plants inside the set are usually denoted by $G_p(s) \in \mathcal{P}$.

4.2.1 Linear nominal model

Assuming that actual plant parameters stay in their nominal value and applying the average hypothesis to the converter under study, a three-phase schematic as the one displayed on Fig. 4.3 can be built. The left part of the diagram contains the averaged model of the converter itself. Note how it is reduced to a controllable voltage source. The converter is connected to the model of the LCL grid filter. The model includes both the resistive and inductive effects of the inductors but considers them a fully linear element. Finally, the grid is represented with the equivalent model described in chapter 3.

The system is assumed to be balanced. The three phases are equivalent in impedance terms. The grid voltage is balanced, as well. So: $C_{0a} = C_{0b} = C_{0c} = C_0$, $R_{xa} = R_{xb} = R_{xc} = R_x$ and $L_{xa} = L_{xb} = L_{xc} = L_x$, where $x = 1, 2, g$.

The linear ordinary differential equations that model the converter nominal behavior are the following [Bueno, 2005]:

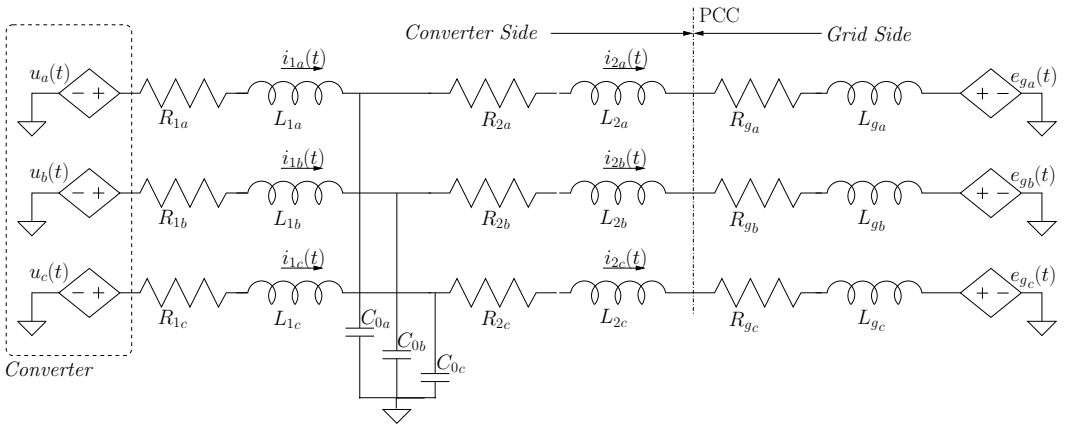

Figure 4.3: *Average linear model of the converter conection to the grid.*

$$\begin{cases} u_k(t) = R_1 i_{1k}(t) + L_1 \dfrac{di_{1k}(t)}{dt} + u_{ck}(t) \\ i_{1k}(t) = i_{2k}(t) + C_0 \dfrac{du_{ck}(t)}{dt} \\ u_{ck}(t) = (R_2 + R_g) i_{2k}(t) + (L_2 + L_g) \dfrac{i_{2k}(t)}{dt} + e_k(t) \end{cases} \qquad k = a, b, c \tag{4.2}$$

If the Park transform is applyed to the previous model, the following model is obtained:

$$\begin{cases} \boldsymbol{u}(t) = R_1 \boldsymbol{i}_1(t) + L_1 \dfrac{d\boldsymbol{i}_1(t)}{dt} + j\omega L_1 \boldsymbol{i}_1(t) + \boldsymbol{u}_c(t) \\ \boldsymbol{i}_1(t) = \boldsymbol{i}_2(t) + j\omega C_0 \boldsymbol{u}_c(t) + C_0 \dfrac{d\boldsymbol{u}_c(t)}{dt} \\ \boldsymbol{u}_c(t) = (R_2 + R_g) \boldsymbol{i}_2(t) + (L_2 + L_g) \dfrac{d\boldsymbol{i}_2(t)}{dt} + j\omega L_2 \boldsymbol{i}_2(t) + \boldsymbol{e}(t) \end{cases} \tag{4.3}$$

where,

- $\boldsymbol{i}_1(t) \in \mathbb{C}$ represents the dq transform of the current flowing through the converter-side inductors $[i_{1a}(t), i_{1b}(t), i_{1c}(t)]$. It is composed of the d and q-axis components $\boldsymbol{i}_1(t) = i_{1d} + j i_{1q}$.
- $\boldsymbol{i}_2(t) \in \mathbb{C}$ represents the dq transform of the grid-side current signals $[i_{2a}(t), i_{2b}(t), i_{2c}(t)]$. It is composed of the d and q-axis components $\boldsymbol{i}_2(t) = i_{2d} + j i_{2q}$.
- $\boldsymbol{u}(t) \in \mathbb{C}$ represents the dq transform of the converter average ouput voltage signals $[u_a(t), u_b(t), u_c(t)]$. It is composed of the d and q-axis components $\boldsymbol{u}(t) = u_d + j u_q$.
- $\boldsymbol{u}_c(t) \in \mathbb{C}$ represents the dq transform of the LCL filter capacitor voltage signals $[u_{ca}(t), u_{cb}(t), u_{cc}(t)]$. It is composed of the d and q-axis components $\boldsymbol{u}_c(t) = u_{cd} + j u_{cq}$.
- $\boldsymbol{e}(t) \in \mathbb{C}$ represents the dq transform of the grid voltage signals $[e_a(t), e_b(t), e_c(t)]$. It is composed of the d and q-axis components $\boldsymbol{e}(t) = e_d + j e_q$.

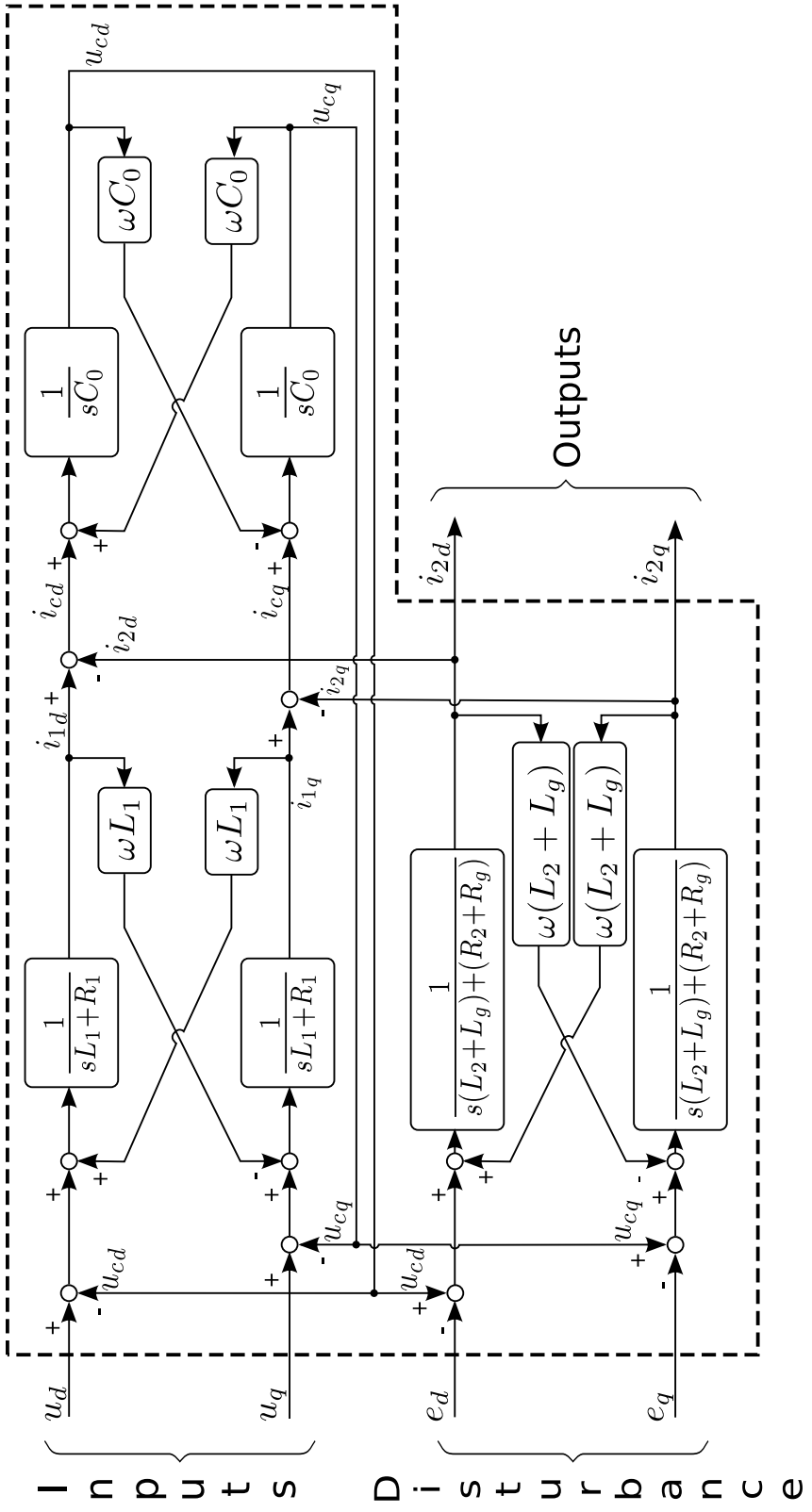

Figure 4.4: *Block diagram of the nominal model of Eq. 4.3.*

A block diagram representing this nominal model is displayed on Fig. 4.4.

At this point, let us assume that the grid voltage source is null, i.e. $e(t) = 0$, it will be introduced later. Considering a state vector $x(t)$, an inputs vector $u(t)$ and an outputs vector $y(t)$ given by:

$$\begin{aligned} x(t) = [i_{1d}(t) \quad i_{1q}(t) \quad i_{2d}(t) \quad i_{2q}(t) \quad u_{cd}(t) \quad u_{cq}(t)]^T, \\ u(t) = [u_d(t) \quad u_q(t)]^T, \\ y(t) = [i_{2d}(t) \quad i_{2q}(t)]^T, \end{aligned} \tag{4.4}$$

one valid state space representation for the model is the following:

$$\begin{cases} \dot{x}(t) = Ax(t) + Bu(t) \\ y(t) = Cx(t) + Du(t) \end{cases} \tag{4.5}$$

$$A = \begin{pmatrix} \frac{-R_1}{L_1} & \omega & 0 & 0 & \frac{-1}{L_1} & 0 \\ -\omega & \frac{-R1}{L_1} & 0 & 0 & 0 & \frac{-1}{L_1} \\ 0 & 0 & \frac{-R_2 - R_g}{L_2 + L_g} & \omega & \frac{1}{L_2 + L_g} & 0 \\ 0 & 0 & -\omega & \frac{-R_2 - R_g}{L_2 + L_g} & 0 & \frac{1}{L_2 + L_g} \\ \frac{1}{C_0} & 0 & \frac{-1}{C_0} & 0 & 0 & \omega \\ 0 & \frac{1}{C_0} & 0 & \frac{-1}{C_0} & -\omega & 0 \end{pmatrix}, \tag{4.6}$$

$$B = \begin{pmatrix} \frac{1}{L_1} & 0 \\ 0 & \frac{1}{L_1} \\ 0 & 0 \\ 0 & 0 \\ 0 & 0 \\ 0 & 0 \end{pmatrix}, \quad C = \begin{pmatrix} 0 & 0 \\ 0 & 0 \\ 1 & 0 \\ 0 & 1 \\ 0 & 0 \\ 0 & 0 \end{pmatrix}^T, \quad D = \begin{pmatrix} 0 \end{pmatrix}$$

The input/output diagram of this model is shown in Fig 4.5.

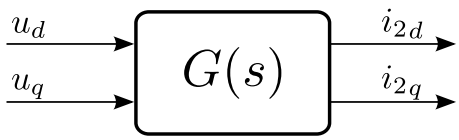

Figure 4.5: *Block diagram of the nominal plant model.*

Disturbance model

When the converter is connected to the grid, given the uncontrolled nature of the grid equivalent voltage value, it can be considered a disturbance over the process model described

in the previous subsection. This disturbance can be modelled applying the superposition theorem to the circuit in Fig. 4.3. A block diagram of the assumed disturbance model is displayed in Fig. 4.6.

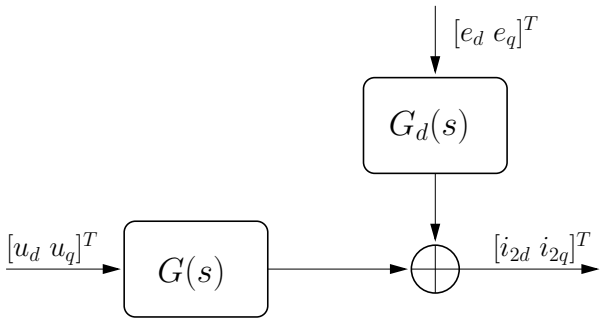

Figure 4.6: *Block diagram of the grid disturbance model.*

The disturbance affects the original system $G(s)$ adding to its outputs the output of a second system $G_d(s)$. $G_d(s)$ expresses the relationship between the plant grid currents ($[i_{2_d} \quad i_{2_q}]$) and the grid equivalent voltage generator ($[e_d \quad e_q]$). An state space representation of the transfer function $G_d(s)$ is the following:

$$\begin{cases} \dot{x}(t) = Ax(t) + B_d u(t) \\ y(t) = Cx(t) + Du(t) \end{cases} \qquad where \quad B_d = \begin{pmatrix} 0 & 0 \\ 0 & 0 \\ \frac{1}{L_2} & 0 \\ 0 & \frac{1}{L_2} \\ 0 & 0 \\ 0 & 0 \end{pmatrix} \tag{4.7}$$

Sample-time model and computational delay

All the control algorithms presented in this dissertation yield discrete-time implementations suitable for its programming in digital processors. This fact makes it advisable to obtain a *discrete-time* equivalent of the proccess model. Among the possible discrete-time equivalents of the plant, the chosen one is the *Zero Order Hold* (ZOH in the following) equivalent because it closely approximates the behavior of a continuous plant when seen from a digital signal processor.

The selection of the sampling time, named T_s, deserves a particular attention due to the influence it has in the final system. Several authors have proposed different criteria for this choice [Levine, 1996]. In general terms, the criteria give an acceptable range of possible values. Among them, the best choice is often the maximum sampling time that guarantees a certain performance.

When controlling power electronics devices, the sampling time has more influence on the system under control than in other kinds of systems. The reason is that the actuation signals are, in fact, PWM signals. The switching frequency of this signals has a direct influence over system effiency and is closely related to the sampling frequency.

More concretely, a typical PWM scheme, that is also used for this thesis, centers the

high level portion of the PWM signal around the sampling instants, allowing to actualize the actuation twice in each switching period. This PWM scheme is described in Fig. 4.7.

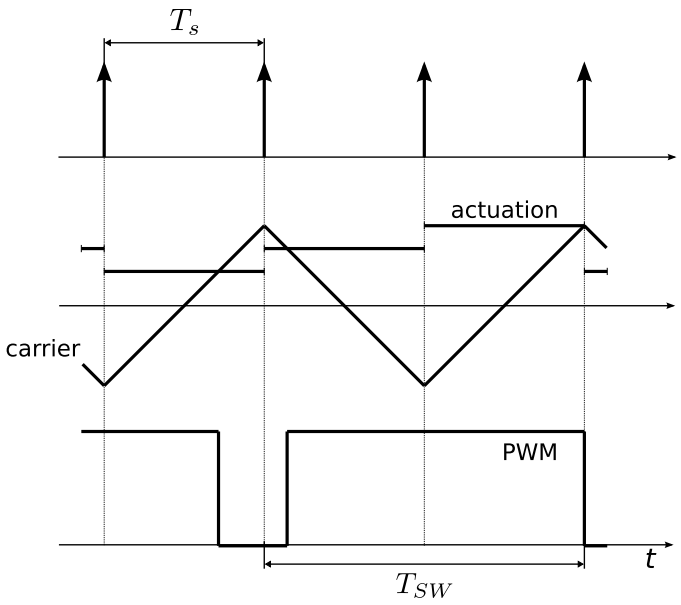

Figure 4.7: *Switching time - sampling time relationship.*

The algorithms proposed in this dissertation are tested in the experimental set-up described in chapter 6, but should be valid for higher powers. For this reason the sample time is chosen to be $T_s = 200\ \mu s$. This sampling time was used in the experimental platform described in [Bueno, 2005] and is also the default in the electronic control platform used for this thesis.

Note that the model to be discretized should be the one in (4.5) and (4.6), i.e. the one without the disturbance inputs, as they are not controlled and affect the plant directly without a zero order hold.

Additionally, as it will be justified on chapter 6, the practical digital implementation of the current controller creates a delay situated on both inputs of the discrete-time model. This situation is displayed in Fig. 4.8.

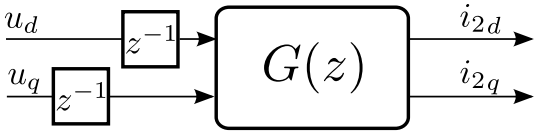

Figure 4.8: *Delays included in the discrete-time equivalent.*

The adding of this delays into the model is done by modifying the discrete-time equivalent model. Let us assume that the following model expressed in state space variables is a good approximation of the continuous model in Eq. 4.5:

$$\begin{cases} x_{k+1} = Gx_k + Hu_k \\ y_k = Cx_k + Du_k \end{cases} \tag{4.8}$$

The input delays can be included in the model by generating a new one:

$$\begin{cases} x_{k+1} = G_d x_k + H_d u_k \\ y_k = C x_k + D u_k \end{cases} \tag{4.9}$$

where

$$G_d = \begin{pmatrix} G & H \\ 0 & 0 \end{pmatrix}, \quad H_d = \begin{pmatrix} 0 \\ I \end{pmatrix} \tag{4.10}$$

This model will be the one used for the optimal *Linear Quadratic* design procedures that will be described in chapter 5.

4.2.2 Uncertainty model

As previously described, in general situations, and specially in the case of converters used in *Distributed Generation Systems*, the grid equivalent inductance, L_g, and resistance, R_g, are only approximately known. The uncertainty can be expressed by means of minimum and maximum value of grid parameters,

$$\begin{array}{c} R_g \in \mathbb{R}, R_g \in [R_{g_{min}}, R_{g_{max}}] \\ L_g \in \mathbb{R}, L_g \in [L_{g_{min}}, L_{g_{max}}] \end{array} \tag{4.11}$$

or, in other terms:

$$\begin{array}{ll} R_g = R_{g_{nom}}(1 \pm \delta_{R_g}\Delta_{R_g}), & \left\|\Delta_{R_g}\right\|_\infty \leq 1 \\ L_g = L_{g_{nom}}(1 \pm \delta_{L_g}\Delta_{L_g}) & \left\|\Delta_{L_g}\right\|_\infty \leq 1. \end{array} \tag{4.12}$$

A graphical model of this uncertainty is shown on Fig. 4.9.

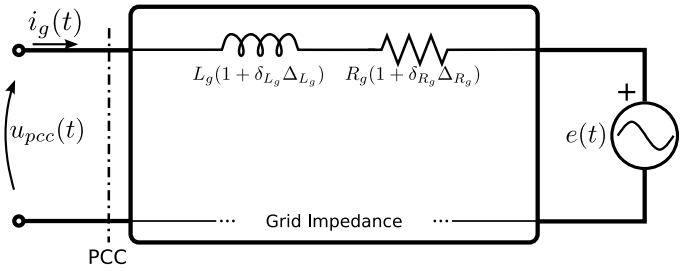

Figure 4.9: *Uncertain resistive-inductive grid.* $\left\|\Delta_{L_g}\right\|_\infty, \left\|\Delta_{R_g}\right\|_\infty \leq 1$

This kind of uncertainty is usually referred to as *Parametric or Structured Uncertainty* [Skogestad and Postlethwaite, 2005]. In this case, the structure of the model is known but some of the parameters are uncertain.

Due to the dynamical character of the plant under control, the grid equivalent resistance and inductance, and the grid-side inductor and resistance L_2 and R_2 can be associated in a virtual grid side inductor and resistor $L_2' = L_2 + L_g$ and $R_2' = R_2 + R_g$ respectively. This notation simplifies the following mathematical expressions.

Without loss of generality, the uncertainty can be translated to the new virtual elements:

$$R'_2 = R'_{2nom}(1 \pm \delta_{R'_2}\Delta_{R'_2}), \quad \left\|\Delta_{R'_2}\right\|_\infty \leq 1 \tag{4.13}$$

$$L'_2 = L'_{2nom}(1 \pm \Delta_{L'_2}\delta_{L'_2}), \quad \left\|\Delta_{L'_2}\right\|_\infty \leq 1 \tag{4.14}$$

With this uncertainty, the set of equations 4.3 can be expressed as:

$$\begin{cases} \boldsymbol{u}(t) = R_1\boldsymbol{i}_1(t) + L_1\dfrac{d\boldsymbol{i}_1(t)}{dt} + j\omega L_1\boldsymbol{i}_1(t) + \boldsymbol{u}_c(t) \\ \boldsymbol{i}_1(t) = \boldsymbol{i}_2(t) + j\omega C_0\boldsymbol{u}_c(t) + C_0\dfrac{\boldsymbol{u}_c(t)}{dt} \\ \boldsymbol{u}_c(t) = R'_2(1 \pm \Delta_{R'_2}\delta_{R'_2})\boldsymbol{i}_2(t) + L'_2(1 \pm \Delta_{L'_2}\delta_{L'_2})\dfrac{d\boldsymbol{i}_2(t)}{dt} + j\omega L'_2(1 \pm \Delta_{L'_2}\delta_{L'_2})\boldsymbol{i}_2(t) + \boldsymbol{e}(t) \end{cases} \tag{4.15}$$

A block diagram describing this set of equations is displayed in Fig 4.10.

Parametric uncertainty

The parametric uncertainty[1] description serves as an useful tool in order to represent the uncertainty induced by uncertain parameters in the process model. The analysis of the grid influence perfectly matches with this paradigm. As shown in Fig. 4.10, this parametric uncertainty affects to the four blocks marked with the symbol Δ in that figure.

The best approach to model this uncertainty is to make use of the *Linear Fractional Transformations* [Doyle, 1984] (LFT in the following). Particullary, for this thesis the upper LFT [Doyle, 1984] will be used. This way:

- An uncertain constant $b = b_0(1+\delta_b\Delta_b), \quad \|\Delta_b\|_\infty \leq 1$, where b_0 is referred to as *nominal* value, can be represented in upper-LFT following the block diagram displayed in Fig. 4.11.

- An uncertain inverse constant $\dfrac{1}{a} = \dfrac{1}{a_0(1+\delta_a\Delta_a)}$, where $\dfrac{1}{a_0}$ is, again, referred to as *nominal* value and $||\Delta_a||_\infty < 1$, can be represented in upper-LFT following the block diagram displayed in Fig. 4.12.

The two kinds of uncertain transfer functions — shaded and marked with a Δ symbol in Fig. 4.10 — can be modelled making use of the two previous expressions as shown in Fig. 4.13 and Fig. 4.14.

This way, the uncertainty is *pulled-out* of the system model. As it will be seen later, this principle is basic in order to get a model expressed in NΔ-Structure. This structure is the basis for most of the existing robust algorithms and particularly for the robust stability analysis described in the next section. Fig. 4.15 shows an schema of such an NΔ-Structured uncertain model.

[1] In real applications, there are often other common uncertainty types such as structured uncertainty, of which parametric uncertainty is a subset, unstructured uncertainty, coprime uncertainty, etc. A detailed description can be found in [Skogestad and Postlethwaite, 2005][Zhou, 1998].

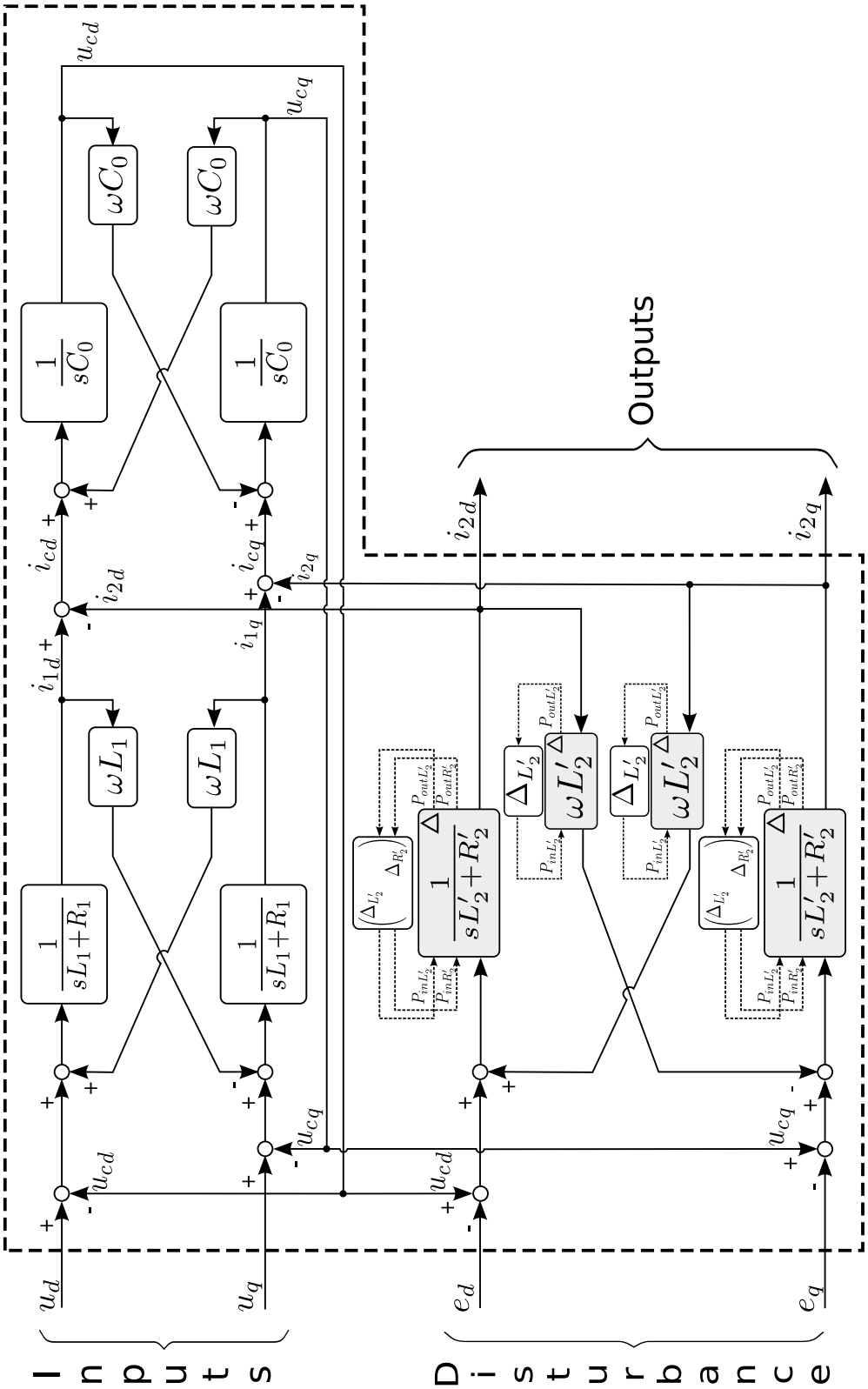

Figure 4.10: *Block diagram of the uncertain converter model with uncertain grid parameters.*

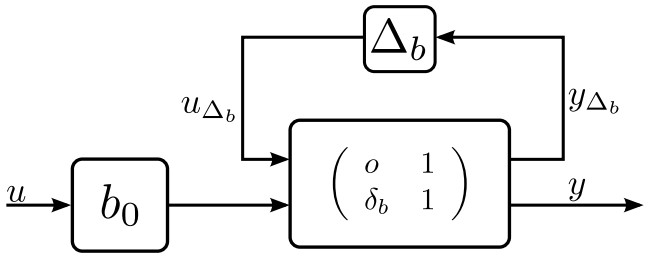

Figure 4.11: *Upper Linear Fractional Transformation of an uncertain direct parameter b.*

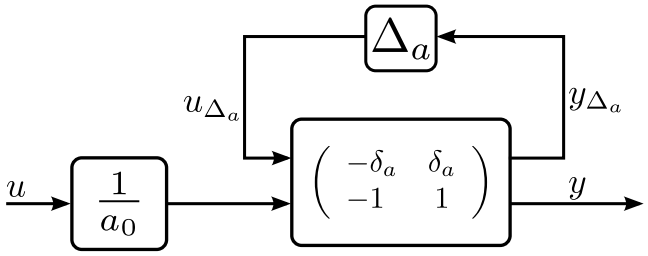

Figure 4.12: *Upper Linear Fractional Transformation of a uncertain inverse parameter* $\frac{1}{a}$.

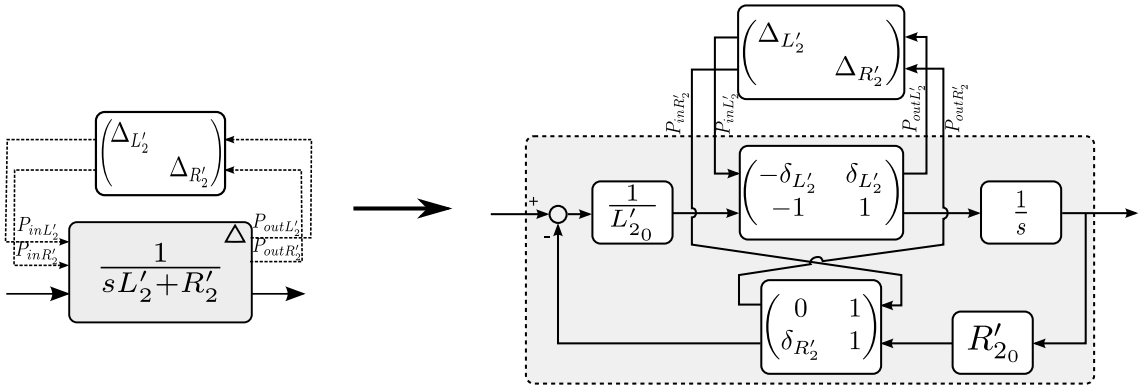

Figure 4.13: *LFT representation of uncertain block.*

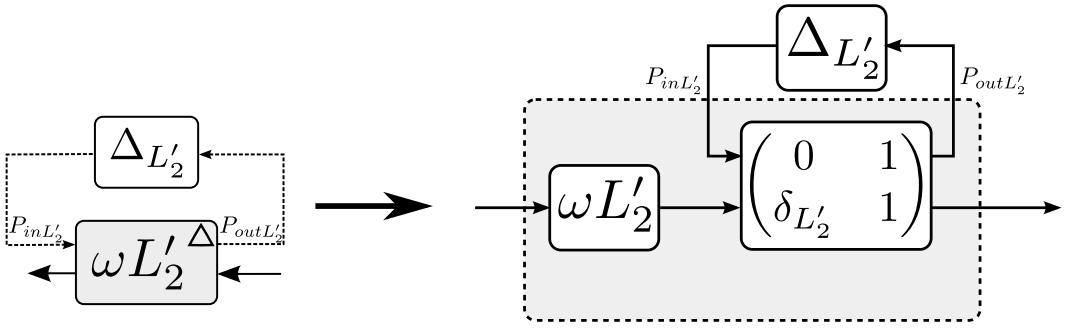

Figure 4.14: *LFT representation of uncertain block.*

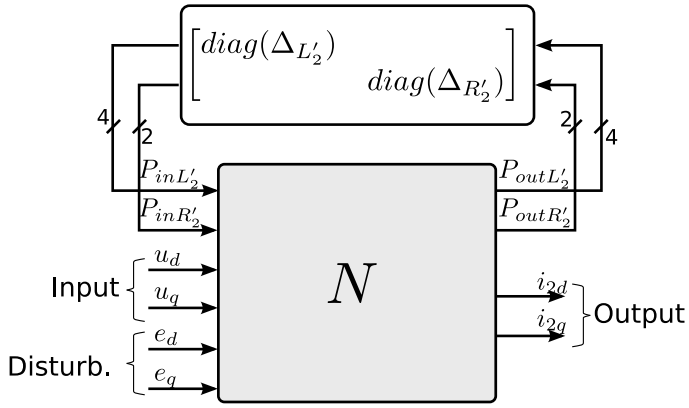

Figure 4.15: *N*Δ*-Structured model.*

4.3 Robust stability of grid converters linear current controllers

4.3.1 Introduction

Previous part of the chapter has modelled the uncertainty that is assumed to be present in the grid dynamics and the way it affects to the model that perceives the current control loop of a grid converter. This section studies how this uncertainty in the control plant model affects to the stability of a linear current controlled grid converter. Regarding this, the stability procedure that is presented here is illustrated with its appliance to three control structures that, for convenience, have been chosen to be similar to the one proposed in chapter 5 of this dissertation. It should be noted that, however, this procedure is general enough to be applied to other cases.

This study is performed applying the robust stability concept. This way, the section proposes a method for extracting reliable margins in the grid uncertain parameters that ensure stability of VSC whose current control is performed by means of linear control schemes that were not designed to present robustness properties. The restriction of the study to the linear controller case enables the use of robust control analysis framework. This framework is powerful enough to handle with this kind of issues and, additionally, it is very developed and documented and is present in popular control software tools such as Matlab.

4.3.2 Robust stability analysis theoretical background statement. Structured singular value μ

Several definitions can be found for *stability* of dynamic systems. In the case of linear time-invariant systems, those definitions are equivalent and fuse in the following:

A system is (internally) stable if none of its components contain hidden unstable models and the injection of bounded external signals at any place in the system results in bounded output signals measured anywhere in the system [Skogestad and Postlethwaite, 2005].

From the definition, a signal $u(t)$ is said to be bounded if there exists a constant $c \in \mathbb{R}^+$ such that $u(t) \leq c$ for all t. The term internal stability stresses on the need to study the

stability of all transfer functions involved in the scheme, and not only the one relating certain inputs with certain outputs.

Another result expresses the relationship between the position of the poles of a LTI system and its stability [Skogestad and Postlethwaite, 2005]:

A linear dynamic system $\dot{x} = Ax + Bu$ is stable if and only if all its poles are in the open left-half plane (LHP); that is $Re\{\lambda_i(A)\} < 0\ \forall i$. A matrix with such a property is said to be "stable" or Hurwitz.

The previous theorem gives a straightforward procedure to test the stability of a system. Although the method is exact, it does not give extra information relating perturbation in plant parameters and the corresponding pole movement. This fact limits its use for robust stability margin extraction in plants with serveral perturbation sources. Additionally, it does not give information about sensible frequencies that could generate stability problems. This limitation can be overcome by using system norms theory. A second result, known as *Small Gain Theorem* introduces the use of norm theory in the stability analysis (and synthesis):

Consider a system with a stable loop transfer function L(s). Then the closed-loop system is stable if

$$\|L(j\omega)\| < 1 \quad \forall\omega$$

where $\|L\|$ denotes any matrix norm satisfying $\|AB\| \leq \|A\| \cdot \|B\|$.

Using this result, the following theorem can be demonstrated [Zhou, 1998]:

Suppose $M \in \mathcal{RH}_\infty$ and let $\gamma > 0$. Then the interconnected system shown in Fig. 4.16 is internally stable for all $\Delta(s) \in \mathcal{RH}_\infty$ with

$$\begin{array}{lll} (a)\ \|\Delta\|_\infty \leq 1/\gamma & \text{if and only if} & \|M(s)\|_\infty < \gamma \\ (b)\ \|\Delta\|_\infty < 1/\gamma & \text{if and only if} & \|M(s)\|_\infty \leq \gamma \end{array}$$

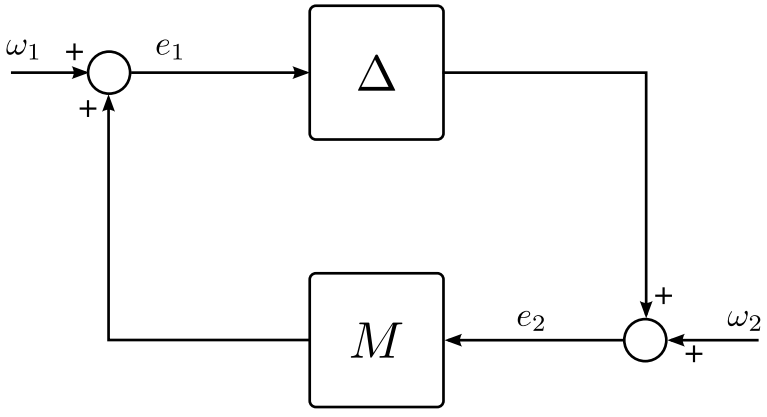

Figure 4.16: *MΔ loop for stability analysis.*

Recasting the uncertainty model obtained in previous section, and represented by means of the NΔ structure displayed on Fig. 4.15, it results easy to adapt the problem to previous theorems. If the *input* and *output* ports in the NΔ structure of Fig. 4.15 is connected to a certain current controller, a MΔ structure that matches with the one in Fig. 4.16 is obtained.

Previous theorem represents a keystone in Robust Control Theory. It should be noted, however, that despite the double implication that the theorem contains, it is, to some extent, conservative. This conservativeness is the result of the lack of restrictions in the structure of Δ block uncertainty. Without structure restrictions, the Δ matrix may represent both unstructured and structured uncertainty sources. As displayed in Fig. 4.15, the considered parametric uncertainty makes the uncertain matrix Δ to be diagonal. This restriction in the structure of the uncertain matrix induces stability margins equals or bigger than the obtained in the unstructured case. For this reason, the *Small Gain Theorem* gives a sufficient condition for parametric robust stability, but not a necessary condition. To obtain such a condition the structured singular value μ was introduced.

The structured singular value μ is defined as follows [Doyle, 1982][Safonov, 1982]:

Let M be a given complex matrix and let $\Delta = diag(\Delta_i)$ denote a set of complex matrices with $\bar{\sigma} \leq 1$ and with a given block-diagonal structure. The real non-negative function $\mu(M)$, called structured singular value, is defined by

$$\mu(M) := \frac{1}{\min\{k_m | \det(I - k_m M\Delta) = 0 \text{ for structured } \Delta, \bar{\sigma}(\Delta) \leq 1\}} \tag{4.16}$$

The Structured Singular Value (SSV) μ can be directly used for robust stability analysis. The result is a scalar frequency function. If the value of μ is less than 1 for all frequencies, the system under study achieves robust stability. The value of μ is actually more useful. If $\mu_\Delta(M) > 1$, it means that the system would only achieve robust stability if $\|\Delta\|_\infty \leq 1/\mu_\Delta(M)$. In the other case, when $\mu_\Delta(M) \leq 1$ the system would be robustly stable for the initial uncertain set, that is included in the bigger (or equal) defined by $\|\Delta\|_\infty \leq 1/\mu_\Delta(M)$. That is, μ does not only serves to study whether a close-loop system is stable, but it also gives a rich measure of the stability bounds.

Computational available tools for the calculation of the SSV are based on a numerical optimization problem. This problem is fully solved for the case of complex uncertainty matrices Δ. When the parameters are not (fully) complex, which is usually the case, the tools yield an upper and lower bound. The interpretation of these bounds is meaningful: the upper bound gives the actual achievable robust stability margin. This measurement alone does not give information about conservativeness of the result but, in any case, gives a reliable robust stability bound that always verifies. The lower bound, usually more difficult to calculate properly, is itself a measure of the accuracy of the analysis. Roughly speaking, the lower bound gives the minimum known perturbation norm that *ensures* system instability. If both values are close, it means that the analysis has been very accurate. Far values, particularly with very low lower bounds mean that the upper bound is probably very conservative.

4.3.3 μ-analysis applied to a power converter

Recasting the model described in Fig. 4.15 obtained in previous section, it is direct to build the required model for μ-analysis. By connecting the controller under study to the *input* and *output* terminals, as displayed on Fig. 4.17, the MΔ structure, needed to apply the SSV analysis, is obtained.

This section describes the adopted solution to solve some practical issues that appear in the case under study and to give some practical examples of its use.

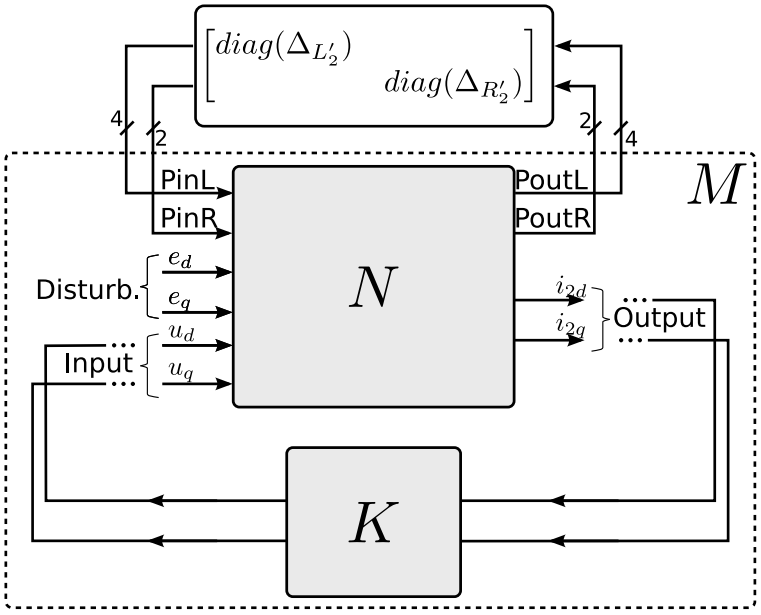

Figure 4.17: *Connection of the controller to the NΔ structure. The result is an MΔ block.*

Practical issues

- *Pure Real Analysis.*

  A plant parameter can suffer real or complex perturbations. In the case under study, the grid equivalent parameters, inductance and resistance, are affected by pure real perturbation.

  The condition for robust stability $\|\Delta\|_\infty \leq 1$ used previously, does not place restriction to the complex or real nature of the perturbation in the parameters. In general terms, the stability bounds obtained for complex perturbation are smaller than the bounds obtained for real ones. However, the analysis assuming a pure real perturbation block induces convergence problems in computational algorithms used to compute the SSV. These problems often yield a very low lower bound. Two approaches may be taken:

  – Approximate the real uncertainties by complex uncertainties, assuming the corresponding conservativeness in the obtained results.
  – Add a part of artificial complex uncertainty to the real uncertain parameters. This is a fix with good practical justification [Balas et al., 2007]. The solution is to assume that there is always some part of complex uncertainty present in the parameters. This transformation is described on Fig. 4.18.

  In this process, each real parameter has been replaced by a real parameter plus a smaller complex parameter. Rather than computing robustness margins to purely real parameters, the modified problem determines the robust stability characteristics of the system with respect to predominantly real uncertainties, though each uncertainty is allowed to have a very small complex part. This slight variation in the uncertainty model is easy to accept in engineering problems, since models of uncertainty are

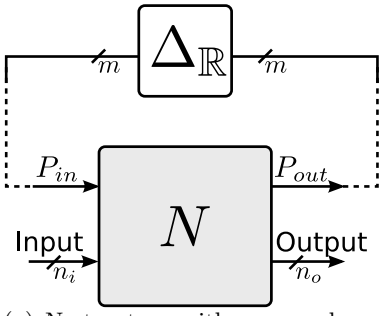

(a) N structure with pure real uncertainty.

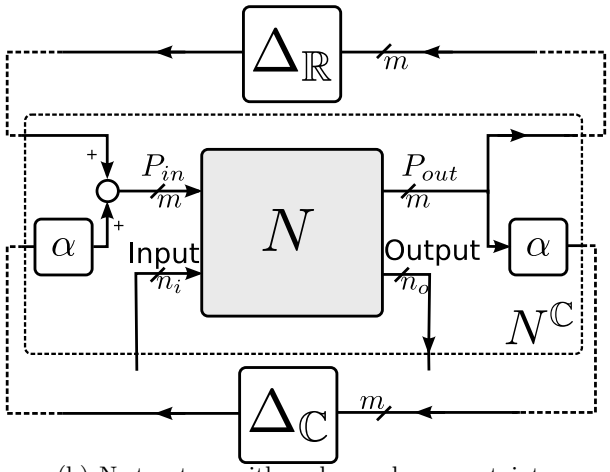

(b) N structure with real-complex uncertainty.

Figure 4.18: Complexification *of N matrix.*

rarely fixed, and small amounts of phase in coefficients of physical models can be usually explained by some underlying dynamics that have been ignored. It can also be proven that as the parameter α converges to 0, the calculated robustness margin, which is a function of α, converges to the robustness margin associated with just the original real parameters. Usually, the chosen value for α is 0.1. It should be always less than 0.5.

Expressed in matrix notation, the new $N^{\mathbb{C}}$ is the following:

$$N^{\mathbb{C}} = \begin{pmatrix} I_{m\times m} & 0_{m\times n_o} \\ \alpha_{m\times m} & 0_{m\times n_o} \\ 0_{n_o\times m} & 0_{n_o\times n_o} \end{pmatrix} N \begin{pmatrix} I_{m\times m} & \alpha_{m\times m} & 0_{m\times n_i} \\ 0_{n_i\times m} & 0_{n_i\times m} & I_{n_i\times n_i} \end{pmatrix}, \tag{4.17}$$

where m stands for the number of perturbation inputs and outputs, n_i stands for the number of plant inputs (not disturbances) and n_o stands for the number of plant outputs. If the original plant, N, has dimensions $(m + n_o) \times (m + n_i + n_d)$, where n_d stands for the dimension of the disturbance input, the complexified plant $N^{\mathbb{C}}$ has the following dimensions: $(2m + n_o) \times (2m + n_i + n_d)$.

- *μ-analysis of sampled-data systems.*

  Most computer aided control design tools provide methods to perform μ-analysis for full continuous-time schemes. There exist solutions also for parametric uncertainty in full discrete-time systems [Packard and Doyle, 1993]. Unfortunately none of both possibilities matches the requirements of the problem under study.

  The case under study is a hybrid problem. The plant to control is continuous, and more important, the uncertain model is developed in the continuous domain. It is important to remark this fact: if the uncertain plant is discretized following, for instance, a Zero Order Hold approximation procedure, the perturbation would not be restricted to the initial parameters anymore and would rather be spread to most of the elements of the new A,B,C,D state matrix. The result is a much more complex uncertain model that, additionally, has fewer relationship with the real plant. On the other hand, the final controller is designed to be executed in a digital signal processor and, thus, is developed in a discrete-time framework.

  The analysis of such a hybrid problem is not included in commercial toolboxes. However, making use of the frequency-wise computation of μ that performs, for example, the Robust Control Toolbox included in Matlab, the process can be carried out making a frequency characterization of all transfer function involved in the closed-loop problem. A simplified diagram of the used analysis-bench is represented in Fig. 4.19.

- *Frequency Sampling.*

  Due to the frequency-wise calculation of μ, the sampling of the frequency space used to make a frequency characterization of the plant under analysis can produce severe errors. If under-sampled, the analysis can give lower values to upper bound generating false robust stability results. This situation is represented in Fig. 4.20. The only way to solve this is to use an iterative process, starting with a rough analysis and including more detail where peaks are detected.

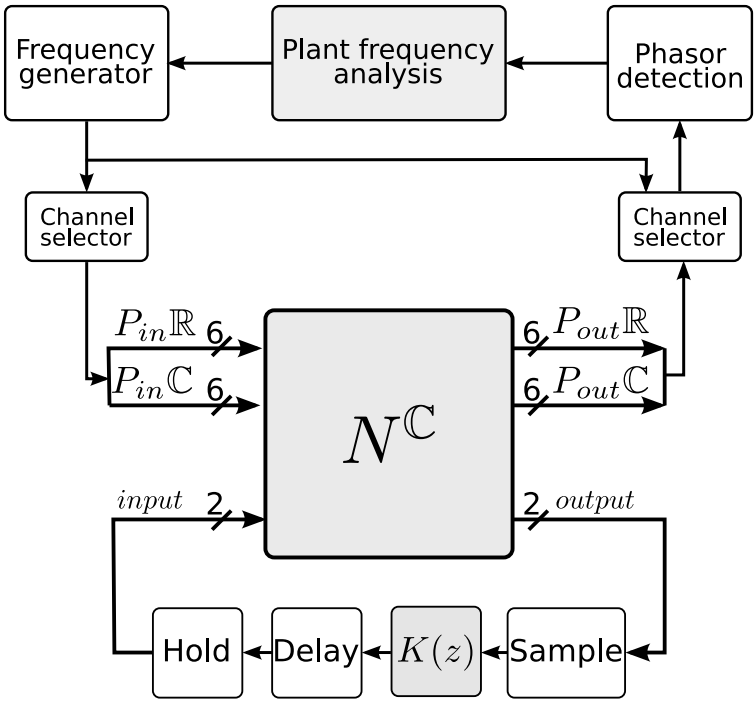

Figure 4.19: *Frequency characterization of the N-plant under study.*

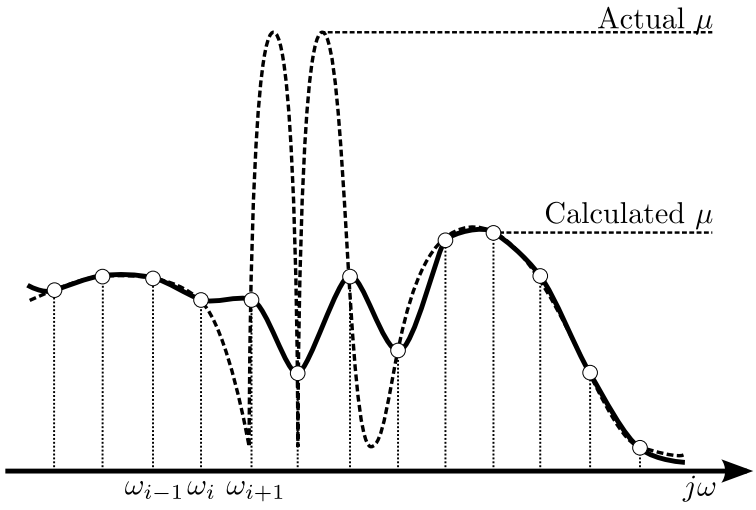

Figure 4.20: *Frequency undersampling of structured singular value μ.*

Study case. Cascaded SISO controllers

The first study case is dedicated to the control scheme proposed in [Bueno et al., 2004]. This proposal considers a feedback structure able to control the grid side current of a converter connected to the grid through an LCL filter. The proposed scheme follows the cascaded control strategy briefly described in chapter 2. This controller is applied in a syncronous reference frame (dq axes).

The internal structure of this control scheme is based on the application of cascaded SISO controllers that are individually responsible for controlling one of the state variables of the plant. More concretely, it has a first layer of two controllers responsible of stabilizing the d and q grid-inductor current components. This layer receives as inputs the external references and the grid current measurements. The output of the controllers are the d and q components of the LCL capacitor voltages. A second control level uses this references, compares them with the components of the actual capacitor voltage and generates a third reference. These references are then compared with the converter-side currents, obtaining the converter voltage final actuation signals. A block diagram of the closed-loop system is displayed on Fig. 4.21.

This control strategy is probably the most popular way to control a grid-converter with LCL filter. The main reason is the fact that the design procedure involves handling with PI and P controller design over SISO approximations of sections of the system dynamics. For this reason, the design is similar — but more complex — to an L filter control design procedure.

In practice, despite the apparent easiness of design, the channel coupling and the cascaded approximations make the constant design tricky, involving an arbitrary trial and error process. The design process is also not necessary adaptable to different grid filters sizes or structures so it has to be repeated for each particular case. Additionally, due to the approximations involved, it results very difficult to impose robustness requirements during the design, and it is difficult to extract robustness bounds after it.

This study case will analyze a particular implementation of this controller, applied to the following LCL filter:

- $L_1 = 0.5\ mH,\ R_1 = 1.55\ m\Omega$
- $L_2 = 0.25\ mH,\ R_2 = 2.08\ m\Omega$
- $C_0 = 100\ \mu F$

The considered grid was assumed to follow the model introduced at the first section of chapter 3 and present the following intrinsic parameters $L_g \in [0, 0.75mH]$ and $R_g \in [0, 0.3\ m\Omega]$. The election of the grid varying parameters is not specially important because the stability margins are — logically — independent of this parameter. The complete scheme was introduced in the μ analysis test.

After several iterations to obtain an accurate SSV, the analysis yielded the frequency function displayed on Fig. 4.22.a. The maximum value of this function is $\mu = 3.37$ which is greater than the unity and, thus, the analysis claims that the analyzed controller is not robustly stable for the defined perturbed set. Moreover, the test ensures that the system is robustly stable only for Δ blocks, with $\|\Delta\|_\infty \leq 1/\mu \backsimeq 0.296$.

Two issues must be solved before extracting stability conclusions. The first one refers to the grid intrinsic parameter (or parameters) that is making the system loose robust stability.

μ theory contemplates an special analysis case just to solve this issue. It is named *Skewed-μ* analysis and, roughly speaking, it locks all perturbed variables except one and analyzes its effect over system stability. This process is repeated with all involved uncertain variables, obtaining a good measure of which variables or variable combinations are compromising stability. For the case under study, these tests showed a clear responsibility of the grid equivalent inductance uncertainty. The second issue to solve is which sign of the real perturbation is getting the system to instability. By means of simulation, it was observed that an overestimation of the grid inductance deteriorates the system stability.

So, as a conclusion, the studied system presents robust stability to grids whose equivalent inductance $L_g \in [0.25mH, 0.48mH]$. Probably the top bound is not tight, but no more conclusions can be obtained with a single SSV analysis. To extract more information about the top bound, the uncertainty interval should be shifted up in inductance values in order to keep the low margin far enough.

Figs. 4.22.b and c show the evolution of the closed-loop system poles for different values of the grid inductance and resistance. Again, in these figures, it results clear to see that the effect of a perturbation in the grid resistance is negligible. This is ratified in Fig. 4.22.e, that shows three step responses corresponding to the nominal system, the system with $R_g = R_{g_{max}}$ and $R_g = R_{g_{min}}$. The three curves are very similar.

Regarding the inductance, however, in subfigure b, it can be observed that a negative perturbation in the grid inductance makes the system instable. It is interesting to note that, when the perturbation matches the norm extracted in the μ analysis, some system poles accurately stay on the unity circumference, signaling critical stability. This coincidence demonstrates the accuracy of the SSV analysis. In the plot below, it results clear to see how the system becomes oscillatory and very close from instability for this perturbation magnitude. The increase in the grid inductance, always inside the analyzed range, does not compromise stability.

Study case. Observer based servo-controller

The second study case is dedicated to analyze the influence of grid uncertainty over the stability of a servo-controller scheme. This servo-controlled is basically a state feedback regulator, with a plant augmentation to guarantee null perfect tracking to constant references. In order to reduce the number of system sensors, some of the state variables are estimated by means of a predictor estimator [Ogata, 1994]. Fig. 4.23 shows a block diagram of this control structure applied to the converter plant.

Although it does not represent one of the most used control schemes, its popularity is growing, particularly when designed following an LQ minimization. Several remarkable published proposals are [Alepuz et al., 2006] [Brabandere, 2006] [Huerta et al., 2008b]. One of the reasons of its increasing popularity is its design flexibility and easiness. Basically, the design process consists in selecting the position of the final closed-loop system directly giving it, or applying a minimization process that calculates it. Anyway, once some eigenvalue or cost function is selected, the process is directly applicable to different scenarios.

The controller that is analyzed in this study case is designed to present null steady state error to constant references in the grid-side currents (dq axes). State variables are estimated by means of a predictor estimator configured to have all its eigenvalues near the z-plane origin to minimize convergence time. A complex pair of poles is situated near the unity circumference so they have a dominant presence in the system and specify the whole

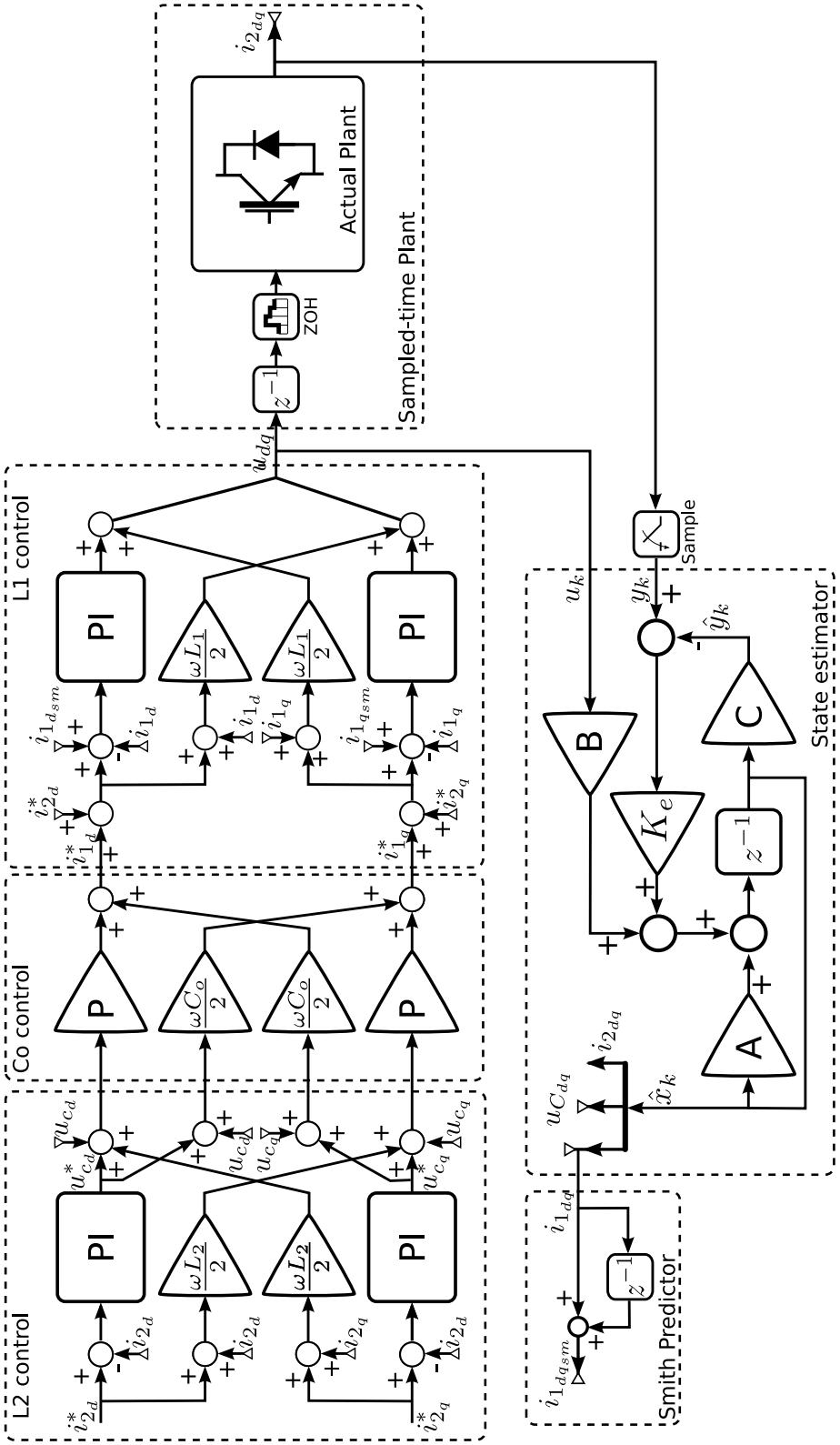

Figure 4.21: *Cascaded SISO controller block diagram.*

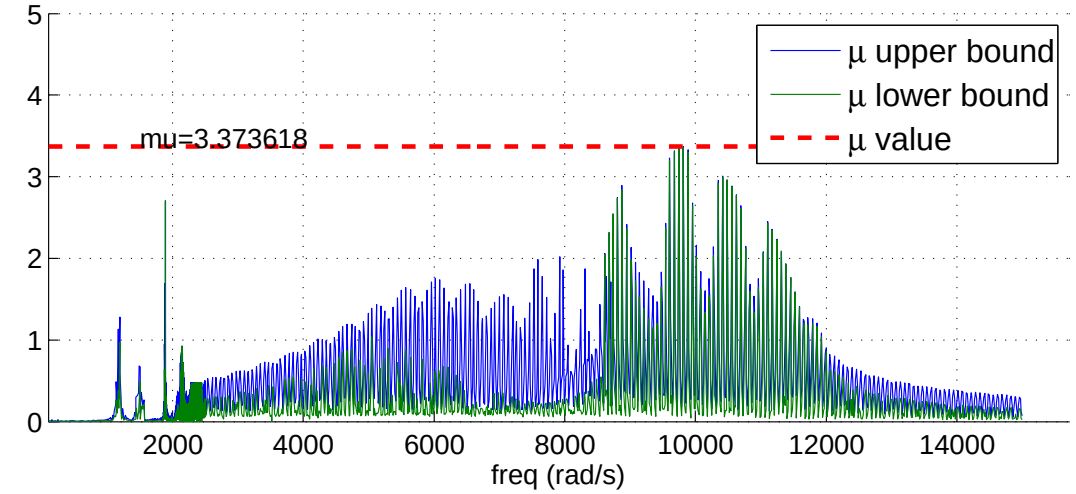

(a) μ structured singular value.

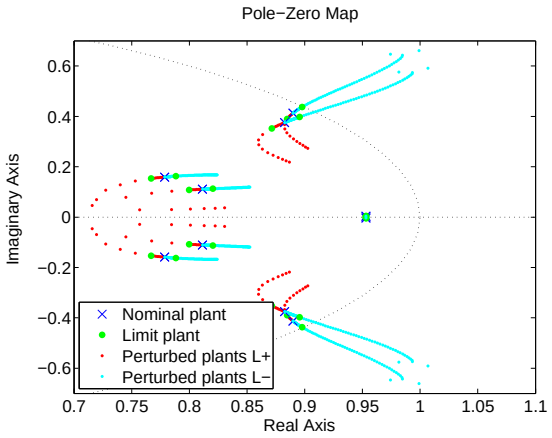

(b) Closed-loop pole disp. with perturbed L.

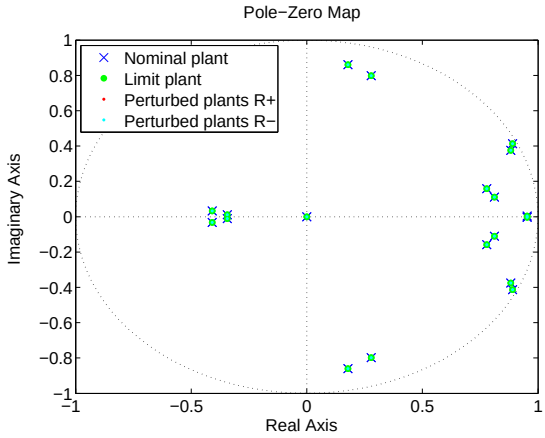

(c) Closed-loop pole disp. with perturbed R.

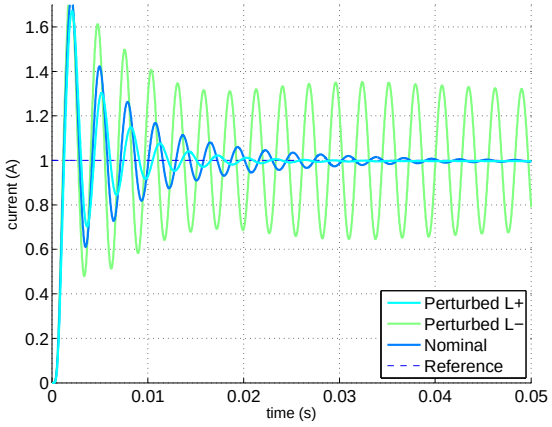

(d) Step response under different L perturbations.

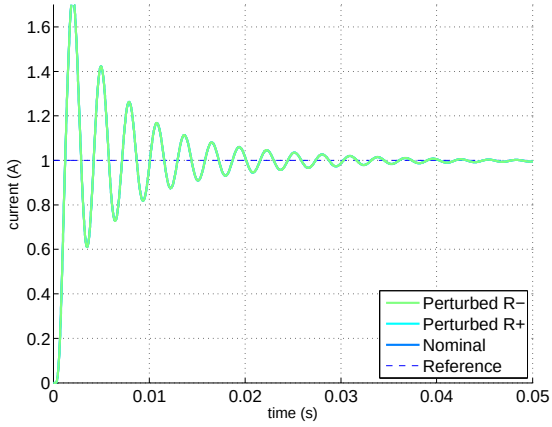

(e) Step response under different R perturbations.

Figure 4.22: *Stability analysis of a cascaded SISO-controller.*

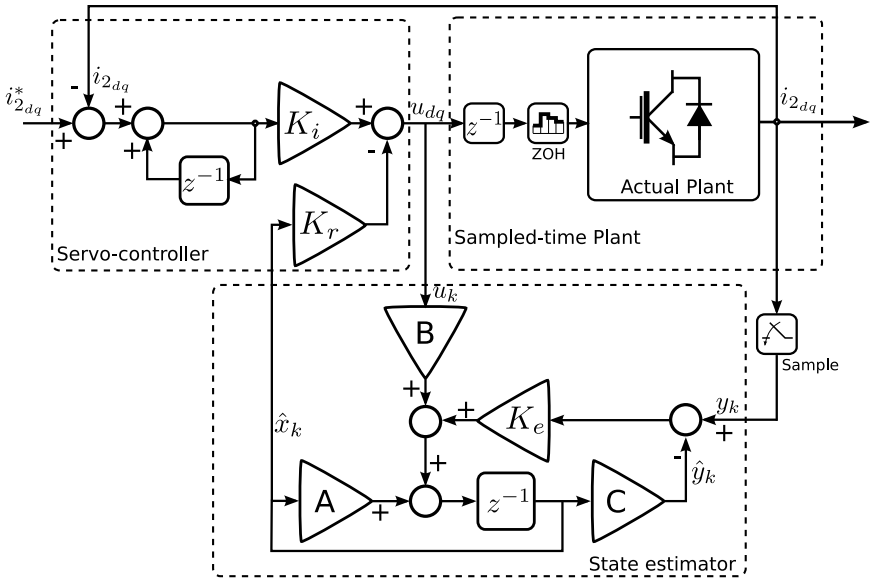

Figure 4.23: *MIMO servo-controller block diagram.*

closed-system behavior. The rest of the poles are placed as near as possible to the z-plane origin in order to limit their influence in the closed-loop system response.

The concrete LCL grid filter configuration is the following:

- $L_1 = 3.4\ mH,\ R_1 = 28.8\ m\Omega$
- $L_2 = 1.7\ mH,\ R_2 = 18.6\ m\Omega$
- $C_0 = 100\ \mu F$

and the grid is only known to have its intrinsic parameters inside the following ranges: $L_g \in [0, 15.7\ mH]$ and $R_g \in [0, 167\ m\Omega]$.

Fig. 4.24.a shows the results obtained by applying μ analysis to the described setup. Again, the obtained SSV is greater than 1, more concretely $\mu = 11.084$, meaning that the controller does not achieve robust stability in the perturbed set. As in the previous case, the skewed-μ analysis revealed that the influence of the inductance variation is more important than the resistance perturbance.

In this occasion, the uncertain interval resulted to be rather centered, and simulations showed that instability was reached both for inductance under — and over — estimation. Particularly, robust stability is ensured for the subset of plants defined by $\|\Delta\|_\infty \leq 1/\mu \backsimeq 0.09$ or, in other terms, $L_g \in [7.1\ mH, 8.5\ mH]$.

This situation was verified by plotting the pole positions of different plants in the subset. Fig. 4.24.b and c show these plots for different grades of negative and positive inductance and resistance perturbation respectively.

The plots verify the stability analysis, and show the sensitivity of the poles positions to inductance perturbation. A fact deserves more attention. Non-dominant poles, that where situated as far from the unstable zone as possible, are the poles that make the system unstable when it suffers the necessary perturbation. The dominant pole, however, remains in practically the same position for all the perturbed set.

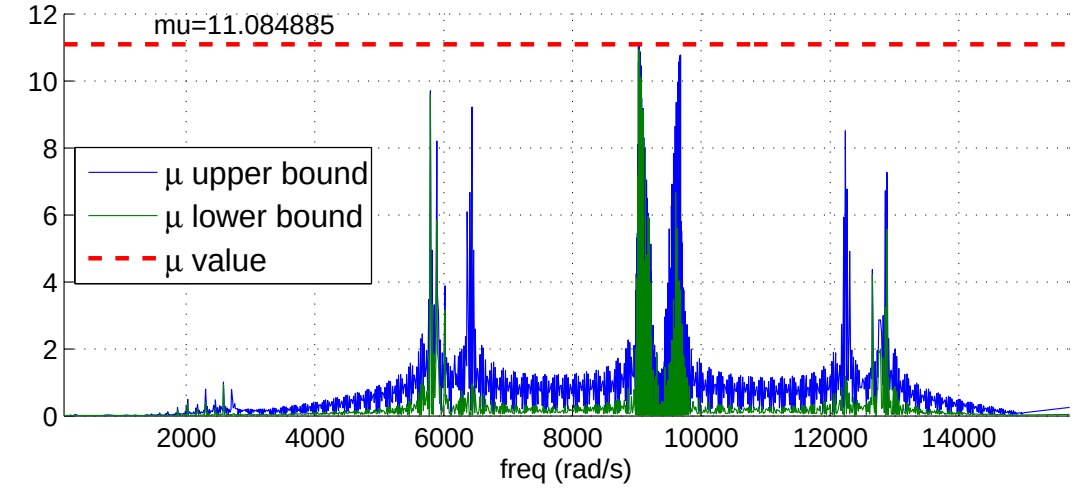

(a) μ structured singular value.

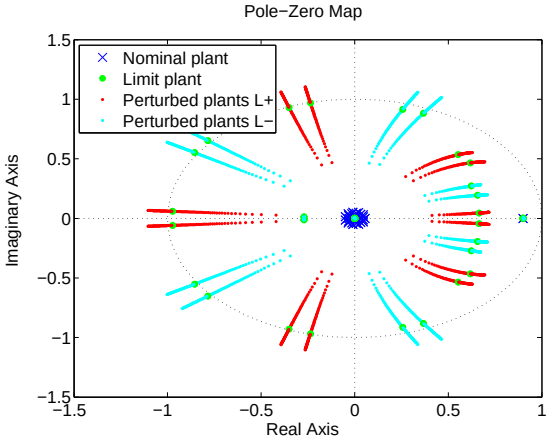

(b) Closed-loop pole disp. with perturbed L.

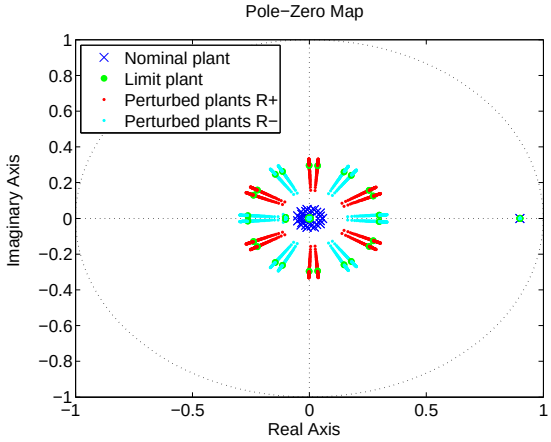

(c) Closed-loop pole disp. with perturbed R.

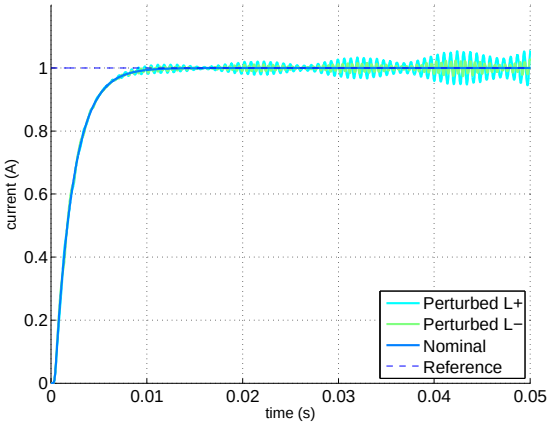

(d) Step response under different L perturbations.

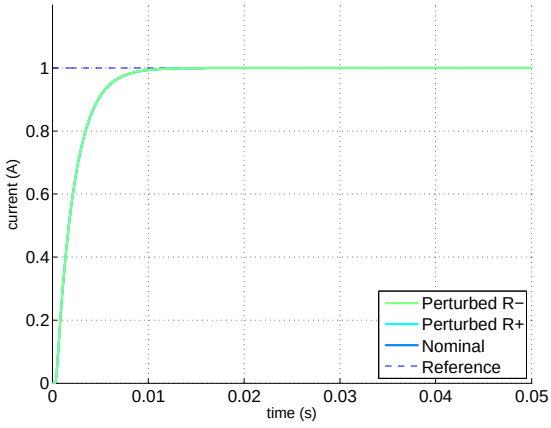

(e) Step response under different R perturbations.

Figure 4.24: *Stability analysis of a servo-controller.*

This fact is represented in the step response plot of Fig. 4.24.d. The three traces, obtained for plants sligthly more perturbed than the SSV maximum bound, show very similar plots, except for the oscillation that increases its value and finally makes the system unstable. This masking of pole movements compromises system stability in a way that can be unspected.

Study case. Robust design

Last of the analyzed cases is dedicated to study the influence of an uncertain grid over a controller that was designed to present robust stability to the considered perturbed set. The controller is a $\mathcal{H}_\infty$ suboptimal controller similar to the one presented in chapter 5 of this dissertation. The interconnection structure is displayed on Fig. 4.25.

Again, the converter under control is connected to the grid through an LCL filter whose main parameters are the following:

- $L_1 = 3.4\ mH,\ R_1 = 28.8\ m\Omega$
- $L_2 = 1.7\ mH,\ R_2 = 18.6\ m\Omega$
- $C_0 = 18\ \mu F$

and the grid is, as in the previous study case, only known to have its intrinsic parameters inside the following ranges: $L_g \in [0, 15.7mH]$ and $R_g \in [0, 167\ m\Omega]$.

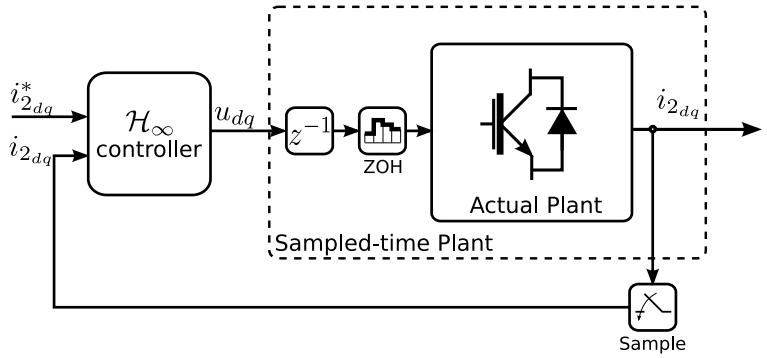

Figure 4.25: *MIMO $\mathcal{H}_\infty$ controller block diagram.*

Fig. 4.26 shows the result of applying μ analysis to the described scheme. As expected, the maximum value is lower than the unity, verifying robust stability for the predefined perturbed set. It results interesting to see the pole movements when the grid inductance and resistance are perturbed. This movement is displayed on Figs. 4.26.b and c, respectively. Firstly, as in previous occasions, it is easy to see that the closed-loop system has little influence from resistance perturbation as shown in the minimum pole movement. Regarding the inductance influence, it is interesting to see how the perturbation is mapped in nearly concentric trajectories, that do not cross with the unitary circumference.

Figs. 4.26.d and e show the steps responses for the nominal an limit inductance and resistance values of the perturbed set.

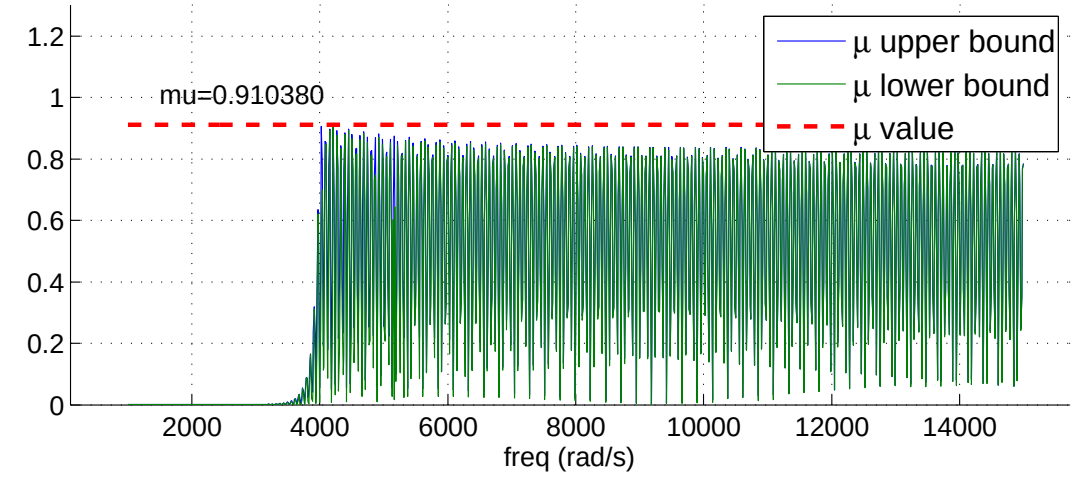

(a) μ structured singular value.

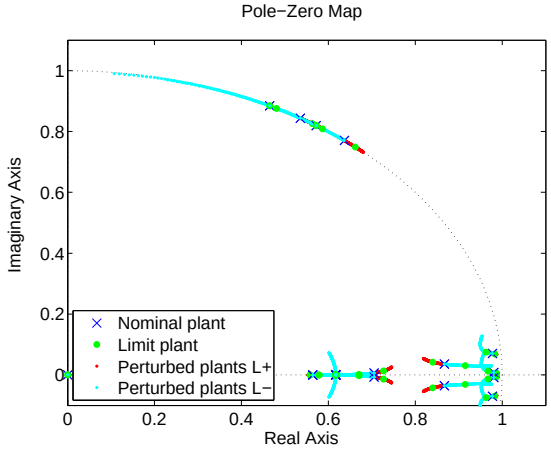

(b) Closed-loop pole disp. with perturbed L.

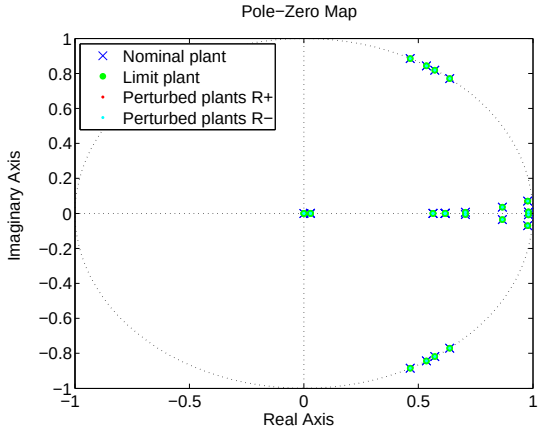

(c) Closed-loop pole disp. with perturbed R.

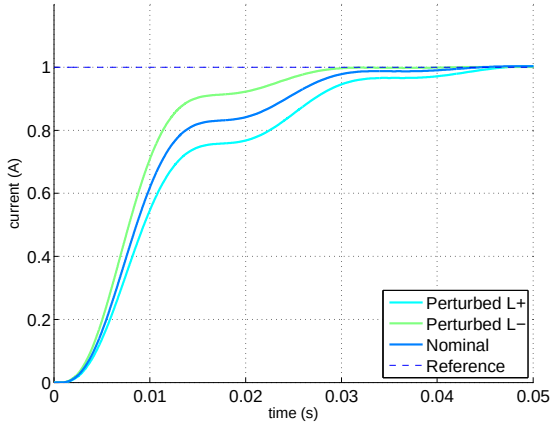

(d) Step response under different L perturbations.

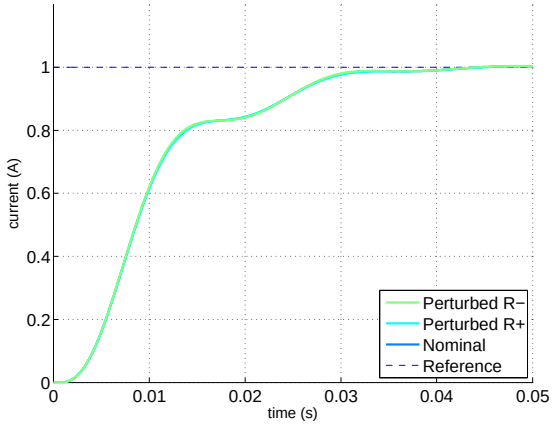

(e) Step response under different R perturbations.

Figure 4.26: *Stability analysis of an $\mathcal{H}_\infty$ − controller.*

4.4 Influence over non-linear current controllers

The application of hysteresis controllers [Bose, 1990] to grid converters (and machine drives) is a popular solution because of their robust behavior, their quick dynamics and the ease on their design. The connection of this kind of controller through higher order grid filters such as LCL structures, that would improve the related THD has not received great attention in the literature [Dahono, 2002] [Serpa et al., 2005]. Experimental testing indicates that the influence of the grid in this configuration is not negligible and can introduce quality and even stability issues.

On this direction, although hysteresis controllers have been spreadly used in real applications (mostly on L configuration), there has not been any important study analyzing the stability of these controllers. The hard non linear behavior of these controllers makes the characterization of robustness and stability as it can be done in linear controllers a difficult task.

This section will perform an analysis of the influence that a non-ideal R-L grid may have over hysteresis controllers of grid converters. This influence will be studied for the particular case of a converter connected to the grid by means of L and LCL filter. The section will describe the different possible configurations in both cases, analyzing the effect of a general $R_g - L_g$ grid. Limit values for both grid inductance and resistance are given for the L structure. In the case of LCL connection, the analysis will overview important issues such as active damping, switching behavior and stability issues.

4.4.1 L- filter configuration

As it was stated in the introduction, hysteresis control on grid converters connected to the grid through an L filter has been one of the most popular control strategies. The block diagram of this strategy is displayed on Fig. 4.27.

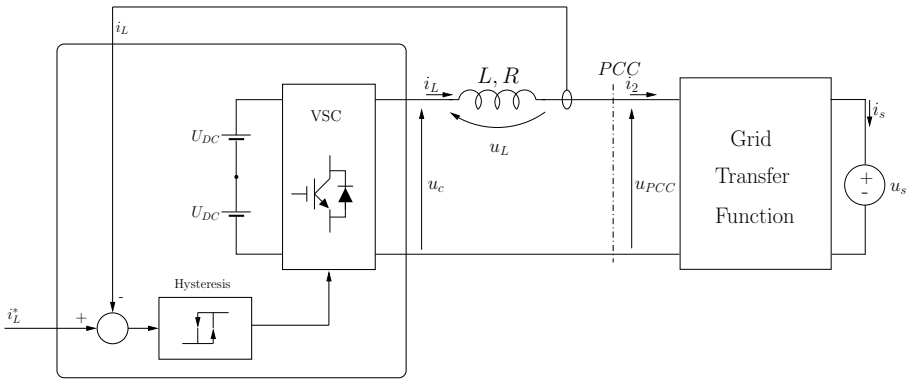

Figure 4.27: *Hysteresis controller applied to a grid converter using L filter.*

Effect of an R_g-L_g grid

The study of the effect of this kind of grid is quite direct. Let us assume that the grid presents an inductive component of value L_g, a resistive component of R_g and that the grid filter is built by means of an inductance L with an associated resistive effect of value R. An equivalent system could be built with $L_{eq} = L + L_g$ and $R_{eq} = R + R_g$.

The transfer parameters of the grid filter plus grid impedance get the expression:

$$\begin{pmatrix} U_C \\ I_1 \end{pmatrix} = \begin{pmatrix} 1 & (L+Lg)s + (R+Rg) \\ 0 & 1 \end{pmatrix} \begin{pmatrix} U_s \\ I_s \end{pmatrix} \tag{4.18}$$

Where now, the grid can be considered ideal, and, thus, all previous results about adaptivity of the hysteresis band [Buso et al., 2000] [Bose, 1990] to keep the switching frequency aproximately constant, can be directly applied.

Grid limit values

The grid transfer function $\frac{i_L}{U_{PCC}}(s)$ determines the current evolution when the converter switches to any of the poles $(U_{DC}, -U_{DC})$ of the DC-bus. In order to keep the feedbacked current $i_L(t)$ inside the hysteresis band, or in other words, tracking the reference, some limit values for both the resistive component of the grid and the inductive component of the grid must be taken into account.

Limit grid inductance value

Keeping the slope of the current above the maximum slope of the reference when the inverter switches to any of its poles is a neccesary condition that must be accomplished by the system in order to track the reference. Otherwise, the grid current would flow below the lower hysteresis band limit (or above the higher one). The consequence of this would be a reference loss until the next half-cycle of the grid arrives, resulting in signal distortion. During regular system operation, whenever the grid current reaches the lower (higher) bound of the hysteresis band, the controller should immediately switch the converter to the positive (negative) pole of the DC-bus. The grid current evolution will follow, under this situation, a positive (negative) step response given by the following expression:

$$\frac{I_L(s)}{U_L(s)} = \frac{1}{R+sL} \longrightarrow i_L(t) = \frac{U_L}{R} - \frac{U_L}{R} e^{-\frac{R}{L}t} \tag{4.19}$$

where $u_L(t)$ is the voltage across the system inductor. The instantaneous value of this voltage is obtained by simply subtracting the grid instantaneous voltage to the DC bus voltage.

The obtained waveform can be approximated by a constant slope of value:

$$\frac{di_L(t=0)}{dt}|_{t=0} = \frac{U_L}{L} e^{-\frac{R}{L}t}|_{t=0} = \frac{U_L}{L} \tag{4.20}$$

The worst situations will come in positive — negative — switchings in the converters with maximum — minimum — grid voltage because the voltage over the inductor and, consequently, the current slope, will both be minimum. Assuming a sinusoidal grid voltage of value:

$$u_S(t) = \hat{U}_S sin(\omega_{grid} t + \phi) \tag{4.21}$$

this constant slope in eq. (4.20) will get the value:

$$\frac{di_L}{dt}|_{t=0} = \frac{U_{DC} - \hat{U_S}}{L} \tag{4.22}$$

On the other hand, assuming a sinusoidal reference of instanteous value:

$$i_L^*(t) = \hat{I}_L sin(\omega_{grid} t), \tag{4.23}$$

it results clear that the maximum modulus of the reference slope happens in its zero crossings. It takes the value:

$$\left|\frac{di_L^*}{dt}\right|_{max} = \hat{I}_L \omega_{grid} \tag{4.24}$$

Note that the worst situation happens when the grid voltage sinusoid has a phase-lag of $\pi/2$ rad relative to the current reference. Finally, thus, a sufficient condition to guarantee correct operation in all conditions, is:

$$\frac{U_{DC} - \hat{U_S}}{L} > \hat{I}_L \omega_{grid} \longrightarrow L < \frac{U_{DC} - \hat{U_S}}{\hat{I}_L \omega_{grid}} \tag{4.25}$$

Fig. 4.28 shows the resulting current of an experimental hysteresis modulator with degradated output due to lack of slope in the hysteresis sawtooth waveform. Note that this degradation is related with an excess in the line inductance combined with high baseband reference frequencies (active filters) and low supply voltages.

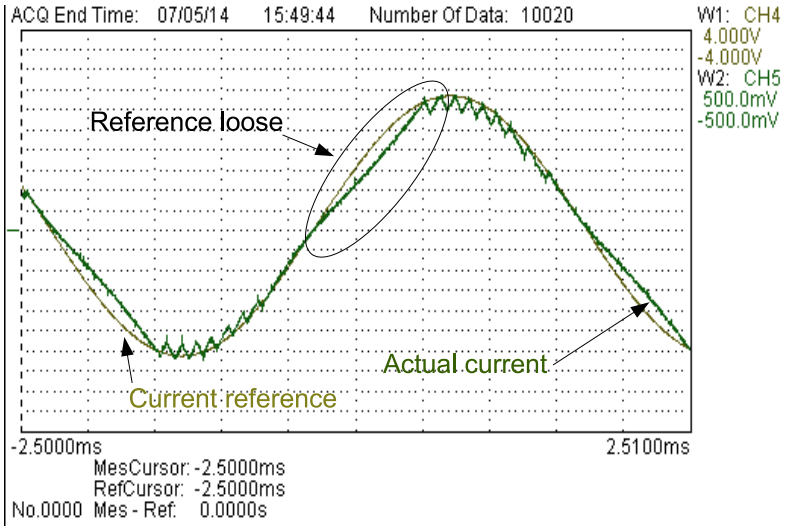

Figure 4.28: *Hysteresis controller current degradation because of inductance excess.*

Limit grid resistance value

The equivalent filter+line resistance value limits the maximum current available in the system. If the current reference is above this limit, the system will present saturation effects, creating distortion on the current signal. To ensure a correct operation of the hysteresis controller, the maximum achievable current should be several times higher than the maximum reference value. The worst situation now happens in the maximum and

minimum points of a sinusoidal current reference when it is in phase with the grid voltage waveform. The resulting condition is as follows (without signs):

$$\frac{U_{DC} - \hat{U_S}}{R} >> \hat{I_L} \longrightarrow R << \frac{U_{DC} - \hat{U_S}}{\hat{I_L}} \tag{4.26}$$

This kind of degradation offers the following typical current waveform displayed on Fig. 4.29.

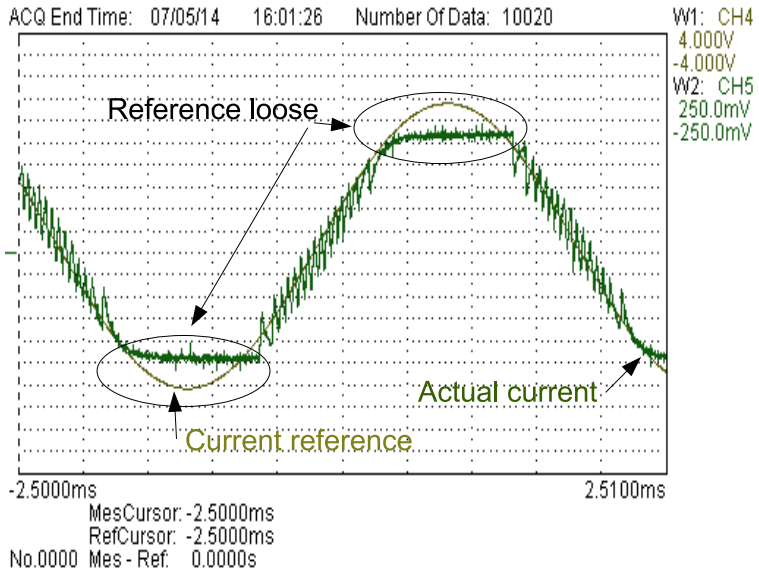

Figure 4.29: *Hysteresis controller current degradation because of resistance excess.*

4.4.2 LCL-filter configuration

As described in chapter 2, two different general control schemes have been traditionally considered when dealing with the inner loop of converters connected to the grid through LCL filter depending on the current that is desired to track a certain reference: the converter-side current or the grid-side current.

Contrary to the linear controller case, the intrinsic behavior of a hysteresis controller makes the control of the grid current i_2 not attractive: Let us assume that this hypothetic scheme is stable and is running properly. Under this ideal conditions, one could expect an evolution of the grid current oscillating in a limit cycle between two values separated by a distance that depends on the hysteresis band amplitude. The result is that far from removing ripple from grid current waveform, this hypothetic control scheme will generally result in more ripple than the one of a simple L scheme and, thus, its use is not advised. For this reason, the most suitable control algorithm will be the one of Fig. 4.30, where the feedbacked current is the converter-side one, named i_1. Its behavior will be next described.

General Operation

Assuming a set-up according to Fig. 4.30, the circuit operation can be split into two different phases. First, the hysteresis controller will track a low frequency current sinusoidal

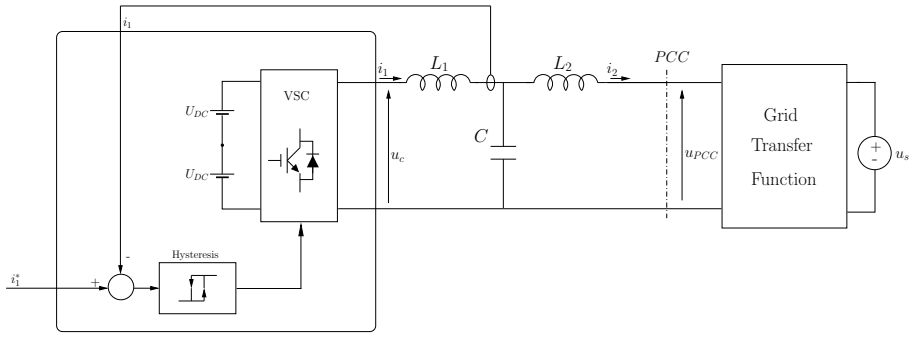

Figure 4.30: *Hysteresis controller applied to a grid converter using LCL filter.*

reference with an associated transfer function relating the voltage at the converter output with the current flowing through L1 inductor ($\frac{I_1(s)}{U_C(s)}$). The resulting $i_1(t)$ current will have two different components: one of low frequency, tracking the reference, and a high frequency sawtooth waveform due to hysteresis switching.

On a second phase, the transfer function $\frac{I_2(s)}{I_1(s)}$, relating the $i_1(t)$ current and the actual grid injected current, named $i_2(t)$, will act as a low-pass filter removing the high frequency ripple from the current and behaving as a bypass in the low frequencies used by the reference. The global scheme is depicted in Fig. 4.31.

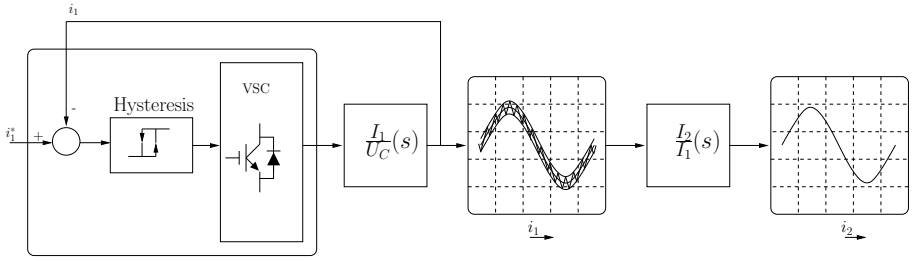

Figure 4.31: *General Operation of hysteresis on LCL topologies.*

Mathematical Model

Again, let us assume an R_g-L_g grid structure. Under this conditions, the relationship between the converter voltage and the first inductor current is described by the symbolic expression:

$$\frac{I_1(s)}{U_C(s)} = \frac{(L_2 + L_g)C_0 s^2 + (R_2 + R_g)C_0 s + 1}{D(s)} \tag{4.27}$$

with $D(S)$:

$$\begin{aligned} D(s) = (L_2 + L_g)L_1 C_0 s^3 + ... \\ ... + C_0(L_2 R_1 + L_g R_1 + L_1 R_2 + L_1 R_g)s^2 + ... \\ ... + (L_1 + L_2 + L_g + (R_2 + R_g)R_1 C_0)s + R_1 + R_2 + R_g \end{aligned} \tag{4.28}$$

On the other hand, the $i_2(t)$ and $i_1(t)$ currents will have a relationship given by the following transfer function:

$$\frac{I_2(s)}{I_1(s)} = \frac{1}{(L_2 + L_g)C_0 s^2 + (R_2 + R_g)C_0 s + 1} \tag{4.29}$$

It is important to remark that in the transfer function in eq. (4.27), the hysteresis amplitude band and the current reference waveform are the only responsible of the global system stability. Once stability is ensured, the frequency response of the transfer function in eq. (4.29) will have a better or worse effect on the actual grid current, but stability will not be compromised.

Relationship between $i_2(t)$ and $i_1(t)$

Although the transfer function showed in eq. (4.29) does not influence the system stability, it may introduce undesired oscillations in $i_2(t)$ current. This oscillation is generated by a resonance generated by the LC branch. More precisely, it is situated in the frequency:

$$\omega_{res} = \frac{1}{\sqrt{(L_2 + L_g)C_0}} \tag{4.30}$$

and presents a maximum modulus of:

$$\left|\frac{I_2}{I_1}(s)\right|_{\omega_{res}} = \frac{1}{R_2 + R_g}\sqrt{\frac{L_2 + L_g}{C_0}} \tag{4.31}$$

Resonance damping

The problem of dealing with the $L_2 - C_0$ resonance in LCL schemes has been intensively discussed in literature for linear controllers. One of the most popular techniques is an algorithm called *Active Damping* [Dahono, 2002] [Blasko and Kaura, 1997] [Liserre et al., 2006c] [Liserre et al., 2004a]. The basic idea of this algorithm is to introduce damping in the system in order to decrease the quality factor of the resonance by means of the virtual resistive elements into the plant transfer function.

The problem, when applied to hysteresis controlled converters, differs in some issues. Although this resonance does not compromise the system stability, it would introduce an oscillation in the $i_2(t)$ current that may degradate the output current quality. The active damping algorithms are perfectly suitable for these systems but they should be restricted to some limitations:

- Any virtual element added to the system should be applicable as a modification over the current reference as there is no possibility to modify any other controller behavior in an hysteresis system.
- The current reference modification should be possible to implement in a computational platform. Pure signal derivatives should be avoided.
- L_1 damping is not a possibility in hysteresis controllers. This kind of damping, although useful in other families of controllers, will only limit the maximum available current on the $\frac{I_1(s)}{U_C(s)}$ loop, without modifying the resonance behavior of the resonance in eq. (4.29) (see eqs.(4.30) and (4.31)).

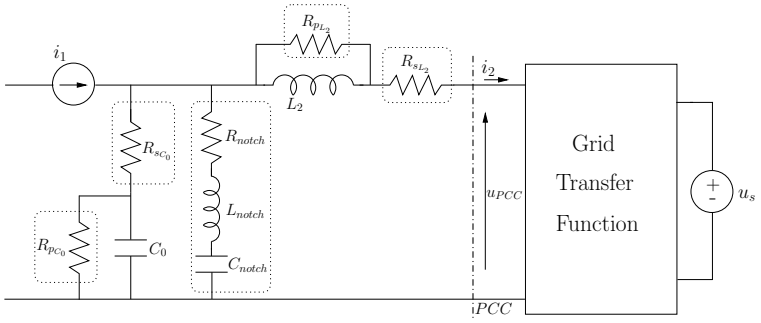

Figure 4.32: *Different active damping possibilities*

Table 4.1: *Active damping algorithms.*

Active element	Implementation	Derivative	Phase-lag
R_{pC_0}	$i^*_{1_{damp}} = i^*_1 - \frac{u_{C_0}}{R_{p_{C_0}}}$	-	Yes
R_{sC_0}	$i^*_{1_{damp}} = i^*_1 - \frac{di_{C_0}(t)}{dt} R_{s_{C_0}}$	Yes	-
R_{pL_2}	$i^*_{1_{damp}} = i^*_1 - \frac{u_{PCC} - u_{C_0}}{R_{p_{L_2}}}$	-	-
R_{sL_2}	$i^*_{1_{damp}} = i^*_1 - \frac{di_2(t)}{dt} R_{s_{L_2}} C_0$	Yes	Yes
$R_{notch}, L_{notch}, C_{notch}$	$i^*_{1_{damp}} = i^*_1 - \frac{u_{C_0}}{R_{notch} + sL_{notch} + \frac{1}{sC_{notch}}}$	-	-

- The introduction of active elements on the LCL structure will modify the phase and amplitude between the current reference and the $i_2(t)$ actual current at the reference frequencies (i.e. 50 Hz). Although this phase-lag could be corrected *a posteriori*, combinations with the minimum impact are preferred. This problem becomes more severe in high frequency current reference applications as for example active filtering devices.

Some typical active damping combinations are shown in Fig. 4.32 and briefly described in table 4.1. Their effect on output current is depicted in Fig. 4.33.

Effect of a generalised R_g-L_g grid

A variation in the value of R_g and L_g affects the hysteresis current controller in an LCL as it modifies the transfer functions involved in the process. Eqs. (4.30) and (4.31) give exact expressions for the frequency and magnitude of the resonance due to the interaction between C_0 and L_2. These expressions closely depend on the value of the grid parameters. More concretely:

- An increase in the inductive component of the grid will generate a decrease in the resonance frequency and an increase in the magnitude of the resonance due to the increase in the quality factor of the resonance.

- An increase in the resistive component of the grid will keep the resonance frequency

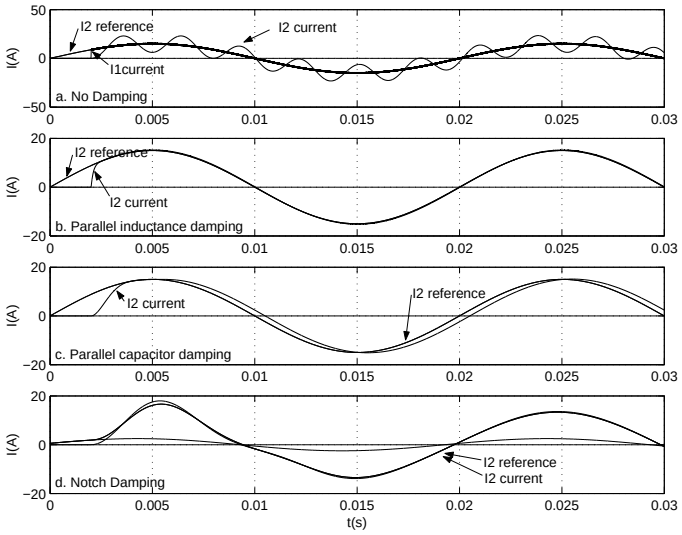

Figure 4.33: *Active damping algorithms effect.*

untouched but will decrease the quality factor of the filter, decreasing the magnitude of the resonance.

Next subsections describe some particular aspects where this impedance value has a remarkable influence.

System stability

The global stability necessary and sufficient condition of this kind of hysteresis controlled systems (also known as *Relay Feedback Systems*) remains an open and active research topic of hybrid and nonlinear automatic control theory. Several theoretical approaches have been reported in the specialized literature as [Goncalves et al., 2001] [Iannelli et al., 2003] [Johansson and Rantzer, 1996]. This section aim is to give some practical guidelines to avoid stability issues:

- The desired switching band of frequencies should be kept well above the LCL resonance in order to obtain a proper filtering of the switching components. A change in the grid equivalent impedance values is easy to be taken into account in this case: the most restrictive situation regarding the grid inductance is in this case a null grid equivalent impedance (maximum resonant frequency); the designer should design the filter assuming a null grid inductance values; its actual value will always be higher.

- Severe stability issues may occur if the resonant band of the transfer function described in eq. (4.27) interferes with the current reference band. Fig. 4.34 shows a simulation of a hysteresis controlled converter tripping due to this interference. In this ocassion, an uncontrolled increment in the grid equivalent inductance would push the resonance frequency to lower values so a proper design should be conservative in this issue. The problem is more severe, again, in the case of active filtering application where the reference frequencies are higher.

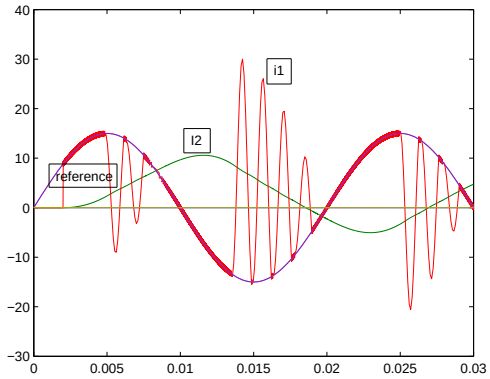

(a) Unstable behavior.

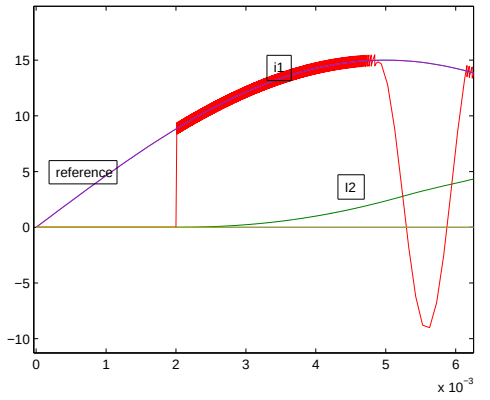

(b) Detail.

Figure 4.34: *Reference-resonance bands interaction.*

An increase in the resistive component of the grid will not represent a stability problem because the resonance frequency will remain untouched and the quality factor of the filter will be smaller.

Switching behavior

One of the key issues when dealing with a hysteresis current control scheme is the relationship between the grid connection filter, the operation point and the resulting switching frequency; or in other words, how to keep the switching frequency relatively static while tracking a sinusoidal reference. As long as the grid inductance and resistance modify the transfer function of the hysteresis control, $\frac{I_1(s)}{U_C(s)}$, they modify the switching behavior of the system as well.

As long as the grid inductance is kept in a safety range according to the stability guidelines given in previous subsection, the $\frac{I_1(s)}{U_C(s)}$ step response will be nearly a constant slope inside the hysteresis band and thus, all adaptive algorithms from L connection, except the ones that explicitly use a concrete value of filter inductance and resistance, will be fully directly available. In addition, as it is displayed in Fig.4.35, in the switching zone of the

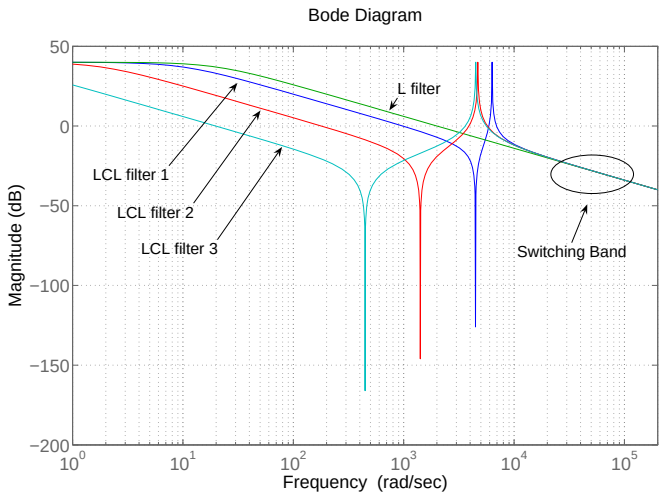

Figure 4.35: *L dynamic equivalent of an LCL hystereis controlled system.(L_1=0.5mH, C=100uF, L_{2_1}=0.5mH, L_{2_2}=5mH, L_{2_3}=50mH)*

bode plot of $\frac{I_1(s)}{U_C(s)}$, the system behaves approximately as an L-R filter structure where the L equivalent gets a value of L_1 and the R equivalent has a value of R_1. This last feature makes the LCL connection quite attractive, because the L_2 and R_2 variation is somehow isolated from the switching behavior of the system.

$L_2 - C_0$ resonance damping

This variation in the grid resistance and inductance also directly affects the active damping schemes that have been adopted in the controller. From a point of view of robustness of the controller, the increase of the resistive component will only generate an increase in the time constant of the plant making the system behave slower. More critical is the increase in the inductive component: if the damping algorithm was not correctly rated, some oscillations could appear in the grid current.

To compensate this situation, the solution should be different depending on the damping algorithm that is being used in the controller. If a pure resistive damping has been chosen, a simple increase in the damping will compensate the resonance displacement. The value of this damping is a trade between controller robustness and the speed of the system response: high damping ratios will admit higher inductance values without presenting oscillations in the grid current but will make the global system slower. If the active damping is being applied by a notch filtering scheme, the filter parameters will have to be modified in order to decrease the filter frequency and increase the quality factor and its gain. This modification will nearly not modify the system response speed, but it is not trivial. Adaptive algorithms could be suitable for this situation.

4.5 Conclusions

Uncertainty in the grid dynamic behavior inductance and resistance affects negatively to the connection of converters to the grid controlled. This chapter has analyzed its effects

on linear and non-linear current control schemes.

For the linear case, the analysis has been developed in using the SSV μ analysis framework. To that end, the uncertainty in the grid dynamics has been modelled as a parasitic impedance representing a grid equivalent inductance and resistance that are uncertain to some extent. This uncertainty in the modelled grid integrates into the converter model that faces the linear current controller. A complete NΔ model has been developed.

This NΔ model is the basis of the μ stability analysis that has been later applied. Several practical issues, that are found when applying the analysis to the current control of a power converter, are described. Additionally, this procedure has been tested on three standard current control configuration applied to LCL grid connected converters: a cascaded control approach based on simple SISO controllers, a servo-controller approach and an $\mathcal{H}_\infty$ approach.

The main conclusions extracted from these study cases are:

- The movement of the poles when the grid equivalent impedance is under — or over — estimated is unpredictible and significantly varies with each particular control scheme or filter configuration.

- Sensitivity of poles is also unpredictable. Poles aparently far from the unstable region can quicly move towards it with small plant perturbations. Other poles by design much closer to the unity circumference may be much more static or follow non-dangerous trajectories.

- Previous facts recommend to apply some kind of robust stability analysis to controllers that where not designed with robustness constraints.

μ analysis reveals as a very useful tool for the evaluation of the controllers robustness. Explored examples demonstrated a good accuracy. Additionally, it is very easily scalable to uncertainty in other parameters, as for example, the converter-side inductor, grid fundamental frequency, LCL capacitor or in unmodelled dynamics of the device.

In the non-linear case, the analysis is restricted to hysteresis controllers. Two scenarios are analyzed: the connection through an L grid filter and through an LCL filter.

In the case of the L filter, an increase in the value of the grid inductance or resistance could compromise system stability for values above the limits showed in the study.

In the case of an LCL filter, this grid variation could also affect system stability by moving the $L_2 - C_0$ resonance. Additionally, resonance damping methods and switching frequency equalization algorithms should be designed to compensate variation in the resonance values. However, the study of the LCL global stability is complex and falls outside of the scope of this dissertation.

Once uncertainty in the grid has been demonstrated to have a not negligible influence over the current control loop of grid converters, an inverse problem may be formulated: given a previously defined uncertainty range in grid parameters, is it possible to design a controller valid for the whole set. Two main approaches may be taken:

- The application of an adaptive control scheme able to adapt to each grid belonging to a considered uncertain set. This solution would yield good results. Unfortunately none of the proposed grid identification algorithms present the minimum requirements to ensure global stability in such a scheme. The presented proposal, for instance,

needs a stable current controller in order to make a correct estimation and, thus, is not valid for this purpose. However it represents a promising topic and, for this reason, it is considered as one of the main future work lines of this dissertation.

- The application of a control scheme designed to stabilize a previously defined set of plants. This approach is valid without the need of an identification scheme and produces high quality controllers able to accept uncertainty not only in certain model parameters (as happens in the adaptive control case) but also from other unstructured sources as, for example, actuators, unmodelled dynamics, etc. The design of such a controller is the topic of the next chapter of this dissertation.

Chapter 5

Grid current control

This chapter proposes two different approaches to perform control of the injected current by power converters connected to the grid by means of LCL filters. The first one is based on Linear Quadratic optimization, which is preferably used when state variables measurements are available. The second one gives a robust stability design procedure suitable for cases where state variables have to be estimated.

5.1 Introduction

The previous chapter of this dissertation has dealt with the influence that uncertainty in the dynamic of the grid where a converter is connected exerts on the stability of the current controller loop of a grid converter. To that objective, the chapter has proposed the use of the SSV μ to perform a robust stability analysis.

This proposed analysis procedure is able to accurately extract the security margins in the grid equivalent impedance and resistance that ensure stability of an scheme controlled with a controller that was not designed with robustness constraints.

The approach of the present chapter is the complementary. Once it has been demonstrated that grid dynamics may generate stability issues in the current controller, the present chapter proposes a design procedure that, given a set of possible grid dynamics, extracts a controller that ensures stability of the closed-loop system.

To that end, the chapter actually proposes two controllers. The first controller, an LQ based controller, is given as it represents an easy design procedure, suitable for different filter configuration that often produce satisfactory results. It additionally presents some robustness properties and settles the discrete-time framework necessary to perform the second procedure.

The second proposal is a control design procedure that, given a range of values for the grid intrinsic parameters, minimizes the influence of the grid from the *disturbance rejection* point of view and ensures some given performance criteria. This situation is depicted on Fig. 5.1.

Chapter 2 made a review of existing current controllers regarding different criteria: (i) according to the control nature, (ii) according to the control reference frame, (iii) according to the control structure, (iv) according to the controlled variable, and (v) according to the control objective. The control proposals presented in this chapter are designed following the next premises:

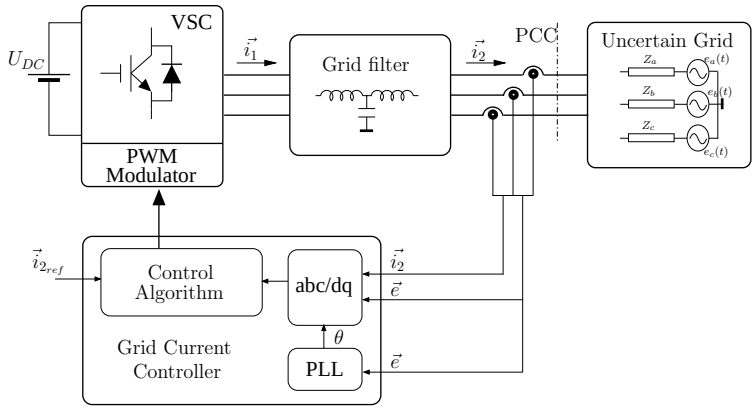

Figure 5.1: *Control problem block diagram.*

- Regarding the control nature, the controllers proposed in this chapter are designed in a linear framework. The linear design procedure offers a large set of control possibilities already proposed in control theory and, more interesting, allow to add robustness requirements to the control specifications or to a-posteriori analyze the achieved system robustness.

- Regarding the control reference frame, the proposal is formulated in a *dq* synchronous reference frame. This transformation allows to consider constant references for the controlled outputs.

- Due to the *dq* transformation, the plant under control is transformed into a MIMO system. For this reason, the control is faced from a MIMO point of view.

- The controlled variable is desired to be the grid-side current, named $i_2(t)$. The direct control of this variable gives actual injected current closed-loop control even in the presence of uncertainty in the grid dynamics.

- Regarding the control objective, both proposals presented in this chapter present different motivations. The LQ design procedure presented first is an energy optimization driven procedure although it partially presents some fair robustness properties when all state variables are available.

Additionally, the grid phase reference, θ, is assumed to be known and may be estimated from the voltage measurements by means of a *Phase Lock Loop* (PLL). This phase will be used to synchronize with the grid angle, and translate the whole control problem into a rotating synchronous reference frame by means of the Park transformation [Krause et al., 1995].

Finally, regarding the actual converter configuration, the whole development will be illustrated by the results obtained for the particular case of the experimental set-up used for this dissertation. The set-up most important characteristics are shown in table 5.1. This platform will be described in detail in chapter 6.

The grid equivalent dynamics are uncertain and assumed to follow the model described in chapter 4. Only a rough knowledge is available:

- $L_g \in [0, 15.7\ mH]$

- $R_g \in [0, 167\ m\Omega]$

The selection of this margin is not supported for any study of grid impedance variation in the actual power system. These data would improve the study interest, but they are unfortunately difficult to obtain and usually require a big infrastructure. For this reason, the uncertain margins where deliberately chosen to be rather high. This way, the results here provided could be directly applied to less uncertain scenarios or be modified following the design rules that are presented below to obtain tighter results.

The present chapter is divided into two main sections.

The first section, named *LQ grid current control*, is dedicated to describe a LQ servo-controller design process for cases lacking tight robustness requirements and where all the measurements are available. The section begins describing the adopted discrete approximation method, and the way to introduce computational delays in the plant model. After that, the LQ minimization rule for the servo-controller application is described. For cases where state variables are not measured and robustness is not an issue, the most popular estimation techniques and the way to introduce them in the servo-controller scheme are described. Second part of the section is dedicated to study the algorithm implementation for its application to a power converter. The section gives some thumb-rules and tips to correctly chose the LQ design matrices Q and R. The proposed estimators are evaluated under different noise conditions.

The second section, named *Output feedback grid current robust control*, is dedicated to describe a Loop-shaping $\mathcal{H}_\infty$ design procedure for cases where the robustness requirements are tight and the only available measurements are the output variables. The section starts with a brief description of the theoretical background and the systematic design procedure that is used in the problem. Again, the second part of the section is dedicated to describe the application of this control algorithm to the current control of a grid converter. First pages are dedicated to describe the effects of grid equivalent impedance uncertainty over the maximum singular values of the plot with the aim of getting criteria to design sensible loop shaping functions. These shaping functions are described later. Once the controller is practically designed, it is verified and analyzed by means of ν-gap *distance*. Next subsection is dedicated to analyze the achieved final close loop performance for both reference tracking and disturbance rejection in the presence of voltage dips, by means of frequency analysis and experimental testing. Last subsection elaborates on some implementation issues as final DSP programming structure and anti-windup protection.

Experimental waveforms of the methods obtained with the set-up presented in chapter 6, controlled by the methods presented in this chapter, are shown on the last section of

DC-Bus Voltage:	700V
Switching technology:	IGBT
Control sampling time:	200μs
PWM switching frequency:	5kHz
Filter inductor 1 parameters (L_1, R_1):	L_1=3.4mH, R_1=28.8mΩ
Filter inductor 2 parameters (L_2, R_2):	L_2=1.7mH, R_2=18.6mΩ
Filter capacitor (C_o):	18μF
Grid voltage:	230Vrms

Table 5.1: *Set-up parameters.*

the chapter.

Finally, the chapter will end with a summary of the extracted conclusions.

5.2 LQ grid current control

5.2.1 Introduction

This section describes the application of the LQ optimal control theory to the control problem described in previous sections. The LQ controller theory reached maturity in the 1960's. It was mainly developed to cope with the incoming problems in space control and rocket guidance with minimum fuel consumption. This kind of problems could be well defined and easily formulated as *optimization* problems. Although other control problems are not so easily suited into the LQ framework, its use is still a recurrent option when dealing with MIMO problems.

In general terms, LQ regulators present the following attractive features:

- They yield satisfactory results when applied to Linear Time Invariant processes if an accurate plant description is available.
- Many of the most popular control design procedures are either restricted to the SISO case or their application to the MIMO case makes them loose their major advantages. LQ designs behave well in the MIMO case, and the design criteria are easy to handle with.
- The procedure naturally extends to discrete-time problems. Additionally, it results easy to introduce computational delays in the model avoiding part of their negative effect.
- Although it does not represent a robust design procedure, in the case that all system states are directly measured, an thus, a state estimator is not used, it presents some interesting robustness properties that give it its versatile character.

These reasons make the LQ servo-control an attractive idea, at least as a first approximation to the problem. Additionally, it serves as a good starting point to check if all initial assumptions have been sensible and the design method presents a high adaptability rate being easy to apply to the control of other state variables. The method hereby presented has been published by the author in [Huerta et al., 2008a] and [Huerta et al., 2008b].

5.2.2 Discrete-time LQ Control design procedure

Consider a continuous linear time-invariant system described by the state space equations:

$$\begin{cases} \dot{x}(t) = Ax(t) + Bu(t) \\ y(t) = Cx(t) + Du(t) \end{cases} \tag{5.1}$$

where $A:\ n \times n$, $B:\ n \times m$, $C:\ p \times n$, $D:\ p \times m$ are the matrixes in eq. (5.1).

A discrete-time *Zero Order Hold* equivalent, with sample time T_s can be obtained following the state space equations [Ogata, 1994]:

$$\begin{cases} x_{k+1} = Gx_k + Hu_k \\ y_k = Cx_k + Du_k \end{cases} \tag{5.2}$$

where

$$G = e^{AT_s} \quad H = \left(\int_0^{T_s} e^{A\tau} d\tau \right) B \tag{5.3}$$

As stated in chapter 4 and justified in chapter 6, due to the final implementation of the electronic control platform, one computational delay appears in the input of the system. This delay is easily modelized, building a system with state space equations:

$$\begin{cases} x_{d_{k+1}} = G_d x_{d_k} + H_d u_k \\ y_k = C_d x_{d_k} + D_d u_k \end{cases} \tag{5.4}$$

where,

$$x_{d_k} = \begin{bmatrix} x_k & v_k \end{bmatrix} \tag{5.5}$$

$$G_d = \begin{bmatrix} G_{nxn} & H_{nxm} \\ 0_{mxn} & 0_{mxm} \end{bmatrix} \tag{5.6}$$

$$H_d = \begin{bmatrix} 0_{nxm} \\ I_{mxm} \end{bmatrix} \tag{5.7}$$

$$C_d = \begin{bmatrix} C_{pxn} & D_{pxm} \end{bmatrix} \tag{5.8}$$

$$D_d = \begin{bmatrix} 0_{pxm} \end{bmatrix} \tag{5.9}$$

Note that this state space formulation introduces m more states.

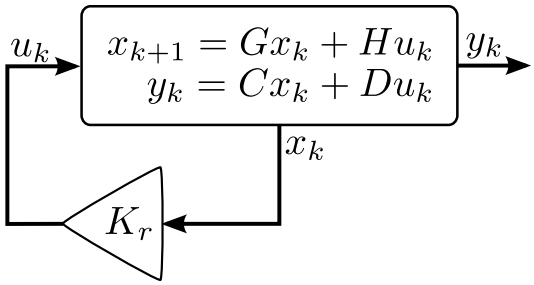

Figure 5.2: *LQ regulator basic scheme.*

Servo-controller application

The standard LQ regulator framework is formulated to perform a state feedback in order to keep the states properly regulated as shown on Fig. 5.2. This structure lacks several important features as reference inputs and null tracking error in the presence of plant model mismatch or output disturbance signals. Some modifications can be made in the control scheme in order to include these features. Following the internal model principle [Francis and Wonham, 1976], a null tracking error can be obtained introducing in the loop

function (i.e. the transfer function between the error signal and system output) infinite gains elements at the desired frequencies. In the application under study, it is desirable to have null error to a step reference change in all the input channels. For this reason, discrete-time integrators are included in the diagram. This control scheme is displayed on Fig. 5.3.

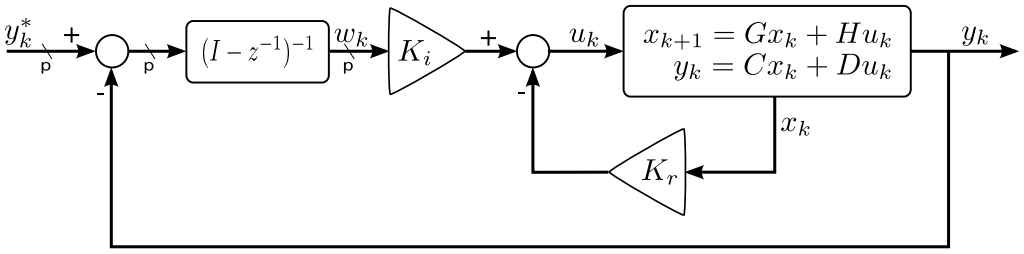

Figure 5.3: *Servo controller structure for step reference tracking.*

Although this scheme is different from the LQ regulator one, a simple operation can make it suitable for this kind of problems. Let us consider a new state vector $\tilde{x}_k$ built as follows:

$$\tilde{x}_k = \begin{bmatrix} x_k^T & w_k^T \end{bmatrix}^T, \tag{5.10}$$

where w_k is a column vector that includes in the system the new integrated variables (see Fig. 5.3). Similarly, a new virtual state space system can formulated with the following state space equations:

$$\begin{cases} \tilde{x}_{k+1} = \tilde{G}\tilde{x}_k + \tilde{H}u_k \\ y_k = \tilde{C}\tilde{x}_k + Du_k \end{cases}. \tag{5.11}$$

Given

$$\tilde{G} = \begin{bmatrix} G & 0 \\ -CG & I \end{bmatrix}, \quad \tilde{H} = \begin{bmatrix} H \\ -CH \end{bmatrix}, \quad \tilde{C} = \begin{bmatrix} C & 0 \end{bmatrix}, \tag{5.12}$$

where variables x_k, u_k, y_k, G, H, C and D are as defined in eq.(5.2) (note that the process also allows the existence of pure delays in the plant inputs), the matrices K_r and K_i in Fig. 5.3 can be obtained as parts of the resulting $\tilde{K}_r$ from a regulator solution for the system in 5.11 [Ogata, 1994]:

$$\tilde{K}_r = \begin{bmatrix} K_r & -K_i \end{bmatrix}. \tag{5.13}$$

LQ optimization rule

An optimum linear quadratic regulator can be obtained by solving the Riccati equation associated with the extraction of the regulator matrix $K = K_{LQ}$ that minimizes the quadratic performance index [Ogata, 1994]:

$$J = \frac{1}{2}\sum_{k=0}^{\infty}\left(\tilde{x}_k^T Q \tilde{x}_k + u_k^T R u_k\right), \tag{5.14}$$

where Q is a positive semidefinite Hermitian matrix and R is a positive definite Hermitian matrix, which determine the quadratic cost weights on the state vector $\tilde{x}_k$, and input vector u_k, respectively. The i^{th} diagonal element of Q, named $q_{i,i}$, determines the direct weight on the i^{th} state. Note that these two matrices are the only design parameters that need to be chosen. Except in classical energy optimization problems, it is not trivial to choose them and this process usually requires some trial and error iteration. Later in this section, some empirical criteria to set these weights in the application under study, will be given.

LQ regulator robustness properties

When no state estimation is performed, i.e. all the state variables are measured, an LQ controlled system is known to present some robustness characteristics if the weight R is chosen to be diagonal [Kalman, 1964][Safonov and Athans, 1977][Skogestad and Postlethwaite, 2005]. More concretely, under these previous assumptions, the system sensitivity transfer function, as expressed in the used notation:

$$S = (I - K_{LQ}(zI - \tilde{G})^{-1}\tilde{H})^{-1}, \tag{5.15}$$

satisfies the Kalman inequality

$$\bar{\sigma}(S(j\omega)) \leq 1, \ \forall\omega. \tag{5.16}$$

It is necessary to remark that, although the LQ presents some robustness guarantees, they are very general conditions which, generally, do not allow to ensure robustness when parametric uncertainty is present. For this reason, the present LQ design should be used in cases where the model is not expected to have significant errors or be analyzed by the methods exposed in chapter 4. Rigorously speaking, this robustness properties do not allow to perform a robustness-driven design, but they are an indicator of well-posedness of the control design for standard cases. For pure robustness problems, $\mathcal{H}_\infty$-based design techniques may be used.

5.2.3 LQ power converter control. Weights matrices selection

The Q and R matrices in eq.(5.14) are the only design parameters of the whole regulator design. As stated above, Q matrix weights the different states. The state vector was defined in 5.10 and has the following states:

$$X_k = [i_{1_d},\ i_{1_q},\ i_{2_d},\ i_{2_q},\ u_{c_d},\ u_{c_q},\ u_{d_{k-1}},\ u_{q_{k-1}},\ \omega_d,\ \omega_q], \tag{5.17}$$

where ω_d and ω_q are the integrated value of the error signals, as described in Fig. 5.3.

Matrix R weights the actuation variables. The practical design of the LQ current regulator typically requires some iteration until desired performance is achieved. The following thumb-rules give some design criteria extracted from practical experience [Wu and Lehn, 2006][Dutton et al., 1997]:

- The elements out of the diagonal of these matrices represent relations between different states. They are usually set to zero because its correct selection is difficult, non-intuitive and brings bad consequences to system global robustness.

- Heavy weights, $q_{1,1}$ and $q_{2,2}$, should be placed on i_{1_d} and i_{1_q} to ensure fast, well-damped transient current response.

- The impedance of the capacitor is fairly high and little current is shunted through it, thus $i_{1_{dq}}$ and $i_{2_{dq}}$ will show a similar behavior. Hence they should have similar associated weights, $q_{3,3}, q_{4,4} \approx q_{1,1}, q_{2,2}$.

- The voltage in the capacitor $u_{c_{dq}}$ should be allowed to move as dictated by the grid in order to avoid converter saturation. Low or zeros weight may be placed on this state. Thus $q_{5,5}, q_{6,6} \approx 0$.

- Weights on the states associated to the input time delays should initially be close to zero $(q_{7,7}, q_{8,8})$. While an increase in these weights will limit the amount of control effort used, it will also decrease damping and performance. For the same reason, input weight matrix R should initially be set to identity.

- Fairly heavy weights, $q_{9,9}, q_{8,8}$, should be placed on the integrators states in order to achieve high bandwidth. This increase comes at the expense of a loss in robustness.

- The actuators, u_{dq} can be limited by increasing either the weights related to the time delays or the matrix R elements.

Fig. 5.4 shows the position of the system closed-loop poles for different values of matrix Q. Figs. 5.5 and 5.6 show the step and disturbance responses, respectively, for different values of the same matrix.

Following the given criteria, the following LQ weights were chosen:

$$Q = \begin{bmatrix} q_{1,1} & 0 & \cdots & 0 \\ 0 & q_{2,2} & \cdots & 0 \\ \vdots & \vdots & & \vdots \\ 0 & 0 & \cdots & q_{10,10} \end{bmatrix}, \quad R = I_{2x2} \tag{5.18}$$

where $q_{1,1}, q_{2,2}, q_{3,3}, q_{4,4} = 25$, $q_{5,5}, q_{6,6} = 0$, $q_{7,7}, q_{8,8} = 1$ and $q_{9,9}, q_{10,10} = 5$. R is chosen as an identity matrix.

5.2.4 State estimation

The regulator scheme showed above implies, in the best cases, an increase in the global system cost, as probably more sensors are needed. In worse cases, probably the LQ regulator cannot be applied because some state is simply not-measurable.

A possible solution, if the system under study is observable in the discrete plane [Ogata, 1994], is to estimate the internal states from the inputs and the outputs of the system by means of a state estimator. This situation is shown on Fig. 5.7. Again, it is important to remark that the robustness properties previously described are lost when states are not directly measurable [Doyle, 1978].

Two classical state estimation structures are described in this dissertation:

- Predictor state estimator.

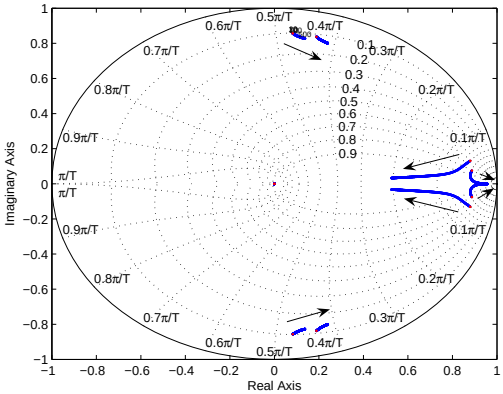

(a) Eigenvalues of the closed loop system for the variation: $1 < q_{11},\ q_{22},\ q_{33},\ q_{44} \leq 500$.

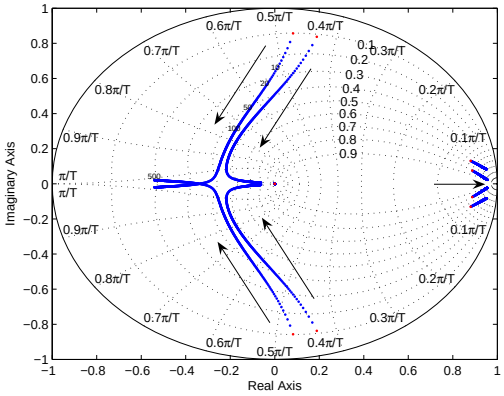

(b) Eigenvalues of the closed loop system for the variation: $1 < q_{55},\ q_{66} \leq 500$.

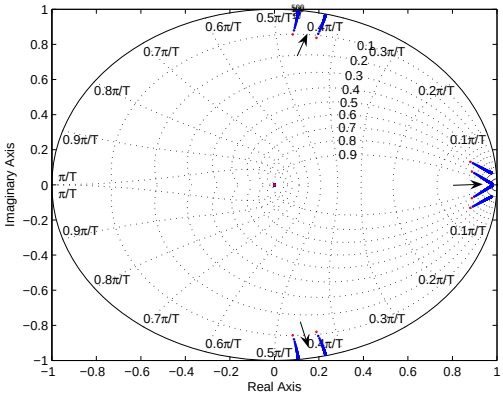

(c) Eigenvalues of the closed loop system for the variation: $1 < q_{77},\ q_{88} \leq 500$.

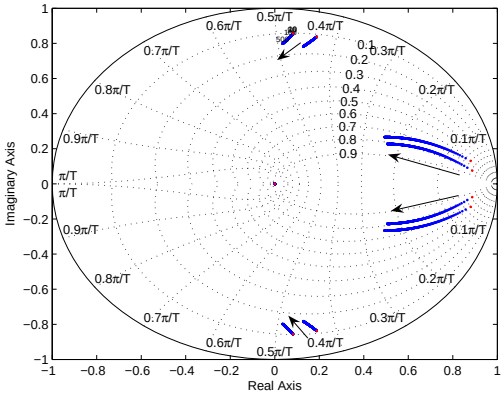

(d) Eigenvalues of the closed loop system for the variation: $1 < q_{99},\ q_{1010} \leq 500$..

Figure 5.4: *LQ closed-loop pole places for different values of matrix Q.*

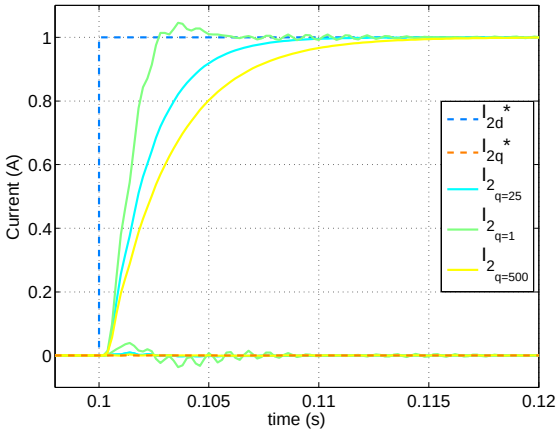

(a) i_{2d} reference step response for different values of q_{11}, q_{22}, q_{33}, q_{44}.

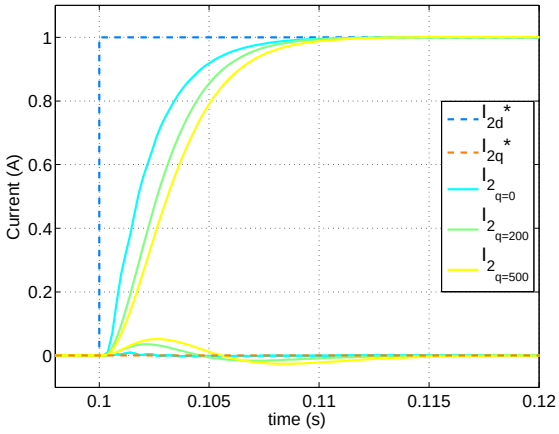

(b) i_{2d} reference step response for different values of q_{55}, q_{66}.

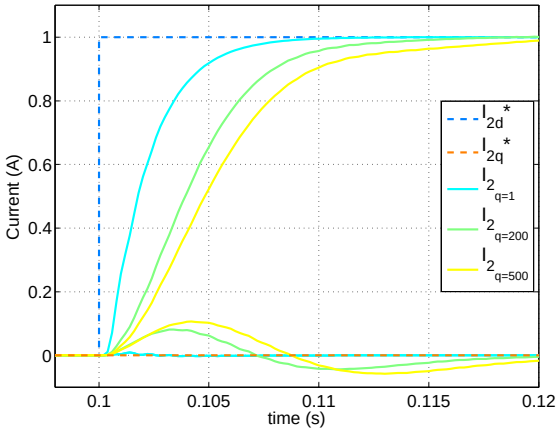

(c) i_{2d} reference step response for different values of q_{77}, q_{88}.

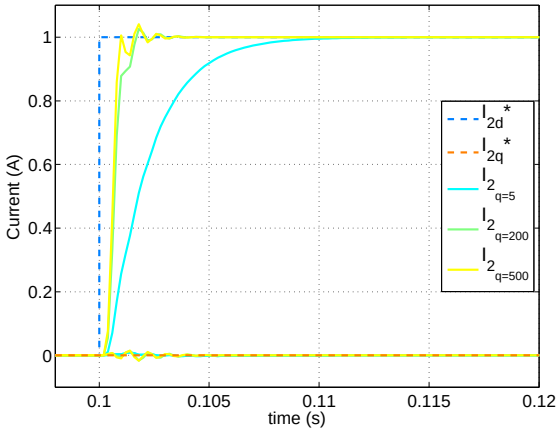

(d) i_{2d} reference step response for different values of q_{99}, q_{1010}.

Figure 5.5: *LQ closed-loop step responses for different values of matrix Q.*

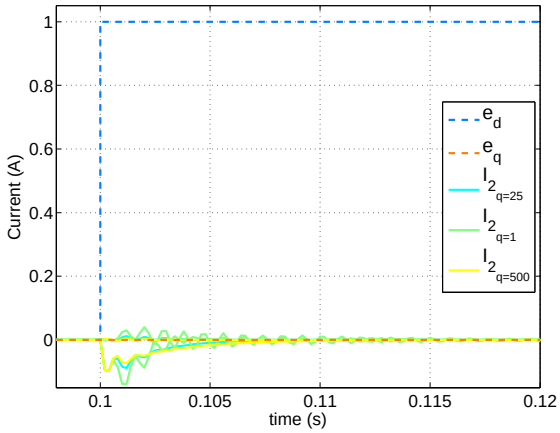

(a) e_d perturbance step response for different values of $q_{11},\ q_{22},\ q_{33},\ q_{44}$.

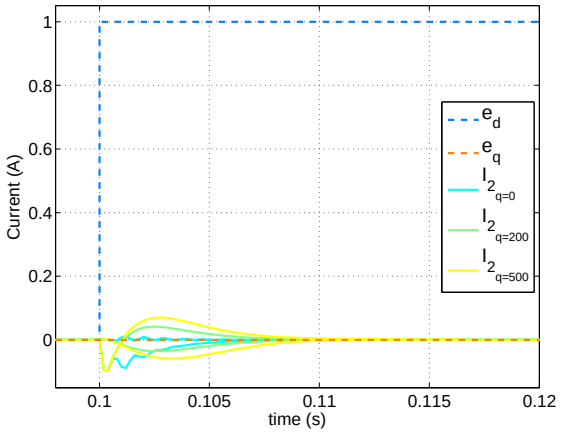

(b) e_d perturbance step response for different values of $q_{55},\ q_{66}$.

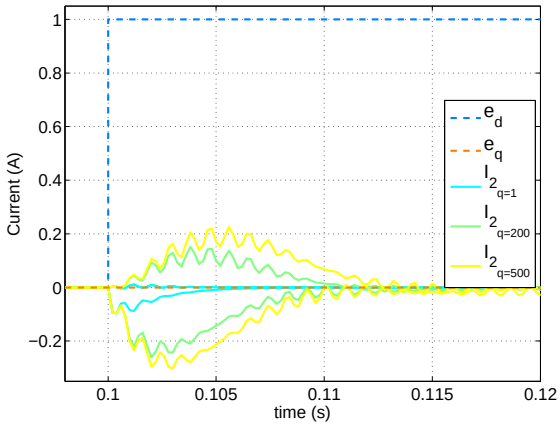

(c) e_d perturbance step response for different values of $q_{77},\ q_{88}$.

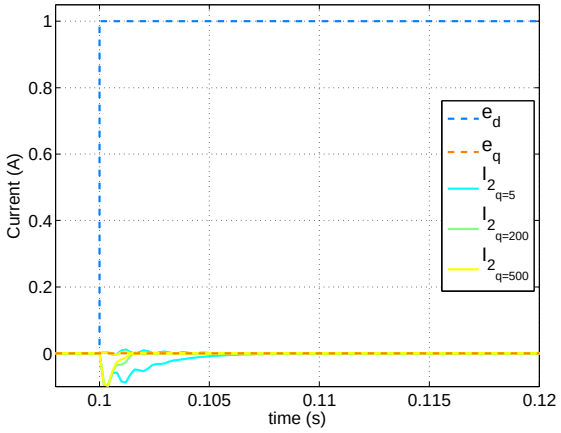

(d) e_d perturbance step response for different values of $q_{99},\ q_{1010}$.

Figure 5.6: *LQ closed-loop disturbance responses for different values of matrix Q.*

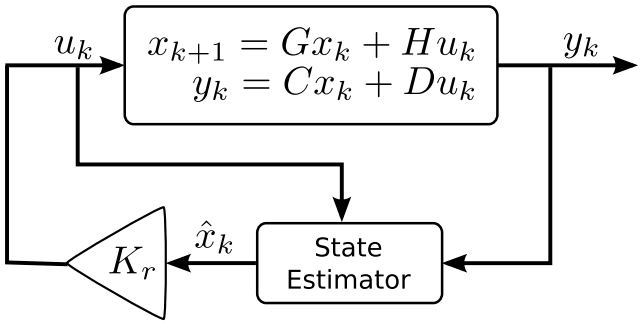

Figure 5.7: *General block diagram of a system regulation with state estimation.*

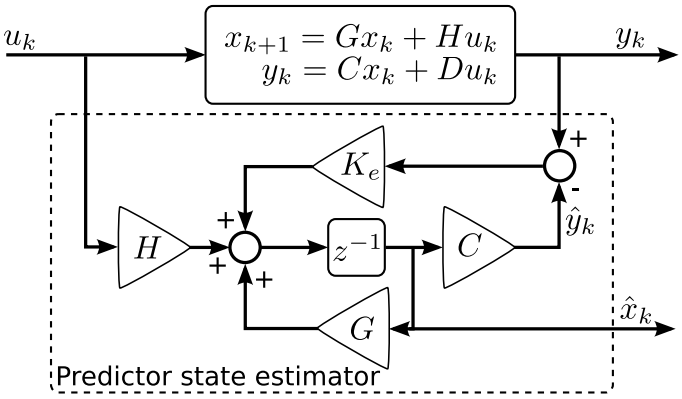

Figure 5.8: *Block structure of the predictor state estimator.*

- *Current*[1] state estimator.

In the case of the predictor state estimator, whose structure is shown on Fig. 5.8, the dynamics are fixed by:

$$\hat{x}_{k+1} = G\hat{x}_k + Hu_k + K_e[y_k - \hat{y}_k], \tag{5.19}$$

where K_e is the feedback gain matrix of the estimator. Another expression of eq.(5.19) is:

$$\hat{x}_{k+1} = (G - K_eC)\hat{x}_k + Hu_k + K_ey_k. \tag{5.20}$$

In this last equation, if the matrix $(G - K_eC)$ is a stable matrix, $\hat{x}_k$ will converge to x_k for any $x(0)$ and $\hat{x}(0)$.

The *Current* state estimator, whose block diagram is represented in Fig. 5.9, presents the following state estimation equations [Ogata, 1994] [Dutton et al., 1997] :

$$\begin{cases} \hat{x}_{k+1} = z_{k+1} + K_e(y_{k+1} - Cz_{k+1}) \\ z_{k+1} = G\hat{x}_k + Hu_k \end{cases} \tag{5.21}$$

The estimation process consists of a two-step procedure: prediction stage and correction stage. In the first step, z_{k+1} is determined, which is an approximation of x_{k+1} based on $\hat{x}_k$ and u_k. In the second step, y_{k+1} is used to improve z_{k+1}, getting $\hat{x}_{k+1}$.

Defining the estimation error as follows:

$$e_k = x_k - \hat{x}_k, \tag{5.22}$$

then:

$$e_{k+1} = (G - K_eCG)e_k. \tag{5.23}$$

Convergence of the error variable is ensured if $(G - K_eCG)$ is a stable matrix.

[1]To avoid nomenclature confusion, the word *current*, referred to an estimator, will appear always in italic style. The word current, in regular style, will be only used to name the electrical magnitude all along this dissertation.

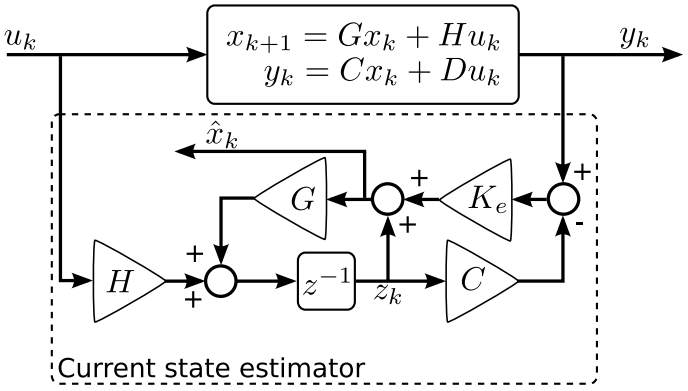

Figure 5.9: *Block structure of the* Current *state estimator.*

When the output signals are contaminated with additive noise, a regular observer, which is usually designed as a dead-beat observer, will barely filter it, getting erroneous values in the estimated state vector. If the dynamic performance is relaxed, the system becomes more immune to measurement noise. Actually, the selection of this eigenvalues involves a trade decision difficult to solve, except in one case: assuming that the additive noise added to the output variables is unbiased, white and Gaussian, the optimum estimator is the Kalman Filter [Kalman, 1960]. The Kalman Filter is easily implemented from the *Current* state estimator structure, with the particularity that the matrix K_e is updated in each of the iterations:

$$K_{e_k} = \tilde{P}_k C^T (C\tilde{P}_k C^T + P_V)^{-1}, \tag{5.24}$$

where

$$\tilde{P}_k = GP_{k-1}G^T + P_\omega, \tag{5.25}$$

$$P_k = (I - K_{e_k}C)\tilde{P}_k. \tag{5.26}$$

The matrices P_v and P_ω have to be previously designed. Intuitively, they represent the measurement uncertainty in the output measurements and model respectively. The design of the latter is quite difficult and is usually set to a null matrix. The design of the former is critical and represents the variance of the output measurement stochastic process [Bishop and Welch, 2001] [Brown and Hwang, 1992].

State estimation of power converter variables

Two different state estimator structures have been evaluated, the predictive estimation structure and the *Current* estimation structure, both previously described. Both structures are perfectly suitable for the estimation of the states in the case under study as the system is observable.

The dynamic behavior of the estimators is controlled by the feedback matrix K_e: by a pole-placement procedure, it is possible to select the desired eigenvalues for the closed-loop estimation process. It is a common practice to select the matrix to place all the eigenvalues in the origin of the z-plane. With these eigenvalues, the estimator gets a dead-beat behavior

and, in absence of modelling errors and additive noise, converges to the actual state vector value n sample periods, being n the number of system states.

These good dynamics properties come at the cost of poor noise rejection capabilities. If this behavior is not desired, eigenvalues should be placed in slower positions. The problem here arises in selecting this new positions.

Figs. 5.10, 5.11 and 5.12 show the behavior of three different estimators: a dead-beat predictor estimator, a dead-beat *Current* estimator and a Kalman Filter when the plant output variables (that are inputs in the estimators) are polluted with different additive white Gaussian noise (AWGN) and switching ripple.

Fig. 5.13 shows a comparison study of the performance of the described estimation techniques in the presence of several noise conditions. Regarding dead-beat and *current* estimators, it is difficult to select one of them as a best option. The study shows that they offer different performance depending on the nature of the noise and the estimated variable. Assuming that variable $i_2(t)$ is feedbacked directly from the measurements and not from the estimator, predictor scheme offers better quality in the converter-side current and capacitor voltage estimation.

Kalman filter clearly offers better performance in all cases. It is important to remark that this performance is deceptive to some extent because the considered plant model in the study closely represents the actual one and noise is perfectly modelled. Introduction of plant uncertainty in the Kalman filter design process is not a trivial task and is one of the reasons to apply an estimation/control scheme based on $\mathcal{H}_\infty$ optimization for the plant state estimation or, in general, control. In spite of that, it is still an optimum approach under AWGN conditions.

5.3 Output feedback grid current robust control

The proposed LQ controller presents some robustness properties if all involved state variables are directly measurable. When the use of either full or reduced order observers is mandatory, this schema looses them. This poor feature extends, as well, to other optimal control schemes as $\mathcal{H}_2$ controllers and, particularly to LQG structures [Doyle, 1978]. $\mathcal{H}_\infty$ theory provides a way to design (sub)-optimal[2] controllers that satisfy robustness specifications even in the case that some state variables need to be estimated. The loop-shaping design procedure described in this subsection is based on $\mathcal{H}_\infty$ robust stabilization combined with classical loop shaping. It was firstly proposed in [McFarlane and Glover, 1990] and since then, it has been successfully applied to several practical problems [Duc and Ballois, 1994] [Samar et al., 1996] [Samar et al., 1995]. It is essentially a two step design process. First, the open loop plant is augmented by pre- and post-compensators to give a desired shape to the singular values open-loop frequency response. This step could be based on an initial controller design or on the designer expertise in classical loop-shaping design procedures. On a second step, the resulting shaped plant (initial loop shape) is robustly stabilized (*robustified*) with respect to the quite general class of coprime factor uncertainty using $\mathcal{H}_\infty$ optimization.

[2]The research for an optimal $\mathcal{H}_\infty$ controller increases the optimization computational complexity and brings few or no advantages. Usually, the objective is the obtaining of a controller that stabilizes a set of plants and not the maximum number of plants because this usually implies a not necessary performance reduction.

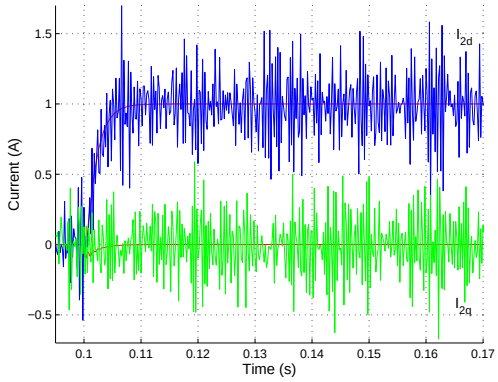

(a) Predictor estimation of i_2 under AWGN noise.

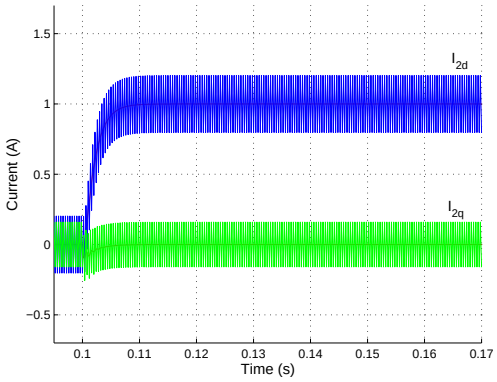

(b) Predictor estimation of i_2 under switching ripple presence.

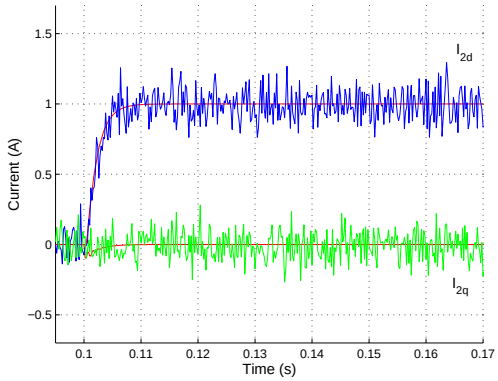

(c) *Current* estimation of i_2 under AWGN noise.

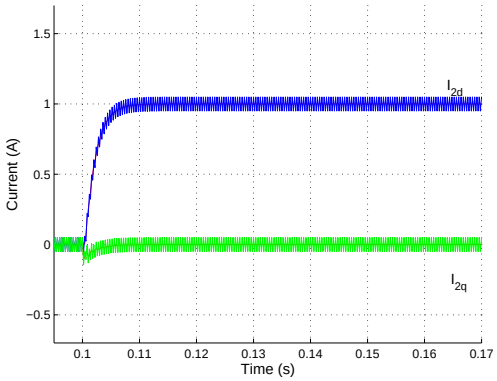

(d) *Current* estimation of i_2 under switching ripple presence.

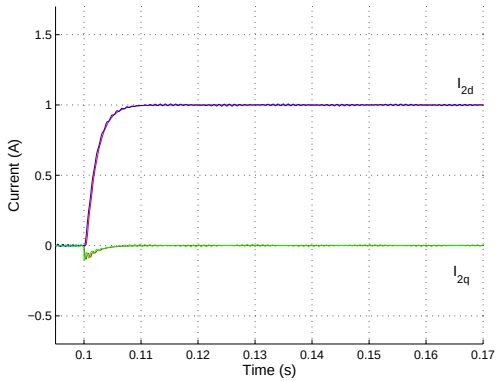

(e) Kalman estimation of i_2 under AWGN noise.

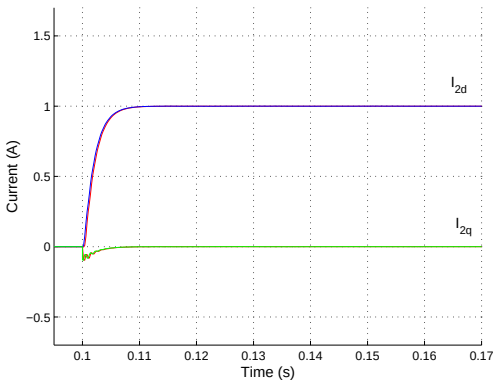

(f) Kalman estimation of i_2 under switching ripple presence.

Figure 5.10: *Comparison of the estimation of the output currents i_{2d} and i_{2q}.*

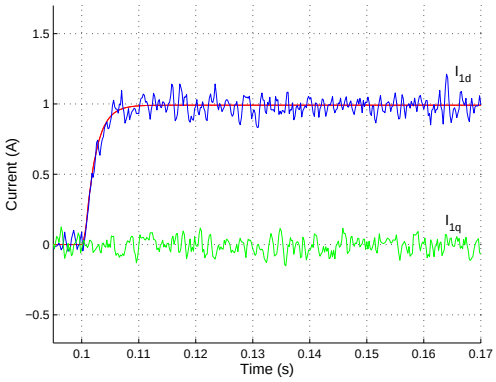

(a) Predictor estimation of i_1 under AWGN noise.

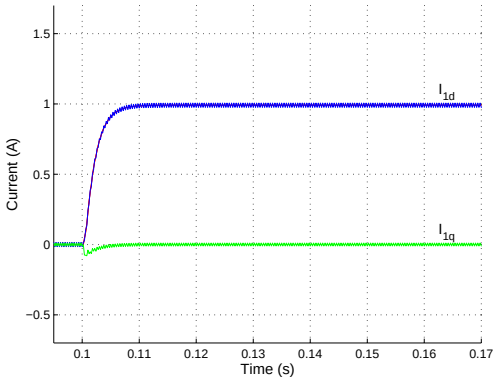

(b) Predictor estimation of i_1 under switching ripple presence.

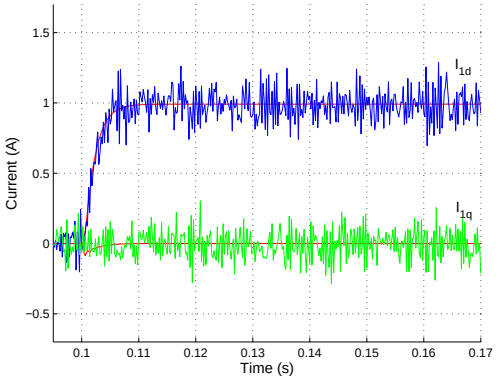

(c) *Current* estimation of i_1 under AWGN noise.

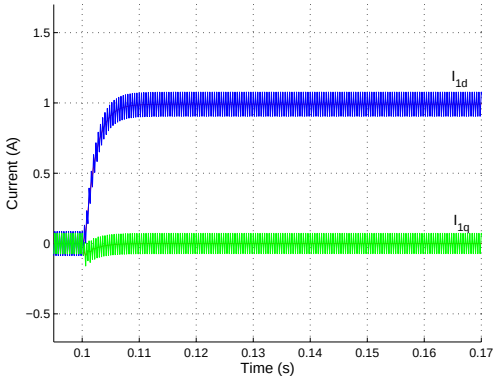

(d) *Current* estimation of i_1 under switching ripple presence.

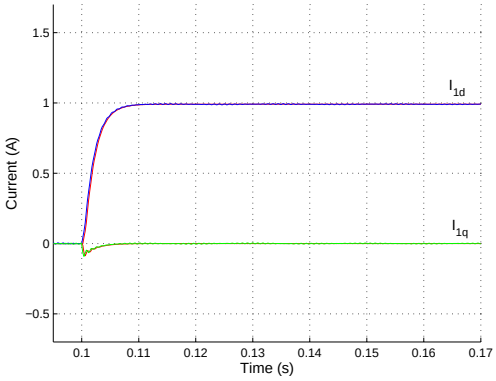

(e) Kalman estimation of i_1 under AWGN noise.

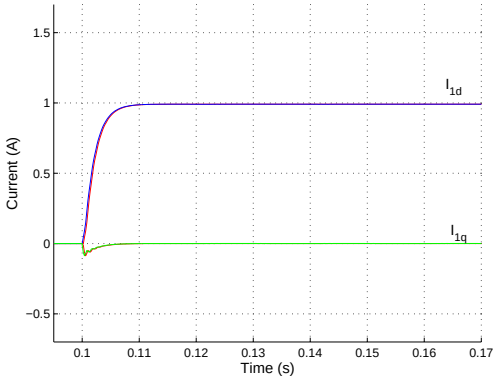

(f) Kalman estimation of i_1 under switching ripple presence.

Figure 5.11: *Comparison of the estimation of the output currents i_{1d} and i_{1q}.*

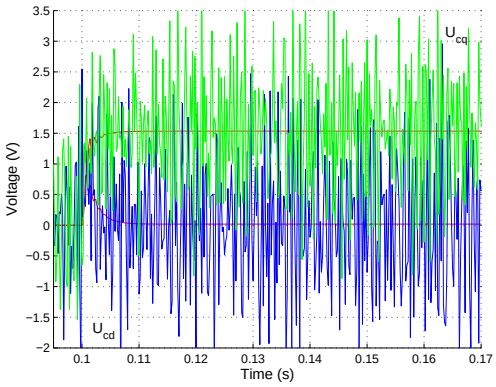

(a) Predictor estimation of u_c under AWGN noise.

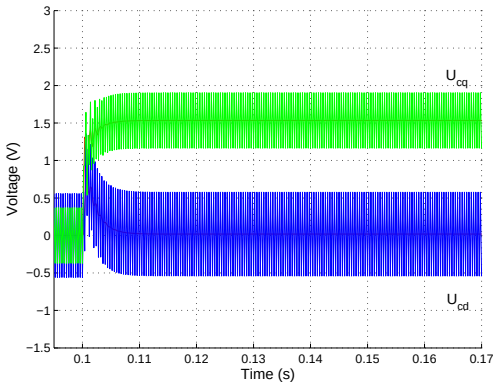

(b) Predictor estimation of u_c under switching ripple presence.

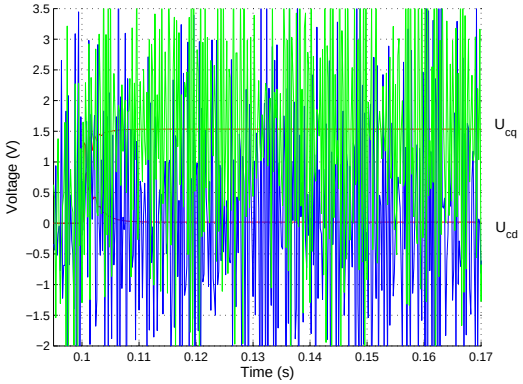

(c) *Current* estimation of u_c under AWGN noise.

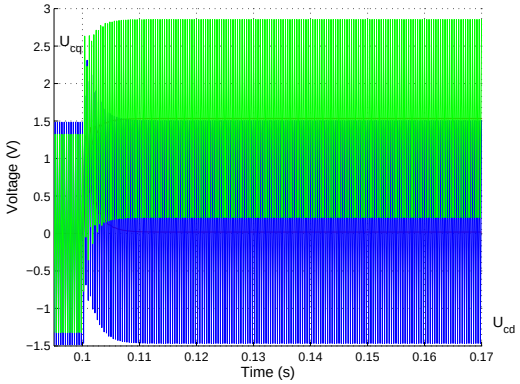

(d) Predictor estimation of u_c under switching ripple presence.

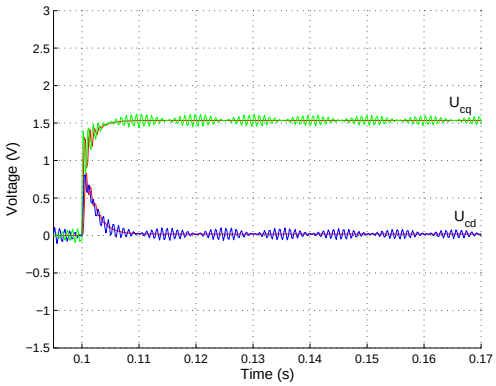

(e) Kalman estimation of u_c under AWGN noise.

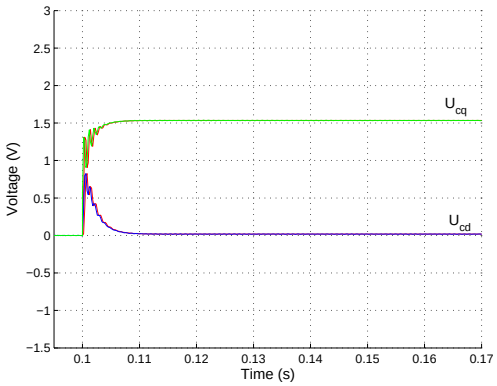

(f) Kalman estimation of u_c under switching ripple presence.

Figure 5.12: *Comparison of the estimation of the capacitor voltages u_{cd} and u_{cq}.*

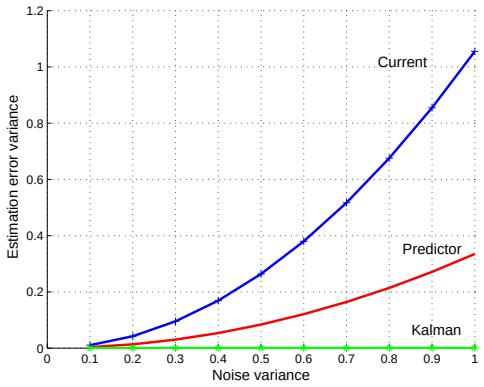

(a) Comparison of estimation techinques for i_1 under AWGN noise.

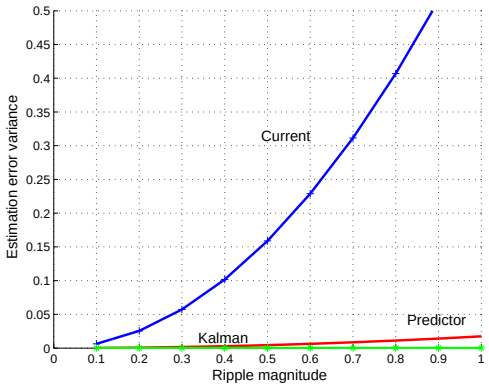

(b) Comparison of estimation techinques for i_1 under switching ripple presence.

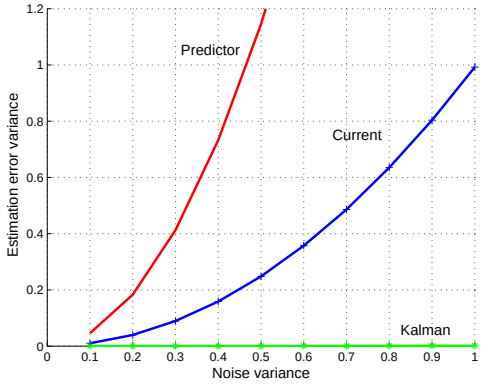

(c) Comparison of estimation techinques for i_2 under AWGN noise.

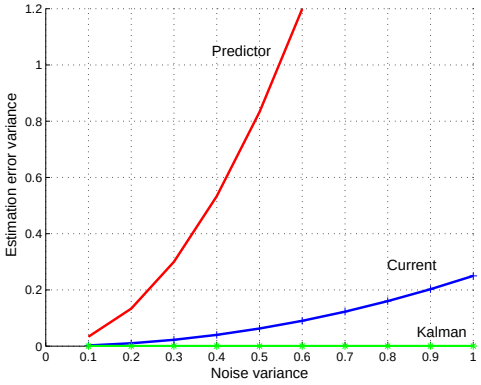

(d) Comparison of estimation techinques for i_2 under switching ripple presence.

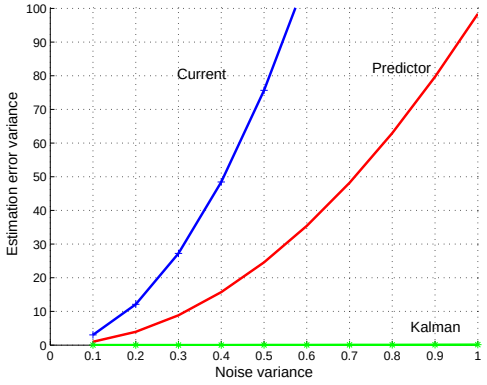

(e) Comparison of estimation techinques for u_c under AWGN noise.

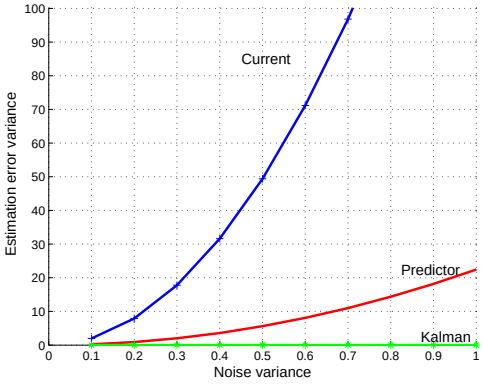

(f) Comparison of estimation techinques for u_c under switching ripple presence.

Figure 5.13: *Comparative study of estimation techniques under different noise pollution situations.*

Simultaneously, the shaped perturbed set is evaluated by means of the ν-gap norm. This tool *measures* the distance between two plants in terms of its coprime factors.

Both tools allow to design a controller that achieves robust stability when applied to each of the plants of a perturbed set that may be defined in terms of parametric uncertainty.

5.3.1 Design flow and terminology

Robust synthesis is the process that allows to extract a controller that produces a stable closed-loop when applied to an a-priori known set of plants. In other words, it can be viewed as a controller that stabilizes a plant that is *uncertain* to some extent.

Plant uncertainty, as described in chapter 4, can be classified into two big groups depending on its nature: unstructured and structured uncertainty. This section focuses on the synthesis of a robust current controller for a VSC connected to a grid with uncertainty in its equivalent resistance and inductance (described in chapter 4). This kind of uncertainty is a parametric, structured uncertainty.

The most general design process inside the Robust Control Theory that is applicable to this problem is the structured singular value μ-synthesis approach [Zhou, 1998]. This approach is general enough to manage parametric uncertainty in a linear plant where some performance constraints are imposed. Unfortunately, for the moment, a systematic procedure to synthesize such a controller is not available. The current method relies on a combination of $\mathcal{H}_\infty$ synthesis and μ analysis that can give good results. This process presents severe convergence issues when the uncertain parameters can get values only in the real line. The issues are still bigger when dealing with discrete-time processes. Both cases match the needs of the design presented in this dissertation. Moreover, μ-synthesis procedure often yields very high order controllers that are very near to be optimal. It is necessary to remark the inconvenience of getting an optimal design in these cases: an optimal controller means that the controller satisfies stability (performance) constraints *if and only if* the plant under study belongs to the initial perturbed set. This translates in systems that are very robust to modelled uncertainty but very sensitive to not modelled uncertainty.

For this reason, this thesis proposes the use of well established and tested $\mathcal{H}_\infty$ techniques to solve the problem. Several approaches are available when using this optimization depending mostly on the kind of uncertainty considered: additive, multiplicative, input, output direct or inverse. A particularly useful design technique, valid in a very wide set of situations, are the $\mathcal{H}_\infty$ techniques applied to plants with *coprime factor uncertainty* [McFarlane and Glover, 1990]. This uncertainty representation simultaneously combines the properties of the other ones and leads to a very useful robust stabilization problem. For this reason, this is the approach used for the work described in this dissertation.

ν-gap (δ_ν) [Vinnicombe, 2001] is an analysis tool that perfectly complements with the robust stabilization of coprime factor uncertain plants. In general terms, the δ_ν of two plants gives the distance between them in terms of their coprime factor. The robust stabilization of coprime factor uncertain plants yields a controller and a stability margin in coprime factor terms. For this reason, a very convenient design procedure is to calculate the maximum δ_ν in the set of uncertain plants and test if this number is smaller than the coprime factor stability margin. If affirmative, the system will achieve robust stability and the design is valid.

A general view of the whole design process is depicted in Fig. 5.14. The process starts

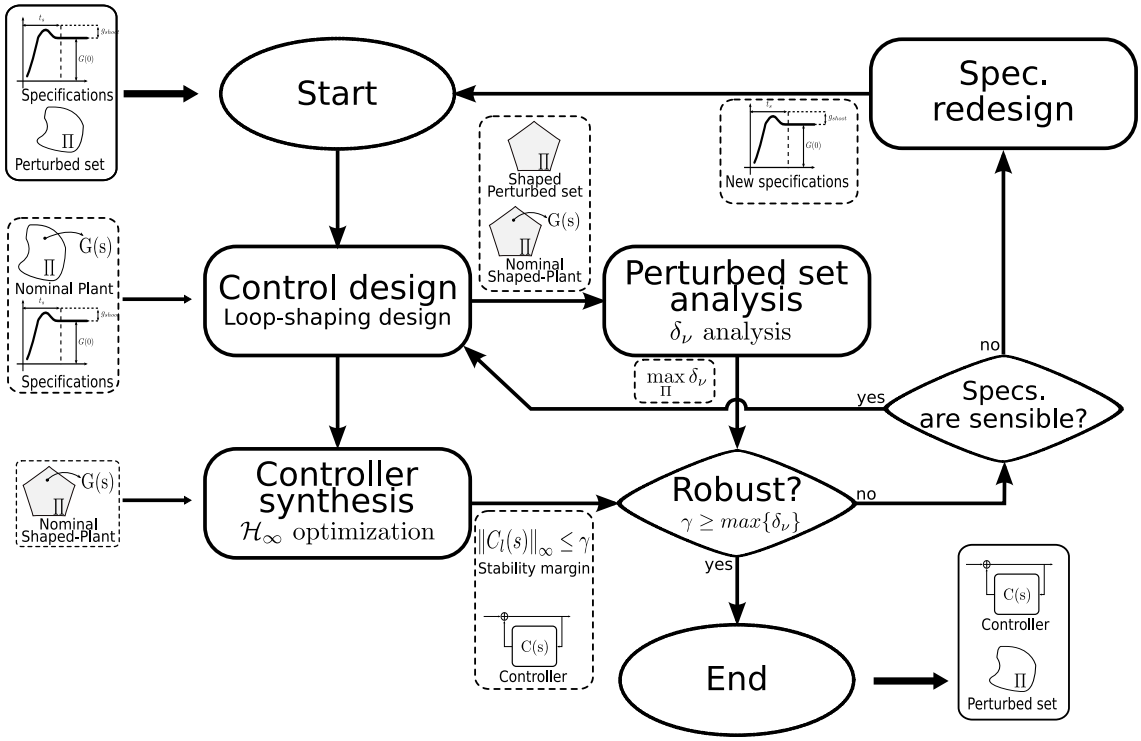

Figure 5.14: $\mathcal{H}_\infty$ - ν-*gap robust control design flow diagram.*

performing an analysis of the problem objectives. These objectives translate into a robust stability specification and, perhaps, a robust performance specification.

The robust stability specification actually is the set of plants that the controller has to stabilize. It is usually named *perturbed set* or *uncertain set* and represented by $G_p(s)$, $G_p(z)$ or Π. In the case under study, the uncertain set is composed of all the possible plants that result of the modification of grid equivalent impedance and resistance. A special plant belonging to the perturbed set is the one that will be used to perform all the computations. This plant is named *Nominal plant*, G(s) or G(z).

The first step in the design process is the series association of the nominal plant with a transfer function. This process, named *loop-shaping*, has a double function: to incorporate the performance specification in the design and to minimize the existing maximum δ_ν of the uncertain set. It has to be remarked that this loop-shaping process is an intuitive procedure and it is the only point where the designer is involved.

Once the plant has been properly shaped, the resulting plant is introduced inside a regular $\mathcal{H}_\infty$ procedure that will yield a controller and the corresponding stability margin, named γ. Simultaneously, the shaping function is applied to the uncertain set, yielding another set named *Shaped perturbed set*. This set is analyzed by means of the ν-gap tool to extract the maximum existing distance between the nominal shaped plant and any plant belonging to the shaped uncertain set.

If the maximum δ_ν is bigger than the obtained stability margin, robust stability is not ensured and the loop-shaping process needs some tuning. If, after several iterations, robust stability is not achieved, the initial performance specifications are probably too tight for the considered uncertain set, and they should be relaxed. This process continues until

$\max_{\Pi} \delta_\nu < \gamma$.

5.3.2 Theoretical Background

Coprime factors and factorization of a discrete-time linear transfer function

The pair $(\tilde{M}, \tilde{N})$ constitutes a *left coprime factorization* of a transfer function $G(z)$ if:

- $G = \tilde{M}^{-1}\tilde{N}$,
- $\tilde{M}, \tilde{N} \in RH_\infty$ and that there exist X, $Y \in RH_\infty$ such that $\tilde{M}X + \tilde{N}Y = I$, and
- $det(\tilde{M})(\infty) \neq 0$.

Additionally, a left coprime factorization of G is said to be *normalized* if M, N satisfy:

$$\tilde{M}\tilde{M}^* + \tilde{N}\tilde{N}^* = I, \tag{5.27}$$

where $\tilde{M}^* = \tilde{M}^T(z^{-1})$, etc. A state space contruction for a normalized left coprime factorization can be obtained as follows [Walker, 1990][Walker, 1991][Samar et al., 1996]. Given $G(z) = C(zI - A)^{-1}B + D$, let $R_1 = I + D^T D$, $R_2 = I + DD^T$, and let $P = P^T$ be the non-negative definite stabilizing solution to the algebraic Riccati equation

$$BR_1^{-1}B^T - P + \Phi P\Phi^T - \Phi PC^T(R_2 + CPC^T)^{-1}CP\Phi^T = 0, \tag{5.28}$$

then

$$[\tilde{N} \quad \tilde{M}] = \left[\begin{array}{c|cc} A + HC & B + HD & H \\ \hline Z_2C & Z_2D & Z_2 \end{array}\right] \tag{5.29}$$

is a normalized left coprime factorization of G, where $\Phi = A - BR_1^{-1}D^TC$, $H = -(APC^T + BD^T)(R_2 + CPC^T)^{-1}$, and Z_2 satisfies

$$Z_2^T Z_2 = (R_2 + CPC^T)^{-1}. \tag{5.30}$$

In a similar way, let Q be the non-negative definite solution to the algebraic Riccati equation:

$$\Phi^T Q\Phi - Q - \Phi^T QB(R_1 + B^T QB)^{-1}B^T Q\Phi + C^T R_2^{-1}C = 0, \tag{5.31}$$

then

$$\begin{bmatrix} N \\ M \end{bmatrix} = \left[\begin{array}{c|c} A + BF & BZ_1 \\ \hline C + DF & DZ_1 \\ F & Z_1 \end{array}\right] \tag{5.32}$$

is a *right coprime factorization* [Gu et al., 2005] of G, where $\Phi = A - BR_1^{-1}D^TC$, $F = -Z_1Z_1^T(B^TQA + D^TC)$, and Z_1 satisfies

$$Z_1Z_1^T = (R_1 + B^TQB)^{-1}. \tag{5.33}$$

Robust stabilization against normalised coprime factor perturbations

Using the above presented factorization procedure, a perturbed plant transfer function can be described by:

$$G_\Delta = (\tilde{M} + \Delta_{\tilde{M}})^{-1}(\tilde{N} + \Delta_{\tilde{N}}), \tag{5.34}$$

where $(\Delta_{\tilde{M}}, \Delta_{\tilde{N}})$ are unknown but stable transfer functions that represent the uncertainty (i.e. the perturbation) in the nominal plant model. The design objective of robust stabilization is to stabilize not only the nominal model G, but the family of perturbed plants defined by:

$$G_p = \{(\tilde{M} + \Delta_{\tilde{M}})^{-1}(\tilde{N} + \Delta_{\tilde{N}}) : ||\Delta_{\tilde{M}} \quad \Delta_{\tilde{N}}||_\infty < \epsilon\}, \tag{5.35}$$

where $\epsilon > 0$ is the *stability margin*. Using a feedback controller K, as shown schematically in Fig. 5.15, and the Small Gain Theorem, the feedback system (G_p, K, ϵ) is robustly stable if and only if (G, K) is internally stable and

$$\left\| \begin{vmatrix} K \\ I \end{vmatrix} (I - GK)^{-1} \tilde{M}^{-1} \right\|_\infty \leq \epsilon^{-1}. \tag{5.36}$$

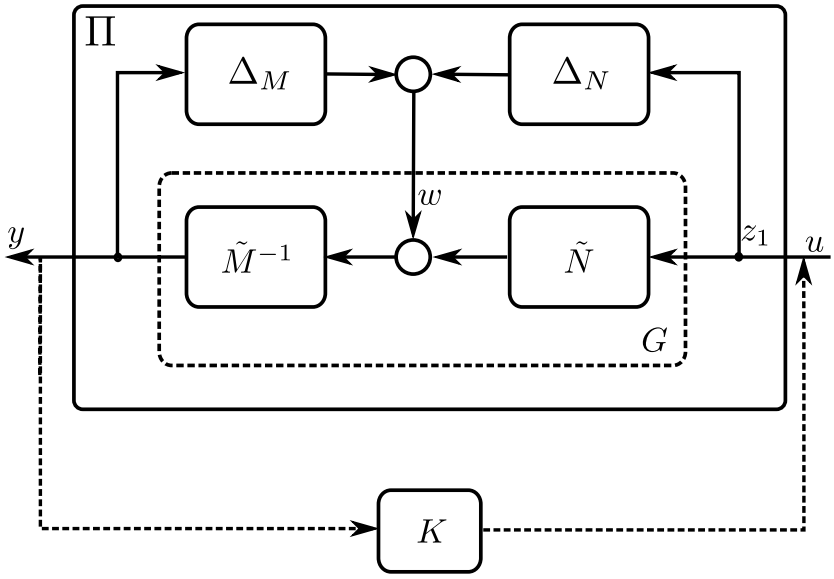

Figure 5.15: *Robust stabilization with regard to coprime factor uncertainty.*

Defining $\gamma = \epsilon^{-1}$, the design of a robust controller can be formulated as a regular $\mathcal{H}_\infty$ problem, where the objective is to find a sub-optimal controller K such that, the following transfer function:

$$\left\| \begin{vmatrix} K \\ I \end{vmatrix} (I - GK)^{-1} \tilde{M}^{-1} \right\|_\infty \leq \gamma. \tag{5.37}$$

In order to apply a standard $\mathcal{H}_\infty$ optimization procedure, it is necessary to express the plant G in the generalized structure displayed in Fig. 5.16, that is, to build the generalyzed system:

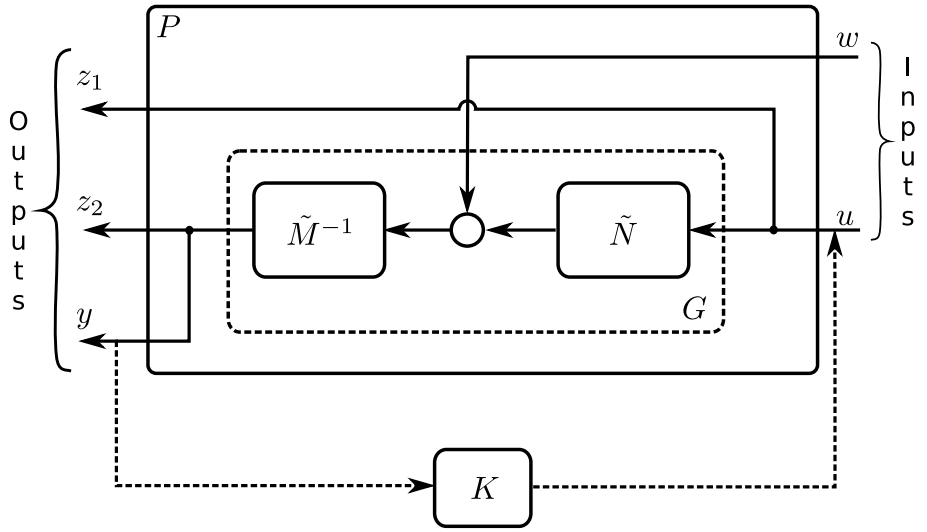

Figure 5.16: *Standard configuration for $\mathcal{H}_\infty$ optimization.*

$$\begin{bmatrix} z_1 \\ z_2 \\ y \end{bmatrix} = P \cdot \begin{bmatrix} w \\ u \end{bmatrix}. \tag{5.38}$$

This system can be expressed in state space equations as follows:

$$P(z) = \left[\begin{array}{c|cc} A & -HZ_2^{-1} & B \\ \hline \begin{bmatrix} 0 \\ C \end{bmatrix} & \begin{bmatrix} 0 \\ Z_2^{-1} \end{bmatrix} & \begin{bmatrix} I \\ D \end{bmatrix} \\ C & Z_2^{-1} & D \end{array}\right] =: \left[\begin{array}{c|cc} A & B_1 & B_2 \\ \hline C_1 & D_{11} & D_{12} \\ C_2 & D_{21} & D_{22} \end{array}\right] \tag{5.39}$$

Coprime factorization $\mathcal{H}_\infty$ optimization advantages

One big advantage of using a coprime factorization description is the possibility of obtaining an *a-priori* analytical value for the lowest achievable value of γ, referred to as γ_{opt} [Walker, 1990]:

$$\gamma_{opt} = \epsilon_{max}^{-1} = (1 - \left\| \tilde{N}\tilde{M} \right\|_H^2)^{-1/2}, \tag{5.40}$$

where $||\cdot||_H$ denotes the Hankel norm. Another valid expression is

$$\gamma_{opt} = \epsilon_{max}^{-1} = (1 + \lambda_{max}(PQ))^{1/2}, \tag{5.41}$$

where $Q = Q^T$ is the non-negative definite stabilizing solution to the algebraic Riccati equation:

$$C^T R_2^{-1} C - Q + \Phi^T Q \Phi - \Phi Q B (R_1 + B^T Q B)^{-1} B^T Q \Phi = 0. \tag{5.42}$$

$\lambda_{max}(\cdot)$ denotes the largest eigenvalue, and R_1, R_2, Φ and P are as defined above.

Additionally, given the simplified structure of the loop-shaping created plant, the standard H_∞ procedure gets simplified to the solution of another Riccati equation, avoiding the classical iteration. X_∞ is the solution of this third discrete Riccati equation:

$$A^T X_\infty A - X\infty - \tilde{F}^T (R + \begin{pmatrix} -Z_2^{-1} H^T \\ R_2^{-1/2} B^T \end{pmatrix} X_\infty \begin{pmatrix} -H Z_2^{-1} & B R_2^{-1/2} \end{pmatrix}) \tilde{F} + C^T C = 0, \quad (5.43)$$

where

$$\tilde{F} = -(R + \begin{pmatrix} -Z_2^{-1} H^T \\ R_2^{-1/2} B^T \end{pmatrix} X_\infty \begin{pmatrix} -H Z_2^{-1} & B R_2^{-1/2} \end{pmatrix})^{-1} \quad (5.44)$$
$$(\begin{pmatrix} -Z_2^{-1} C \\ D^T R_1^{-1/2} C \end{pmatrix} + \begin{pmatrix} -Z_2^{-1} H^T \\ R_2^{-1/2} B^T \end{pmatrix} X_\infty A)$$

and

$$R = \begin{pmatrix} Z_2^{-2} - \gamma^2 I_p & Z_2^{-1} R_1^{-1/2} D \\ D^T R_1^{-1/2} Z_2^{-1} & I_m \end{pmatrix}. \quad (5.45)$$

Further, by defining $\tilde{F} = \begin{pmatrix} F_1 \\ F_2 \end{pmatrix}$, where $F_1 :\ p\ x\ n$, and $F_2 :\ m\ x\ n$, a suboptimal H_∞ controller can be constructed as

$$K(z) = \left[\begin{array}{c|c} A_K & B_K \\ \hline C_K & D_K \end{array} \right]. \quad (5.46)$$

where

$$\begin{aligned} A_K &= \hat{A}_K - \hat{B}_K D (I + \hat{D}_K D)^{-1} \hat{C}_k \\ B_K &= \hat{B}_K (I + D \hat{D}_K)^{-1} \\ C_K &= (I + \hat{D}_K D)^{-1} \hat{C}_K \\ D_K &= \hat{D}_K (I + D \hat{D}_K)^{-1}, \end{aligned} \quad (5.47)$$

with

$$\begin{aligned} \hat{D}_K &= -(R_2 + B^T X_\infty B)^{-1} (D^T - B^T X_\infty H) \\ \hat{B}_K &= -H + B \hat{D}_K \\ \hat{C}_K &= R_2^{-1/2} F_2 - \hat{D}_K (C + Z_2^{-1} F_1) \\ \hat{A}_K &= A + HC + B \hat{C}_K. \end{aligned} \quad (5.48)$$

Robust stability assessment.

The previous subsection gives a procedure to design a controller for a set of plants G_p whenever they satisfy condition 5.35. This condition is expressed in terms of amount of coprime uncertainty. In other words, a controlled K extracted with the previous method, stabilizing a plant P_0 with a stability margin ϵ, stabilizes all plants of the set:

$$G_{\delta_x,\epsilon} = \left\{ G_i = \tilde{M}_i^{-1}\tilde{N}_i : \delta_x(G_0, G_i) \leq \epsilon \right\} \tag{5.49}$$

if and only if $\epsilon < \epsilon_{max}$. The key point is to find an appropriate way to calculate the function δ_x. There are several candidates in the related literature, the most remarkable are:

- The $\|\cdot\|\infty$ norm $\left\| \begin{pmatrix} \tilde{N}_0 \\ \tilde{M}_0 \end{pmatrix} - \begin{pmatrix} \tilde{N}_i \\ \tilde{M}_i \end{pmatrix} \right\|_\infty$, proposed in [McFarlane and Glover, 1990].
- The directed gap $\bar{\delta}(G_0, G_i) = \inf_{Q \in H_\infty} \left\| \begin{pmatrix} \tilde{N}_0 \\ \tilde{M}_0 \end{pmatrix} - \begin{pmatrix} \tilde{N}_i \\ \tilde{M}_i \end{pmatrix} Q \right\|_\infty$ as proposed in [Georgiu and Smith, 1990][Sefton and Ober, 1993].
- The gap metric $\delta_g(G_0, G_i) = sup\{\bar{\delta}(G_0, G_i), \bar{\delta}(G_i, G_0)\}$ [Georgiu and Smith, 1990][Sefton and Ober, 1993].
- The point-wise gap metric $\delta_\mu(G_0, G_i)$ as defined in [Qiu and Davison, 1992].
- The l_2-induced gap metric $\delta_\nu(G_0, G_i)$ as defined in [Vinnicombe, 1993][Vinnicombe, 2001].

So, any controller achieving a stability margin ϵ, as described in (5.36) will stabilize all plants within a distance to the nominal value smaller than ϵ, this distance being one of the five measures mentioned above.

It is necessary to stress on the great interest of solving the $\mathcal{H}_\infty$ (5.36) in conjunction with one of the five metrics indicated above, that is to say using one of the gaps as a design indicator. For instance, choosing a nominal model, G_0, for the synthesis of the controller, one can obtain a maximum stability margin ϵ_{max} and then verify that for all the other models $G_1, \cdots, G_n$, $\delta_x < \epsilon_{max}$. In this situation it would be possible to choose a suboptimal controller with margin ϵ with the expression above described [Duc and Ballois, 1994].

Furthermore, for any ϵ, the set $G_{\nu,\epsilon}$ defined by the l_2-induced gap metric δ_ν is known to be larger than the others [Vinnicombe, 1993] and moreover, the distance $\delta_\nu(G_0, G_i)$ is easy and fast to compute. These are the reasons of the choice of this metric for the work described in this dissertation.

A systematic discrete-time H_∞ loop-shaping design procedure

Previous subsections showed a direct method to robust stabilize a plant from its decomposition in coprime factors. However, robust stabilization alone is not very useful in practice because the designer is not able to specify any nominal performance nor robust stability requirements. To introduce design capabilities, [McFarlane and Glover, 1990] proposed a

pre- and post-compensator approach to tune the open-loop singular values prior to robust stabilization of this *shaped* plant.

If W_1 and W_2 are pre- and post-compensators respectively, then the shaped plant (initial loop-shape) G_s is given by

$$G_s = W_2 G W_1 \tag{5.50}$$

as shown in Fig. 5.17. The controller K is synthesized as described in past subsection, by solving the described robust stabilizing procedure for the shaped plant G_s with a normalized left coprime factorization $G_s = M_s^{-1} N_s$. The above procedure contains all the essential ingredients of classical loop-shaping.

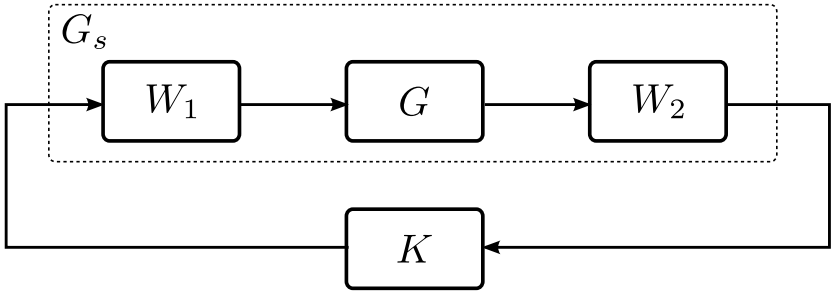

Figure 5.17: *Shaped plant and controller*

Although skill is required in the selection of the weights (W_1 and W_2), experience on real applications has shown that robust controllers can be designed with relatively little effort by following a few simple rules. The following set of rules has been tested in several practical applications as [Postlethwaite et al., 1999][Duc and Ballois, 1994][AlSwailem, 2004] [Samar et al., 1996] and in the work presented in this dissertation:

1. Design the desired shaped plant to address the performance objectives according with classical control rules:

   (a) Scale and reorder the inputs and outputs so that the plant is as diagonal as posible. The Relative Gain Array [Bristol, 1966] gives useful information here.

   (b) W_1 is the responsible of making the *dynamic loop-shaping*, so that the transfer function $W_2 G W_1$ has desirable singular values. This usually means to get a high gain at low frequencies in order to get a low tracking error, to get roll-off rates of approximately 20 dB/decade (slope of about -1) at the desired bandwidth, with higher rates at high frequencies in order to get a robust design.

   (c) W_2 is usually used to emphysize the importance of one output among the others.

2. Evaluate the design indicators:

   (a) Compute ϵ_{max} for the shaped plant (note that this value only depends on the shaped plant. This is a great facility in the control design process). If $\epsilon_{max} << 1$, the controller is unable to stabilize a sufficiently large set of plants, thus the process returns to point 1.

(b) Compute the l_2-induced gap metric δ_ν between the nominal shaped plant $W_2G_0W_1$ and all the plants $W_2G_iW_1$ where the plants G_i belong to the original perturbed set Π. If $\delta_\nu(W_2G_0W_1, W_2G_iW_1) > \epsilon_{max}$ for some i, return to point 1.

(c) Choose $\epsilon_{opt} = \max_{G_i \in \Pi} \delta_\nu(W_2G_0W_1, W_2G_iW_1)$.

3. Robustify the design:

(a) Use the $\gamma_{opt} = \epsilon_{opt}^{-1}$ as the input to the suboptimal controller synthesis described above.

(b) In the strange case that exactly the optimal controller is needed, the presented procedure is not valid anymore as singularities appear in the solution. This makes the controller unimplementable. This problem can be resolved using the procedure in [Safonov et al., 1989].

Extended $\mathcal{H}_\infty$ stabilization procedure

One of the common criticisms to the use of this design process is its occasional conservatism. This apparent conservatism is due to the fact that both the robust index γ and the ν-gap metric δ_ν are punctual measurements. Despite of it, actually both indexes are calculated as the maximum point of two frequency-wise functions that can be computed:

Let the function $\rho(G_s, K)$ be a point wise version of the robust index $\epsilon = \gamma^{-1}$[Vinnicombe, 2001]:

$$\rho(G_s, K)(j\omega) = \frac{1}{\bar{\sigma}\left(\begin{bmatrix} G_s \\ I \end{bmatrix} (I - KG_s)^{-1} \begin{bmatrix} -K & I \end{bmatrix}\right)} \tag{5.51}$$

The previously defined margin ϵ, provided the pair $[G_s \quad K]$ is stable, is, then:

$$\epsilon = \left\| \begin{bmatrix} G_s \\ I \end{bmatrix} (I - KG_s)^{-1} \begin{bmatrix} -K & I \end{bmatrix} \right\|_\infty^{-1}. \tag{5.52}$$

In a similar way, a point-wise version of the ν-gap metric can be found, named $\kappa(j\omega)$, that for two different plants G_1, G_2 is defined as follows:

$$\kappa(G_1, G_2)(j\omega) = \bar{\sigma}(\tilde{P}_2 P_1)(j\omega), \tag{5.53}$$

where $P_i = \begin{bmatrix} N_i \\ M_i \end{bmatrix}$, being $\{N_i \ M_i\}$ a normalized right coprime factorization of G_i, and $\tilde{P}_j = \begin{bmatrix} -\tilde{M}_j & \tilde{N}_j \end{bmatrix}$, being $\{\tilde{N}_j \ \tilde{M}_j\}$ a normalized left coprime factorization G_j.

Now, given a perturbed plant G_i belonging to the set Π of possible perturbed versions of the nominal plant G_0. The plant G_i feedbacked with the controller K is stable if [Vinnicombe, 2001]

$$\rho(G_0, K)(j\omega) > \kappa(G_i, G_0)(j\omega), \ \forall\omega. \tag{5.54}$$

Note that this condition is less (equal, in the worst case) conservative than the one in eq. 5.49. The easiness of extracting frequency information of the ν-gap metric is one of the

strongest reasons for using it among all the other possibilities and can be used to build an extended procedure.

The significance of the last paragraph can be illustrated using Fig. 5.18 [Zhou, 1998]. In the example shown, $\delta_\nu(G_0, G_j) > \epsilon_{G_0,K}$. Thus a frequency-independent stability test cannot conclude that a stabilizing controller K for G_0 will stabilize G_j. However, the frequency-dependent test in the preceding paragraph shows that K stabilizes both G_0 and G_j since $\kappa(G_0, G_j)(j\omega) < \rho(G_0, K)(j\omega),\ \forall\omega$.

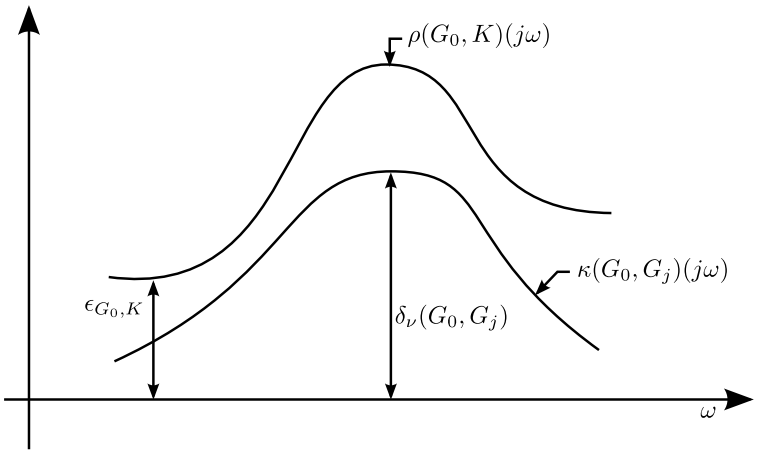

Figure 5.18: *K stabilizes both G_0 and G_j since $\rho(G_0, K)(j\omega) > \kappa(G_i, G_0)(j\omega),\ \forall\omega$.*

Usually, the norm of the transfer function $\|G\|_\infty$ (see Fig. 5.16) obtained after the $\mathcal{H}_\infty$ optimization procedure has an approximately flat maximum singular value for all frequencies. Intuitively, this flatness implies that the resulting controller, if designed to fulfill robustness (5.54) at frequencies where the ν-gap distance $\kappa(G_0, G_j)(j\omega)$ of the perturbed plant is high, will necessarily be conservative at the rest of the frequencies. This situation is illustrated in Fig. 5.19.

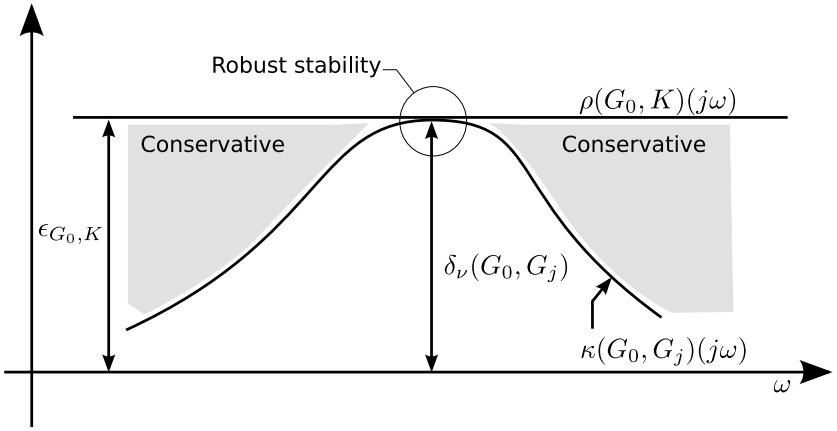

Figure 5.19: *Typicall flat characteristic of suboptimal $\mathcal{H}_\infty$ design.*

More tight results could be obtained if the maximum value of the generalized system could be shaped to approximately match the distance between plants $\kappa(G_0, G_j)(j\omega)$. This

can be made by minimizing the generalyzed plant

$$\left\| \begin{bmatrix} I \\ K \end{bmatrix} (I - GK)^{-1} \tilde{M}^{-1} W \right\|_{\infty} < \gamma, \tag{5.55}$$

where $W(z)$ is a stable and minimum phase rational transfer function with the desired shape in the stability margin $\rho(P_0, K)$. The block diagram of the generalized plant expressed in eq. 5.55 is represented in Fig. 5.20.

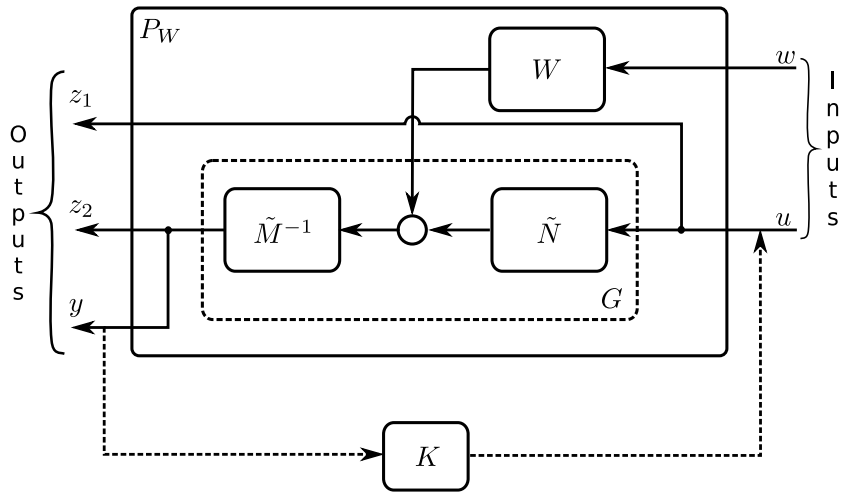

Figure 5.20: *Generalized plant to perform the extended $\mathcal{H}_\infty$ optimization procedure.*

The state space formulation of this generalized plant is the following:

$$P_w(z) = \left[\begin{array}{cc|cc} A & -B_m D_m^{-1} C_W & -B_m D_m^{-1} D_W & B \\ 0 & A_W & B_W & 0 \\ \hline \begin{bmatrix} 0 \\ C \end{bmatrix} & \begin{bmatrix} 0 \\ D_m^{-1} C_W \end{bmatrix} & \begin{bmatrix} 0 \\ D_m^{-1} D_W \end{bmatrix} & \begin{bmatrix} I \\ D \end{bmatrix} \\ C & D_m^{-1} & D_m^{-1} D_W & D \end{array}\right] =: \left[\begin{array}{c|cc} A & B_1 & B_2 \\ \hline C_1 & D_{11} & D_{12} \\ C_2 & D_{21} & D_{22} \end{array}\right] \tag{5.56}$$

given

$$G = \left[\begin{array}{c|c} A & B \\ \hline C & D \end{array}\right], \quad W = \left[\begin{array}{c|c} A_W & B_W \\ \hline C_W & D_W \end{array}\right], \quad \tilde{M} = \left[\begin{array}{c|c} A_m & B_m \\ \hline C_m & D_m \end{array}\right]. \tag{5.57}$$

5.3.3 Loop shaping $\mathcal{H}_\infty$ control of a power converter

The robust design procedure described above can be applied to the control of the grid-side current of a VSC connected to the grid through an LCL filter. The concrete control objectives have been stated in the introduction of this chapter and a detailed description of the plant to control has been given in chapter 4 of this dissertation.

Loop Shaping procedure

As explained in section 5.3.2, the loop-shaping procedure covers the design of two weight transfer function matrixes: $W_1(z)$ and $W_2(z)$. Whilst the function of $W_1(z)$ is to settle the desired nominal performance and robust stability feature over the loop function $L = W_2(z)G(z)W_1(z)$, and thus it is mandatory to select it, in the case of the second matrix, named W_2, its function limits to weight the importance of one output channel among the others. Clearly, in the case under study, this does not apply, as in most cases the final close-loop function is desired to be fully symmetrical. This last reason makes it a good choice to fix:

$$W_2(z) = \begin{pmatrix} 1 & 0 \\ 0 & 1 \end{pmatrix}. \tag{5.58}$$

A good first step regarding the selection of weight matrix $W_1(z)$ is to make a study of $G(z)$ open loop singular values. This previous study gives a valuable information about what features are missing in the original shape and should be included in the new weights. In the same direction, the initial open-loop study quality would increase if the singular values of whole uncertain set are plotted simultaneously. This way, it results easier to see how and where do the uncertain elements affect the singular values of the nominal plant. The plant under study presents parametric uncertainty. For this reason, a good way to obtain this curves is to make a parameter sweep.

Fig. 5.21.a shows the singular values of the plant, when a sweep in the grid equivalent resistance, in the interval $R_g \in [0, 167\ m\Omega]$, is induced. Figures 5.21.c and .e make a more detailed view of the effects of the variation (perturbation) of this parameter over the first resonance (c) and the second and third resonance (e) respectively. From the observation of the three plots, it is direct to extract the following conclusions:

- The variation of this parameter does not create a big influence on the nominal plant singular values except in the ressonances.
- The resonance frequencies remain stable under this resistance variation.
- An increment in the grid equivalent resistance reduces the quality factor of a resonance peak.

On the right column, Fig. 5.21.b shows the singular values of the open-loop plant under a sweep in the grid equivalent inductance in the range $L_g \in [0, 15.7\ mH]$. Again, Figures 5.21.d and .f show a more detailed view of the effects of the perturbation of these parameters. The following conclusions may be extracted:

- The frequency of the first resonance peak remains static independently of the grid equivalent inductance value.
- The band of the first resonance peak decreases when the inductance increases. However the maximum value of this resonance is, again, independent of the inductance value.
- Regarding the second and third resonance peaks (Fig. 5.21.f), even slight variations in the grid inductance induce changes in all frequency, peak value and bandwidth of the resonance peaks.

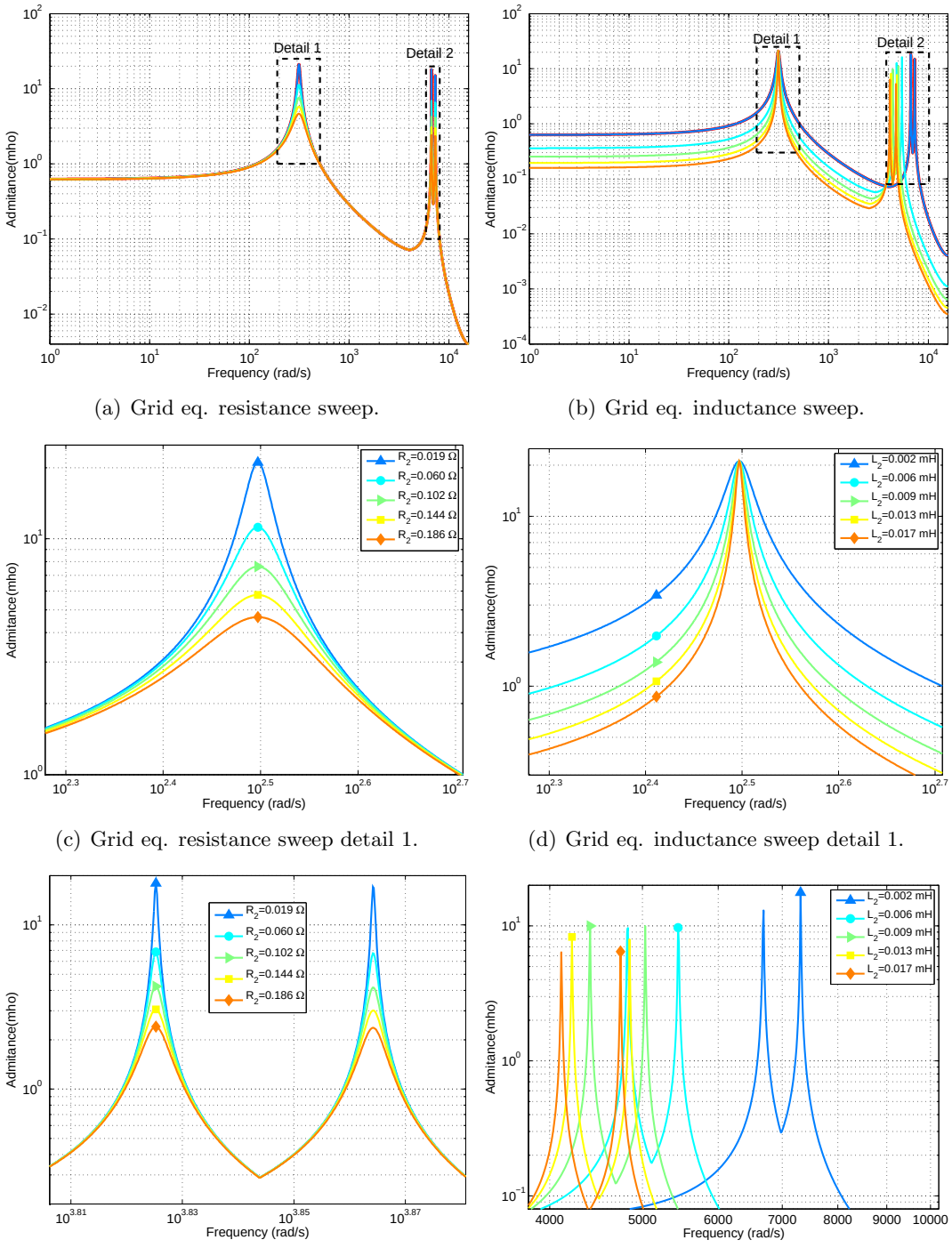

(a) Grid eq. resistance sweep.

(b) Grid eq. inductance sweep.

(c) Grid eq. resistance sweep detail 1.

(d) Grid eq. inductance sweep detail 1.

(e) Grid eq. resistance sweep detail 2.

(f) Grid eq. inductance sweep detail 2.

Figure 5.21: *Plant open loop maximum singular values.*

As described in subsection 5.3.2, the loop function after the shaping process is desired to have some basic properties as:

- Infinite gains at frequencies where null error is mandatory. This implies that the shaping weight $W_1(z)$ should present integrator behavior at null frequency in order to achieve null error to step reference changes, as the present application requires.
- At high frequencies, where usually unmodelled dynamics uncertainty and sensor noise is present, the loop-shaping function should present both a big attenuation and a big slope (more than 20 dB/decade).
- The slope of the singular values frequency function in the neighborhood of the desired crossover frequency [Skogestad and Postlethwaite, 2005] should be approximately 20 dB/decade. This slope is related with the stability margin obtained in the $\mathcal{H}_\infty$ optimization, γ. Low slopes yield low values for γ and, thus, good robustness indexes.

Additionally to obtaining a good stability margin in the design process, a second objective of the shaping weight $W_1(z)$ is to reduce the existing ν-gap between shaped plants: $\delta_\nu(G(z)W_1(z), G_p(z)W_1(z))$. Given the complexity of the exact relationship between the singular values of the plants and the resulting ν-gaps between them, it is difficult to extract qualitative conclusions. However, it results clear that uncertain regions below the crossover-region, and, thus, inside the closed-loop system bandwidth will have a big influence in the ν-gap measure between shaped plants.

As it will be shown below, the first resonance may be let fall inside the closed-loop bandwidth. This action has clear benefits, as it improves the settling time of the closed-loop system, and the disturbance rejection response around these same frequencies. In the last resonances cases, their influence over system robustness is much more critical and, as it will be shown later, these resonances peaks must be kept well below the 0 dB limit.

Shaping weights can be chosen directly in discrete-time by means of transfer functions in z domain. However, it usually results easier to design them in continuous time and convert to discrete-time by a *Tustin* approximation [Samar et al., 1995] [Samar et al., 1996]. As explained in chapter 4, the sampling time is fixed to $T_s = 200\ \mu s$.

For the application under study, the chosen weight was decomposed in a three factor product:

$$W_1(s) = diag(W_{11}(s) \cdot W_{12}(s) \cdot k). \tag{5.59}$$

Qualitatively, W_{11} inserts the desired tracking capabilities. In its simpler version, which is the case, W_{11} would normally be a simple integrator to achieve null error in steady state integrator:

$$W_{11} = \frac{1}{s} \tag{5.60}$$

W_{12} is desired to be a weight that increases the robustness to high frequencies perturbations, as, for example, the second and third resonances of the open-loop plant and the unmodelled high frequencies dynamics. For this reason, in the application under study, it is chosen to be a double pole of the form:

$$W_{12} = \left(\frac{k_{12}}{s + k_{12}} \right)^2, \tag{5.61}$$

where, after some iterations, the constant was selected to be $k_{12} = 2370$.

Finally, the constant k is the responsible of introducing a *dc* gain in the singular values in order to settle the desired crossover frequency and, consequently, approximately, the closed-loop bandwith. In the application, the constant d is designed to be $k = 785$.

The shaping weight transfer matrix, in the continuous domain, is, then, as follows:

$$W_1(s) = \begin{pmatrix} \frac{k \cdot k_{12}^2}{s \cdot (s+k_{12})^2} & 0 \\ 0 & \frac{k \cdot k_{12}^2}{s \cdot (s+k_{12})^2} \end{pmatrix} = \begin{pmatrix} \frac{785 \cdot 2370^2}{s \cdot (s+2370)^2} & 0 \\ 0 & \frac{785 \cdot 2370^2}{s \cdot (s+2370)^2} \end{pmatrix} \tag{5.62}$$

The singular values of shaping matrix and the matrices that compose it are displayed in Fig. 5.22.

When this transfer matrix is discretized ($T_s = 200\ \mu s$), the resulting shaping weight results as follows:

$$W_1(z) = \begin{pmatrix} 0.00288 \cdot \dfrac{(z+1)}{(z-1)} \cdot \dfrac{(z+1)^2}{(z-0.6168)^2} & 0 \\ 0 & 0.00288 \cdot \dfrac{(z+1)}{(z-1)} \cdot \dfrac{(z+1)^2}{(z-0.6168)^2} \end{pmatrix} \tag{5.63}$$

ν-gap analysis and robust stability

Revisiting eq. 5.35, and the guides given for loop-shaping design together with the conclusions of the last subsection, it results clear the dual responsibility of the loop-shaping process. On one hand, the loop-shaping process should be chosen to (sub-)optimally minimize the *infinity* norm of the closed-loop transfer function. This minimization implies a maximization in terms of unstructured uncertainty. On the other hand, while unstructured uncertainty assumption is sensible in some design problems, in the present case, the uncertainty is clearly structured, and, moreover, parametric. This parametric dependency forces a detailed study of the effects of shaping function over the resulting ν-gap distance between the shaped plants belonging to the perturbed set. In other words, the following question should be asked: *Which is the shaping function that minimizes the distance between plants while achieving a good robustness margin γ?*. Previous subsections indicated the tips to achieve a good robustness margin, but no a-priori design guides are available to minimize distance between gaps. This section is dedicated to gain some insight into this problem studying the effects of each of the resonances uncertainty on the ν-gap distance

The effect of a plant perturbance in either the grid equivalent resistance or inductance, on the first resonance, situated around 100 $rad\ s^{-1}$, as displayed in Fig. 5.21, affects the shape of the resonance but leaves untouched the resonant frequency. This fact makes it possible to let this resonance fall inside the loop function bandwidth without compromising controller robustness. Fig. 5.23 shows maximum existing ν-gap in the perturbed set when the nominal plant is shaped with three different shaping functions. These shaping functions are essentially the same except for the constant k. The constant has been chosen to produce a loop function that lets the resonance out of the loop bandwidth ($k = 10$), the value of

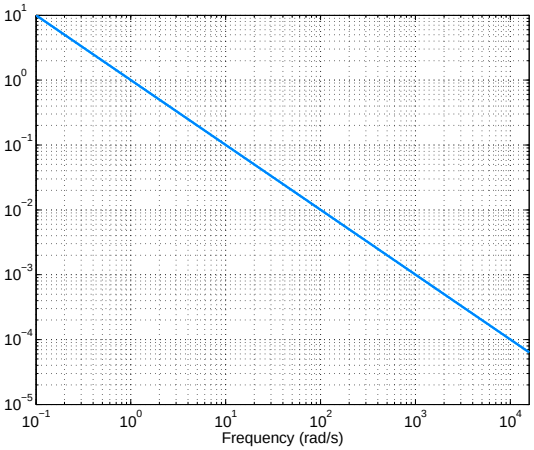

(a) Singular values of sub-shaping weight $W_{11}(s)$

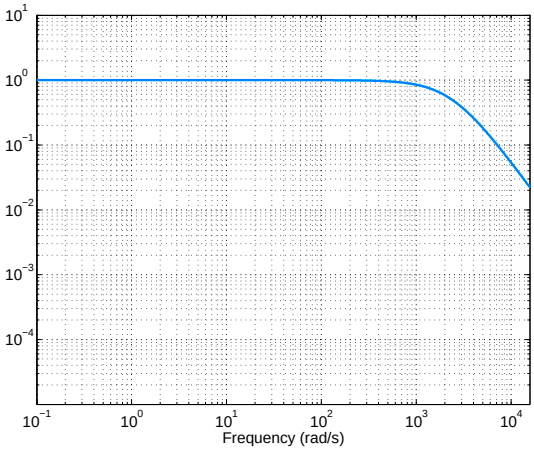

(b) Singular values of sub-shaping weight $W_{12}(s)$

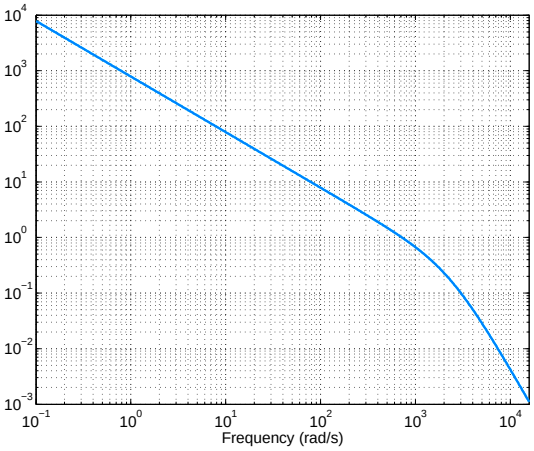

(c) Singular values of continuous shaping weight $W_1(s)$

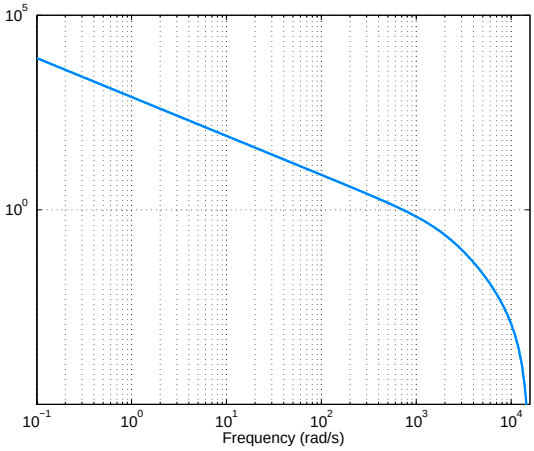

(d) Singular values of the discrete-time shaping weight.

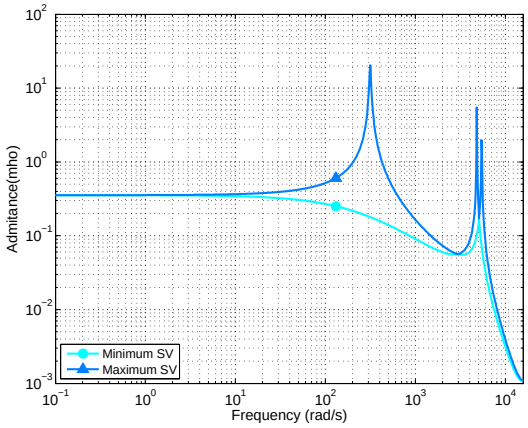

(e) Singular values of the nominal open-loop plant.

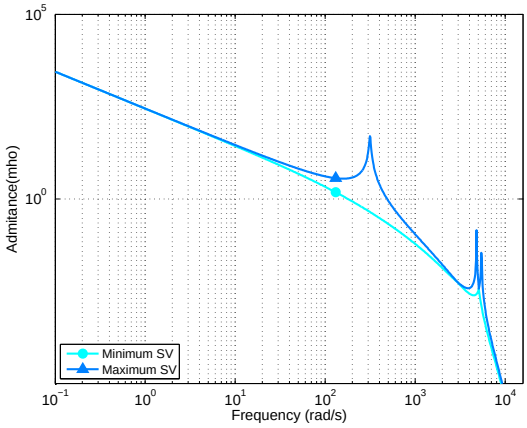

(f) Singular values of the shaped plant.

Figure 5.22: *Singular Values plot of the continuous shaping weight.*

the final design ($k = 785$) and a higher value that clearly makes the resonance be inside the loop bandwidth ($k = 5000$). Fig 5.23.a shows the singular values of the shaped loop function for the three k values. Subplots b,c and d show the corresponding existing ν-gap considering a resistive, inductive and resistive-inductive perturbance respectively. It can be seen that, when the plant is inductively perturbed, the ν-gap is bigger in the cases where the resonance has bigger gain. In the resistive case, however, the ν-gap shows a big spike in the lower gain case, probably by the proximity of the resonance to the 0 dB lines, that is likely to create sensitive results.

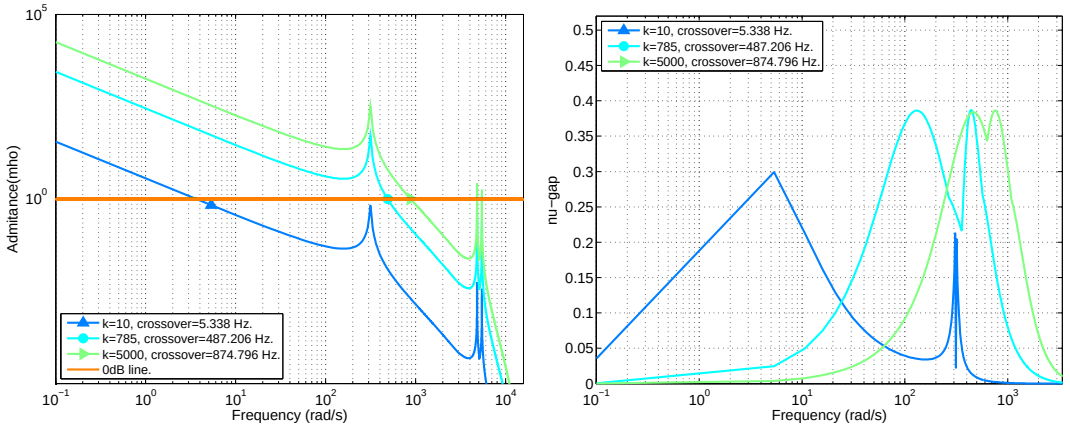

(a) Shaped loop function for three different k values.

(b) ν-gap distance for L_2 perturbation. 1st resonance.

(c) ν-gap distance for R_2 perturbation. 1st resonance..

(d) ν-gap distance for L_2 and R_2 perturbation. 1st resonance..

Figure 5.23: *Effect on the ν-gap of changing the gain of the shaping function. Detail of first resonance.*

The study of the perturbation effect on the perturbed set ν-gap in the case of the second resonance follows the same main principles. Again, the nominal plant has been shaped with the shaping function, described previously, modifying the constant k to leave the resonance out of the bandwidth ($k = 200$), in the place of the final design ($k = 785$) and to inside the loop bandwidth ($k = 2e5$). Fig. 5.23.a shows the singular values of the studied shaped loop functions. Subplots b,c and d show the corresponding existing ν-gap considering a resistive, inductive an resistive-inductive perturbance respectively. As

depicted in Fig. 5.21, when the grid equivalent impedance changes its inductive behavior, the resonance changes its resonant frequency. It results clear from Fig. 5.23.b that this shifting produces a great influence in the ν-gap whenever the resonance is in frequencies in the crossover region. This fact, and the proximity of the Nyquist bound to the resonances, practically limits the maximum achievable performance of the closed loop system in a double sense. First of all, it limits the maximum achievable crossover frequency, and, thus, the minimum settling time of the closed-loop system. It results clear that more speed means more sensitivity to parameter variation. On the other hand, the gain at resonant frequencies is also limited. This limit, as will be shown later, will have a direct influence over the disturbance response performance. Intuitively, it is easy to see that in frequencies with low gain in the loop-function, the system will have poor performance in its disturbance rejection behavior. Resistance variation, similarly to the first resonance case, presents a limited influence over the ν-gap of the perturbed set and does not represent a problem in design terms.

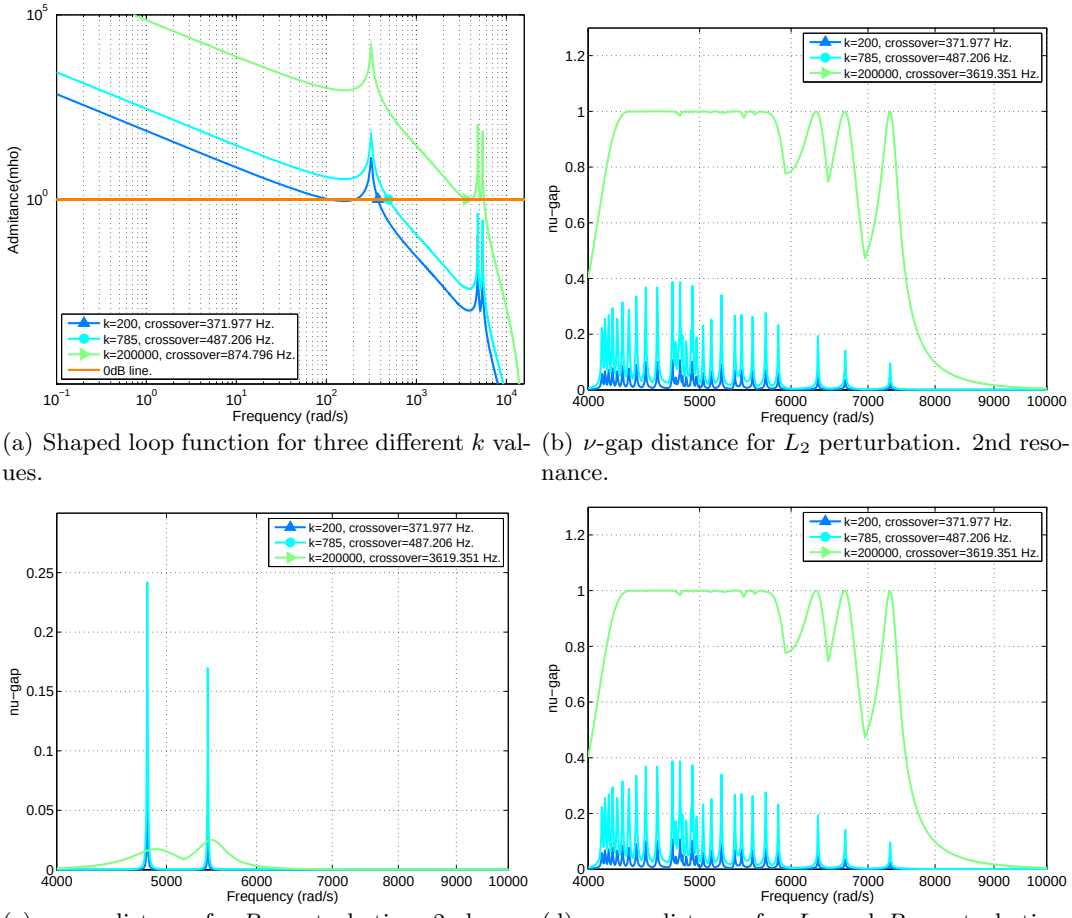

(a) Shaped loop function for three different k values.

(b) ν-gap distance for L_2 perturbation. 2nd resonance.

(c) ν-gap distance for R_2 perturbation. 2nd resonance.

(d) ν-gap distance for L_2 and R_2 perturbation. 2nd resonance.

Figure 5.24: *Effect on the ν-gap of changing the gain of the shaping function. Detail of second resonance.*

Fig. 5.25 shows the influence of a variation in the grid resistance and inductance parameters simultaneously over the system stability. It results clear to see that the effect

of an inductance variation over the perturbed set ν-gap is much bigger than the effect of resistance variation.

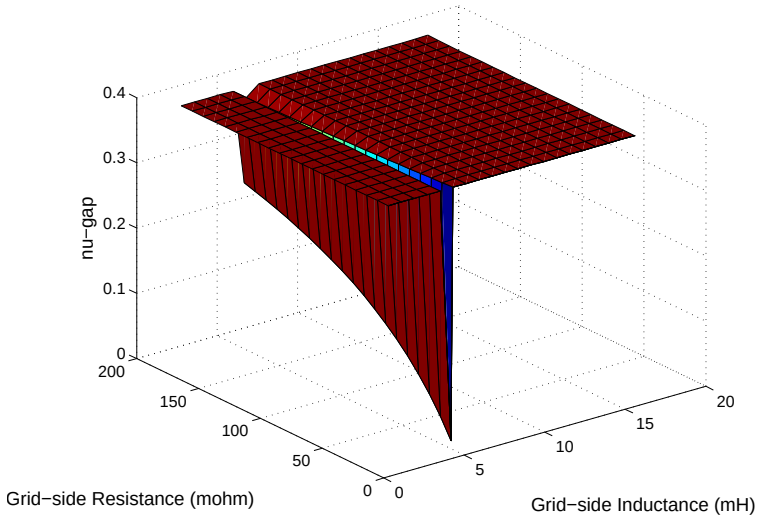

Figure 5.25: *ν-gap evolution for different L_2 and R_2 values.*

Closed-loop controller performance and robustness

Final controller design, as described in eq. (5.63), achieves robust stability when the considered perturbed set presents the uncertainty in the grid equivalent resistance and inductance values:

$$R_g \in [0, 0.18]\ \Omega, \quad L_g \in [0, 17]\ mH \tag{5.64}$$

This uncertainty represents a 10 p.u. uncertainty with respect to the grid-side grid filter inductor intrinsic parameters. The $\mathcal{H}_\infty$ minimization process yielded a stability margin $\gamma = 0.39$. The maximum ν-gap of the perturbed set is 0.389, thus, robust stability is guaranteed. Fig. 5.26 shows a simultaneous frequency plot of the maximum ν-gap in the perturbed set and the controller achieved stability margin. The ν-gap always falls below the stability margin.

Closed-loop functions S and T are specially important in the evaluation of the closed-loop performance of the system. The *sensitivity* function S is the transfer function (matrix) that relates the disturbance input to the output. It is represented for some plants of the perturbed set in Fig. 5.27.a. The *Complementary sensitivity* function, T, relates the reference (and measurement noise) input with the closed-loop system output. It is represented for a subset of plants belonging to the perturbed set in Fig. 5.27.b.

These two functions show, in general terms, that the design was carried out in a satisfactory way except around $\omega = 160\ rad\ s^1$, where the S and T functions show some undesirable overshoot.

Robustness stability has been analyzed using the SSV μ robust stability analysis method described in chapter 4. Fig. 5.28 shows the result of this analysis that verifies robust stability for the presented controller in the considered uncertain set.

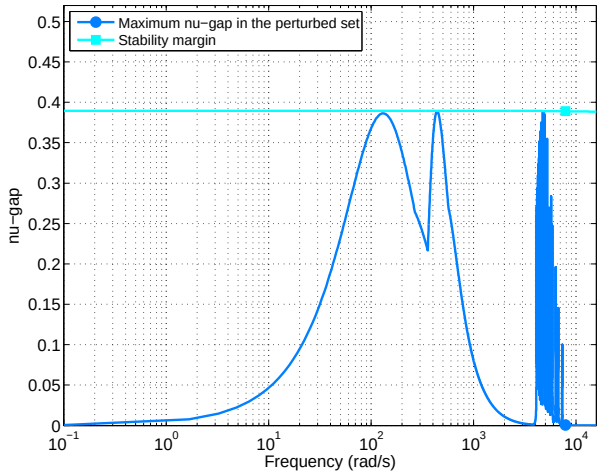

Figure 5.26: *Stability margin and maximum ν-gap of the perturbed set.*

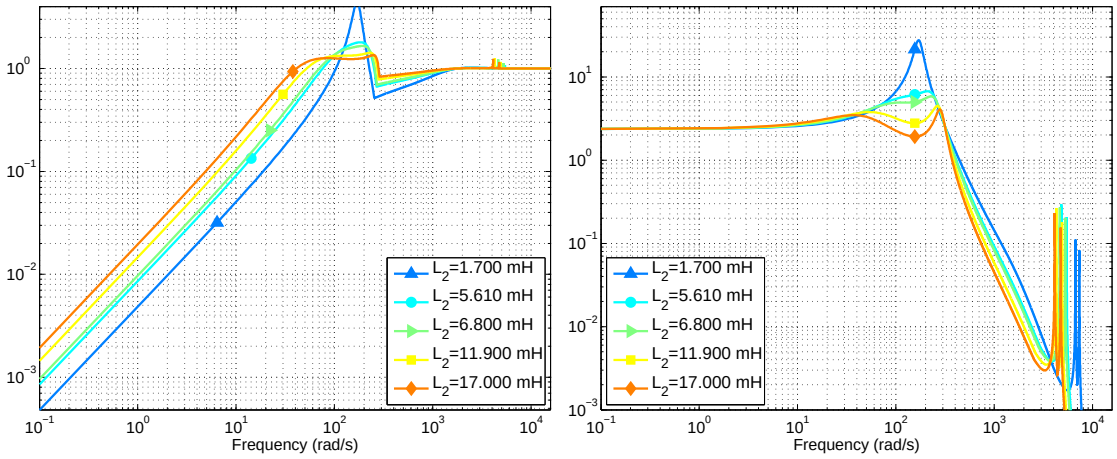

(a) Sensitivity function S. (b) Complementary sensitivity function T.

Figure 5.27: *Sensitivity and complementary sensitivity functions.*

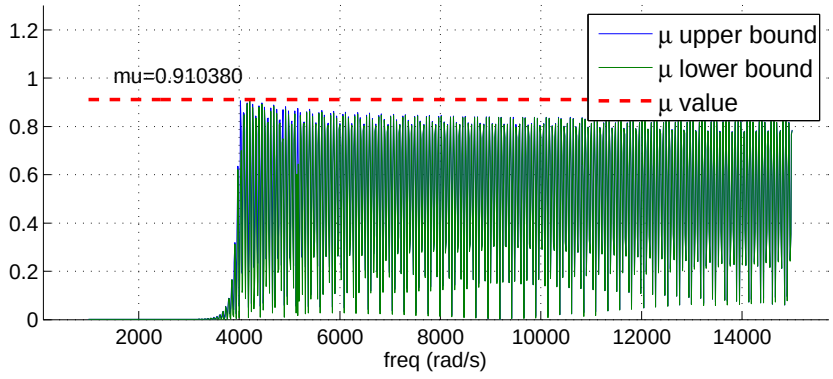

Figure 5.28: *Structured singular value of the designed controller.*

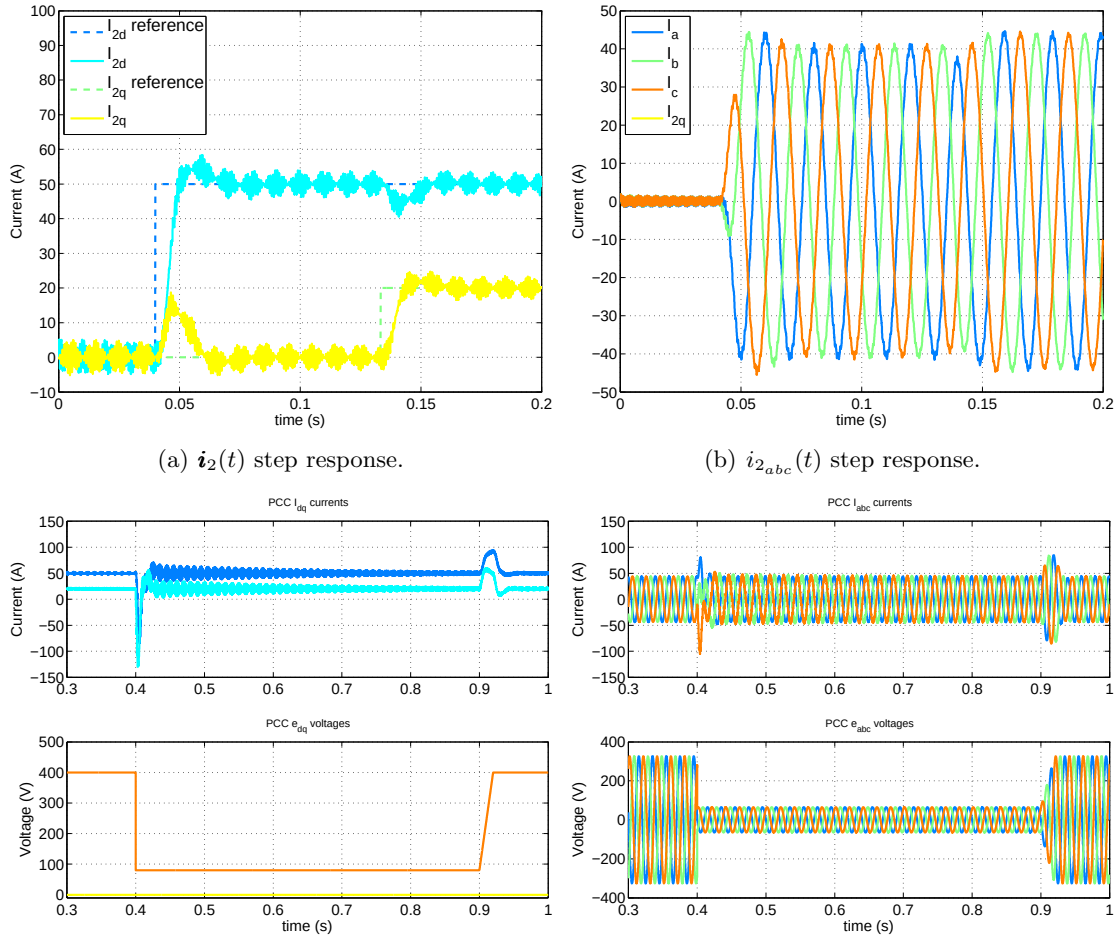

(a) $\boldsymbol{i}_2(t)$ step response.

(b) $i_{2_{abc}}(t)$ step response.

(c) $\boldsymbol{i}_2(t)$ dip response.

(d) $i_{2_{abc}}(t)$ dip response.

Figure 5.29: $\mathcal{H}_\infty$ *controller simulation results.*

The present proposal achieves a settling time of approximately one grid cycle time for the nominal plant used for the design, situated at the first third of the uncertain set. Compared with other proposals, as, for example the ones analyzed in chapter 4, the controller can be considered to be slow. This lack of speed causes a negative influence over higher (in hierarchy) controllers, particularly over the voltage controller as described in the introduction of this dissertation. The performance of the voltage control loop hardly depends on the performance of the current one. To ensure independent operations, the dynamics of the voltage control loop are usually deliberately slowed down around 10 times comparing with the current loop dynamics. In a parallel way, results displayed in Fig. 5.29.c and .d, showed an improvable disturbance rejection behavior. Disturbance rejection performance finally relies on the magnitude of the loop function, named L, compared with the magnitude of the grid disturbance transfer matrix, named $G_d(s)$. If the loop function presents high gain at a certain frequency, the steady state error at that frequency will be small, resulting in good disturbance rejection. Unfortunately, in the case under study, the disturbance transfer matrix presents resonance peaks that are uncertain and placed at the same positions of the second group of resonances of the plant model, displayed on Fig. 5.21.e and .f. Given the necessity of placing the crossover frequency before the second resonances group of the plant, and keeping it well attenuated to minimize ν-gap distance, disturbances cause poorly damped transients.

To some extent, this is the price to pay for robustness. In fact, from the study performed in the previous section, the placement of the crossover frequency relative to the resonance groups (see Fig. 5.21) creates three basic design possibilities:

- To place the crossover frequency after the second resonance group. This strategy would yield the best results as very high bandwidth controllers would be produced. Once the uncertain resonance group is fully introduced inside the system bandwidth, its influence over the perturbed-set ν-gap falls again to sensible values that can be stabilized by a synthesized controller. Unfortunately, this option is not available for the presented experimental set-up because of two reasons: (i) the Nyquist frequency is located very close to the end of this resonance and (ii) the maximum stability margin of the controller is lower than the gap in nearly every case. This resonance group is indeed a very uncertain region that could be considered the start of the high frequency unmodelled dynamics zone of the plant. Introducing it inside the bandwith clearly reduces the robust character of the controller. For this reason, this problem would be a classical application of μ robust design theory.

- A decrease in the crossover frequency would place it in the surroundings of the second resonance group. This strategy allows to synthesize a controller but the ν-gap of the perturbed set quickly goes to the unity (maximum value) even for small perturbations in the grid equivalent inductance. This strategy would allow to significantly increase the system bandwidth but is not feasible.

- To place the crossover frequency between both resonances groups. This strategy forces to externally attenuate the second resonance group in order to avoid that it crosses the 0 dB line for any plant in the perturbed set. This is the chosen option and probably the best one for many filter configurations. The performance of the resulting controller mainly depends on the gain of the loop transfer function in the first resonance peak. This resonance is also present in the disturbance transfer function

so it has a direct influence on disturbance rejection behavior. Roughly speaking, high gains will produce better rejection and additionally will increase the crossover frequency, improving step response, as well.

In fact, the amount of gain that can be placed in this resonance peak hardly depends on the distance between resonance groups. LCL filters with separated groups allow to give a big gain to the first resonance and let the loop function fall slowly (20 dB/decade) and still place the required attenuation over the second resonance group to keep the gap in sensible values. Of course this distance has significant practical consequences in the final equipment as it is related with the converter switching period (T_{SW}), the desired attenuation over switching frequency (THD) and the filter size.

A last remark has to be made regarding controller robustness. A third grid parameter that is always uncertain is the grid fundamental frequency. Grid operators of developed countries guarantee a narrow safety operation margin. This grid frequency uncertainty mainly creates synchronization issues that fall out of the scope of this study. Assuming that the synchronization system is able to accurately adapt to the fundamental frequency and is correctly translating measurements into the synchronous reference frame, the grid still creates a parametric perturbation over the plant model. Observing Fig. 4.4 and Fig. 4.10, it can be noted that the ω parameter directly affects to the inter-channel coupling terms: ωL_1, ωC_0 and $\omega L_2'$. This uncertainty is not included neither in the stability analysis of chapter 4 nor in the perturbed set defined in the present chapter. However, the low variation of the grid frequency is likely to be assumed by the robustness of the designed controller. On this issue,the sub-optimal nature of the proposed procedure makes its conservativeness a positive feature. Fig. 5.30 shows the effects of a grid variation in the interval $\omega \in [2\pi 40\ rad\ s^{-1}, 2\pi 60\ rad\ s^{-1}]$ over the limit models in the perturbed set: the model with less grid equivalent resistance and inductance and the one with the biggest values.

Implementation issues

The most direct way to implement the previously designed controller is represented in Fig. 5.31. This configuration has been found to be useful [Skogestad and Postlethwaite, 2005] because the references do not directly excite the dynamics $K(z)$, which can result in large amounts of overshoot in the case the controller presents derivative behavior. The pre-filter is used to ensure a steady-state gain of 1 between the references and the outputs, assuming that $W_1(z)$ contains integral behavior.

The controller requirement is to achieve null error in steady-state. To obtain this feature, the pre-compensation weight has to include a DC integrator to achieve infinite gain at null frequency in the loop gain. This behavior is well known to present problems in the usual case of plants with amplitude limitations in the actuators. In the power converter case, amplitude of the actuation should be limited to avoid the converter from entering in the non-linear over-modulation zone. Being u_d, u_q the actuation signals, and U_{DC} the voltage level in the DC-side of the power converter, a particular safety limit for this variables may be expressed as[3]:

[3]Several saturation strategies are reported in the technical literature [Ottersten, 2003]. The design of such a saturator falls out of the scope of this dissertation, whose aim limits to present a valid anti-windup procedure suitable for generic situations.

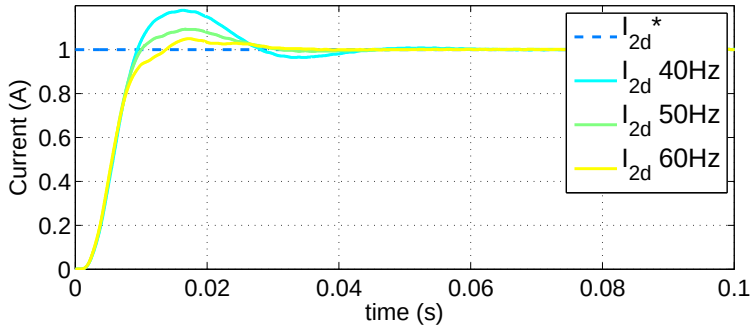

(a) Response with $\Delta_L = -1$, $\Delta_R = -1$.

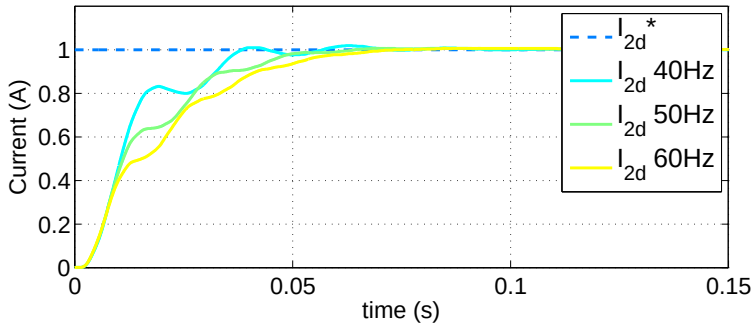

(b) Response with $\Delta_L = 1$, $\Delta_R = 1$.

Figure 5.30: *Effects of grid fundamental frequency over closed-loop step response.*

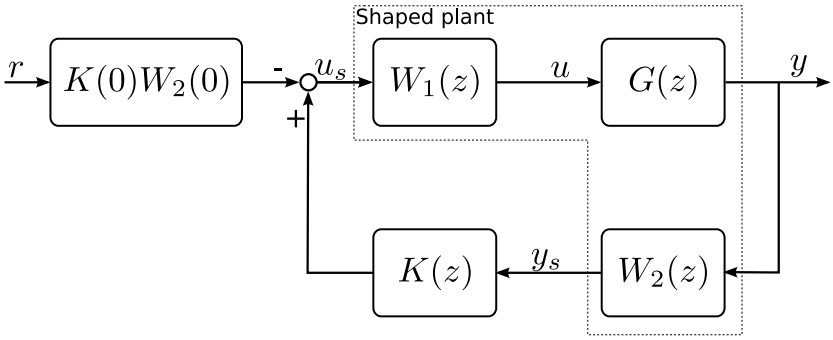

Figure 5.31: *Practical implementation of the H_∞ discrete-time loop-shaping controller.*

$$u_d^2 + u_q^2 < \left(\frac{U_{DC}}{2}\right)^2 \tag{5.65}$$

During input variable saturation, the integrators that exist in the controller continue to integrate their input causing windup problems. Several methods have been proposed in the literature to avoid this kind of problems. Provided that the transfer function that can cause windup problems is invertible (i.e. $D \neq 0$) and minimum-phase, a good approach is to implement it in its *self-conditioned* or *Hanus* form [Skogestad and Postlethwaite, 2005] [Hanus et al., 1987]. In the loop-shaping $\mathcal{H}_\infty$ controller case, the anti-windup action can be restricted to the pre-compensator W_1 as it is the only element that presents integral behavior. So, let the weight W_1 have a state space realization:

$$W_1 := \left(\begin{array}{c|c} A_w & B_w \\ \hline C_w & D_w \end{array}\right) \tag{5.66}$$

and let u_{dq} be the input to the plant actuators and e_{dq} the input to the shaped plant (i.e. the error signal). When implemented in *Hanus* form, the expression for u_{dq} becomes:

$$u_{dq} = \left(\begin{array}{c|cc} A_w - B_w D_w^{-1} C_w & 0 & B_w D_w^{-1} \\ \hline C_w & D_w & 0 \end{array}\right) \begin{pmatrix} e_{dq} \\ \breve{u}_{dq} \end{pmatrix}, \tag{5.67}$$

where $\breve{u}_{dq}$ is the actual plant input, after the actuator saturation process. The *Hanus* form prevents windup by back-propagating the actual plant input to W_1 states, keeping them consistent under saturation situations. It is easy to see, that when there is no saturation, and consequently $u_{dq} = \breve{u}_{dq}$, the dynamics remain unaffected and eq. 5.67 simplifies to eq. 5.66. However, when saturation happens and $u_{dq} \neq \breve{u}_{dq}$, the dynamics are inverted and the states remain consistent with the actual plant input. Fig. 5.32 shows how this anti-windup strategy is integrated in the control loop.

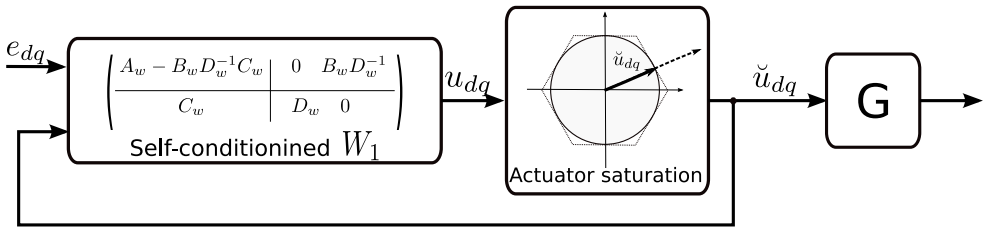

Figure 5.32: *Anti-windup strategy in weight W_1.*

In order to evaluate the performance of this anti-windup scheme, the system was deliberately saturated at low actuation voltage, and reference currents where set-up at very high values to intensify saturation undesirable effects. Fig. 5.33 shows the effect produced by the proposed anti-windup system when applied to the converter control problem. In the left column of the figure the responses of the *dq* output currents, the *dq* actuation voltages and the *abc* output currents can be seen. The right column of the figure shows the responses of the same signals when no anti-windup scheme is present. As the figure shows, the anti-windup effect is clearly positive.

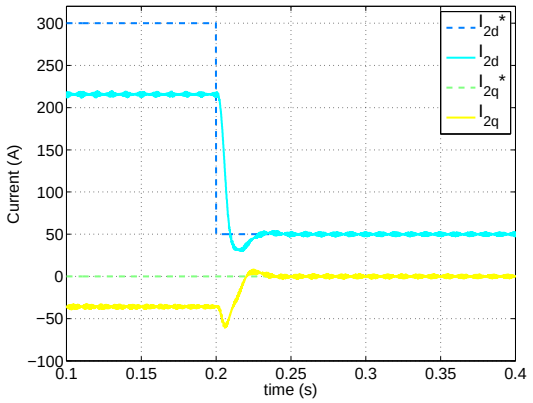

(a) Output dq currents response in anti-windup presence.

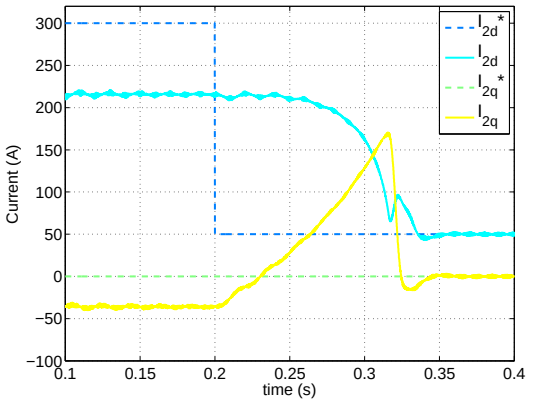

(b) Output dq currents response without anti-windup presence.

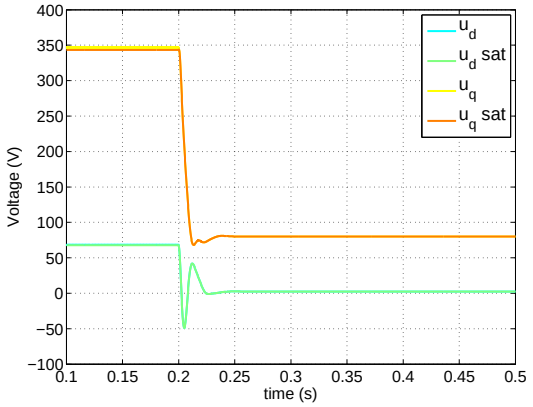

(c) Actuation dq voltages response in anti-windup presence.

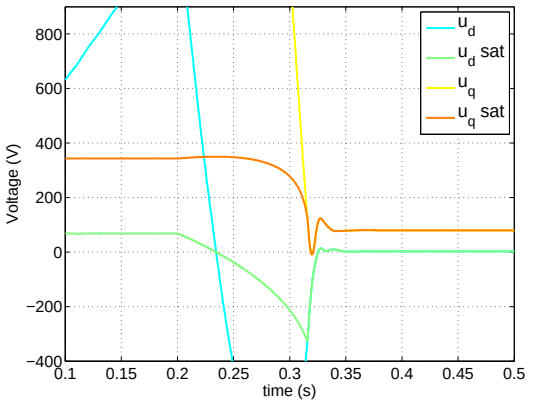

(d) Actuation dq voltages response without anti-windup presence.

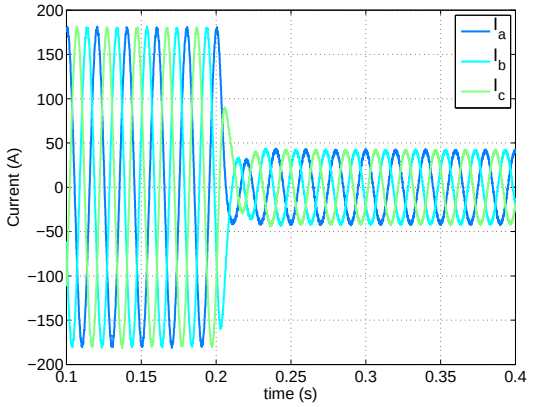

(e) Output abc currents response in anti-windup presence.

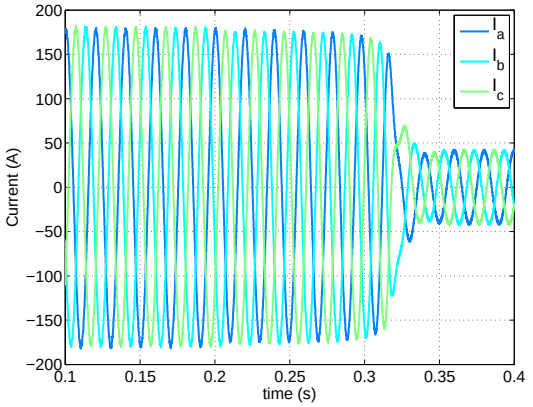

(f) Output abc currents response without anti-windup presence.

Figure 5.33: *Anti-windup effect*

5.3.4 Robustness comparison with other controllers

The main difference between the presented controller and previous approaches for controlling the grid-side current of an LCL filter is the final objective of design process itself. This approach main finality is to obtain a controller that stabilizes an uncertain set of plants. Other approaches are basically focused on transient or steady performance. It results clear to see that, by the use of the analysis procedure proposed in chapter 4, the maximum values for the grid equivalent inductance and resistance can be extracted for such a non-robust controllers. However, that design processes are often difficult (or impossible) to adapt to a particular robustness requirement: if a certain controller is not robust enough, there is no a-priori criteria to modify it in order to increase its robust features. The opposite direction, to improve the performance if the controller is more conservative than it should, is also an issue.

$\mathcal{H}_\infty$ approach, however bases its design precisely on this kind of considerations, and, thus, can yield more appropriate controllers for circumstances where robustness is an issue.

Regarding the effects of uncertainty, it is difficult to make a systematic comparison with other controllers due to the great variability of filter configurations and controller designs, mostly when referred to a cascaded SISO approach where each of the PI elements is designed individually. Despite of that, each structure is influenced in a particular way when the intrinsic grid parameters are modified. Two representative approaches of the grid-side LCL current control have been used for this comparison: a cascaded SISO approach as the one described in [Bueno et al., 2004] and a MIMO servo-controller approach as the one described in [Huerta et al., 2008b].

Fig. 5.34 shows the step responses for different inductance and resistance perturbations. As displayed, the schemes demonstrates to be very robust to inductance under-estimation at the cost of loosing the steady state null error. This increase in the robustness when the null steady state error is relaxed is common to other many problems as even the proposed $\mathcal{H}_\infty$ procedure, that may achieve much faster results in this situation. The control scheme presents a more critical sensitivity to inductance underestimation, that creates signals oscillations and finally instabilizes the closed-loop. As expected, uncertainty in the grid equivalent resistance induces little effect.

The MIMO pole-placement grid-side current control approach presents a more systematic design method. As displayed on Fig. 5.35, it does not loose the null steady state error when the plant is perturbed in either its equivalent inductance or resistance. The presented scheme is based on a dominant pole placement. It is interesting to remark that the position of the dominant poles is hardly changed under perturbed situations. This makes this design quite robust, in performance terms, provided the design is not unstabilized. However, the design is sensitive to both inductance under- or over-estimation. Again, the sensitivity to resistance variation is minor.

Finally, Fig. 5.36 shows the effects of the grid perturbation over the step response of the system controlled by the proposed $\mathcal{H}_\infty$ scheme. As in the previous case, the closed-loop system does not loose the steady-state performance. It assumes a great perturbation for inductance perturbation, particularly for inductance under-estimation. This kind of perturbation degrades the transient performance: the system gets more slow when the grid equivalent inductance is increased. As in previous cases, the sensitivity to resistance variation is minor.

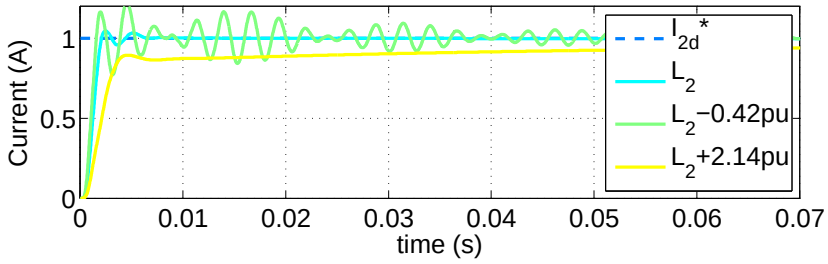

(a) Grid inductance variation.

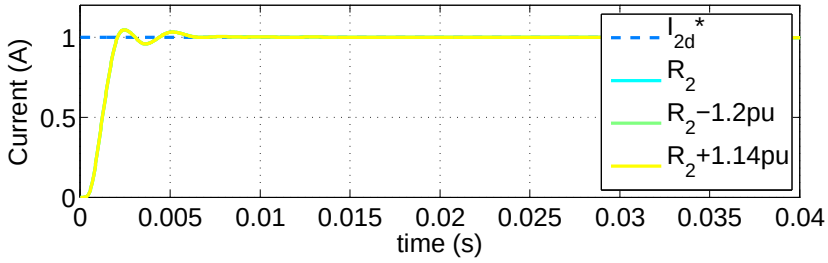

(b) Grid resistance variation.

Figure 5.34: *Response of the cascaded SISO system in [Bueno et al., 2004] under different grid conditions.*

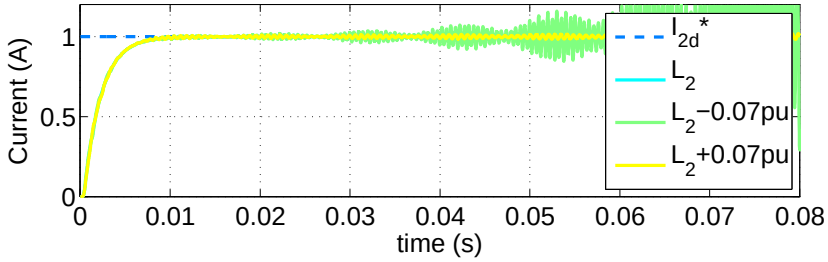

(a) Grid inductance variation.

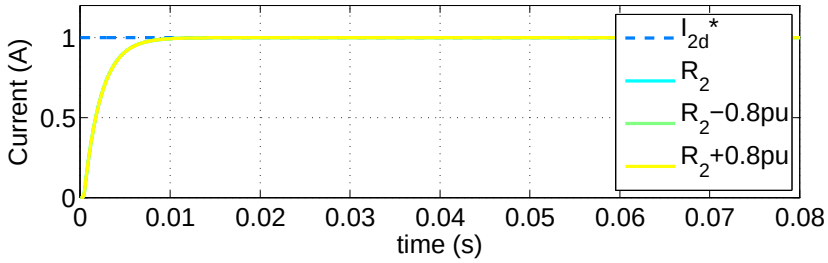

(b) Grid resistance variation.

Figure 5.35: *Response of the pole-placement MIMO servo-controlled system in [Huerta et al., 2008b] under different grid conditions.*

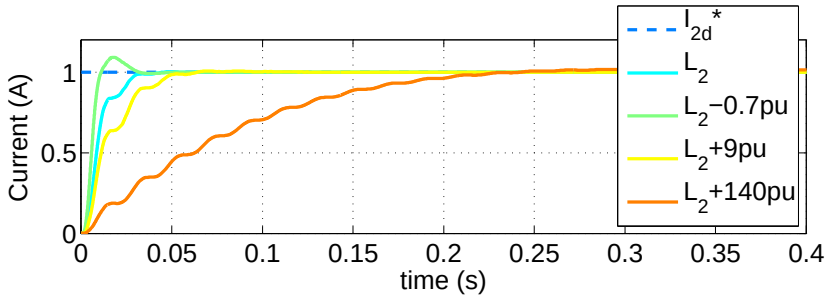

(a) Grid inductance variation.

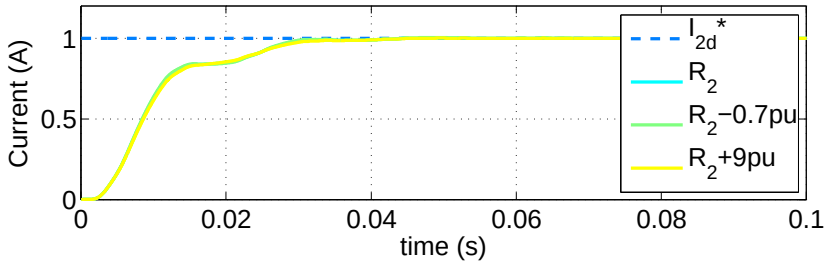

(b) Grid resistance variation.

Figure 5.36: *Response of the proposed loop-shaping $\mathcal{H}_\infty$ controlled system under different grid conditions.*

5.4 Experimental results

The proposals presented in this chapter have been evaluated under experimental testing. The experimental set-up that was used during the experiments is described in detail in chapter 6.

Fig. 5.37.a shows the step response obtained by the LQ procedure described in this chapter when all state variables are directly measurable. Fig. 5.37.b shows a scope capture of the obtained *abc* current signals. Fig. 5.37.c and .d show the step response and the *abc* currents, respectively, of the system when controlled by an LQ control scheme with state variables estimated by a predictor estimator. Fig. 5.37.e and .f show the step response and the *abc* currents, respectively, of the system when controlled by an LQ control scheme with state variables estimated by a *Current* estimator. Fig. 5.37.g shows the tracking error during a step change for the LQ scheme without states estimation. Fig. 5.37.h shows the harmonic content obtained by the application of the presented LQ design procedure.

Fig. 5.39.a and .b shows the step response and the corresponding *abc* signals obtained when the system is controlled by means of the proposed $\mathcal{H}_\infty$ procedure. Fig. 5.39.c shows the error tracking during a step change in the current references of a system controlled by the robust design procedure. Finally, Fig. 5.39.d shows the harmonic content obtained with this control scheme.

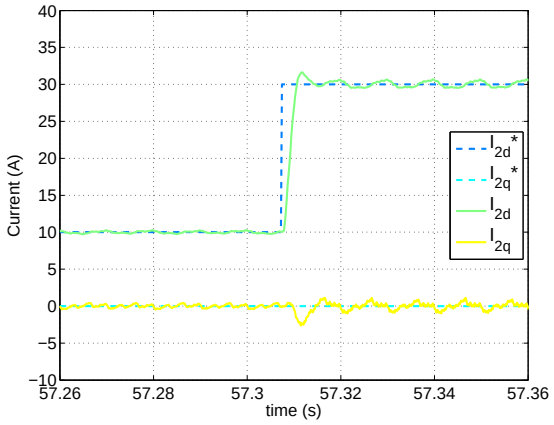

(a) LQ *dq* step response. Measured states.

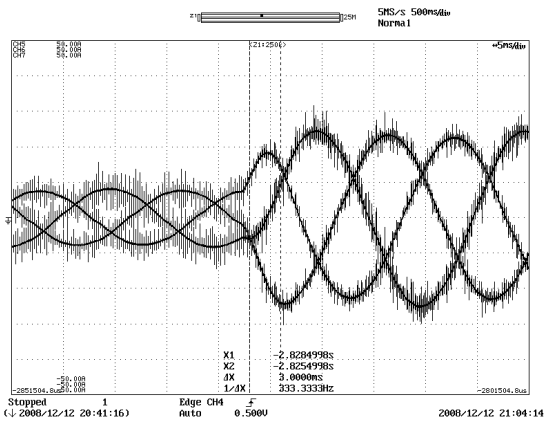

(b) LQ *abc* current signals. Measured states.

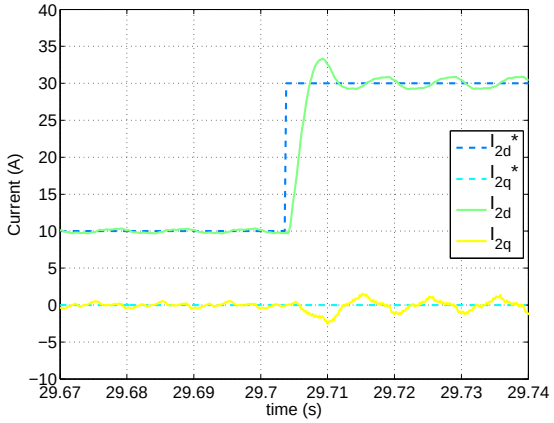

(c) LQ *dq* step response. Predictor estimator.

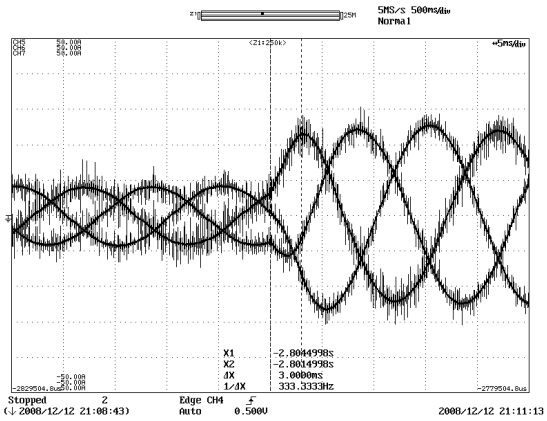

(d) LQ *abc* current signals. Predictor estimator.

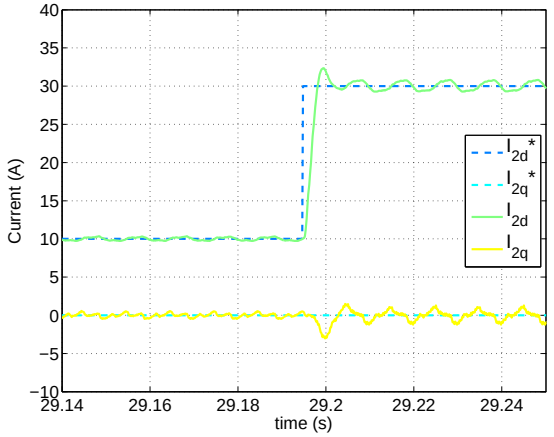

(e) LQ *dq* step response. *Current* estimator.

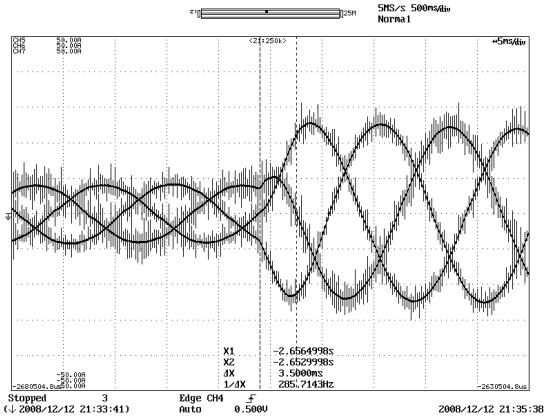

(f) LQ *abc* step response. *Current* estimator.

Figure 5.37: *Experimental step responses of the presented LQ controllers.*

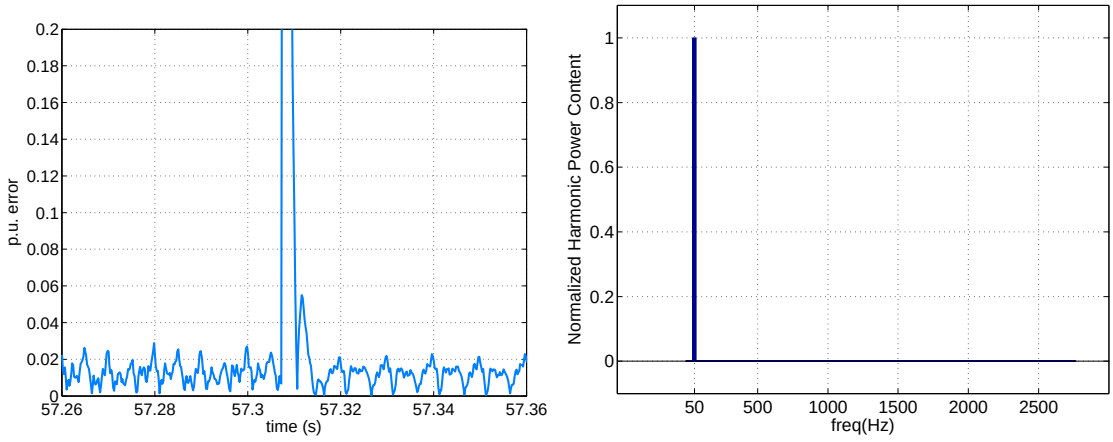

(a) LQ tracking error. Predictor estimator.

(b) LQ harmonic content. Predictor estimator.

Figure 5.38: *Experimental evaluation of the LQ proposal.*

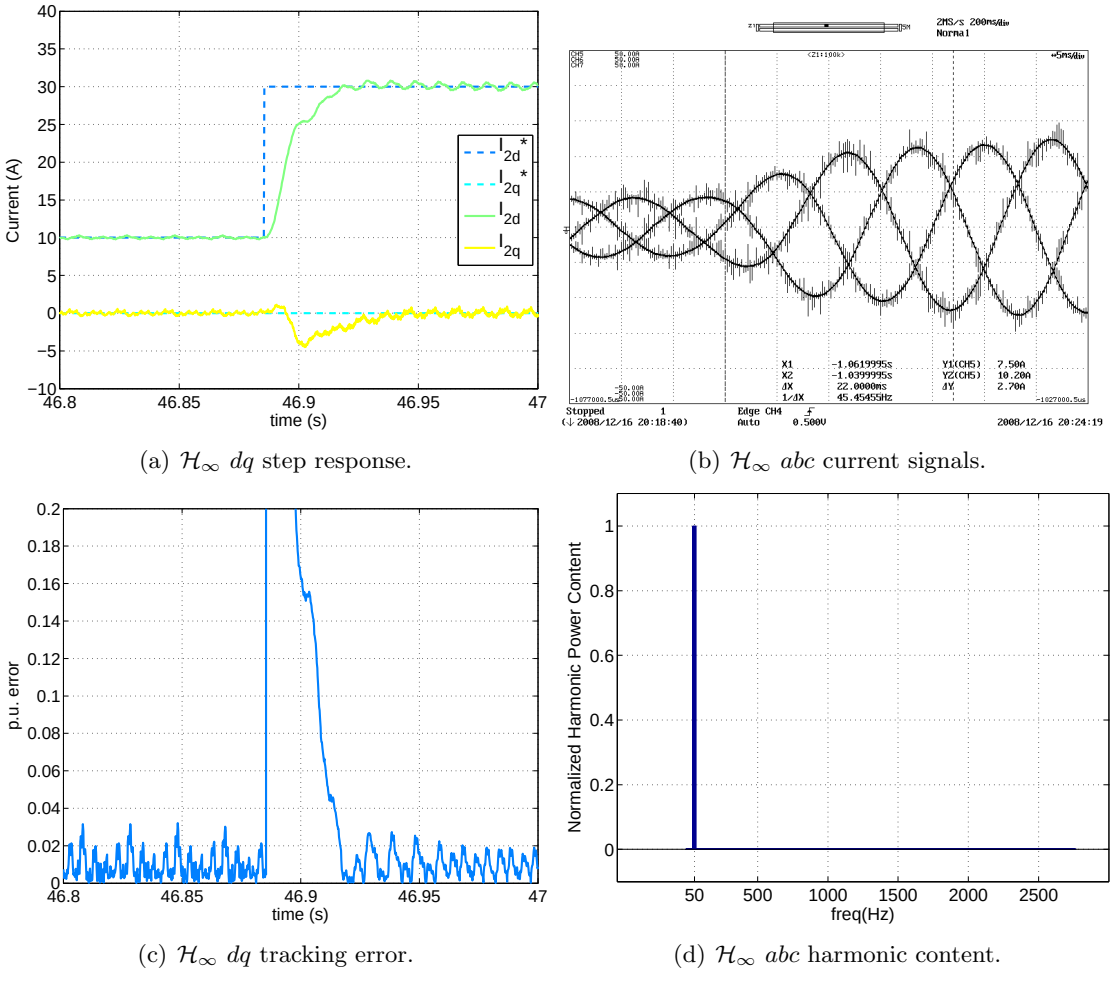

(a) $\mathcal{H}_\infty$ *dq* step response.

(b) $\mathcal{H}_\infty$ *abc* current signals.

(c) $\mathcal{H}_\infty$ *dq* tracking error.

(d) $\mathcal{H}_\infty$ *abc* harmonic content.

Figure 5.39: *Experimental testing of the proposed $\mathcal{H}_\infty$ controller.*

5.5 Conclusions and main contributions

This chapter has presented two approaches for the MIMO current control of VSC connected to the grid trough LCL filters. Following lines state the main extracted conclusions and contributions.

First part of the chapter has proposed an LQ servo-controller design procedure. This technique has demonstrated to be a successful design approach whenever strict robustness constraints are not present. Experimental results have demonstrated the very good performance of the closed-loop system. The design method is easily applicable to different filter structures, allows the introduction of null steady-state error requirements and can be applied to discrete-time plants, even including computational delays, being fully suitable for its appliance in the control of power converter by means of a DSP platform.

For the case where a decrease in the number of system sensors is desired, the chapter has proposed the use of three well-known estimator schemes: the predictor, *Current* estimators and Kalman filter. The use of these sensors allow to perform a full control using only the grid-current sensors. The chapter has analyzed the influence of different kinds of noise on the estimation behavior. The chapter has also shown the behavior of the LQ scheme when state variables are estimated by means of predictor and *Current* estimators.

Second part of the chapter has proposed an $\mathcal{H}_\infty$ design procedure. This technique is able to synthesize a controller from an uncertain description of the plant model. The design procedure has demonstrated to produce satisfactory results and its robust stability has been verified by simulations and structured singular value μ analysis. The resulting controller has also been verified under experimental testing.

The concrete design technique that has been used in this thesis, Loopshaping $\mathcal{H}_\infty$, offers a simple design process based on a simplified loopshaping procedure. Its combination with the ν-gap norm creates a powerful set of tools that allows to handle with structured or unstructured uncertain processes.

This is the main contribution of this thesis. Previously applied control schemes may result in controllers with better or worse robustness properties. Perhaps a particular PI-based design applied to a particular LCL filter gives a very robust controller, however, there is no way to a-priori know or modify these robustness properties. The presented proposal gives actual control of final design in robustness issues.

Additionally, the use of $\mathcal{H}_\infty$ techniques may be understood not only as a design procedure but also as a very strong analysis tool that allows the designer to have an accurate idea of the influence of a particular uncertainty over the hypothetical final closed-loop system. This fact brings a valuable base for an engineering oriented design, as it can give information about the best possible controller for certain assumed uncertainty.

Chapter 6

Experimental set-up and results

This chapter describes the experimental set-up that was developed and used to verify the results proposed in this dissertation. The description covers system architecture, task description and design and final system performance. The second part of the chapter summarizes the obtained experimental results.

6.1 Introduction

This chapter presents the experimental set-up that has been used for evaluating the algorithms[1] proposed in this dissertation.

The design of this system has been developed by the *Industrial Electronics applied to Renewable Energy Systems* group, GEISER, from the UAH, in collaboration with the company Sedecal Control S.L.. Its design is framed inside the the project CONDOR II, entitled *"Design and evaluation of protection and control solution for distributed generation systems in the presence of grid faults and disturbances"*. This project is funded by the Spanish Science and Technology Ministry (ENE2005-08721-C04-01).

The experimental set-up consists of a Voltage Source Converter connected to the grid by means of an LCL grid filter and controlled by means of an digital electronic control platform.

The presented system is divided in two components:

- A Power Electronics System (PES in the following). This system represents the power electronics circuitry of the whole experimental set-up. Roughly speaking, it is composed of a DC/AC IGBT-driven Voltage Source Converter, a grid connection filter and the ancillary circuitry needed for safety and flexibility issues.
- An Electronic Control System (ECS in the following). This system represents the control logic of the experimental set-up. It is basically composed of a high-performance computing unit connected to co-processor that generates the necessary periphery and communication capabilities to properly interface with the PES and a control host or other controllers in a distributed scheme.

Fig. 6.1 shows a block diagram of the complete experimental set-up.

[1] Figs. 4.29 and 4.28 displayed in chapter 4 where captured with a hysteresis controlled converter used in the Electrical Engineering Lab of the UPC.

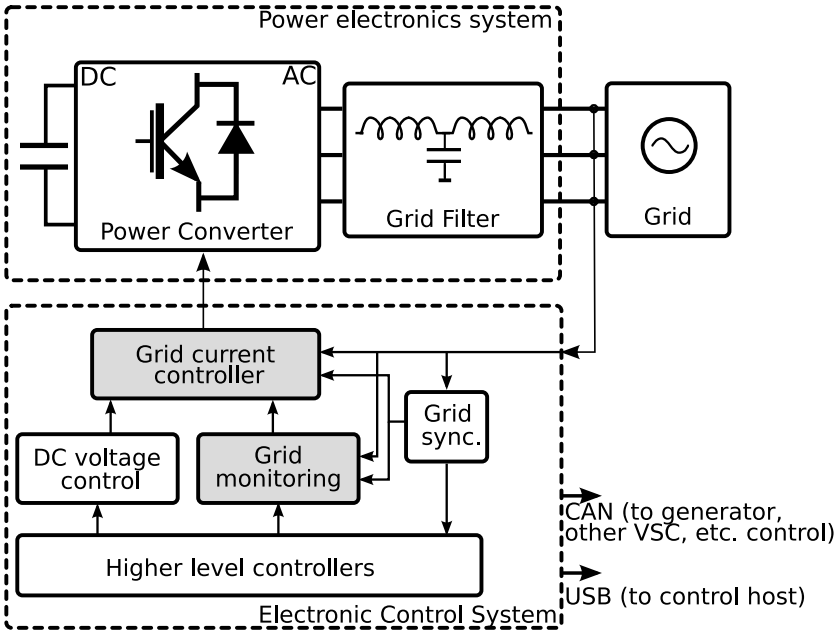

Figure 6.1: *Experimental set-up general block diagram.*

6.2 Power Electronics System

As stated in the introduction, the Power Electronics System represents the power processing part of the whole experimental set-up. Fig. 6.2 shows a block diagram of it. The PES core component is a 17.5 kVA Voltage Source Converter, built with IGBTs.

The VSC is designed to be connected to the grid through an LCL filter that serves as an interface between the VSC and the grid and provides the desired attenuation at switching frequencies.

Besides these core components, the PES also contains other important devices that play an auxiliary role in the converter operation. The PES contains a diode drive auxiliary rectifier (see Fig. 6.2). This rectifier primary function is to perform a DC-bus pre-charge to place the VSC into linear modulation zone before starting the PES control algorithm. The rectifier is complemented with a set of three resistors that appear in the bottom part of Fig. 6.2. This devices are placed to limit the maximum current entering the diode rectifier.

The connection or disconnection of this rectifier is carried out by means of the so-called *Auxiliary contactor*. This element controls the connection or disconnection of the three-phase input signals to the rectifier input. The function of the named *Time-triggered contactor* protects the main contactor from incorrect activations.

In the same direction, *General* and *Main contactors* control the connection of the whole PES to the grid. The combination of both devices allow several interesting system configurations. For example, it can be connected in back-to-back configuration with the VSC to make experiments of the DC-bus controller under non-linear DC-bus loading or even to connect it in shunt configuration, and to test active filter algorithms in the VSC.

Finally, the so-called *Filter contactor* in association with the damping resistances R_{da}, R_{db} and R_{dc}, are used to create a configurable damping of LCL resonance. This external damping is not usually used in production systems but can result useful for algorithm

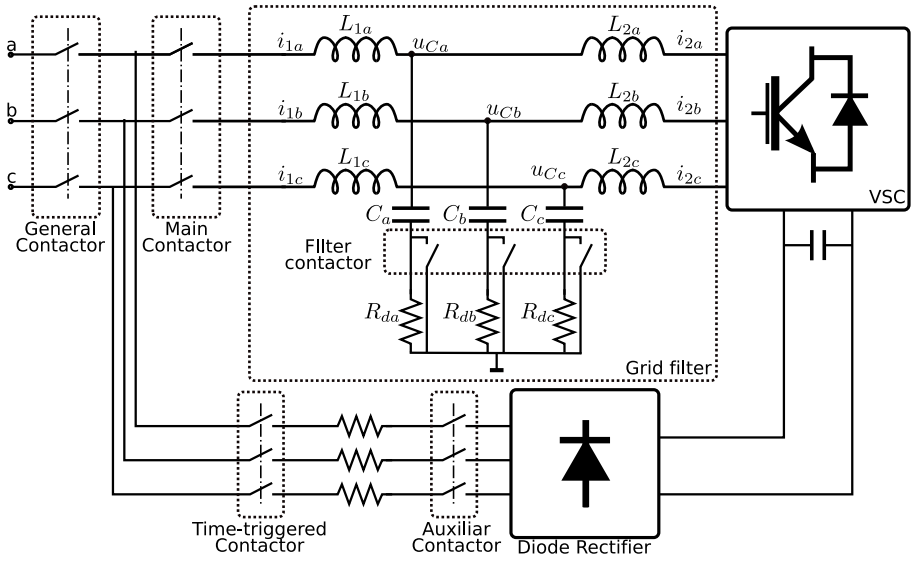

Figure 6.2: *Power Electronics System block diagram.*

development and testing.

6.2.1 Power converter

The main component of the PES is the Power Converter. The converter is a regular IGBT-driven Voltage Source Converter. This topology is very popular due to its great flexibility. Its schematic is displayed on Fig. 6.3.

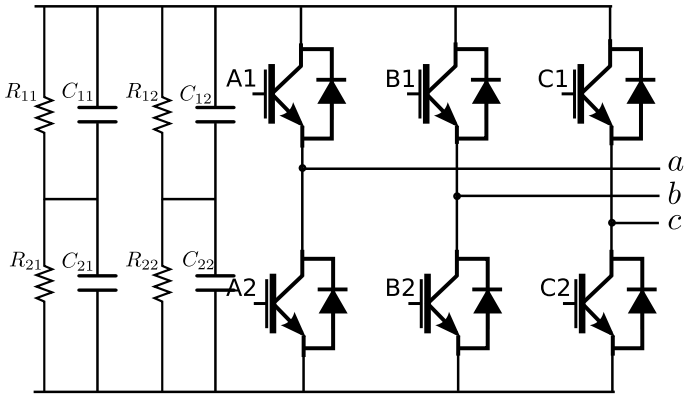

Figure 6.3: *Schematic of the power electronics.*

The IGBT used for its construction are the SKM1506B123D devices. The DC-bus is build by means of four associated 3300 μ electrolytic capacitors.

6.2.2 Grid filter

As described in previous chapter, the Power Converter that is used in this thesis is connected to the grid by means of an LCL filter. This topology brings some advantages in filter

costs, dynamic capabilities and harmonic attenuation that make it attractive for its use as a grid interface. Some of the control problems that appear with its use can be considered to be the main topics of this dissertation.

The schematic of such a filter is displayed on Fig. 6.4.

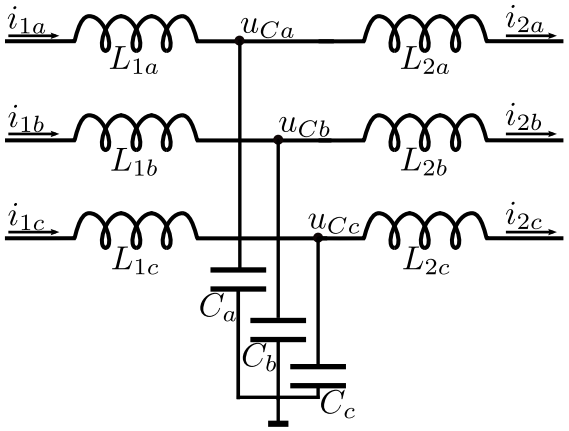

Figure 6.4: *Schematic of the LCL filter.*

The nominal value of the components of this filter are:

- Converter-side inductance: $L_1 = 3.4\ mH$.
- Grid-side inductance: $L_2 = 1.7\ mH$.
- Capacitor: $C = 18\ \mu F$.

The values for this filter where selected following IEC-61000-3-4 regulation. This regulation states that current harmonics above the 33rd should be smaller than 0.6% of the nominal.

Additional requirements, such as the ratio between the inner and outer inductors and the idle production of reactive power by the filter, are needed to derive a design expression. In the regulation, it is stated that the ratio between the inductors is a trade between low resonance frequency and low current ripple in the inner inductor L1. A good compromise is obtained if the inner inductor is twice the size of the outer inductor. Furthermore, an idle reactive current of 5% of the nominal line current is considered reasonable. Hence, the additional requirements are given by

$$\begin{aligned} L_1 &= 2 \cdot L_2 \\ C &= 0.05 \cdot C_{base}, \end{aligned} \tag{6.1}$$

where $C_{base} = I_{base}/(U_{base}\omega_{base})$ and I_{base} and U_{base} represent the nominal line rms current and voltage, respectively.

6.2.3 PES - ECS interface

Three interfaces link the PES with the ECS:

- ECS ⟶ PES interface. This interface contains the actuation information that was computed by a control algorithm loop (for instance, one of those presented in this dissertation) and is transmitted to the PES. These variables are transmitted as PWM signals over an optical communication layer. The optical nature of this interface is very convenient for two main reasons: (i) it allows to physically separate the PES from the ECS without introducing undesirable noise and losses. (ii) it provides electrical insulation.

- PES ⟶ ECS interface. This interface contains the measurements of physical variables performed in the PES. These data are transmitted to the ECS. There, they are compared with some references and feedbacked inside the control loop. To increase the system noise immunity, all measurements are performed by means of transductors and data are transmitted in current mode.

- Interface with contactors. Some of the contactors placed in the system (see Fig. 6.2) can be accessed directly from the ECS. To enable this capability, the system has several relayed digital inputs/outputs that can be read or written from the ECS.

6.3 Electronic Control System

The computational platform that hosts all the system control algorithms, required auxiliary functions and periphery, as displayed in Fig. 6.1, is the Electronic Control System (ECS).

Its initial objective was the control of a back-to-back three-level converter. The control complexity of this kind of converters induced a design that simultaneously presented a high computational power, usually present in floating point DSP and a big and complete periphery to handle with PWM generation and signal acquisition of such a system.

The main goals of the design of this control platform are:

- To build a laboratory equipment, flexible enough to be suitable for research and final prototyping. This flexibility may be understood in two directions: (i) The set-up should accept the most popular ways of programming, i.e. C programming and Matlab/Simulink cross-compiling. (ii) the electronic control platform should be usable for the control of power electronics equipment different than the original one.

- The platform should present enough computing power to be suitable for developing state algorithms that may have an elevated degree of complexity and are not optimized.

- The system should be scalable in the sense of accepting the connection to other control systems that may operate simultaneously in a distributed control scheme. For this reason, the electronic control platform should present real-time high-speed communication capabilities as, for example, CAN and USB.

This facts and its main final purpose for technical research recommended to split the ECS in two subunits: (i) a pure high-performance computational unit focused on efficiently solving computational algorithms, and (ii) a configurable logic device able to support all the periphery logic, data acquisition and some other ancillary functions.

This design paradigm makes the board design over-dimensioned for some industrial applications. For its use as a research and development tool, however, it reveals to be a very flexible tool able to handle real-time requirements for complex controllers and subsystems, allowing its programming by non programmers users using Matlab and Simulink, and allowing a high-detail real-time debugging and waveform viewing.

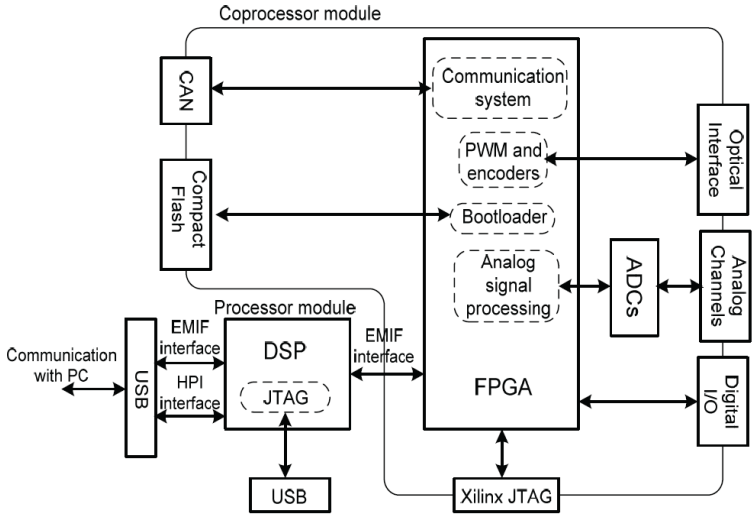

Figure 6.5: *Electronic Control System block diagram.*

Tasks distribution between the processing devices

The split of the Electronic Control System into two devices brings a great flexibility and power regarding controller implementation. However, despite this bigger computational power, a new problem arises: what pieces of the control algorithm should execute each of the units. In general terms, the distribution of tasks between these two devices is determined by the main characteristics of DSPs and FPGAs and the following considerations based on the task type:

- Some tasks are constrained or linked by data dependences. Their location should be in the same device to avoid high data exchange rates between devices.
- Since the selected DSP has limited integrated periphery, some tasks, like encoder reading or PWM generation, should be implemented in the FPGA.
- Tasks with very high computational load that may result too heavy for the the DSP to execute them in real-time, or tasks the DSP could execute, but at the cost of a too high computational charge, may be processed in the FPGA. For example: a state estimator, a complex Kalman Filter, an accurate FFT, etc.
- A very repetitive task that rarely changes may be programmed in the FPGA, independently on its computational complexity. For example: the Delay Signal Cancellation algorithm, an FFT, a FIR filter used for the grid voltage main harmonic filtering, etc.

- Tasks with low or low-medium computational load, which are often modified by the programmer, may be executed in the DSP. Such tasks are mainly control algorithms.
- Non-critical tasks, such as signal representation, are not constrained, so they can be placed in the DSP due to its ease of programming.

In general terms, in the final set-up, as displayed in Table 6.1, the DSP executes the synchronization tasks (PLL), synchronous reference frame direct and inverse transformations, the grid current controller, the grid monitoring system and the DC-bus controller. The FPGA holds more mechanical tasks as PWM generation, encoder capture, peripheral control, whole system synchronization and input data preprocessing.

DSP
Current vectorial controller.
Synchronous reference frame direct and inverse transformations.
DC-bus voltage controller.
Grid monitoring tasks.
Grid synchronization: PLL, frequency estimation and sequence decoupling.
FPGA
System global synchronization.
PWM generation.
Peripheral control.
ADC acquisition logic.
ADC input signals filtering and preprocessing.
Encoder capture.

Table 6.1: *System task distribution.*

6.3.1 Central Processing Unit

The Central Processing Unit is formed by the DSP TMS320C6713 by Texas Instruments. This computational platform is based on a VLIW architecture together with floating-point arithmetic-logic units. This platform represents a very powerful DSP architecture able to handle with complex algorithms. The choice was motivated by several reasons:

- The fact of using a floating-point structure — versus a typical fixed-point one — drastically facilitates the algorithm prototyping, minimizing implementation time and errors.
- Its great computational power ensures the availability of enough processor time to include new emerging control algorithms such as complex system identification techniques and modern control schemes executing in full real time.
- This concrete platform is supported by MATLAB cross-compiler and can be interfaced via Simulink. Although this kind of code is no very suitable for final applications, it results very useful when doing initial prototyping.
- This DSP is shipped with a fast external bus, named EMIF, which allows an easy peripherals design.

On the other hand, however, the platform has some drawbacks. Perhaps the most important one its the complexity involved in a design based on this device. This design complexity gets decreased if the design is based on, for example, one of the development kit designed by third parts as the TMS320C6713 DSK developer kit by Spectrum Digital. Making use of this system, the designer can firstly focus on the design for a particular application that inserts in the connectors of the development board. Once this specific design is finished, tested and implemented, it is still possible to redesign the DSP mother board and focus in a more application dependent objective.

The second drawback associated with this family of devices is their limited number of peripheral units. From its initial conception, these DSPs were mainly designed as powerful cores. For this reason, their direct use as controllers for power electronics systems is quite limited. The co-processor module that is described below has been designed to solve these limitations.

DSP programming

The development tool used for the DSP programming is Code Composer Studio v.3.3 by Texas Instrument, using C as programming language and the real-time operating system DSPBIOS also by Texas Instruments. The flowchart in Fig. 6.6 represents the control algorithms executed by the DSP.

After the DSP is initialized, it waits for two external interruptions, numbered 4 and 5. Both interruption signals are generated by the FPGA and both of them transfer the execution flow to the DSP. The external Interruption 4 is activated in the event of a fault in the system as, for example, a driver fault. Under these circumstances, the DSP stalls the execution of the program in a safe way (stop_system() in Fig. 6.6). Otherwise, the DSP stands idle until the external Interruption 5 is periodically activated every 200 μs. This interruption is associated with the control algorithm execution.

The interrupt service routine, marked as c_init(5) in Fig. 6.6 starts sending the acquisition signal to the analog-to-digital capture units. This process is the first to ensure the maximum accuracy in the synchronization of the capture with the maximum and minimum points of the carrier signal. If the acquired values fall outside of previously defined security ranges, execution is safely stalled as in the case of interruption 4.

After this process, the actuation variables that where computed in the previous sample period are applied to the plant. This artificial delay of the actuation variables ensures that the actuations are always applied at the same moment of each sampling period (independently of control algorithm complexity) at the cost of introducing an extra delay at the plant input. This input delay affects in a negative way to global system stability. For this reason, it should be properly modelled as part of the process under control. An example of such a modelling process was given in chapter 4 of this dissertation.

Once the new measurements are captured and previous actuations are applied, the system starts computing the actual control loop. The process starts with system synchronization routines: grid phase and frequency estimation and sequence decoupling. With the estimated values, the input measurements are translated into two synchronous reference frames: a conventional reference frame synchronized with grid phase, to be used in the current control algorithm and the new one introduced in chapter 3 for its use in the grid monitoring system.

The grid monitoring task is evaluated first, as it is the responsible of detecting abnormal

grid situations as, for instance, islanding situation. The grid monitoring task essentially consists of a two steps procedure: (i) A recursive least-squares procedure that estimates the grid equivalent impedance, and (ii) an estimation evaluation procedure that evaluates the estimates quality sending signals to the current controller if needed. The CPU execution time of this task is 17 μs.

The DC-bus voltage controller, whose design is not covered by this thesis, is executed next. This control block outputs reference values to the inner current control task described next.

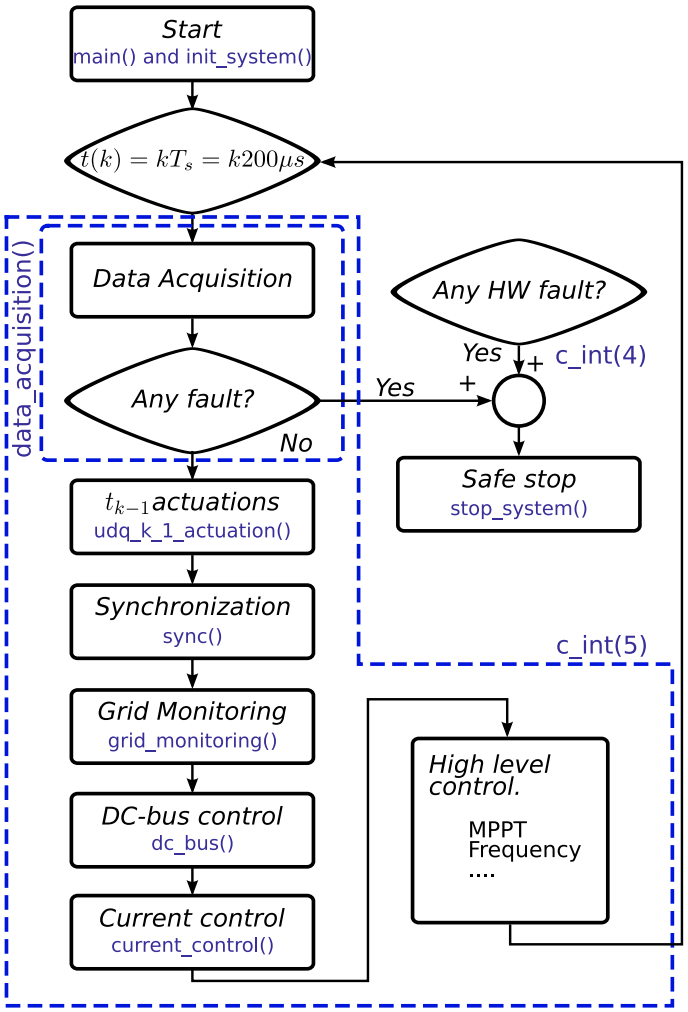

Figure 6.6: *DSP software flowchart.*

The current controller, as described in chapter 5, consist in a feedback association of three discrete-time linear time-invariant system: the feedback system, the loopshaping system and the dc-gain adjust system. All blocks are programmed following a state space model. This procedure guarantees an easy reprogramming, order reducing and tuning of the control algorithm. Fig. 6.7 plots the execution times of seven different controllers: the three LQ-based controllers presented in the first part of chapter 5, and four Loop-shaping $\mathcal{H}_\infty$ controllers with a different number of poles in the shaping function. The controller

proposed in this dissertation presents 3 poles in the shaping function of each of the input channels.

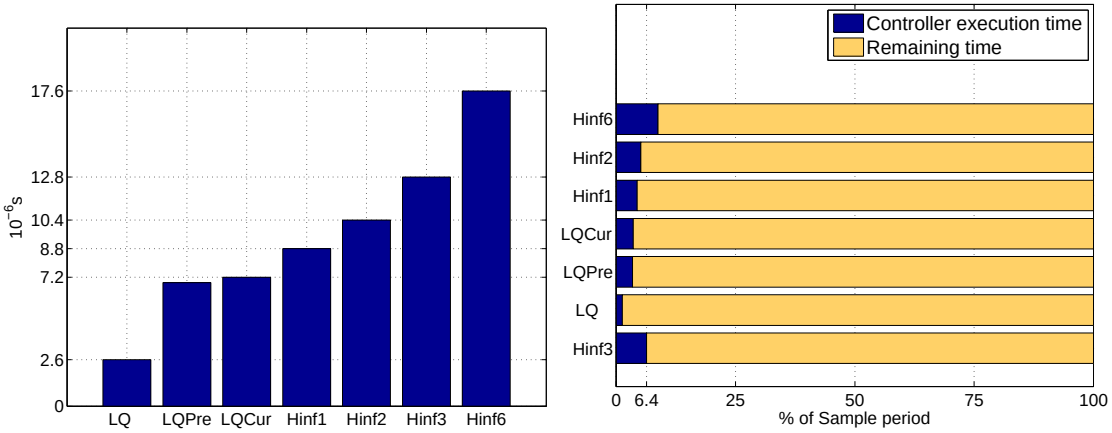

(a) Comparison of proposed controllers execution time.

(b) Execution percentage in a sample period of 200 μs.

Figure 6.7: *CPU control task execution time.*

The complete synchronization, identification and control scheme presented in this thesis is fully executed in less than 60 μs, which represents a 30% of the available computing time. It has to be remarked that no effort has been dedicated to optimize the execution time, being the proposal fully executable in real-time.

USB communications

The developed system is provided with high-speed communication USB capabilities. The capabilities allow to have a complete log of all the signals involved in the converter operation. More concretely, assuming a sampling period of 200 μs and a set of 13 internal variables to be sent, this amounts to a minimum data-flow rate of 320 kbytes/s. This represent a small part of the maximum available data-rate of 21 Mbytes/s.

Practical experience using this communication system evidences the great advances that can be obtained by its use at the cost of a negligible computational charge in the DSP core. ECS real-time high-speed high-detail communications opens the possibility of a very detailed log that can serve as a powerful tool for system debugging and fault tracking.

6.3.2 Co-Processor Unit

The Co-Processor Unit, mainly composed by the FPGA device, implements the necessary periphery to adapt the CPU core to the connection to the Power Electronics System described above. For this reason, this unit can be understood as an interface layer between the DSP and the power converter. The connection of both ECS units is sustained on the use of the EMIF interface. On the other side, the communication between the Co-Processor and the Power Electronic Converter flows through the different modules implemented in the FPGA, such as the acquisition block, PWM generator, etc. Fig. 6.8 depicts the block diagram of the design implemented in the FPGA device.

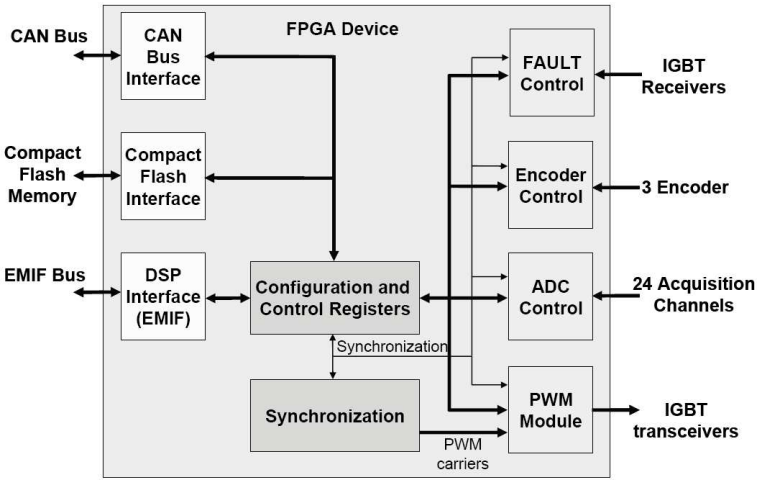

Figure 6.8: *FPGA-based Co-Processor block diagram*

CPU - Co-processor unit synchronization

Despite its secondary nature, when viewed from a synchronization point of view, the Co-Processor Unit plays the role of system master. The synchronization module is the responsible of the generation of a periodic pulse (SYNC) to determine the sampling period T_S=200 μs. This SYNC pulse is used to periodically interrupt the DSP so both devices can synchronize their operation every 200μs. SYNC signal is the last responsible of the real-time operation of the whole control system. Furthermore, this pulse is also sent to other modules to synchronize their operation. Its frequency may also be modified by means of a register available in the FPGA device.

Fig. 6.9 shows the timing of the different events in the DSP and the FPGA and how they are synchronized as mentioned before. After generating the SYNC signal at instant k, the FPGA acquires samples from the ADCs and encoders, while the DSP remains stalled until the acquired data are available in the FPGA. Then the FPGA transmits these data to the DSP, and the DSP transmits the new references to the FPGA PWM generator. These references are obtained by the algorithms computed at the instant $k-1$. With the acquisition data at instant k and the references applied at k, the new references to be applied at the instant $k+1$ are computed.

Co-processor main modules

The main modules implemented in the Co-processor device are the following:

- Configuration and Control Registers. The FPGA maps several sets of configuration and control registers in the EMIF bus memory map. This represents the main communication methods between the two entities. The most remarkable register sets are: Global configuration register, dead-time configuration register, IGBT state monitoring register, USB control registers and interruption masks register.
- PWM Module. This module generates the PWM control signal for different VSC configurations: from a simple VSC to a back-to-back association of two three-level VSCs.

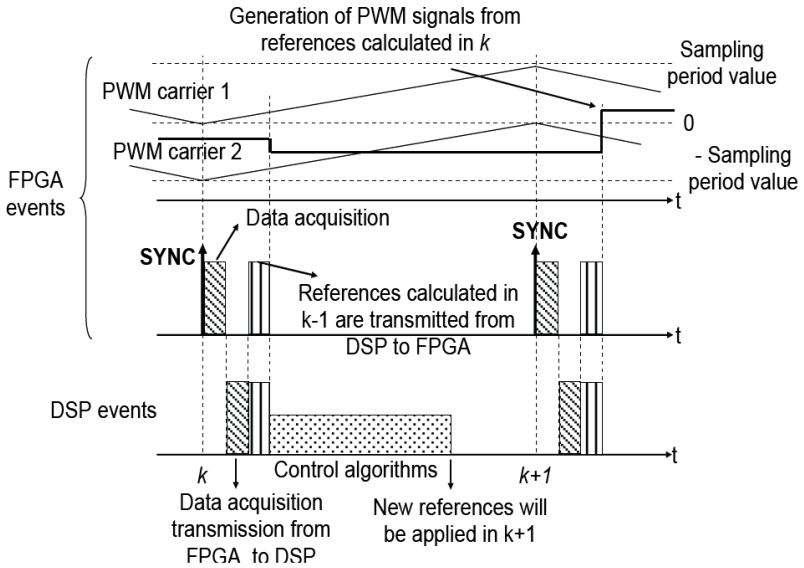

Figure 6.9: *CPU-Co-processor Synchronization timing.*

- Acquisition Module. The acquisition module is able to simultaneously sample up to 24 analog channels at a configurable frequency (5 kHz for the presented set) syncrhonized with the SYNC signal. The sampled signals resolution is 12bit. Several configurable digital filter-based pre-processing channels can be applied to the incoming samples.
- Encoder Module. The ECS is able to acquire the data coming from up to three different encoders.
- Storage Module. The Co-processor also provides the ECS with storage capabilities. Particularly the system ships a Compact Flash interface that can be used for both firmware loading and log file.

6.4 Experimental set-up images

This section shows some photographs from the final experimental set-up. Fig. 6.10 displays the different components of the Electronic Control System. Fig. 6.10.a shows a top-view of the DSP boards and Fig. 6.10.b shows a photograph of the Co-processor system.

Fig. 6.11 displays different components of the complete set-up. Fig. 6.11.a shows a detail of the grid converter, Fig. 6.11.b shows a top view of the set-up and Fig. 6.11.c shows a general view of the complete set-up.

6.5 Summary of experimental results

Although experimental results have already been displayed in their corresponding chapters, a very brief summary of the most important results and waveforms is displayed below.

Fig. 6.12 shows the behavior of the grid synchronization system. Fig. 6.13 displays the PCC variables expressed in the synchronous reference frame used for the grid identification process. Fig. 6.14 and Fig. 6.15 represent the evolution of the grid equivalent impedance

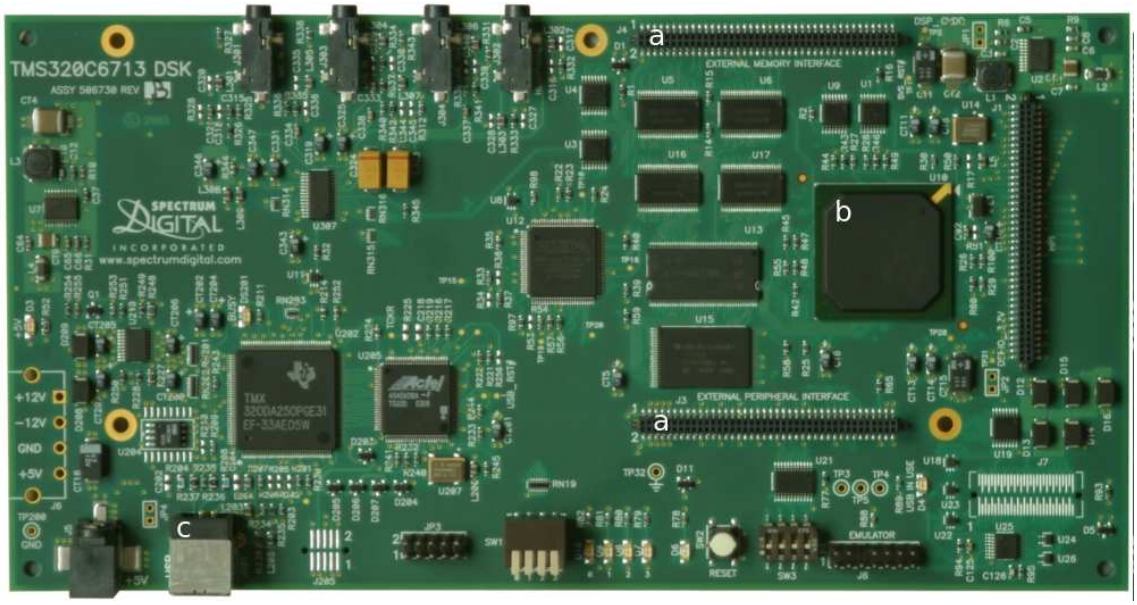

(a) TMS320C6713 DSP card top view. a. EMIF interface ports. b. DSP CPU. c. USB JTAG interface.

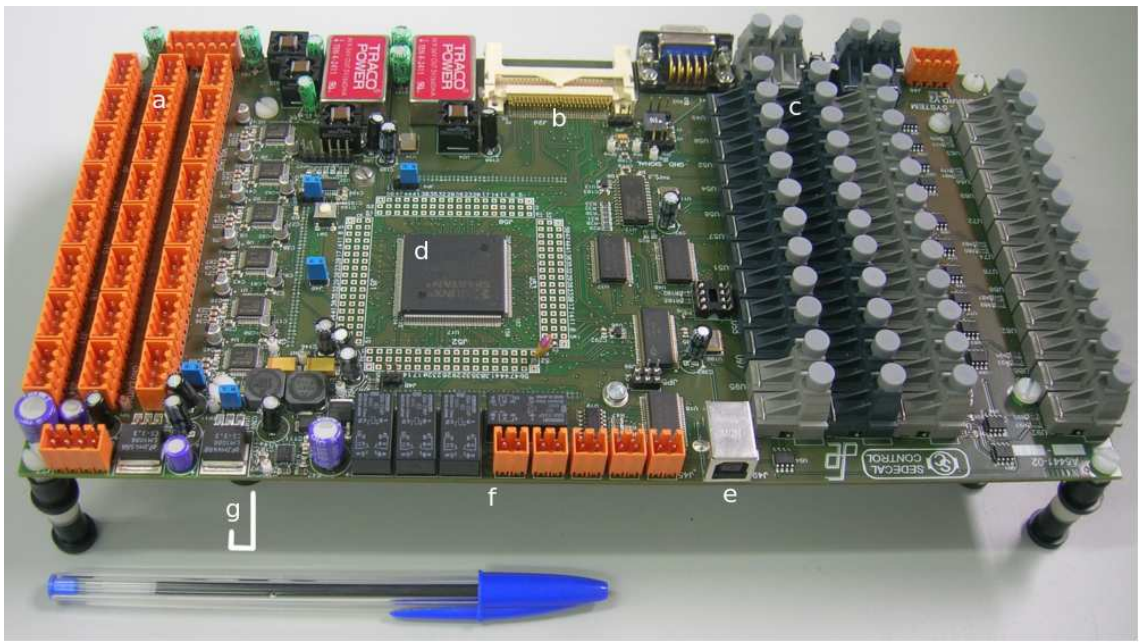

(b) FPGA card view. a. Analog channels. b. Compact Flash interface. c. IGBT optic interfaces. d. FPGA. e. High-speed USB interface. f. Relay outputs. g. TMS320C6713 DSK board (below).

Figure 6.10: *Electronic Control System snapshot.*

(a) Grid Converter. a. DC-bus capacitors. b. Driver boards. c. IGBT. d. Heat sink. e. IGBT optic interface.

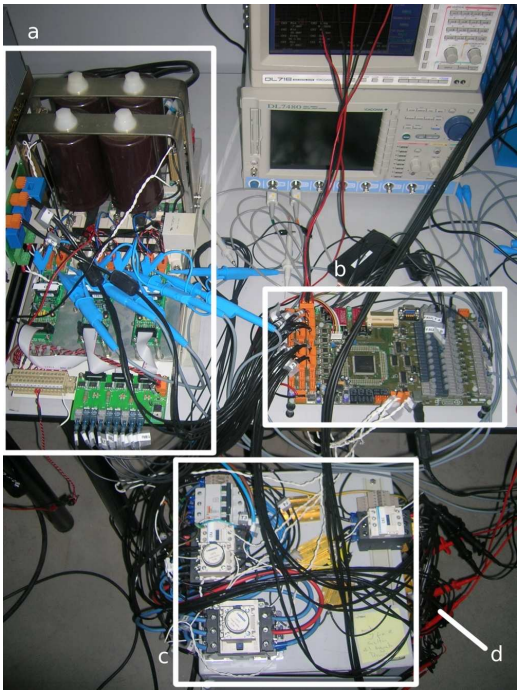

(b) Experimental set-up top view. a. Grid converter. b. Electronic Control System. c. Grid interface filter. d. Sensors.

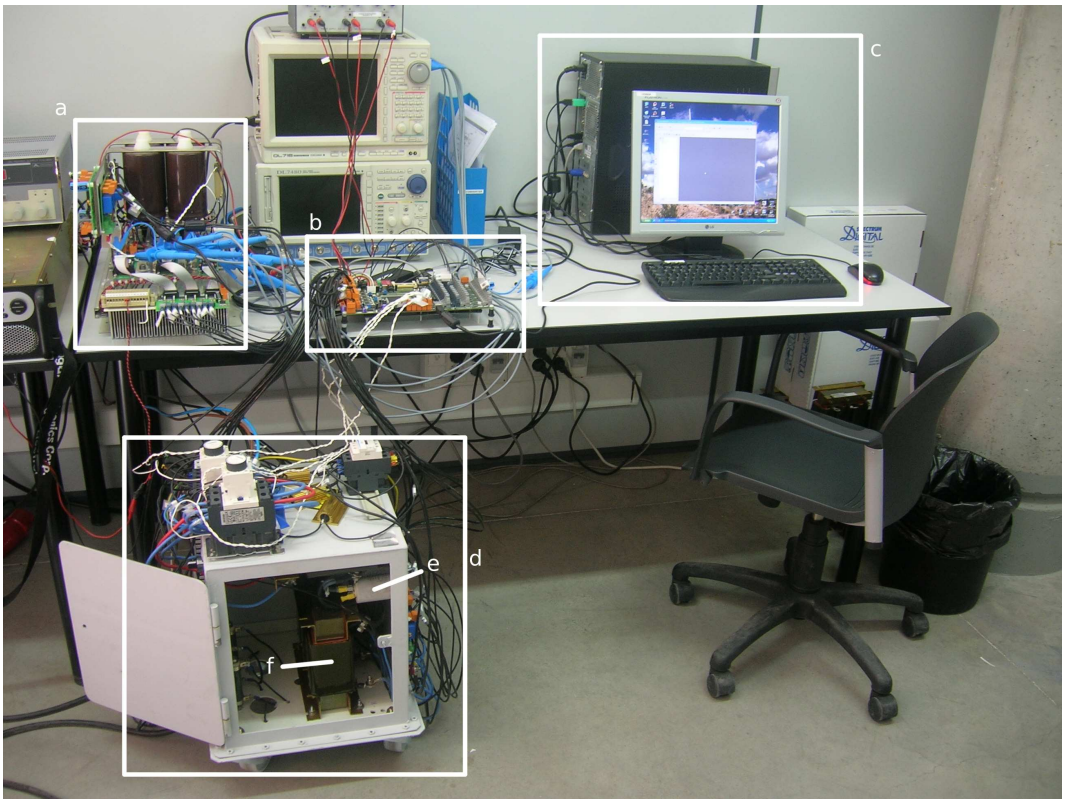

(c) Experimental set-up general view. a. Grid Converter. b. ECS. c. PC control host. d. Grid filter. e. Filter capacitors. f. Filter inductors.

Figure 6.11: *Experimental Plant details*

and voltage source respectively when using the input data displayed in Fig. 6.13. Fig. 6.16 shows the step responses of the set-up when the grid converter is controlled with different combinations of LQ controllers, Fig. 6.17 displays the tracking error and harmonic content of the LQ proposals when all state variables are measured. Finally, Fig. 6.18 represents the step response, tracking error and harmonic content of the proposed $\mathcal{H}_\infty$ controller.

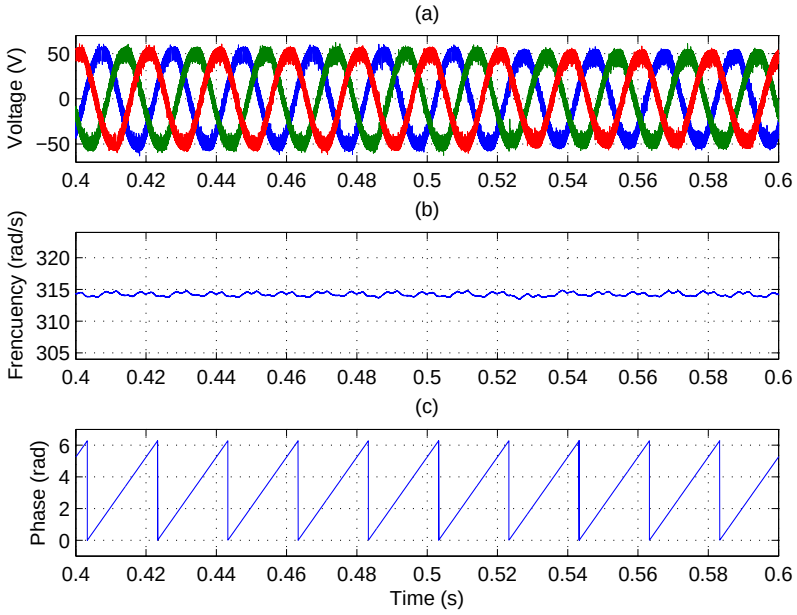

Figure 6.12: *Time evolution of the Grid synchronization system. (a) Three-phase PCC voltage measurement. (b) Frequency estimation. (c) Phase estimation.*

6.6 Conclusions

This chapter gives a description of the experimental platform that has been used for the work presented in this dissertation. The experimental part is based in a *Power Electronics System*, or PES, which represents the actual electronic interface between the power generator and the grid. This electronic interface is controlled by means of the *Electronic Control System* which consists in a high performance general purpose DSP communicated with a application oriented slave card which serves as a peripheral generator, mathematical coprocessor and communication and debug interface. Final part of the chapter shows some photographs of the final experimental set-up and summarizes some remarkable experimental waveforms obtained during this dissertation.

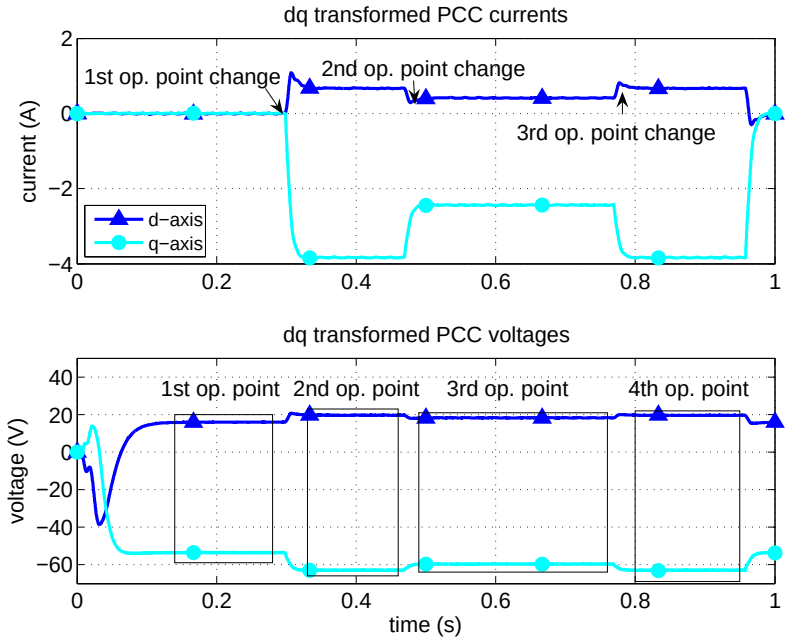

Figure 6.13: *Values of the measured currents and voltages in PCC transformed into monitoring system dq reference frame.*

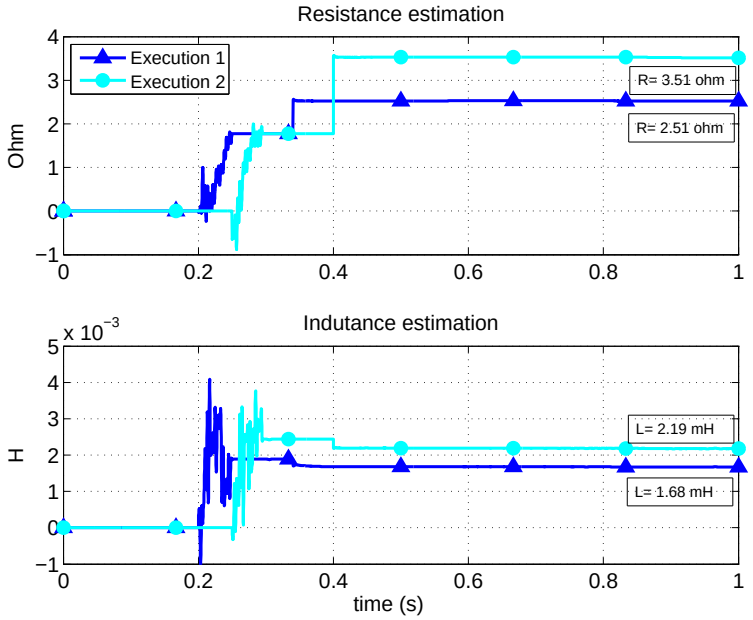

Figure 6.14: *Experimental impedance estimation.*

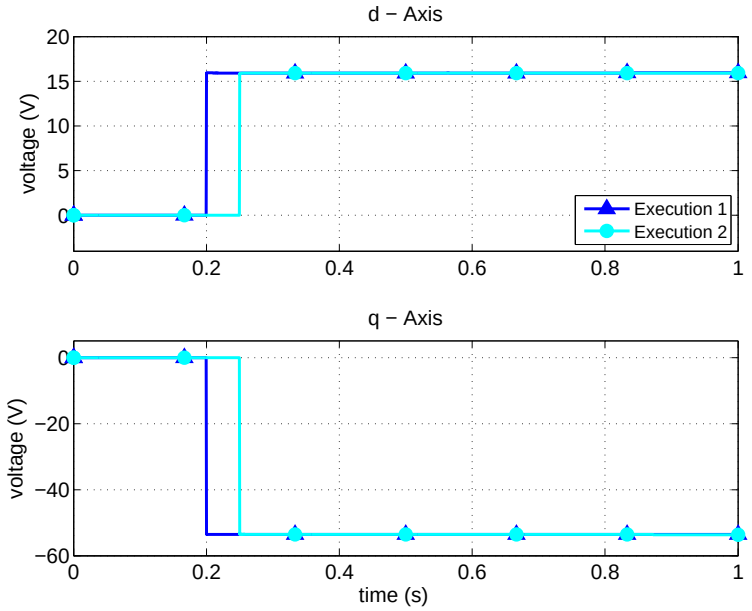

Figure 6.15: *Experimental grid equivalent voltage source estimation.*

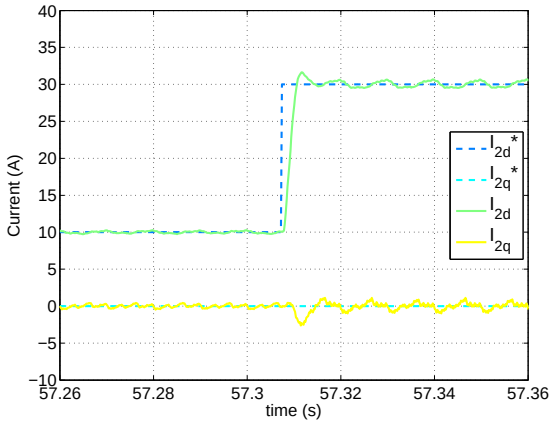

(a) LQ *dq* step response. Measured states.

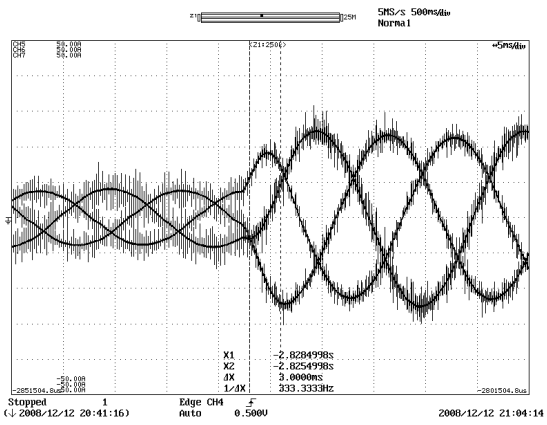

(b) LQ *abc* current signals. Measured states.

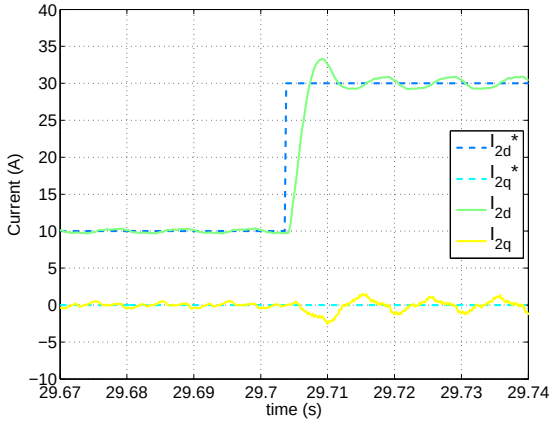

(c) LQ *dq* step response. Predictor estimator.

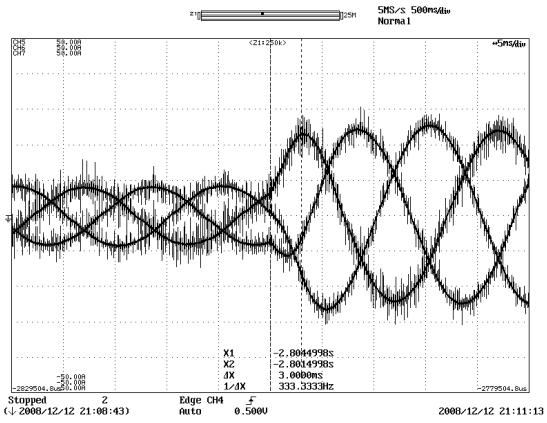

(d) LQ *abc* current signals. Predictor estimator.

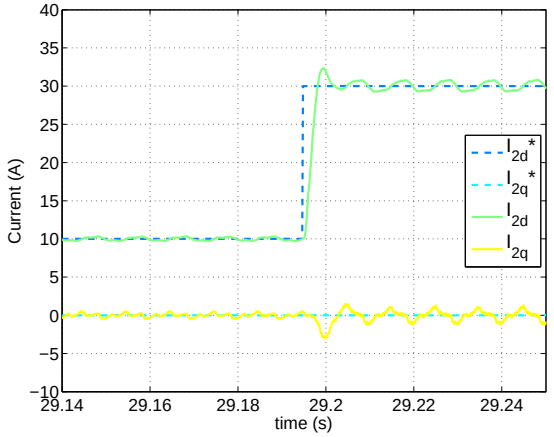

(e) LQ *dq* step response. *Current* estimator.

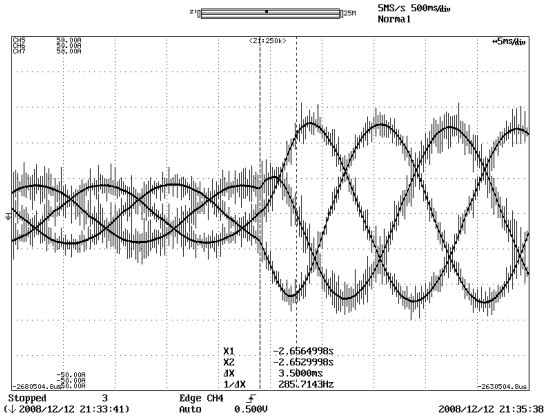

(f) LQ *abc* step response. *Current* estimator.

Figure 6.16: *Experimental step responses of the presented LQ controllers.*

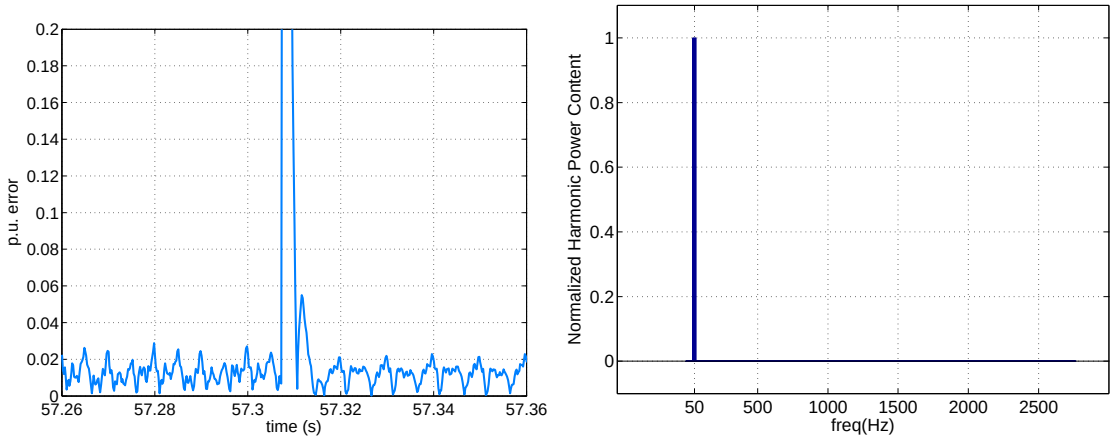

(a) LQ tracking error. Predictor estimator.

(b) LQ harmonic content. Predictor estimator.

Figure 6.17: *Experimental evaluation of the LQ proposal.*

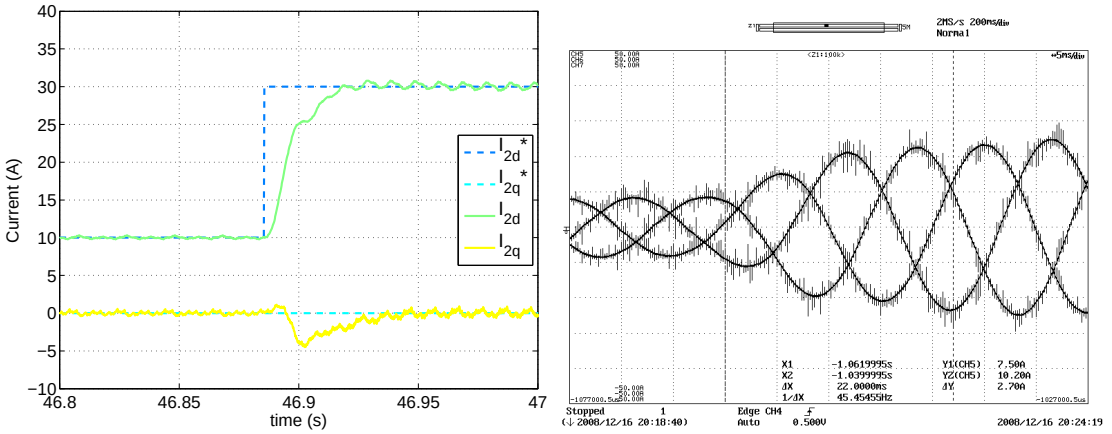

(a) $\mathcal{H}_\infty$ *dq* step response.

(b) $\mathcal{H}_\infty$ *abc* current signals.

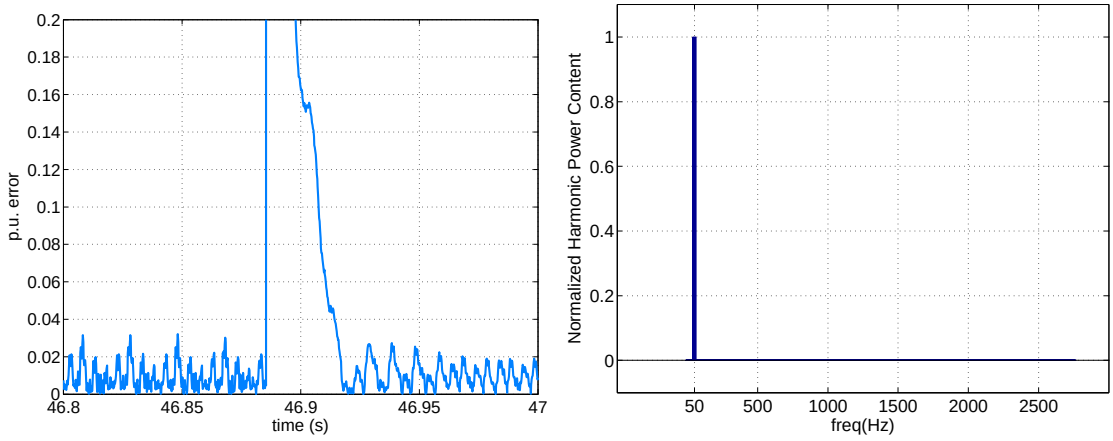

(c) $\mathcal{H}_\infty$ *dq* tracking error.

(d) $\mathcal{H}_\infty$ *abc* harmonic content.

Figure 6.18: *Experimental testing of the proposed $\mathcal{H}_\infty$ controller.*

Chapter 7

Conclusions and Future Works

7.1 Introduction

This chapter presents a summary of the contributions, conclusions and future works extracted from the work developed during this thesis. The chapter is divided into two sections. The first section focuses on the topics discussed in this dissertation. For each of them, a summary of the proposed contributions, extracted conclusions and future research lines is presented. The second section provides a statement of the author's publications related with the work developed in this thesis.

7.2 Summary of contributions, conclusions and future works

7.2.1 General conclusions

Resuming the objectives presented in chapters 1 and 2, this thesis deals with the (negative) effects that an uncertain grid can have over the stability of current controllers of VSC connected to the grid through LCL filters.

To perform this study, the thesis has faced the problem from a three-fold point of view: identify the uncertain parameters, study the effects of these parameters over current controllers and propose controllers immune to these effects.

These three issues have been the topics of the three main chapters of this dissertation. In general terms, the thesis has demonstrated that the uncertainty parameters exist, can be estimated and an incomplete knowledge of grid equivalent impedance and inductance induces a negative effect over grid converters behavior. This negative effect ranges from a performance degradation to converter instability. As demonstrated, this is a common problem for linear and non-linear control schemes.

Fortunately, the automatic control theory has available tools to handle with this lack of knowledge, or uncertainty. Making use of it, this thesis proposes the use of $\mathcal{H}_\infty$ techniques to design robust controllers. To illustrate this, a particular approach based on two popular tools has been proposed: loopshaping $\mathcal{H}_\infty$ and ν-gap norm. This document has presented a successful robust design based on them. It is necessary to remark that far from offering a definitive solution, this proposal starts a very promising research line towards the introduction of robust design techniques in VSC control. The interest on this issue is huge due to the usual 24x7 requirements of this kind of systems.

The sections below make a more detailed analysis of the extracted contributions, conclusions and future works.

7.2.2 Grid monitoring

Contributions

The grid monitoring system proposed in this thesis was covered in detail in Chapter 3 of this document. The principal proposed contributions are the following:

- This thesis has proposed the use of a linear regression algorithm, operating in the a synchronous reference frame (dq axes) to solve the optimization problem of the estimation of the grid equivalent resistance and inductance.
- An estimation quality evaluation subsystem has been presented. This subsystem calculates a quality index related with the estimation validity in real time that can serve as the basis of higher level system features.
- The estimation evaluation subsystem opens the door to give the monitoring system its quasi-passive nature: The monitoring system stands acquiring data without introducing disturbances into the grid while the estimation quality is above an arbitrary level. Only when the quality falls beyond this level, the converter introduces disturbances into the grid.
- The estimation evaluation subsystem also makes the monitoring method suitable for grid islanding situations detection.
- The thesis has proposed a synchronization method that can be utilized to generate a synchronous reference frame that is not locked with any of the grid voltages components phases.

Conclusions

- The proposed regression method offers successful estimation results and, thanks to the dq transformation, the mathematical algorithm presents a low computational load.
- The regression algorithm inherits the optimum behavior of least-squares-based algorithms in the presence of additive Gaussian noise.
- Synchronization performance has demonstrated to have a critical influence on algorithm accuracy. It is a critical point of the monitoring system.
- The method requires an underlying stable current control loop in order to operate. This fact limits the application of the algorithm in adaptive control schemes.
- The presented method can serve as base for a partial tuning control algorithm as well as a base for a islanding detection system.

Future Works

- The removal of the frequency dependency would drastically improve system robustness and accuracy. The implementation of the optimization algorithm in the $\alpha\beta$ reference frame seems to be quite appropriate for this purpose.
- Introduce switching information into the optimization algorithm to increase estimation accuracy. High frequency switching information is not being considered in the presented proposal, however, it could give valuable information about the behavior of the grid at these frequencies.
- Study the possibility of developing an estimation algorithm suitable for its use in a full adaptive scheme.

7.2.3 Analysis of the grid influence on the behavior of current controllers

Contributions

The topic of analyzing the effect that an uncertain non-ideal grid (i.e. an inductive-resistive grid) induces over the behavior of current controlled grid converter was covered in Chapter 4 of this document. The most important proposed contributions are the following:

- A standard uncertainty NΔ model of the LCL filter under uncertainty in grid equivalent inductance and resistance has been developed. This model is very interesting as it serves as a valuable basis for the use of systematic robust control tools, as, for example, μ-analysis.
- Application of μ structured singular value theory to make a systematic study of the parameter allowable variation or uncertainty that keeps the closed-loop system stable for a previously designed current controller. This tool allows to extract robustness conclusions about controllers whose design motivation was different from robustness.
- A stability analysis of hysteresis current controllers connected to the grid through L filters has been presented. The analysis covers the extraction of stability bounds for the uncertainty of grid considered parameters. For the case of VSC connected through LCL filters, the analysis is limited to make a problem identification and settlement. Some design criteria based on empirical experience are given.

Conclusions

- μ-analysis reveals as a very useful tool for the evaluation of the robustness presented by controllers that are not robust by design, as well as for validating controllers designed with robust techniques. Usually the actual stability is slightly bigger than the theoretical calculated by μ. This is because in general terms, $\mathcal{H}_\infty$ theory, tends to be conservative. More concretely, μ analysis is a little conservative by the assumption of complex uncertainty in the parameters, and not just real uncertainty.
- The accuracy of uncertainty modelling is key point. Uncertain parameters that are not covered by the N-Δ model are not taken into account in the analysis and, thus, can generate erroneous conclusions.

- The L filter behaves well when controlled via hysteresis. This system presents simple and predictable dynamics. As a consequence, the maximum values in the grid inductance and resistance are very well established. In the LCL case, however, the involved LTI system can present a kind of chaotic behavior. This phenomenon is due to the interactions between system modes (resonances), current reference and hysteresis bandwidth. The study of this behavior is difficult due to the hybrid nature of the closed-loop system.

Future Works

Regarding the study in the scope of linear controllers, the following future works are suggested:

- The method presented in this dissertation is limitted to study the robust stability of closed-loop system. This study gives stability margin but no information about the degradation of the closed-loop system performance when parameters are different from the nominal. This study can be performed using a *Robust performance* analysis, that is covered by μ theory. Robust performance analysis could provide a test method to know if a certain controller applied to a certain plant would pass current grid regulations.

- Improvement in the modelling: Some other perturbation effects would increase the model quality and, thus, the analysis accuracy. Some of the most important are the grid parasitic capacitance that is neglected in this thesis, the components possible drifts and initial tolerances and the unmodelled IGBT dynamics.

- The measurement of system current signals implies the choice of a sample time. Regarding this issue some studies give certain criteria to sample in the L filter case. This solution takes profit of the first order dynamics to remove switching ripple noise from current measurements. When this criterium is applied to the sampling of currents in an LCL filter, the switching harmonics are not correctly removed. It is a topic that should be studied in detail to avoid further aliasing problems.

- Regarding the hysteresis case, the stability analysis for this kind of controllers must be generalized to give tight stability margins in the LCL case or even higher order filters. The mathematical framework is already available from the hybrid control theory and has to be adapted to the features of this particular problem.

7.2.4 Grid current control

Contributions

Chapter 5 presented several proposals regarding the MIMO current control of VSC connected to the grid through LCL filters. The proposals covered the estimation of internal state variables and the design following a Linear Quadratic and $\mathcal{H}_\infty$ optimizations. The main proposed contributions are the following:

- An evaluation of MIMO estimators was presented. The most representative state estimators where described, adapted to the problem and compared under different

common circumstances such as additive white Gaussian noise and fixed-frequency switching ripple. Kalman Filter was applied to the problem of state estimation.

- The control of the LCL grid-side current has been performed following a MIMO approach. To test this framework, a state feedback Linear Quadratic controller has been designed and tested. The design has been implemented assuming that all state variables are measured and estimating some of them.

- The control of the LCL grid-side current has been performed by means of $\mathcal{H}_\infty$ control techniques. Particularly, by means of a combination of Loopshaping $\mathcal{H}_\infty$ and ν-gap norm.

- The voltage actuators saturation problems have been overcome by means of the use of an anti-windup system based on the use of the Hannus form.

Conclusions

- The MIMO modelling, estimation and control of the grid converter has demonstrated to be a feasible and, moreover, convenient approach. Two main facts back-up this conclusion: (i) MIMO treatment allows a general design process that is easily applicable to structures that are different to the one initially considered. (ii) Additionally, it avoids to approximate a MIMO plant by several SISO processes and opens the door to modern control and estimation techniques.

- Regarding state estimators, the results of this dissertation allow to conclude that, when designed using dead-beat pole-placement, *Current* and Predictive configurations offer similar results. Performance of both possibilities is different under certain kind of noises, however both sources of disturbance are usually simultaneously present during converter regular operation and, thus, for practical purposes both represent an equally valid option.

- Dead-beat pole-placement for state estimators is usually applied because it allows a quick convergence. However, this comes at the cost of poor noise immunity. Different positions for the eigenvalues would improve this behavior but it is difficult to find a placement criterion that combines performance and noise immunity.

- In this direction, the optimal estimator, Kalman Filter, has demonstrated to be a good alternative. Results show a high grade of immunity of the estimations when output variables are polluted with either additive Gaussian or switching noise. However, this estimation method presents serious theoretical limitations when the assumed model is not accurate.

- Linear Quadratic control techniques represent a successful design approach whenever robustness is not required. In general terms, they provide an easy design procedure that yields a good performance in most situations. The design method is easily applicable to different filter structures and allows the introduction of null steady-state error requirements. As an additional advantage, its design can be applied to discrete-time plants even including computational delays being fully suitable for its appliance in the control of grid converters by means of a DSP platform.

- $\mathcal{H}_\infty$ based design reveals to be a very useful technique for its appliance in current control of VSC because of several reasons. The most important is probably that it allows to include robustness constraints inside a design procedure that directly handles with internal state variable estimation and feedback. Thus, robustness is ensured even when only the output variables are feedbacked. Other important advantages of this approach are the possibility of making a full discrete-time design, also handling with computational delays and the inclusion of steady state error requirements at several simultaneous frequencies.

- The concrete design technique that has been used in this thesis, Loopshaping $\mathcal{H}_\infty$, offers a simple design process based on a simplified loopshaping procedure. Its combination with the ν-gap norm creates a powerful set of tools that allows to handle with structured or unstructured uncertain processes.

- In general terms, $\mathcal{H}_\infty$ may be understood not only as a design procedure but also as a very strong analysis tool that allows the designer to have an accurate idea of the influence of a particular uncertainty on the hypothetical final closed-loop system. This fact brings a valuable base for an engineering oriented design, as it can give information about the best possible controller for certain assumed uncertainty.

  This conclusion has also an interesting interpretation in the opposite direction when the robustness concept is applied to the rest of the filter components: how accurate has to be the modelling, or how small has to be the component tolerance to achieve a certain robust performance in any case. This design flow opens the door of using robust design to decrease system costs.

Future Works

- Introduce robustness constraints inside the estimation scheme. $\mathcal{H}_\infty$ optimization naturally yields a controller with an observer-controller internal structure. This structure may be decoupled in order to obtain a $\mathcal{H}_\infty$ estimation of internal state variables under uncertainty presence.

- The applied Loopshaping $\mathcal{H}_\infty$ procedure gives a good flexibility in the design of the shaping transfer matrix. This facility allows the inclusion of resonant integrators in the loopshaping function. The use of this integrators would enable the proposed control for its use in active filter applications and stationary reference frame control. This topic represents an interesting future research line.

- The inclusion of PCC voltage measurements, that are usually available for synchronization or higher level control purposes, in the control structure, is expected to improve the grid converter current control behavior. This is probably one of the more direct future works extracted from this dissertation.

- Include robust performance constraints in the design process. In a similar way as happens in the robust analysis case, this future work would allow the introduction of specifications directly extracted from regulation and grid-codes specifications into the design process.

- Study more advanced control configurations as, for example, the two degrees of freedom structure (2-DOF) in order to improve disturbance rejection while maintaining robustness properties.
- Explore μ-synthesis possibilities. This design approach is usually not considered because of the convergence issues that appear when dealing with real, structured uncertainty, as is the case in this application. In the case of a successful optimization process, the result is usually a very high order controller that yields a not very different performance when compared with other robust designs and, otherwise, offers very poor robustness to non-modelled uncertainty, that is always present. However, the achievement of such a design is attractive for several reasons and should be explored.
- Extract more general conclusions about best possible disturbance rejection and possible control performance assuming a minimal necessary robustness for the grid-side current control of the VSC.
- Make a robust-driven study of the trade that exists between system performance, filter bandwidth, control sampling time and filter size.
- Explore the use of adaptive control schemes as an alternative to robust control.

7.3 Author's publications related to this thesis

As a result of the work developed during this thesis, several contributions have been published in relevant technical international journals and conferences.

- Santiago Cobreces, Pedro Rodriguez, Daniel Pizarro, Francisco J. Rodriguez, Emilio J. Bueno. *"Complex-Space recursive least squares power system identification"*. Presented in the 38th IEEE Power Electronics Specialists Conference, 2007. (PESC '07).
- Santiago Cobreces, Francisco Huerta, Daniel Pizarro, Francisco J. Rodriguez, Emilio Bueno. *"Three-phase power system parametric identification based in complex-space recursive least squares"*. Presented in the 2007 IEEE International Symposium on Intenlligent Signal Processing (WISP07).
- Santiago Cobreces, Emilio J. Bueno, Daniel Pizarro, Francisco J. Rodriguez, Francisco Huerta. *"Grid Impedance Monitoring System for Distributed Power Generation Electronic Interfaces"*. To be published in IEEE Transactions on Instrumentation and Measurement. Accepted 2008.

The three publications that are presented above are related with the grid monitoring topic described in Chapter 3. In chronological order, they describe the internals of the optimization algorithm, the design of the synchronization algorithm for its appliance in three-phase system and the development of the estimation evaluation subsystem that gives the algorithm its quasi-passive nature.

- Santiago Cobreces, Emilio J. Bueno, Francisco J. Rodriguez, Daniel Pizarro, Francisco Huerta. *Robust Loop-shaping $\mathcal{H}_\infty$ control of grid converters connected to uncertain grids through LCL filters*. To be submitted to IEEE Transactions on Power Electronics on 2009.

This paper describes the $\mathcal{H}_\infty$ proposal, presented in chapter 5.

- Francisco Huerta, Emilio J. Bueno, Santiago Cobreces, Francisco J. Rodriguez, Carlos Giron.*Control of grid-connected voltage source converters with LCL filter using a Linear Quadratic servocontroller with state estimator.* Presented in the 39th IEEE Power Electronics Specialist Conference, 2008 (PESC'08).

This paper presented the Linear Quadratic design procedure that is presented on chapter 5 of this thesis.

- Santiago Cobreces, Emilio Bueno, Francisco J. Sanchez, Francisco Huerta, Pedro Rodriguez. *"Influence Analisys of the Effects of an Inductive-Resistive Weak Grid over L and LCL Filter Current Hysteresis Controllers".* Presented in the 2007 European Power Electronics Conference (EPE '07).

This publication deals with the effects of a non-ideal grid over the behavior of converters whose current is controlled by means of a hysteresis scheme. The study covers the L and LCL connection filter case. The contents of this publication are described in chapter 4 of this dissertation.

- Francisco J. Rodriguez, Santiago Cobreces, Emilio J. Bueno, Alvaro Hernandez, Raul Mateos, Felipe Espinosa. *"Control Electronic Platform based on Floating-Point DSP and FPGA for a NPC multilevel back-to-back converter".* Published in Electronic Power Research. Elsevier 2008.

- Emilio J. Bueno, Santiago Cobreces, Francisco J. Rodriguez, Alvaro Hernandez, Felipe Espinosa. *"Design of a back-to-back NPC Converter Interface for Wind Turbines with Squirrel-Cage Induction Generator".* Published in IEEE Transactions on Energy Conversion. 2008.

The publications listed above are related to the design of the experimental platform used to test the algorithms described in this dissertation. The former is dedicated to describe the internals of the electronic control platform composed of a DSP and an FPGA, the latter is dedicated to describe the whole experimental platform including the power converter. The contents of these papers are described in Chapter 6 of this document.

- Santiago Cobreces, Josep Bordonau, Joan Salaet, Emilio J. Bueno, Francisco J. Rodriguez. *"Exact-Linearization Non-Linear Neutral-Point Voltage Control for Single-Phase Three-Level NPC Converters".* To be published in IEEE Transactions on Power Electronics. Accepted 2008.

This publication proposes a neutral-point voltage control for a single-phase three-level VSC. This work was developed during the first stages of the Ph.D work and is not reflected on this document to its off-topic nature.

Bibliography

[whi, 1997] (1997). *Energy for the future: Renewable Sources of Energy. White Paper for a Community Strategy and Action Plan.* European Commission.

[kyo, 1998] (1998). *Kyoto Protocol to the United Nations Framework Convention on Climate Change.* United Nations.

[ewe, 2005] (2005). *Large Integration of Wind Energy in the European Power Supply: analysis, issues and recommendations. A report by EWEA.* European Wind Energy Association.

[bla, 2005] (2005). *Learning from the Blackouts. Transmission System Security in Competitive Electricity Markets.* International Energy Agency.

[per, 2005] (2005). *Plan de Energías Renovables en España 2005-2010.* Instituto para la Diversificación y Ahorro de la Energia. Ministerio de Industria, Turismo y Comercio.

[eus, 2006] (2006). *European Smartgrids Technology Platform. Vision and Strategy for Europe's Electricity of the Future.* European Commission.

[gre, 2006] (2006). *Green Paper. A European Strategy for Sustainable, Competitive and Secure Energy.* European Commission.

[weo, 2006] (2006). *World Energy Outlook 2006.* International Energy Agency.

[ene, 2007] (2007). *Energy for a Changing World. An Energy Policy for Europe - the need for action.* European Commission.

[sra, 2007] (2007). *Strategic Research Agenda for Europe's Electricity Networks of the Future.* European Commission.

[Abu-Rub et al., 2004] Abu-Rub, H., Guzinski, J., Krzeminski, Z., and Toliyat, H. (2004). Predictive current control of voltage-source inverters. *IEEE Transactions on Industrial Electronics*, 51(3):585–593.

[Alepuz et al., 2008] Alepuz, S., Busquets-Monge, S., Bordonau, J., Cortes, P., Rodriguez, J., and Vargas, R. (2008). Predictive current control of grid-connected neutral-point-clamped converters to meet low voltage ride-through requirements. In *Records of the IEEE Power Electronics Specialists Conference, 2008. PESC 2008.*, pages 2423–2428.

[Alepuz et al., 2006] Alepuz, S., Busquets-Monge, S., Bordonau, J., Gago, J., Gonzalez, D., and Balcells, J. (2006). Interfacing Renewable Energy Sources to the Utility Grid

Using a Three-Level Inverter. *IEEE Transactions on Industrial Electronics*, 53(5):1504–1511.

[Alepuz et al., 2005] Alepuz, S., Salaet, J., Busquets, S., and Bordonau, J. (2005). Load voltage and output current control of three-level voltage source inverters. In *31st Annual Conference of IEEE Industrial Electronics Society, 2005. IECON 2005.*, page 6pp.

[Allmeling, 2004] Allmeling, J. (2004). A control structure for fast harmonics compensation in active filters. *IEEE Transactions on Power Electronics*, 19:508–514.

[AlSwailem, 2004] AlSwailem, S. I. (2004). *Application of Robust Control in Unmanned Vehicle Flight Control System Design*. PhD thesis, Cranfield University.

[Asiminoaei et al., 2004] Asiminoaei, L., Teodorescu, R., Blaabjerg, F., and Borup, U. (2004). A new method of on-line grid impedance estimation for PV inverters. In *Proceedings of APEC'04*, volume 3, pages 1527–1533.

[Bae and Ovaska, 2005] Bae, B. and Ovaska, S. (2005). Reference signal generator for active power filters using improved adaptive predictive filter. *IEEE Transactions on Industrial Electronics*, 52(2):576–584.

[Balas et al., 2007] Balas, G., Chang, R., Packard, A., and Safonov, M. (2007). *The Robust Control Toolbox 3. User guide.*

[Bishop and Welch, 2001] Bishop, G. and Welch, G. (2001). An introduction to the kalman filter. Technical report, University of North Carolina, Department of Computer Science.

[Blanco et al., 2005] Blanco, E., Bueno, E., Espinosa, F., Cobreces, S., Rodriguez, F. J., and Ruiz, M. A. (2005). Fast Harmonics Compensation in VSCs Connected to the Grid by Synchronous-Frame Generalized Integrators. In *IEEE International Symposium on Industrial Electronics 2005.*

[Blasko and Kaura, 1997] Blasko, V. and Kaura, V. (1997). A Novel Control to Actively Damp Resonance in Input LC Filter of a Three-Phase Voltage Source Converter. *IEEE Transactions on Industry Applications*, 33:542–550.

[Bode and Holmes, 2001] Bode, G. and Holmes, D. (2001). Load Independent Hysteresis Current Control of a Three Level Single Phase Inverter with Constant Switching Frequency. In *35th IEEE Power Electronics Specialist Conference.*

[Boroyevich, 2000] Boroyevich, D. (2000). Modelling and design of AC converters. Technical report, CPES-Viriginia Tech.

[Bose, 1990] Bose, B. K. (1990). An Adaptive Hysteresis-Band Current Control Technique of a Voltage-Fed PWM Inverter for Machine Drive System. *IEEE Transactions on Industrial Electronics*, 37(5):402–408.

[Botteron et al., 2003] Botteron, F., de Camargo, R., Hey, H., Pinheiro, J., Grundling, H., and Pinheiro, H. (2003). New limiting algorithms for space vector modulated three-phase four-leg voltage source inverters. *IEE Proceedings on Electric Power Applications*, 150(6):733–742.

[Brabandere, 2006] Brabandere, K. D. (2006). *Voltage and frequency droop control in low voltage grids by distributed generators with inverter front-end*. PhD thesis, Katholieke Universiteit Leuven - Faculteit ingenieurswetenschappen.

[Bristol, 1966] Bristol, E. (1966). On a new measure of interactions for multiple multivariable process control. *IEEE Transactions of Automatic Control*, AC-11(1):1000–1002.

[Brod and Novotny, 1985] Brod, D. M. and Novotny, D. W. (1985). Current Control of VSI-PWM Inverters. *IEEE Transactions on Industry Applications*, IA-21(3):562–570.

[Brown and Hwang, 1992] Brown, R. and Hwang, P. (1992). *Introduction to Random Signals and Applied Kalman Filtering*. John Wiley and sons.

[Bueno, 2005] Bueno, E. (2005). *Optimización del comportamiento de un convertidor de tres niveles NPC conectado a la red eléctrica*. PhD thesis, Politechnic school. University of Alcala.

[Bueno et al., 2005] Bueno, E., Rodriguez, F., Espinosa, F., and Cobreces, S. (2005). SPLL design to flux oriented of a VSC interface for wind power applications. In *32nd Annual Conference of IEEE Industrial Electronics Society, 2005. (IECON 2005)*, page 6pp.

[Bueno et al., 2004] Bueno, E. J., Espinosa, F., Rodriguez, F. J., Ureña, J., and Cobreces, S. (2004). Current control of voltage source converters connected to the grid through an LCL-filter. In *35th IEEE Power Electronics Specialist Conference*, pages 68–73.

[Buso et al., 2000] Buso, S., Fasolo, S., Malesani, L., and Mattavelli, P. (2000). A dead-beat adaptive hysteresis current control. *IEEE Transactions on Industry Applications*, 36:1174–1180.

[Ciobotaru et al., 2007] Ciobotaru, M., Teodorescu, R., Rodriguez, P., Timbus, A., and Blaabjerg, F. (2007). Online grid impedance estimation for single-phase grid-connected systems using PQ variations. In *Proceedings of the 2007 Power Electronics Specialist Conference (PESC07)*, pages 2306 – 2312.

[Cobreces et al., 2007] Cobreces, S., Bueno, E., Sanchez, F. J., Huerta, F., and Rodriguez, P. (2007). Influence analisys of the effects of an inductive-resistive weak grid over L and LCL filter current hysteresis controllers. In *Proceedings of the 2007 European Power Electronics Conference*.

[Dahono, 2002] Dahono, P. (2002). A Control Method to Damp Oscillation in the Input LC Filter of AC-DC PWM Converters. In *33th IEEE Power Electronics Specialist Conference*.

[de Oliveira et al., 1991] de Oliveira, A., de Oliveira, J. C., Resende, J. W., and Miskulin, M. S. (1991). Practical Approaches for AC System Harmonic Impedance Measurement. *IEEE Transactions on Power Delivery*, 6(4):1721–1726.

[Dias et al., 2008] Dias, R., Neves, F., Bueno, E., and Cavalcanti, M. (2008). Robust Virtual Flux Oriented Direct Power Control for Three-Phase Rectifiers. In *Proceedings of the VII Conferência Internacional de Aplicacöes Industrials. INDUSCON'08*.

[Doyle, 1978] Doyle, J. (1978). Guaranteed margins for LQG regulators. *IEEE Transactions on Automatic Control*, 23:756–757.

[Doyle, 1982] Doyle, J. (1982). Analysis of feedback systems with structured uncertainties. *IEE Proceedings D Control Theory and Applications*, 129(6):242–250.

[Doyle, 1984] Doyle, J. C. (1984). Lecture Notes on Advances in Multivariable Control. In *ONR/Honeywell Workshop.*

[Duc and Ballois, 1994] Duc, G. and Ballois, S. L. (1994). Hinf control of a flexible arm: coprime factors design using the gap metric. In *Proceedings of the Third IEEE Conferece on Control Applications*, volume 2, pages 1317–1322.

[Dutton et al., 1997] Dutton, K., Thompson, S., and Barraclough, B. (1997). *The Art of Control Engineering.* Addison-Wesley Longman.

[Enslin and Heskes, 2004] Enslin, J. and Heskes, P. (2004). Harmonic Interaction Between a Large Number of Distributed Power Inverters and the Distribution Network. *IEEE Transactions on Power Electronics*, 19(6):1586–1593.

[Fortescue, 1918] Fortescue, C. L. (1918). Method of symmetrical coordinates applied to the solution of polyphase networks. *Transactions AIEE*, 37:1027–1140.

[Francis and Wonham, 1976] Francis, B. and Wonham, W. (1976). The internal model principle of control theory. *Automatica*, 12(5):457–465.

[Fusco et al., 2000] Fusco, G., Losi, A., and Russo, M. (2000). Constrained least squares methods for parameter tracking of power system steady-state equivalent circuits. *IEEE Transactions on Power Delivery*, 15(3):1073–1080.

[Gabe et al., 2007] Gabe, I. J., Massing, J. R., Montagner, V. F., and Pinheiro, H. (2007). Stability Analysis of Grid-Connected Voltage Source Inverters with LCL-Filters using Partial State Feedback. In *Records of 2007 European Conference on Power Electronics and Applications.*

[Georgiu and Smith, 1990] Georgiu, T. T. and Smith, M. C. (1990). Optimal robustness in the gap metric. *IEEE Transactions on Automatic Control*, 35:673–687.

[Girgis and McManis, 1989] Girgis, A. A. and McManis, R. B. (1989). Frequency Domain Techniques for Modeling Distribution or Transmission Networks Using Capacitor Switching Induced Transients. *IEEE Transactions on Power Delivery*, 4(3):1882–1890.

[Girgis et al., 1993] Girgis, A. A., Quaintance, W. H., Qiu, J., and Makram, E. B. (1993). A time-domain three-phase power system impedance modeling approach for harmonic filter analysis. *IEEE Transactions on Power Delivery*, 8(2):504–510.

[Goncalves et al., 2001] Goncalves, J., Megretski, A., and Dahleh, M. (2001). Global stability of relay feedback systems. *IEEE Transactions on Automatic Control*, 46(4):550–562.

[Gu et al., 2005] Gu, D. W., Petkov, P., and Konstantinov, M. (2005). *Robust Control Design with MATLAB.* Springer-Verlag London Limited.

[Hanus et al., 1987] Hanus, R., Kinnaert, M., and Henrotte, J. (1987). Conditioning technique, a general anti-windup and bumpless transfer method. *Automatica*, 23(6):729–739.

[Harnefors and Nee, 1998] Harnefors, L. and Nee, H.-P. (1998). Model-Based Current Control of AC Machines Using the Internal Model Control Method. *IEEE Transactions on Industry Applications*, 34(1):133–141.

[Huerta et al., 2008a] Huerta, F., Bueno, E., Cobreces, S., Rodriguez, F., and Giron, C. (2008a). Control of grid-connected voltage source converters with LCL filter using a Linear Quadratic servocontroller with state estimator. In *IEEE Power Electronics Specialists Conference, 2008. PESC 2008.*, pages 3794–3800.

[Huerta et al., 2008b] Huerta, F., Cobreces, S., Bueno, E., Rodriguez, F. J., Espinosa, F., and Giron, C. (2008b). Control of Voltage Source Converters with LCL Filter using State-Space Techniques. In *Proceedings of the 34th Annual Conference of the IEEE Industrial Electronics Society (IECON'08).*

[Iannelli et al., 2003] Iannelli, L., Johansson, K., Jonsson, U., and Vasca, F. (2003). Dither for smoothing relay feedback systems. *IEEE Transactions on Circuits and Systems I: Fundamental Theory and Applications*, 50(8):1025–1035.

[Johansson and Rantzer, 1996] Johansson, K. and Rantzer, A. (1996). Global analysis of third-order relay feed-back systems. Technical Report TFRT-7542, Department of Automatic Control, Lurid Institute of Technology.

[Jung and Tzou, 1996] Jung, S. and Tzou, Y. (1996). Discrete sliding-mode control of a PWM inverter for sinusoidal output waveform synthesis with optimal sliding curve. *IEEE Transactions on Power Electronics*, 11(4):567–577.

[Kalman, 1960] Kalman, R. E. (1960). A new approach to linear filtering and prediction problems. *Transactions of the ASME - Journal of Basic Engineering*, 82(D):35–45.

[Kalman, 1964] Kalman, R. E. (1964). When is a linear control system optimal? *Journal of Basic Engineering - Transactions on ASME*, 86(D):51–60.

[Kazmierkowski and Malesanti, 1998] Kazmierkowski, M. P. and Malesanti, L. (1998). Current Control Techniques for Three-Phase Voltage-Source PWM converters: A Survey. *IEEE Transactions on Industrial Electronics*, 45:691–703.

[Kazmierkowsky et al., 2002] Kazmierkowsky, M. P., Blaabjerg, F., and Krishnan, R. (2002). *Control in Power Electronics. Selected Problems.* Elsevier Science (USA).

[Krause et al., 1995] Krause, P. C., Wasynczuk, O., and Sudhoff, S. D. (1995). *Analysis of Electric Machinery.* Institute of Electrical & Electronics Engineers.

[Kuo and Golnaraghi, 2002] Kuo, B. C. and Golnaraghi, F. (2002). *Automatic Control Systems.* Wiley.

[Levine, 1996] Levine, W. (1996). *The Control Handbook.* CRC. Press.

[Lindgren, 1998] Lindgren, M. (1998). *Modeling and Control of Voltage Source Converters connected to the Grid.* PhD thesis, Chalmers University of Technology.

[Lindgren and Svensson, 1998] Lindgren, M. and Svensson, J. (1998). Control of a voltage-source converter connected to the grid through an LCL-filter-application to active filtering. In *Conference record of the 29th Annual IEEE Power Electronics Specialists Conference, 1998. PESC 98.*, volume 1, pages 229–235vol.1.

[Liserre et al., 2005] Liserre, M., Blaabjerg, F., and Teodorescu, R. (2005). Grid impedance detection via excitation of LCL-filter resonance. In *Conference Record of the 40th IAS Annual Meeting Industry Applications Conference*, volume 2, pages 910–916.

[Liserre et al., 2004a] Liserre, M., Dell'Aquila, A., and Blaabjerg, F. (2004a). Genetic Algorithm-Based Design of the Active Damping for an LCL-Filter Three-Phase Active Rectifier. *IEEE Transactions on Power Electronics*, 19:76–86.

[Liserre et al., 2006a] Liserre, M., Pigazo, A., Dell'Aquila, A., and Moreno, V. M. (2006a). An Anti-Islanding Method for Single-Phase Inverters Based on a Grid Voltage Sensorless Control. *IEEE Transactions on Industrial Electronics*, 53(5):1418–1426.

[Liserre et al., 2004b] Liserre, M., Teodorescu, R., and Blaabjerg, F. (2004b). Stability of grid-connected PV inverters with large grid impedance variation. In *Proceedings of the 35th Annual IEEE Power Electronics Specialist Conference*, pages 4773–4779.

[Liserre et al., 2006b] Liserre, M., Teodorescu, R., and Blaabjerg, F. (2006b). Multiple harmonics control for three-phase grid converter systems with the use of PI-RES current controller in a rotating frame. *IEEE Transactions on Power Electronics*, 21(3):836–841.

[Liserre et al., 2006c] Liserre, M., Teodorescu, R., and Blaabjerg, F. (2006c). Stability of Photovoltaic and Wind Turbine Grid-Connected Inverters for a Large Set of Grid Impedance Values. *IEEE Transactions on Power Electronics*, 21(1):263–272.

[Ljung, 1986] Ljung, L. (1986). *System identification: theory for the user*. Prentice-Hall, Inc.

[Loh and Holmes, 2005] Loh, P. and Holmes, D. (2005). Analysis of multiloop control strategies for LC/CL/LCL-filtered voltage-source and current-source inverters. *IEEE Transactions on Industry Applications*, 41(2):644–654.

[Magueed and Svensson, 2005] Magueed, F. and Svensson, J. (2005). Control of vsc connected to the grid through lcl-filter to achieve balanced currents. In *Industry Applications Conference, 2005. Fourtieth IAS Annual Meeting. Conference Record of the 2005*, volume 1, pages 572–578Vol.1.

[Malinowski et al., 2001] Malinowski, M., Kazmierkowski, M., Hansen, S., Blaabjerg, F., and Marques, G. (2001). Virtual-flux-based direct power control of three-phase PWM rectifiers. *IEEE Transactions on Industry Applications*, 37(4):1019–1027.

[Mattavelli et al., 2005] Mattavelli, P., Spiazzi, G., and Tenti, P. (2005). Predictive digital control of power factor preregulators with input voltage estimation using disturbance observers. *IEEE Transactions on Power Electronics*, 20(1):140–147.

[McFarlane and Glover, 1990] McFarlane, D. and Glover, K. (1990). Robust controller design using coprime factor plant descriptions. *Lecture Notes in Control and Information Sciences, Springer-Verlag, Berlin.*, 138.

[Miret et al., 2004] Miret, J., de Vicuna, L., Castilla, M., Cruz, J., and Guerrero, J. (2004). A simple sliding mode control of an active power filter. In *Records of the IEEE 35th Annual Power Electronics Specialists Conference. PESC 04.*, volume 2.

[Mojiri et al., 2007] Mojiri, M., Karimi-Ghartemani, M., and Bakhshai, A. (2007). Estimation of power system frequency using an adaptive notch filter. *IEEE Transactions on Instrumentation and Measurement*, 56:2470–2477.

[Morari and Zafiriou, 1989] Morari, M. and Zafiriou, E. (1989). *Robust Process Control.* Prentice Hall.

[Noguchi et al., 1998] Noguchi, T., Tomiki, H., Kondo, S., and Takahashi, I. (1998). Direct power control of pwm converter without power-source voltage sensors. *IEEE Transactions on Industry Applications*, 34:473–479.

[Ogata, 1994] Ogata, K. (1994). *Discrete-Time Control Systems. 2nd Edition.* Prentice-Hall.

[Ottersten, 2003] Ottersten, R. (2003). *On Control of Back-to-Back Converters and Sensorless Induction Machine Drives.* PhD thesis, Chalmers Univeristy of Technology, Sweeden.

[Ottersten and Svensson, 2002] Ottersten, R. and Svensson, J. (2002). Vector current controlled voltage source converter - deadbeat control and saturation strategies. *IEEE Transactions on Power Electronics*, 17(2):279–285.

[Packard and Doyle, 1993] Packard, A. and Doyle, J. (1993). The complex structured singular value. *Automatica*, 29(1):71–109.

[Pedersen et al., 2003] Pedersen, K. O. H., Nielsen, A. H., and Poulsen, N. K. (2003). Short-Circuit Impedance Measurement. *IEE Procedings on Generation, Transmission and Distribution*, 150(2):169–174.

[Plunkett, 1979] Plunkett, A. B. (1979). A current-controlled PWM transistor inverter drive. In *Conference Record of the IEEE Industrial Applications Society Annual Meeting*, pages 785–792.

[Postlethwaite et al., 1999] Postlethwaite, I., Smerlas, A., Walker, D. J., Gubbels, A. W., Baillie, S. W., Strange, M. E., and Howitt, J. (1999). Hinf control of the NRC Bell 205 fly-by-wire helicopter. *Journal of American Helicopter Society*, 44(4):276–284.

[Pou, 2002] Pou, J. (2002). *Modulation and Control of Three-Phase PWM Multilevel Converters.* PhD thesis, Universitat Politècnica de Catalunya.

[Qiu and Davison, 1992] Qiu, L. and Davison, E. J. (1992). Pointwise gap metrics on transfer matrices. *IEEE Transactions on Automatic Control*, 37:741–758.

[Rahim and Kandlawala, 2004] Rahim, A. and Kandlawala, M. (2004). Robust STATCOM voltage controller design using loop-shaping technique. *Electric Power Systems Research*, 68(1):61–74.

[Rhode et al., 1997] Rhode, J. P., Kelley, A. W., and Baran, M. E. (1997). Complete characterization of utilization-voltage power system impedance using wideband measurement. *IEEE Transactions on Industry Applications*, 33(6):1472–1479.

[Rodriguez et al., 2007a] Rodriguez, J., Pontt, J., Silva, C., Correa, P., Lezana, P., Cortes, P., and Ammann, U. (2007a). Predictive Current Control of a Voltage Source Inverter. *IEEE Transactions on Industrial Electronics*, 54(1):495–503.

[Rodriguez et al., 2007b] Rodriguez, P., Pou, J., Bergas, J., Candela, J. I., Burgos, R. P., and Boroyevich, D. (2007b). Decoupled Double Synchronous Reference Frame PLL for Power Converters Control. *IEEE Transactions on Power Electronics*, 22(2):584–592.

[Safonov, 1982] Safonov, M. (1982). Stability margins of diagonally perturbed multivariable feedback systems. *IEE Proceedings D Control Theory and Applications*, 129(6):251–256.

[Safonov and Athans, 1977] Safonov, M. and Athans, M. (1977). Gain and phase margin for multiloop LQG regulators. *IEEE Transactions on Automatic Control*, 22:173–179.

[Safonov et al., 1989] Safonov, M. G., Limebeer, D. J. N., and Chiang, R. Y. (1989). Simplifying the Hinf theory via loopshifting, matrix-pencil and descriptor concepts. *International Journal of Control*, 50:2467–2488.

[Samar et al., 1995] Samar, R., Murad, G., Postlethwaite, I., and Gu, D.-W. (1995). A discrete time Hinf observer-based controller and its application to an aero-engine. In *American Control Conference, 1995. Proceedings of the*, volume 3, pages 1931–1935vol.3.

[Samar et al., 1996] Samar, R., Murad, G., Postlethwaite, I., and Gu., D.-W. (1996). A Discrete time H-infinity observed-based controller and its application to a glass tube production process. *European Journal of Control*, 2.

[Schauder and Caddy, 1982] Schauder, C. and Caddy, R. (1982). Current Control of Voltage-Source Inverters for Fast Four-Quadrant Drive Performance. *IEEE Transactions on Industry Applications*, IA-18(2):163–171.

[Sefton and Ober, 1993] Sefton, J. and Ober, R. (1993). On the gap metric and coprime factor perturbations. *Automatica*, 29:723–734.

[Serpa et al., 2005] Serpa, L. A., Kolar, J. W., Ponnaluri, S., and Barbosa, P. M. (2005). A Modified Direct Power Control Strategy Allowing the Connection of Three-Phase Inverter to the Grid through LCL Filters. In *Conference Record of the Fourtieth IAS Annual Meeting.*

[Skogestad and Postlethwaite, 2005] Skogestad, S. and Postlethwaite, I. (2005). *Multivariable feedback control*. Wiley.

[Staroszczyk, 2005] Staroszczyk, Z. (2005). A method for real-time, wide-band identification of the source impedance in power systems. *IEEE Transactions on Instrumentation and Measurement*, 54(1):377–385.

[Sumner et al., 2004] Sumner, M., Palethorpe, B., and Thomas, D. (2004). Impedance measurement for improved power quality part 1: The measurement technique. *IEEE Transactions on Power Delivery*, 19(3):1442–1448.

[Sumner et al., 2002] Sumner, M., Palethorpe, B., Thomas, D., Zanchetta, P., and Piazza, M. C. D. (2002). A technique for power supply harmonic impedance estimation using a controlled voltage disturbance. *IEEE Transactions on Power Electronics*, 17(2):207–215.

[Svensson, 1997] Svensson, J. (1997). Inclusion of dead-time and parameter variations in VSC modelling for predicting responses of grid voltage harmonics. In *Proceedings of the 7th European Conference on Power Electronics and Applications. EPE'97.*, volume 3, pages 216–221.

[Tarkiainen et al., 2004] Tarkiainen, A., Pollanen, R., Niemela, M., and Pyrhonen, J. (2004). Identification of Grid Impedance for Purposes of Voltage Feedback Active Filtering. *IEEE Power Electronics Letters*, 2(1):6 –10.

[Teodorescu et al., 2004] Teodorescu, R., Blaabjerg, F., Borup, F., and Liserre, M. (2004). A new control structure for grid-connected LCL PV inverters with zero steady-state error and selective harmonic compensation. In *IEEE Applied Power Electronics Conference and Exposition 2004*.

[Timbus et al., 2007] Timbus, A. V., Rodriguez, P., Teodorescu, R., and Ciobotaru, M. (2007). Line impedance estimation using active and reactive power variations. In *Proceedings of the 2007 Power Electronics Specialist Conference.*, pages 1273 – 1279.

[Timbus et al., 2004] Timbus, A. V., Teodorescu, R., Blaabjerg, F., and Borup, U. (2004). Online grid measurement and ENS detection for PV inverter running on highly inductive grid. *IEEE Power Electronics Letters*, 2(3):77–82.

[Twining and Holmes, 2003] Twining, E. and Holmes, D. G. (2003). Grid Current Regulation of a Three-Phase Voltage Source Inverter With an LCL Input Filter. *IEEE Transactions on Power Electronics*, 18:888–895.

[Utkin, 1993] Utkin, V. (1993). Sliding mode control design principles and applications to electric drives. *IEEE Transactions on Industrial Electronics*, 40(1):23–36.

[Vinnicombe, 1993] Vinnicombe, G. (1993). Frequency domain uncertainty and the graph topology. *IEEE Transactions on Automatic Control*, 38:1371–1383.

[Vinnicombe, 2001] Vinnicombe, G. (2001). *Uncertainty and Feedback. Hinf loop-shpaing an the nu-gap metric*. Imperial College Press. London.

[Walker, 1990] Walker, D. (1990). Robust stailizability of discrete-time systems with normalized stable factor perturbation. *International Journal of Control*, 52(2):441–455.

[Walker, 1991] Walker, D. J. (1991). *Robust Control of Discrete Time Systems*. PhD thesis, Department of Electrical Engineering, Imperial College of Science, Technology and Medicine, University of London.

[Wipasuramonton et al., 2006] Wipasuramonton, P., Zhu, Z., and Howe, D. (2006). Predictive current control with current-error correction for PM brushless AC drives. *IEEE Transactions on Industry Applications*, 42(4):1071–1079.

[Wu and Lehn, 2006] Wu, E. and Lehn, P. (2006). Digital current control of a voltage source converter with active damping of LCL resonance. *IEEE Transactions on Power Electronics*, 21:1364–1373.

[Yuan et al., 2002] Yuan, X., Merk, W., Stemmler, H., and Allmeling, J. (2002). Stationary-Frame Generalized Integrators for Current Control of Active Power Filters With Zero Steady-State Error for Current Harmonics of Concern Under Unbalanced and Distorted Operating Conditions. *IEEE Transactions on Industry Applications*, 38:523–532.

[Zhou, 1998] Zhou, K. (1998). *Essentials of Robust Control*. Prentice-Hall Inc.

[Zmood and Holmes, 2003] Zmood, D. N. and Holmes, D. G. (2003). Stationary Frame Current Regulation of PWM Inverters With Zero Steady-State Error. *IEEE Transactions on Industry Applications*, 18:814–822.

[Zmood et al., 2001] Zmood, D. N., Holmes, D. G., and Bode, G. H. (2001). Frequency-Domain Analysis of Three-Phase Linear Current Regulators. *IEEE Transactions on Industry Applications*, 37:601–610.